UNIVERSITA' DEGLI STUDI DI PAVIA

DIPARTIMENTO DI CHIMICA

DOTTORATO IN SCIENZE CHIMICHE E FARMACEUTICHE (XXXI CICLO)

Direttrice: Chiar.ma Prof. Antonella Profumo

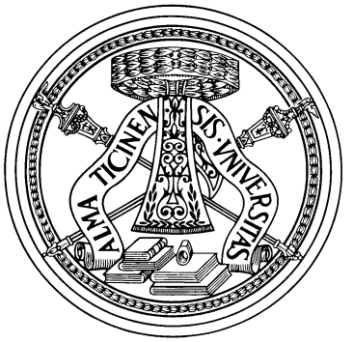

OPTOELECTRONIC SENSORS BASED ON MOLECULARLY IMPRINTED POLYMERS

Relatrice:

Prof. Maria Pesavento

Tesi di Dottorato in Chimica

Simone Marchetti

Anno Accademico: 2017/2018

INDEX

ABSTRACT

The need for more rapid and miniaturized chemical-analytical methods, able to give an "in situ" analysis, stimulated the research on chemical sensors. A chemical sensor is based on the strict integration of a receptor with an instrument able to generate a signal upon the combination with the analyte. Chemical sensors were proposed in combination with different transduction methods, in particular, electrochemical and optical ones. Among these, surface plasmon resonance (SPR) appears to be particularly suited, yet not widely employed because of the difficulties in the miniaturization. This problem has been faced by introducing transduction devices based on plastic optical fiber (POF). This research was focused on the development of new sensoristic methods, based on synthetic biomimetic receptors, obtained by molecular imprinting on polymers and biopolymers, coupled with optoelectronic methods of transduction (Par. 1.3). The activity led to the creation of several selective optical sensors based on surface plasmon resonance (SPR) or on the evanescent wave coupling (EWC) (Par 1.4.4). SPR intrinsic devices are directly developed on plastic optical fiber (POF) with a D-shaped profile [1], while the SPR extrinsic ones are based on a plastic slab (PMMA or PET) as a waveguide, into which the light was injected by a POF [2; 3]. Two kinds of sensing metal layers have been considered, i.e. a homogeneous thin gold film (50 nm) and a set of parallel ink with silver nanoparticles printed lines [2; 3]. Another transduction based on a segmented waveguide (SWS) for EWC was tested, obtained by coupling POF through a material of different RI in the middle [4]. The D-shaped sensor consists of a plastic optical fiber (POF) deprived of the cladding covered by a thin layer of Au in contact with the synthetic receptor (MIP) [1], a similar extrinsic sensor has been developed with a PMMA slab as a waveguide, with a sputtered thin Au layer, in contact with an appropriate synthetic receptor (MIP) [2]. Another extrinsic sensor was realized on a PET slab inject printed with lines of silver nanoparticles intercalated by MIP rows [3]. The segmented waveguide (SWS) is based on two parallel POFs coupled through a trench drilled in between, filled with a molecularly imprinted polymer [4]. Similar cheap and simple instrumentation is required for all the sensors examined: a white light source emitting from 300 nm to 900 nm, i.e. the wavelength range of transmittance of the PMMA POF, or in some configurations even a LED; a spectrophotometer for the same wavelength range, and software for the data analysis. In the intrinsic D-shaped POF-SPR and extrinsic PMMA Slab sensors, the signal of analytical interest is the shift in resonance wavelength, which is evaluated in function of the analyte concentration,

while in the extrinsic PET-line-MIP sensor the intensity of light emerging from the PET collected from a fiber is evaluated. The intrinsic D-shaped platform is able to selectively detect the presence of DBDS or furfural in a real matrix, i.e. a mineral oil at a concentration as low as 6.7 10^{-8}M with a MIP K_{aff} of 5(1) 10^6 M^{-1}. This device was implemented to a multiplexing sensing device, by coupling in series different sensors which differ because of the different thickness of the metal layer. The same device is able to detect the concentration of 2-FAL in the water down to 3 10^{-8} M, the affinity constant in water is noticeably lower than that in transformer oil Kaff of 1.1(3) 10^6 M^{-1}. Despite these good results, intrinsic D-shaped platforms suffer from low reproducibility due to the manual fabrication procedure. Consequently, extrinsic configurations based on a slab waveguide have been investigated, mainly in order to improve the reproducibility of the sensing device. The same molecularly imprinted polymer (MIP) for 2-FAL was used as a receptor. Both the proposed devices were able to selectively detect the 2-FAL in aqueous solution with comparable LOD and affinity constant for MIP to that obtained with the D-shaped configuration previously described. The easy replacement of the chip allows a simplified measurement procedure, this results in an enhancement of the sensors reproducibility. Based on another concept of analysis, in the SWS platform the relative output, i.e. the ratio of the light intensity, emerging from the two fibers (I2 /I1), is plotted versus the concentration of the analyte. LOD and Kaff are comparable with that of SPR platforms but it is more reproducible due to the simplicity of platform fabrication, which also avoids the presence of the possibly irreproducibility of the Au layer. Voltammetric sensor based on screen printed cell (SPC) were also investigated for the sake of comparison (Par. 2.3.3). The SPC-MIP sensor is based composed by a graphite ink working and auxiliary electrodes, and a silver ink quasi-reference electrode with a MIP deposed layer. The analysis was performed with square wave voltammetry (SWV) for furfural analyte, the reduction current is evaluated in function of concentration. The SPC-MIP sensor shows a LOD of 6 10^{-6}M for 2-FAL in water, which is almost one magnitude order higher than that obtained D-shaped POF, confirming optical platform as more suitable and less affected by interference. All these sensors employ a MIP receptor, the identification of appropriate functional monomers has been made by computational method (Gaussian 09). The prepolymer solution of MIP has been prepared by molar ratio 1 (DBDS): 4 (MAA): 40 (DVB) (Par. 2.4). The MIP composition was optimized to be used as a receptor layer on the sensors (Par. 2.4.4). This MIP coupled with the optical transduction methods shows a high selectivity, however, suffer from low dynamic range; so various formulation has been considered in order to obtain different porosity and enhance the MIP loading capacity. The adsorbent properties

of the MIP were characterized by batch and column techniques either by spectrophotometric and electrochemical analysis (Par. 2.3).

Also, new kinds of molecularly imprinted materials have been considered in order to improve the biocompatibility of the sensing devices. In particular silk fibroin has been examined for its good optical and mechanical characteristics (Cap 4.). Moreover, it is a biomaterial already approved for biomedical applications. A research on the development of an imprinted bioreceptor using the silk fibroin protein was carried out at Tufts University in Boston aiming of a further application in sensors which exploit the optical sensing platform here exposed or various silk structures engineered by the Silklab group such as gratings, opals, and waveguides (toroidal resonator). The binding site has been designed considering the primary structure of the silk fibroin as intermolecular folding of the protein around the template allowing non-covalent interactions. A study has been started on the thermodynamics by DFT calculations. Silk was dissolved as exposed in the nature protocol [5]. Fibroin derived protein were employed exploiting different M.W. of the protein with an average value of 69kDa and 47kDa. Samples of imprinted fibroin film for glucose were obtained by deposing and drying 2mL of silk solutions at 6.6% in a PDMS mold at different analyte concentration (140-260-350 mg/L). The films have been water annealed to obtain a water-resistant product. The characterization of the adsorption characteristic of fibroin film imprinted with glucose was performed by batch procedure, by soaking the sample into 5mL of PBS solution (30mM) spiked with an amount of glucose ranging from (160-270-360 mg/L). Colorimetric enzymatic assays based on GOD/HRP enzymes were used to perform the quantitative analysis. Preliminary results on the imprinting of fibroin with glucose have been promising, with an imprinting factor around 2. Moreover, the imprinted material can easily obtain a thin layer, which is particularly suitable for sensor development. A high loading capacity was found, around 5 ($mg_{analyte}/g_{fiborin}$), however, a high specific absorption has been measured. The approximate K_{aff} found of 10^3 M^{-1} is similar to that obtained on MIPs by batch procedure, hence is low, since the sensing of even low-affinity sites is given by this method and considering that in this investigation high concentrations were employed. A strong irreproducibility were found. Further investigations are required to optimize the procedure of analysis.

1 INTRODUCTION

1.1 CHEMICAL SENSORS

The requirement of miniaturized analytical methods, able to give analysis "in situ" in a short time, stimulated the research in the field of chemical sensors. They can be of high interest in many different fields, thanks to the convenience of their use, the rapidity of the analytical response, the low cost of production and the possibility of reuse. A chemical sensor is an analytical system which combines an element for the specific chemical recognition of the analyte, i.e. the receptor, with a transducing device able to generate a signal proportional to the analyte concentration related to the analyte-receptor interaction.

The most common receptors are bioreceptors, as for example enzymes (catalytic receptors) and antibodies and aptamers (non-catalytic receptors). Among the advantages of the biosensors, there is the highly selective response, i.e. able to discriminate between very similar structures or chemical functions, since the analyte-receptor binding is highly selective. Most sensors are actually based on such biological interactions (antibody-antigen, substrate-enzyme, etc.). The bioreceptors, however, have some disadvantages: their use is limited to particular conditions and therefore they can hardly be employed in non-biological environments (at high or low pH, high temperature or in a non-aqueous solvent, etc.), due to the possible denaturation and/or degradation. Moreover, the affinity catalytic bioreceptors such as enzymes do not exist for all the substrates and cannot be synthesized (proteins). Although considering the class of the non-catalytic receptors, such as antibodies, they can be obtained from the immune system of vertebrates animals, nevertheless, they require a long and expensive work for production and purification before the possible use, and still suffer from a low reproducibility. Instead, the aptamers, another receptor of the same class, can be synthesized, but require a long work of research and optimization. Moreover, for all the non-catalytic receptors, the most tedious disadvantage is the required use of markers for the measurement, since the combination of the substrate with the receptor does not directly produce any signal.

In recent years, synthetical receptors instead of biological ones, in particular, those obtained by the molecular imprinting technique (MIP), emerged as very promising tools for sensing since they

offer some advantages, as for example the stability in non-biological matrix, a rapid and low-cost development, and a good reproducibility; however, they're not catalytic, so labels are needed.

Chemical sensors have been proposed based on different transduction methods, in particular, electrochemical and optical ones. However, label-free transduction is preferred due to the better simplicity and rapidity in obtaining the response.

Most commonly used were EIS (electrochemical impedance spectroscopy), QCM (Quarz cristal microbilance) and SPR (surface plasmon resonance).

Among these, surface plasmon resonance (SPR) appears to be particularly suited, yet not being widely used because of the high costs and large dimension of the measuring devices. This problem has been faced by introducing instrumentation based on optical fiber (OF) [6].

The aim of the present research was the development of new sensing methods, based on synthetic biomimetic receptors, obtained by molecular imprinting techniques coupled with optoelectronic transduction based on plastic optical fibers (POF). [7-8]

Several new sensing platforms based on surface plasmon resonance (SPR) and on the evanescent wave coupling (EWC) have been considered with the aim of improving the performance in terms of sensitivity and reproducibility. In the present investigation, commercially available plastic slabs (PMMA or PET) have been considered as a waveguide, into which the light is injected by a POF [8-9]. These slabs present a flat surface, in which the receptor can be omogeneously deposited by a very convenient in situ polymerization procedure, as it has been previously shown in the case of the D-shaped platforms [10]. Again with the aim of improving the reproducibility, different sensing metal layers have been examined in the present research [11-16]. Actually, the metal layer obtained by sputtering, a method which has been typically used in previous researches, can be rather irreproducible, in particular in terms of thickness and presence of metallic nanostructures. Thus another optical transduction principle, not requiring a metal layer as SPR, has been considered too. It is based on a segmented waveguide (SWS) obtained by coupling two POFs through a material of different RI in the middle [17].

The first sensing platform based on POF considered by our research group consisted of a plastic optical fiber (POF) deprived of the cladding, leveled out to a flat surface and covered by a thin layer of Au in contact with the synthetic receptor (D-shaped SPR sensor) [18]. This sensor was successfully used in connection with MIPs, and with bioreceptors, for the determination of different substances

[19], however with a certain irreproducibility due to the fact that the whole preparation of the platform was manually performed, including the decladding and formation of the flat surface of the decladded POF portion. In order to reduce this irreproducibility extrinsic sensor can be considered, based on commercially available plastic slabs, which do not require any manual treatment before the deposition of the metal layer. In particular, in this investigation, a PMMA slab has been tested as a waveguide, with a sputtered Au thin layer [20], and a PET slab with inkjet printed lines of silver nanoparticles [11-21] in contact with the appropriate synthetic receptor (MIP) has been tested.

A possible approach to reduce the irreproducibility of the metal layer can be based on the segmented waveguide (SWS) principle [17]. The SWS platform here proposed consists of two parallel POFs coupled through a trench drilled in between, filled with a molecularly imprinted polymer. For all the platforms proposed a similar cheap and simple instrumentation is required.

In this work, the effectiveness of the coupling of the POF-based optical platforms described with synthetical receptors as MIPs has been investigated.

1.2 MOLECULAR IMPRINTING

Molecular imprinting is a technique used to create artificial receptors by the formation of a polymer network around a template molecule (target). Removal of the template leaves chemically and sterically complementary voids (imprints) in the polymer network, which is able to rebind the template. Although the first paper describing the formation of imprints was published in 1931 [22], research on molecular imprinting was scarce until the 1980s. In an excellent and extensive review, Whitcombe et al. illustrated the maturation of the field by the dramatic increase in publications seen over the past 20 years [23]. From this, it becomes clear that molecular imprinting is an effective and rapidly evolving technology, with many possible applications such as analytical separations, enzyme-like catalysis, chemical sensors and drug delivery [23-27]. Molecular imprinting has proven to be particularly successful for low molecular weight compounds [28-31]. MIPs were proposed as potential substitutes for antibodies as receptors to quantify, for example, certain types of drugs in the blood such as theophylline and diazepam [32]. Although imprinting of larger, more complex molecules such as proteins, DNA, and even whole cells and viruses has been reported [33-36], the number of research papers using such templates is relatively small. This reflects the difficulties faced when trying to imprint large and flexibles biomolecules [37-38]. Generally speaking, recognition of proteins seems to be difficult, because they fold into three-dimensional structures and are vulnerable to harsh conditions such as high/low pH, temperatures, high salt concentrations, and so on. In order to achieve molecular imprinting of proteins, such obstacles should be overcome [39-40]. Much of the pioneering work in the molecular imprinting of peptides and proteins was conducted by Mosbach [41-47] using amino acid derivatives as template molecules. For low molecular weight compounds, highly crosslinked gels are used to ensure the preservation of the imprinted cavity after removal of the template. However, for large template molecules, the highly crosslinking hinder the mass transfer, leading to slow template removal and rebinding kinetics or, in the worst case, to a complete physical immobilization [48]. By employing biomacromolecules as the template, imprinting can generally only be performed in an aqueous environment, which limits the choice of functional monomers. Also, the physicochemical properties of the biomolecules such as charge or hydrophobicity can strongly vary in different regions of e.g. the protein template, and similar regions may be present in other substances. This could lead to high aspecific binding and cross-reactivity of the imprinted polymer. In the present investigation, small molecular weight

templates have been considered since the aim of the research was to demonstrate how a MIP can be successfully implemented in marker-free optoelectronic sensors.

The main topics of concern in the synthesis of imprinted polymers are the selection of the proper functional compounds and the composition of the prepolymer mixture since these determine the structure of the imprints and the selectivity of the adsorption. So, this research has been focused on the optimization of the binding site by the choice of the appropriate functional moieties, supported by computational methods, and on the effect of the presence of the solvent in the prepolymer mixture for the preparation of MIPs.

Other points of relevance for the application of the MIPs as receptors in optoelectronic sensors are in particular their optical characteristics and the physical shape of the receptor layer in contact with the transducer, included its thickness and porosity. Some of these have been examined in the present work in view of the optimization of the sensor performance, in particular considering the reproducibility.

A preliminary investigation has been carried out on a different imprinted material, obtained from silk fibroin. The idea was to imprint a biological polymer, in order to develop biocompatible sensing devices [49] even edible [50] or implantable [51]. Despite these favorable possibilities, only publications on peptide biosensing have been found on proteins [52-54].

1.2.1 MOLECULARLY IMPRINTED POLYMERS (MIP)

In synthetic receptors as MIPs specific cavities must be designed for the target molecule (template) [55]. Since the analyte (template) can be of different types, like proteins, molecules with high molecular mass or small chemical compounds i.e. drugs and pesticides [39; 56], the choice of the prepolymer mixture formulation of the MIP is crucial. The stability of the functional monomers-template aggregate -is important so that the adduct can be maintained during the polymerization process. Figure 1 illustrates the operational steps of the molecular imprinting technique [19; 57].

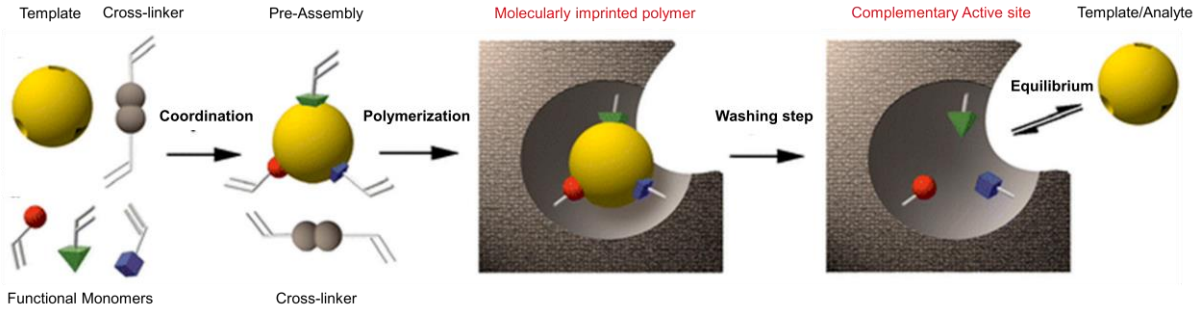

Figure 1. *Representative scheme of the synthesis of MIP.*

1. The molecule which acts as the molecular mold (template)determines the choice of .the functional monomer which can interact optimally with the functional groups of the template molecule building up g the appropriately oriented and selective chemical hooks for the analyte, and that of the cross-linker which will build the real three-dimensional structure of the site;
2. The Self-assembling in solution between the template and functional monomers, which form the adducts or complexes;
3. The polymerization (thermal or UV-VIS) initiated by an adequate initiator;
4. Extraction of the template molecule, in order to expose the complementary site (with fixed functional groups) for the subsequent recombination by a selective recognition of the analyte in a real matrix.

Monomers are chosen which present both a polymerizable moiety and a part able to interact with the analyte forming a polymerizable pre-assembled cluster in a solvent. In presence of a cross-linking agent and an initiator of reaction, polymerization takes place around the pre-assembled

cluster molecules which build the tridimensional structure of the site with a particular spatial arrangement of the functional monomers around the template.

The polymerization usually is performed thermally or by the use of UV rays. At the end of the polymerization process, the template is removed by an appropriate washing procedure with solvents which show high affinity to the template, to produce a polymer with binding sites complementary to the template in size and shape with chemical hooks directed in an appropriate geometry.

Usually, the approach considers non-covalent interactions template-functional monomer such as hydrophobic interactions, hydrogen bonds, ionic interactions, π-π stacking, Van der Waals forces and electrostatic interactions [58]. Even if these are non-specific bonds, by fixing the geometry and designing the site with an adequate amount of interactions in the preassembly cluster, it is possible to obtain sites with the proper selectivity and high stability. Carefully selected functional monomers are needed in order to produce sufficiently stable aggregates in the prepolymer mixture able to persist during the polymerization process.

Functional monomers commonly used in the synthesis of MIPs are shown in Figure 2.

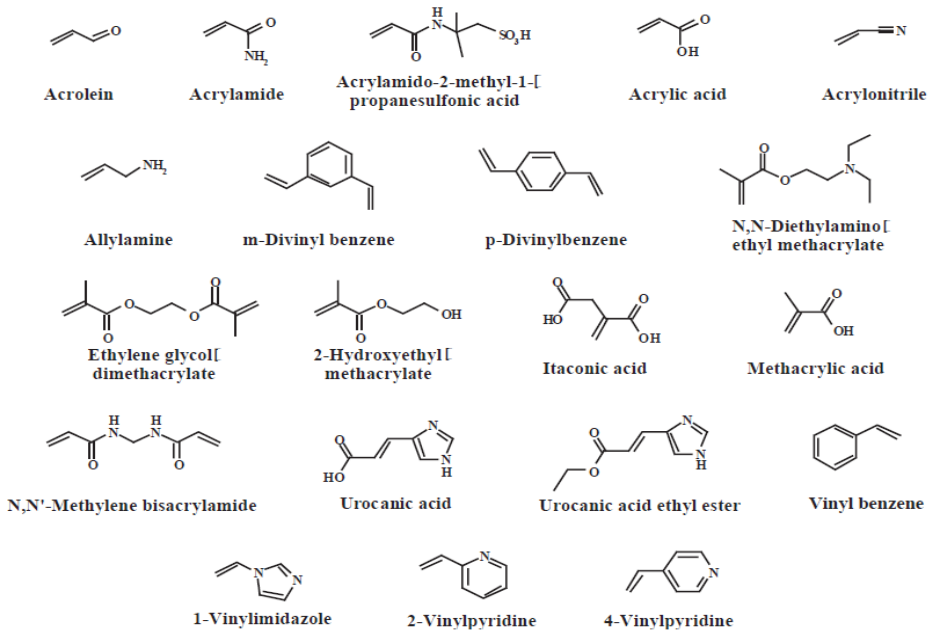

Figure 2. Typical functional monomers used for the synthesis of MIPs [58]

Computational methods for custom synthesis of MIP can be considered as an effective approach [59-62]. The composition of the prepolymer mixture for the formation of a strong pre-assembly between the analyte and the monomers can be studied by computational models. In the present investigation, a computational method (Gaussian 09) has been used to test the interaction between functional monomer and template with the hybrid function at B3LYP / 6-311 + G ** level. The calculation was refined in a Continuous Model of Polarization (PCM) to evaluate the solvent effect, which is also relevant for the strength of the interaction template-functional monomer.

The right ratio between the functional monomer and the template is fundamental for the activity of MIP and should be appropriately chosen, so as not to leave non-structured functional monomers in the MIP, which could give rise to nonspecific absorption as exposed in a work by Prof. Baggiani group [63]. Also important is the role of cross-linker in order to have a certain polymer stiffness. The ratio of the prepolymer mixture reagents can be calculated by the molecular mechanics using "ab initio" calculations [43] or by metadynamics simulations (MTD) based for example on the most recent “adaptively biased molecular dynamics" approach [43]. This calculation has not been performed in this thesis since previously considered by our group.

In this type of imprinting the solvent is crucial to determine the formation of the assembly since the recognition "template-monomers" is related to physical and chemical parameters of the solvent.

For example, hydrogen bonding interactions strongly contribute to the affinity of molecularly imprinted polymers (MIPs). They can be easily established in organic and aprotic solvents but are seriously hampered in water. For this purpose, dichloromethane, chloroform or toluene are often used. Obviously, this is possible only when the template and the functional monomers are sufficiently soluble in the considered solvent. Actually, a sufficiently high concentration of the reagents is needed to form the aggregate template-monomer particularly when the interactions are not very strong. However, this could enhance the aspecific adsorption due to the interaction with residual functional monomers, non-structured in the sites.

Non imprinted polymer (NIP) is commonly used to verify the aspecific absorption. For example, the use of charged functional monomers can lead to strong electrostatic interactions between monomers and template but also to undesired high aspecific binding. Even so, the unspecific adsorption on NIP is an index of the possible interaction of the analyte with the free binding group of the functional monomer. It is pointless to obtain a formulation of NIP where no aspecific

absorption is observed since this means that the coordinative portion (monomers) probably does not interact at all with the analyte considered, and so not any specific site can be formed as explained by Baggiani at all. [38]

The washing steps are also relevant for the performance of the MIP. An appropriate solvent which shows high affinity to the template must be employed. This step allows obtaining the largest number of empty sites in the polymer. Also, other substances such as monomers or oligomeric fragments not completely polymerized, which could interfere with correct sensor performance, for example by interfering in the transduction, need to be eliminated by washing procedure with a suitable solvent.

Fundamental for the microstructure and porosity are the polymerization procedure and the presence of a porogen solvent. Different strategies allow obtaining MIP in different shapes depending on the required use. Bulk polymerization is the most reported method for MIPs [64-66]. This method allows the formation of a polymer highly networked, produced by the polymerization of functional monomers and cross-linking agents around a mold molecule. The result is a hard solid block that needs to be crushed and sieved to select the particles of the required dimension. The main problem of the preparation of MIPs with the bulk technique [65-66] is the production of an irregular mesoporous particulate not suitable for example for the production of stationary phases for HPLC analysis.

Nevertheless, other methods of polymerization can be used including suspension, emulsion, two-step swelling and precipitation [67-73]. Among these, the precipitation polymerization is extensively employed [67-68]. In synthesis, the difference consists in the presence of higher amounts of porogen solvent than in bulk polymerization [69]. The excess of porogenic solvent prevents the formation of a compact mass of the polymer (bulk) so producing polymeric microspheres of regular size and shape. This makes it possible to avoid the step of crushing and sieving to select particles of a given dimension. In fact, a random shape of the particles, like shattered glass, is obtained during the crushing procedure in the bulk polymerization. For separative or chromatographic applications the best shape consists of spheroidal and homogeneous particles; however, the particles dimension distribution can be broad and even on the nanometric scale, not suitable for a chromatographic application (at least 0.5 μm of particles dimension are required) and they must be even bigger in SPE methods (greater than 100 μm).

For the use in sensors, the most used polymerization methods consist of “in-situ” techniques, based on electropolymerization, spin-coating, drop casting or layer preparation of aggregated micro / nano-particles (beads) layers [70]. In this research, the drop casting and spin coating methods were considered in particular in order to obtain a suitable MIP receptor layer over the surface of the sensors with an easy and straightforward procedure.

An overview of the possible uses of MIPs is provided by A. Mayes et al [55], which lists the possible applications of MIPs:

- Stationary phases for separation by HPLC (also enantiomeric)
- Capillary electrophoresis and electrochromatography separation
- Materials for adsorbing phases (SPE)
- Catalysts
- Sensors

A broad description of the use of MIPs in the field of chemical sensors has been presented by Turner et al [74].

1.2.2 SELECTION OF THE PREPOLIMER MIP MIXTURE BY COMPUTATIONAL METHODS

Currently, computational methods are of great importance for the rational design of molecularly imprinted polymers [59-61]. In fact, the characterization of the molecular complexes between the template and functional monomer forms the basis of the investigation of the for the possible application of these polymers, for example giving information about the affinity of the sites for the template. In this work, the interaction of the functional monomers with the template has been studied through the use of the Gaussian09W program. The method is based on the calculation of electronic energies through the Density Functional Theory (DFT) using the hybrid density function B3LYP. The calculation considers the interactions between the electronic densities that occur for interactions such as hydrogen bond, ionic, Van der Waals, hydrophobic, π-π stacking, etc.

The most energy-stable conformations are calculated by rotation of the dihedral angles of each bond in the structure of the reagents (monomer and template) alone in the gas phase vacuum under standard conditions and coupled in cluster conformation. For each functional monomer, the most stable template-monomer complex was identified and the related stabilization energy for "coordination" was calculated, with respect to the electronic energy of the isolated components. The following relationship is used:

$$\Delta E = E\,(model - monomer) - [E\,(template) + E\,(monomer)] \quad \textit{Eq. 1}$$

Geometry optimizations were performed with the algorithm at the B3LYP 6-31G * level. Considering the electrostatic interaction energies, further single point calculations were performed on the optimized geometries using a broader set of bases (B3LYP / 6-311 + G ** level). Finally, for the resultant most stable model the stabilization energy in various solvents was calculated using the Continuous Polarization Model (PCM) considering the Hartree-Fock Atomic States Set (UAHF). Since polymerization occurs in a solvent, the effect of solvent was considered too, because it can lead to changes in the energy and stability of the template–monomer complexes [58]. The solvent may act as a competitor of the functional monomer for the interaction with the template. It considers the solvent as a uniform polarizable medium with a

particular dielectric constant, in which the solute is placed in suitably shaped cavities in the medium [55].

This computational approach has been already widely used in research works with the aim of developing MIPs for sensing applications [60-62].

1.3 BIOIMPRINTING

While MIPs have been prepared for a large number of target molecules and applications [27; 75-77] over the years, both for low molecular weight substances and larger biomolecules such as DNA, protein and so on, the problems of their biocompatibility has been seldom addressed. So, in this work a preliminary investigation on the possibility of performing some imprinting on a biocompatible and poorly immunogenic protein, silk fibroin, has been considered, taking advantage of the coordination properties of some functional groups present in the protein.

The optimal optical properties, i.e refractive index, and transparency, coupled with the impressive mechanical properties, i.e. strength and flexibility, made this material really promising for designing optoelectronic biosensors to be used even in the living organisms. [78-81]

The use of biocompatible materials is of paramount importance for biomedical applications. Polymers such as polylactic acids [82-83] and collagens [84] have been widely studied to design medical device. Recent interest in integrating the biological interface of biomaterials with technological functionalities such as electronics [85-87] or optics [79; 88-89] provides a new path of research. The requirements of mechanical stability, optical clarity, and reliable electronic interfaces present a significant barrier to success because of the impact on material performance. Recent results indicate that silk fibroin possesses a convenient convergence of the features outlined above. Also, silk fibroin has the remarkable properties of a controllable degradation rate from hours to years [90] and the possibility to be chemically modified to alter surface properties [91]. Silk fibroin is already a widely used biopolymer approved by the US Department of Agriculture [92] and it has been shown to be suitable for use as a material platform for sophisticated optical and optoelectronic components with features on the micro- and nanoscale [51; 88-89; 93-100]. These components provide mechanically stable, high-quality optical elements that are fully degradable, biocompatible, and implantable [78]. Silk fibroin based materials have been shown to possess the ability to stabilize labile biological components [80; 101-105], which provides the opportunity for functionalized optical devices, as well as for drug delivery. Silk-based anticancer drug delivery systems have been proposed [106-107]. The results demonstrate a next-generation concept exploitable in different biomedical fields up to new micro-optical devices. The idea was to exploit the ability of several groups in the fibroin molecules to coordinate a given template [52] and to “freeze” the obtained imprinted sites during the drying procedure. Moreover, we aim to develop a

new bio-synthetic imprinted receptor by exploiting the appealing characteristics of this protein, first of all, the possibility of obtaining different insoluble solid structures, which in our case could result imprinted [5] and the refractive index which seems to be appropriate for coupling with optical sensoristic devices [108].

1.4 OPTOELECTRONIC SENSORS BASED ON MOLECULARLY IMPRINTED POLYMERS

1.4.1 SURFACE PLASMON RESONANCE (SPR AND LSPR) PHENOMENA

Surface plasmon resonance (SPR) is an optical phenomenon that derives from the interaction between an electromagnetic wave and the conduction electrons present at the surface of a metallic element, therefore is more evident in those metallic forms with a wider surface such as nanoparticles or thin films [12].

The electrons on the surface of a metal can be considered mobile and can be represented as a high-density fluid (plasma) in which it is possible to induce coherent and simultaneous oscillations, which propagate as waves longitudinally within few nm along the metal-dielectric interface. The propagating plasma waves are called surface plasmon waves (SPW). SPW is a transverse magnetic (TM) or a p-polarized light wave. This wave is longitudinal and has a magnetic vector vertical to the plane of incidence. The magnetic vector travels along the upper surface of the metal film. Moreover, the electromagnetic field is distributed as follows. At the interface, the intensity of the field is the strongest and diminishes exponentially into both materials with a decay depth on the order of about a light wavelength. The major part of the field is located in the dielectric [109]

Figure 3 shows a sketch of the plasmon-polariton propagating at the metal-dielectric interface. The electromagnetic field of the SPW has a maximum intensity that exponentially decreases (evanescent wave, EW) into both media with a variable penetration from 100 to 600 nm (for VIS and NIR wavelengths).

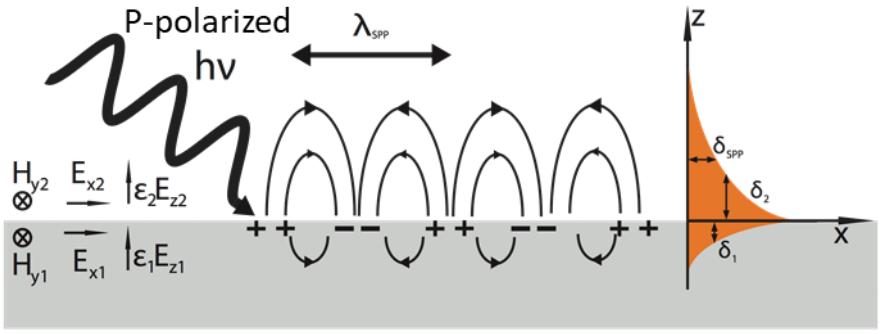

Figure 3: Sketch of the plasmon-polariton propagating over the surface.

The excitation of the plasmons is possible only when a coupling between the moment of the wave vector of a light beam and the mode of oscillation (or oscillation frequency of plasmon) of the free electrons of the surface of a metal takes place [110-111]. It is known that surface plasmons are transverse magnetic waves, so a TM or p-polarized light can excite them. The momentum and the wave vector of the light are increased by passing the light wave through an optically denser medium (e.g. a prism with high dielectric constant). When a beam of light passes from a material with a high refractive index (eg glass) to a material with a low refractive index (eg water), part of the light is reflected by the interface. At the interface, a small portion of the light penetrates the optically thinner medium to a depth of about one wavelength and propagates along the boundary for a distance of approximately half of the light wavelength. Then the light returns to the optically denser medium. The field in the lower refractive index medium is called the evanescent field and the wave corresponding to it is called the evanescent wave (EW) [112]. For sensing purposes the SPW is conveniently excited by the evanescent wave from a waveguide as reported in Figure 4.

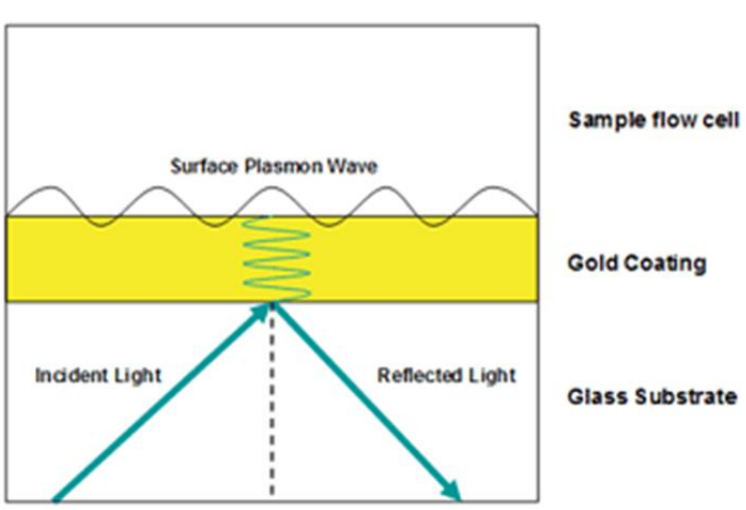

Figure 4: schematic view of the SPR phenomenon excited by EW

If the angle of incidence of the light is higher than a critical value, the light is completely reflected (total internal reflection). The total reflection in the optical fibers is achieved by entrapping the beam of light in the core of the fiber using a cladding with lower RI, as reported in Figure 5. If the waveguide surface (eg the glass surface) is covered with a thin metal film (eg gold), the reflected

light may be attenuated. This effect occurs when the part of the light which emerges as an evanescent wave towards the metal layer is absorbed to excite a surface plasmon. [12]

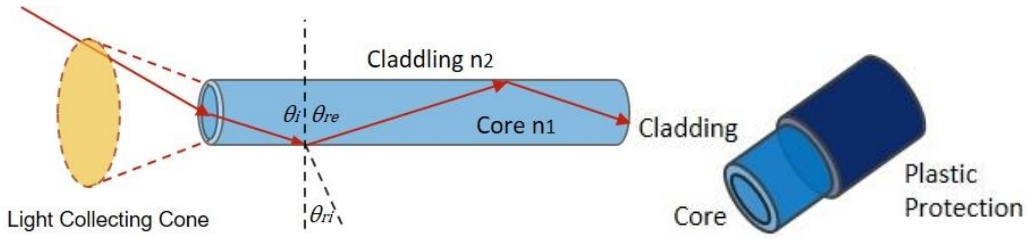

Figure 5: a) Sketch of the total reflecting phenomenon inside the POF. b) Structure of the POF.

By employing a white light in condition of total reflection for all the reflection modes present inside the waveguide, there is a high probability that at least one can generate an evanescent wave which is able to match the condition of the surface plasmon excitation of the metal plasmon, i.e. the surface plasmon resonance (SPR) takes place. This SPR excitation provokes a strong absorption of light; as a result of the transfer of energy an attenuated reflection (ATR) is detected as a sharp dip of the output signal at the specific wavelength known as resonance wavelength, or at a particular incidence angle θ called angle of resonance [110-111].

The resonance condition are defined according to the following expression [10]:

$$K_0 n_c \sin\vartheta = K_0 \left(\frac{\varepsilon_{mr} n_s^2}{\varepsilon_{mr}+n_s^2}\right)^{1/2} ; \; K_0 = \frac{2\pi}{\lambda} \qquad \textit{Eq. 2}$$

The term on the left is the propagation constant (K_{inc}) of the evanescent wave generated by the total attenuated reflection (ATR) of the incident light with angle θ by means of a light coupling system (prism or optical fiber) with refractive index n_c. The term on the right is the propagation constant (K_{SP}) of the surface plasmonic wave (SPW); ε_{mr} indicates the real part of the metal-dielectric constant (ε_m) and " n_s" is the refractive index of the dielectric (the sensing medium). This matching condition of propagation constants is heavily sensitive to even a slight change in the outer refractive index, which makes this technique a powerful tool for sensing.

The confinement of the SPR phenomenon at the nanoscale onto a nanoparticle conductive surface (Figure 6), which is called localized SPR (L-SPR), leads to an enhancement of the optical phenomena. LSPR is a well-studied nanoscale phenomenon similar to SPR [113].

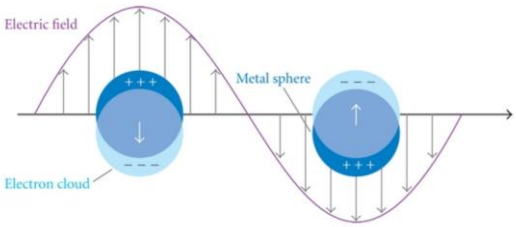

Figure 6: Sketch of the LSPR in a metallic nanostructure [114]

This enhanced field amplitude reflects over the related properties such as magneto-optical properties with an improvement. The SPR decays rapidly away from the nanoparticle/dielectric interface into the dielectric background. So LSPR is a spatial resolution technique with a very high sensitivity (subwavelength), which is modulated only by the size of nanoparticles [13]. Some experiments have also shown that the sensitivity of SPR is higher than that of LSPR, while LSPR has better linearity [115-118]. A brief comparison of SPR and LSPR made by Mayer at all. [119] report that LSPR has a bulk dielectric sensitivity of 10^2 (nm/RIU) and SPR of 10^6; while, the sensing distance is of 10nm and 1000nm respectively.The metal nanoparticles exhibit a strong absorption band in the UV-Vis region, which is not present in the bulk metal layer. Particle optical excitation has a maximum value at the plasmon resonance frequency, which occurs at visible wavelengths for noble metal nanoparticles. Typically sensing for NPs in solution or immobilized on a transparent surface is performed using a p-polarized electromagnetic wave obtained with a UV-vis instrument, but in MIP-POF devices a polychromatic light, non polarized [12; 10; 120] can be used to excite SPW. This makes it possible to employ simple and portable devices at low cost. Excellent reviews on LSPR sensing can be found in the literature [113; 119], so this approach is very promising for future developments. Moreover, LSPR is not affected by variation of the temperature as it happen for SPR.

1.4.2 SPR FOR SENSING

As based on a label-free transduction technique, plasmonic sensors can represent an efficient, low-cost, stable and reusable detection method for different analytes, with possible applications in food, environmental, clinical and biological field, as well as in industrial process controls. Despite the fact that sensing techniques based on SPR have been extensively studied, the exploration of new methods that overcome existing drawbacks and improve the sensing performance is consistently pursued [121]. In particular, the SPR methods based on MIPs appear to be of great help in increasing the actual applicability of sensors outside the lab in real life situations. This could be further improved by the implementation of optical fibers in SPR transduction methods, in particular, plastic optical fibers (POF).

SPR transduction is based on the determination of the variation of the refractive index of the dielectric layer containing the receptor in immediate contact with the metal film, as schematically reported in Figure 7.

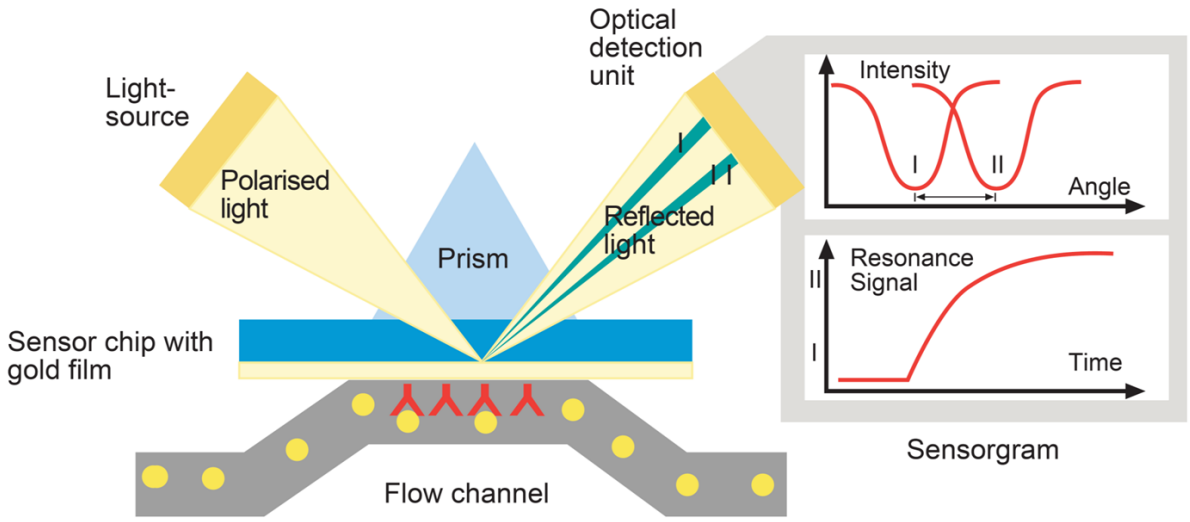

Figure 7 Kretschmann geometry on an SPR sensor *[122]*. Signal obtained from the angular spectrum and sensorgram.

When the refractive index of the interface interposed between the metal film and the dielectric is changed, it causes a change in the propagation constant of the surface plasmon wave. This, in turn, modifies the conditions of coupling between the light waves and the surface itself.

Therefore, the angle of incidence of light for which the excitation of the surface plasmon and/or the wavelength at which excitation takes place changes. [120]

Many of the SPR sensors on the market today are based on prism coupling devices [121]. These devices have an Otto or Kretschmann configuration [122], in which a metal film is deposited directly on a prism face (Figure 7). The sensors based on this type of instrumentation have been commercialized firstly by Biacore and presently by many other firms too. The data obtained by these devices are recorded in real time obtaining a graph called a sensorgram, which represents the variation of the resonance angle (Δθ) as a function of time. Δθ is a function of the variation of the refractive index of the receptor layer, in close contact with the gold layer, and therefore of the amount of substrate that binds, depending in turn on the concentration present in the sample.

Alternatively the variation of the excitation wavelength can is determined. In that case, the surface plasmons are excited by a polychromatic light (thus containing several wavelengths) maintaining the angle of incidence constant. The wavelength that generates the strongest coupling is measured, i.e. the resonance wavelength. Figure 8 shows a possible measurement output with this particular sensor configuration.

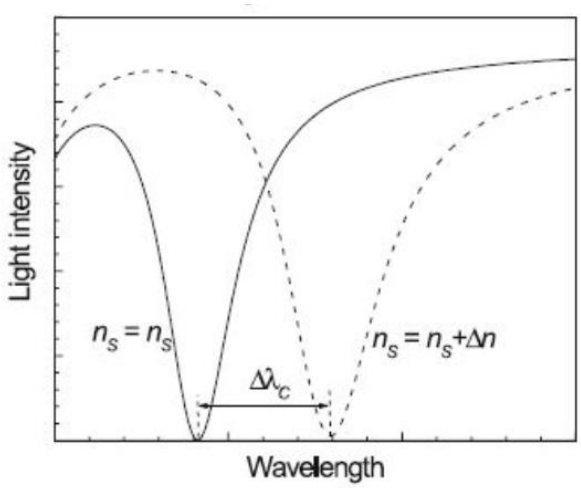

Figure 8. Shift of the resonance wavelength by variation of the refractive index [120]

The analytical signal is obtained from the transmission spectrum and consist in the shift in the resonance wavelength which can be directly related to the variation of the refractive index due to the change of the analyte concentration. Despite the selectivity and sensibility of these techniques,

they are not widely used for sensing, because of the difficulties in the miniaturization, the high cost of the devices and the needed to keep precisely focused the optical prism. The apparatus required is very bulky and expensive, so hardly suitable for out-of-the-lab determinations. To overcome such difficulties Jorgenson et al. have realized SPR sensors in optical fibers, without prism [123], in which the metal layer was directly deposited on the core of the optical fiber. These SPR sensors on optical fiber present a noticeable instrumental simplicity where no adaptive optics or thermal control are needed. They make it possible to reduce the dimensions and lower the price of the sensor system with respect to the most common commercial instrumentation based on the Kretschmann configuration (e.g. Biacore).

Glass optical fibers were initially employed [6; 112; 123-125], but more recently plastic or special optical fibers have been exploited too [18].

SPR sensors based on optical fibers showed noticeably high sensitivity, being able to detect very small variations of the refractive index of the medium (dielectric) in contact with the metal layer, where biological or artificial receptors are present [18]. They selectively recognize the analyte present in the liquid under test, if it is able to produce a local variation of the dielectric's refractive index in the receptor layer in contact with the metal film.

It is worth pointing out that preliminary results [10; 18-19] showed the feasibility of these new sensing methods, but there is still a long way to go before these can be translated into practical sensing devices, thus stimulating further research in the field of plasmonic sensors.

Another aspect to be considered is that the use of an optical fiber, differently from the devices based on the prism configuration, makes the remote sensing straightforward, so as the possibility of integration of SPR sensing platform with optoelectronic devices, eventually leading to “Lab-on-a-chip” [10; 18-19].

SPR sensors based on MIP receptor have been successfully proposed for detection of target analytes in complex and real matrices in several fields, such as, for example, in industrial monitoring for determining low levels of 2-furaldehyde (2-FAL) in power transformer oil [19], in clinical-chemical analysis for the determination of amikacin and cholesterol in human plasma [126], endotoxins monitoring [127], detection of human Hepcidin-25 [128], testosterone and dopamine in aqueous media [129-131], chloramphenicol [132], in environmental analysis like organic

micropollutants with swellable molecularly imprinted poly N-(N-propyl)acrylamide particles [133] or for dangerous species like 2,4,6-trinitrotoluene (TNT) [57].

Recently, SPR sensors based on optical fibers, in particular on POFs, with MIP receptor, have been successfully proposed for detection of target analytes in complex and real matrices, as for example, in industrial monitoring for determining low levels of furfural (2-furaldehyde) and dibenzyl disulfide (DBDS) in power transformer oil [14; 19; 134] or to determine dangerous and toxic species like TNT [10] or L-nicotine [135] in aqueous solutions. In these examples, the sensor was prepared by depositing a layer of gold on the optical fiber without cladding and a layer of MIP on the gold surface. The part of POF without cladding had a typical D-shaped profile, obtained by erasing. The measurement instrumentation used for this type of sensor consists of a halogen lamp and a spectrophotometer, interfaced with a computer via USB output. New optical devices based on SPR on POFs, realized and characterized during this work, are discussed in the following paragraphs.

Since in SPR the binding event shall occur within a depth of 200 nm from the metal surface, this should be the maximum depth of the receptor layer [121]. Many different methods for "in-situ polymerization" have been proposed, among them spin-coating, electropolymerization, micro/nano-beads linked to MIP and other approaches based on the use of nanotechnologies [70]. Among the different strategies for processing MIP to obtain a useful receptor layer, those in which the polymerization is performed "in-situ" (i.e. over the electrode), forming a thin polymeric layer, are particularly interesting since they are convenient and have the advantage of the short distance of the interaction sites and the electrode surface.

1.4.3 EVANESCENT WAVE COUPLING (EWC) FOR SENSING

In SPR transduction the principle of sensing is based on the optical phenomenon of the attenuation of the reflected light inside a waveguide due to the surface plasmon excitation by the evanescent wave. Yet, other attenuation mechanisms can occur, which can also be exploited for sensing. For example, an interesting approach was proposed by Sequeira [136]. Here the variation of the light intensity is due to the evanescent wave coupling which occurs under the condition of total reflection inside a waveguide with a segmented structure, where the segmentation consists of segments with different refractive index. As exposed by J. van Lith et al [137], the RI variation can be achieved by intercalation of a dielectric sensing material (e.g. a MIP selective receptor) so that the variation of the output light intensity depends on the optical properties of the sensing segment. At the interface of each fragment of the waveguide, the intensity of light is transferred in part to the output guided modes and in part to radiation modes which give rise to the evanescent wave, able to penetrate into the dielectric for a depth of 100-600nm. In the structured segments, the evanescent wave scans the sensing length of the segment, after interaction with an analytical solution which results in a change of RI. So, the output light will be modulated differently from the input light. The mismatch between the light inserted and the output will be due to the variation of the optical properties, i.e. the RI, of the sensing material intercalated. In the case of MIP, this is directly related to the concentration of the analyte interacting with the MIP sites.

This sensing principle presented by J. van Lith et al [137] is schematically reported in Figure 9. The instrumentation required is similar to that of SPR sensing method [18].

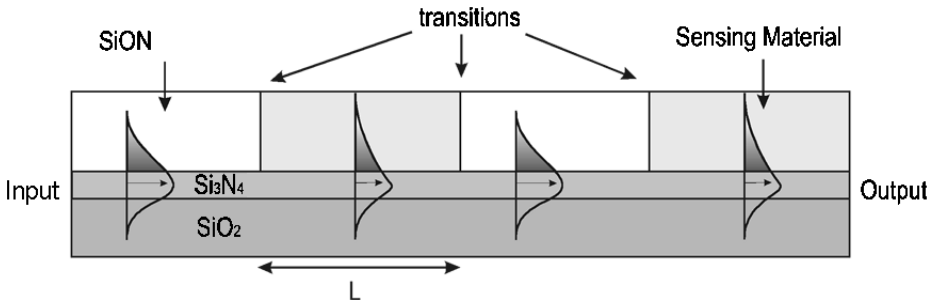

Figure 9: Principle of sensing in a segmented waveguide sensor [137].

The optical waveguide consists of two or more different types of waveguide segments [137-140]. Typically, segmented waveguide sensors (SWS) are based on segmentation of the cladding and the sensing principle is based on the refractive index changes (real and/or imaginary part) of the cladding material. Segmentation of both core and cladding has been proposed too [137-140]. In these approaches both core dimension and cladding refractive index change in the sensing region. SWS has been used both for refractive index and chemical sensing [137-140].

1.4.4 SPR OPTICAL PLATFORM BASED ON POFS

The plastic optical fibers (POFs), for example, those made of poly-(methyl-methacrylate) (PMMA), present indisputable advantages over silica or glass fibers such as exceptional flexibility, simple manipulation, large numerical aperture, big diameter. Also, they are able to withstand smaller bend radii than glass fibers. Therefore, POFs are particularly suitable for the realization of low-cost and miniaturized sensors for application to remote controls [6; 18; 141-145].

Thus, this work was focused on the development of POF/POW-MIP platforms as innovative and powerful optical chemosensors which could combine the interesting characteristic of POFs with the optimal selectivity of the MIP (molecular imprinted polymer) and the high sensibility of the surface plasmon resonance (SPR) or evanescent wave light coupling (EWC) techniques. While many experimental configurations have been proposed to realize this type of sensors [6; 13; 19; 121; 135-136], nevertheless this research was mainly focused on those reported below, which present good characteristics of easy and rapid preparation, reproducibility, re-usability, low price and low detection limit, or detection limits suitable for the required analysis.

The optical fibers sensors (OFSs) based on POFs can be classified in two main types: intrinsic and extrinsic, depending on whether the fiber is interacting with an analyzed medium or if it is used only as a waveguide that allows the propagation of the light to the sensing region, respectively [136].

1.4.4.1 Instrinsic SPR sensors on D-Shaped POF

Surface plasmon resonance (SPR) sensors based on D-shaped POF have been successfully developed for different analytes and different receptors such as antibodies, aptamers and molecularly imprinted polymers (MIP) [10; 134; 146-147] by our research group. It has been shown that the flat part of the D-shaped platform is suitable for an easy deposition of the receptors, in particular, MIPs. Thin, robust and re-usable MIP layers are easily formed over the flat gold film by in-situ polymerization [10; 134]. However, the platforms were obtained by a hand polishing procedure, which could be scarcely reproducible. The performances of the SPR D-shaped POF platform are influenced by the morphology of the D-shaped region (roughness and total depth) [148]. Also, the type and the thickness of the metal layer used in the sensors affect the performance of the platforms [14; 16; 149-150].

1.4.4.1.1 D-shaped POF sensors preparation

The optical fiber used had the following characteristics: a core consisting of polymethylacrylate (PMMA) with a diameter of 980 µm and a fluorinated plastic cladding with 20 µm of thickness and refractive indices respectively of 1.49 and 1.41.

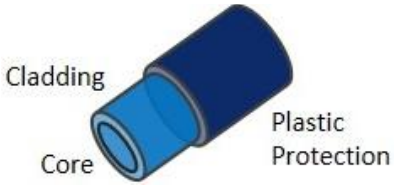

Figure 10. Composition of the POF.

A portion of the optical fiber has been fixed with glue in a groove (width 1000 µm and depth 20 µm), purposely trenched in a resin block. Subsequently, the fiber was polished to remove the cladding and expose the fiber core. Appropriate 5 µm abrasive sheets were used to perform this operation. The part of the fiber protruding from the block was abrased with a gentle "8"-shaped movement. This movement was repeated 20 times. The described operations were then repeated

with 2 µm abrasive paper. All these operations were highly facilitated by the embedding of the POF in the resin holding support.

In Figure 11 the configuration of the platform after the polishing process is shown.

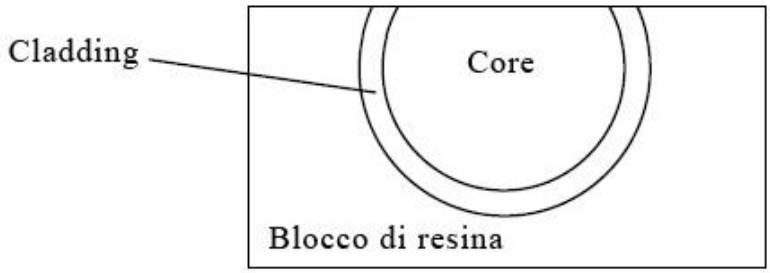

Figure 11. Platform after polishing with the exposed core. The characteristic D-shaped transversal profile is evident.

A photoresist layer is deposited by dropping and spinning by a spin coater in order to obtain a homogeneous layer. The spinning has been performed at 6000 rpm. At the end of the process, the film thickness is about 1.5 µm. Photoresist Microposit S1813 was used as the photoresist (RI= 1.61) [1].

In the last phase, a gold film is formed by sputtering over the photoresist surface by Bal-Tec SCD 500. At the end of the process, 30 or 60 nm of gold was deposited on the surface of the optical platform.

A cross-section view of the D-shaped platform after gold deposition is reported in Figure 12:

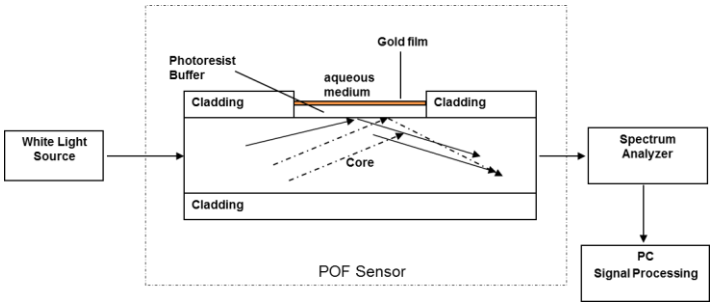

Figure 12: D-Shaped POF configuration.

After the characterization of the bare platform (see 2.2.7.), the platforms were covered with a MIP receptor imprinted for the analyte of interest with a procedure exposed in MIP layer deposition paragraph (see 2.4.4.). The D-shaped POF platforms have good LOD and sensibility, however, they suffer from some practical construction problems and irreproducibility mainly due to the manual preparation.

1.4.4.1.2 Multiplexing sensors based on SPR-MIP-POF D-shaped

A point of particular interest in sensing technology is the possibility of implementation of a multiplexing sensor, able to analyze simultaneously different substances [15]. Several approaches, based on parallel or serial connection have been previously proposed on the basis of theoretical and experimental investigation [15; 151]. The possibility to use surface plasmon resonance on plastic optical fiber with molecularly imprinted polymer (SPR-MIP-POF) sensors for multi-analyte detection has been discussed too [134; 1].

In this work, the possibility of developing a multi-analyte SPR chemical sensor based on MIP by employing multiple SPR D-shaped sensor in series on a unique waveguide, i.e. one POF, has been investigated [1]. In two similar optical sensors [134], with two specific MIP receptors, were considered, for the detection of two analytes of interest for the control of the transformer oil in power transformers, furfural (2-FAL) and dibenzyldisulfide (DBDS). It has been shown in that case that only an experimental set-up with the two sensors in parallel is possible since the surface plasmon resonances are at the same wavelength for the two sensors. This indicates that similar MIPs for two low molecular weight substances have the same refractive index. Here the idea to obtain a separate resonance of the sensors was to use metal layers with different thickness on each D-shaped POF sensor, which is known in the literature, [14; 16; 134; 150] to obtain different resonance wavelengths. A schematic view of the sensors is reported in Fig 13. A different MIP receptor imprinted for the specific analyte has been employed on each platform, which gives the chemical specificity. As a proof-of-principle, the monitoring of the concentration of the two interesting analytes mentioned above in the insulating oil of power transformers is presented, as previously done with the parallel configuration [134]. The prepolymer mixtures for two MIPs were prepared according to the classical procedure reported in [19; 152] and deposed separately over the two platforms.

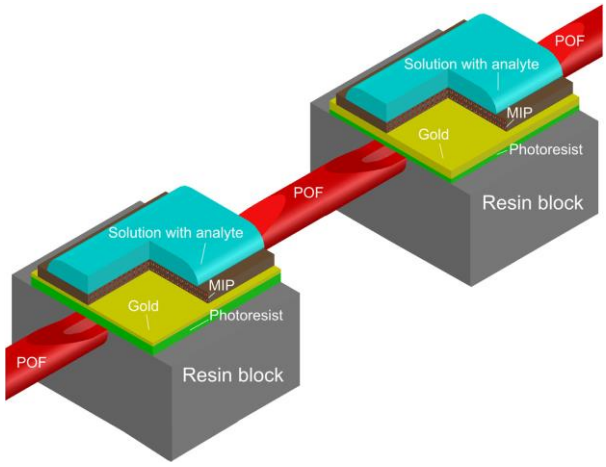

Figure 13: Optical chemical multichannel sensor system based on cascaded SPR-MIP sensors [1].

1.4.4.2 Extrinsic SPR PMMA Slab Optical platform

To overcome the irreproducibility of the D-shaped POF sensor, probably due to the handmade fabrication of the platform, other configurations were studied, in particular, the extrinsic ones, based on PMMA slab. Those sensors based on OFs, but in which OFs are not the waveguide for sensing, being instead employed for injecting the light and for driving it to the detector, are called "extrinsic" sensors. The extrinsic sensor here considered is based on the SPR concept as the D-shaped POF ones, but it was obtained by sputtering a gold layer on the waveguide constituted by a PMMA slab. This was obtained commercially, with a well-controlled rugosity allowing a better reproducibility of the gold layer.

The slab optical platform is schematically shown in Figure 14. It is composed of a removable bilayer chip (a PMMA chip with a gold film on the top), two plastic optical fibers and a holder purposely designed [2; 20]. The removable chip is a PMMA layer, with size 10 mm x 10 mm and 0.5 mm thickness, and a thin gold film deposited on PMMA by sputtering (60 nm thick). The liquid prepolymer mixture for MIP has been deposited by a spin coater over the gold layer. The holder was designed to host the PMMA-gold chip and two POFs, one as a collector and one which drives the source light. A cover equipped with a hole and an o-ring to retain the liquid samples for the analysis completes the holder.

Figure 14 shows a schematic view of the light path in the SPR-MIP sensor platform and the sensing area (MIP dielectric). The exciting light is introduced in the slab waveguide by reflection in a trench (size: 1mm x 1mm and 10mm long), realized directly in the holder. The source path, i.e. the trench, is illuminated by a POF connected to the source positioned at 90° with respect to the slab waveguide. This type of illumination has been made to ensure a full sensible length path illumination of the PMMA slab, in which multiple modes of the light could be driven inside the slab and ensure the SPR plasmon excitation. Actually, a large incident angle is required for the surface plasmon resonance excitation [2; 20]. The POF used has a core of PMMA and cladding of fluorinated polymer, with 1mm of the total diameter. As a collector of output light, another POF was used to carry the signal to a spectrometer.

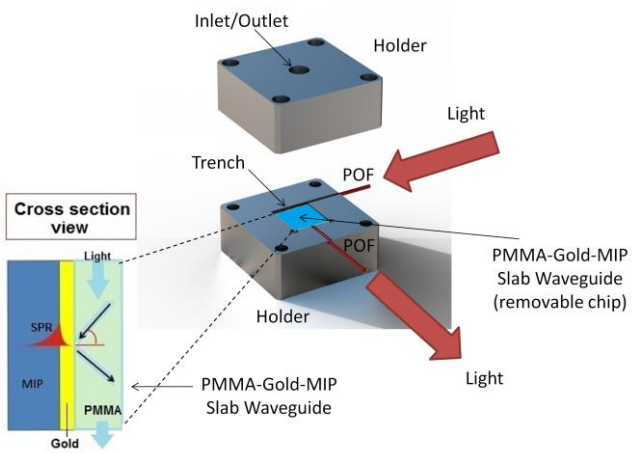

Figure 14 Schematic view of the light path in the SPR sensor with a MIP receptor on the gold film. Top and cross-section view of the sensor system [2]

1.4.4.3 Extrinsic Inkjet printed PET optical waveguide

Printing technique could help in producing electronic and optical devices where small dimension, quick developing times and reasonably priced features are required, compared to traditional silicon electronics [153]. The most relevant techniques for the realization of printed devices are Screen Printing and Inkjet Printing. Screen Printing consists of the deposition of a thick film of material on a substrate through masks and a roller pressure mechanism. Other materials, such as conductive, insulating and other functional layers, can be deposited on the substrate surface so that many different kinds of devices made by Screen Printing are available in [154-156]. The disadvantages of Screen Printing are linked to the use of masks and material waste. On the contrary, Inkjet Printing is a contactless technique allowing the true quick prototyping of electronic component, especially sensors. Some remarkable advantages of Inkjet technologies reside in straight printing, high dimensional resolution, and suitability for several substrates. Polymers like PEDOT-PSS (3, 4-ethylene dioxythiophene) and PANI (Polyaniline) and conductive silver nanoparticles are most widely used with Inkjet Printing technology [11; 157-158]. Examples of devices developed using low-cost Inkjet printers have been reported [159]. The aim was to obtain particular surface patterns by Inkjet printing which could enhance the sensibility of the platform.

In this investigation a novel extrinsic optical platform was developed, i.e. a PET slide waveguide with printed lines of silver nanoparticles and MIP receptor (acting as cladding) [3]. Figure 15 shows the scheme of the transmission extrinsic POF sensor based on a MIP receptor, where two POFs (core of PMMA and cladding of fluorinated polymer, with 500µm of total diameter) connect the optical waveguide sensing region of the PET layer covered with silver lines and MIP, with the light source and the spectrometer. This platform is still based on SPR, possibly enhanced by localized SPR phenomena due to the presence of silver nanoparticle. The MIP receptor has been produced by deposing the prepolymer solution over the printed slab. PET was used because of its flexibility which could make the development of flexible devices possible. The light propagated in the PET slab with printed AgNPs-MIP by total internal reflection (TIR), with the evanescent field interacting with the selective MIP sensing layer. The evanescent wave radiation penetrates into the MIP cladding layer (about 100nm) and decays exponentially with distance from the surface of the PET slab [141].

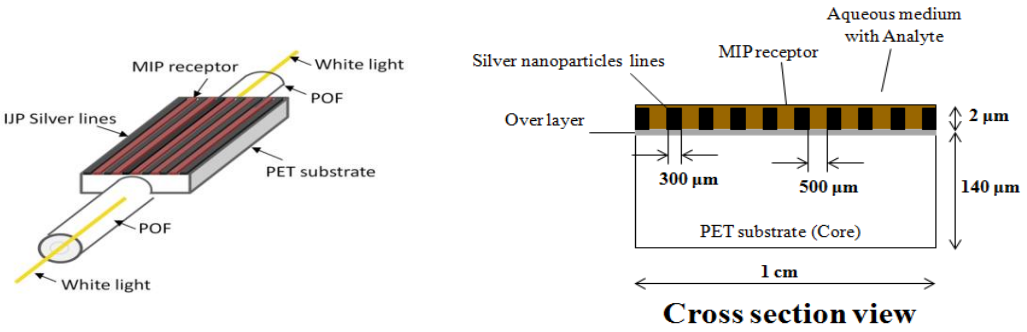

Figure 15. Design of the Extrinsic PET line Inkjet printed optical waveguides and cross-section view.

1.4.4.3.1 Fabrication of the optical sensing platform based on PETs

The printing process adopted to deposit the parallel lines of silver nanoparticles on a PET (polyethylene terephthalate) substrate uses a low cost WF-2010 piezo Inkjet printer (Epson, Suwa, Japan) and a metal ink for the creation of conductive patterns. The latter is a silver nanoparticles solution, "Metalon® JS-B15P" by Novacentrix (Austin, TX, USA). The PET slide adopted is the Novele™ IJ-220 Printed Electronics Substrate by Novacentrix, which is suited to low-cost and low-temperature applications and specially designed for Inkjet-compatible conductive inks. The dimensions of the PET slide are 1x5 cm and 140 µm of thickness. The parallel lines pattern is shown in Figure 13. The thickness of the silver nanoparticles lines on the PET substrate is about 2 µm, the length (L) is 5cm, the spacing (S) is 500 µm and the width (W) is 300 µm. On this pattern of silver nanoparticles, the MIP prepolymer mixture (200µL) has been dropped and spinned for 2 min at 1000 rpm. Thermal polymerization was then carried out for 16 h at 80 °C.

1.4.4.4 OPTICAL SEGMENTED WAVEGUIDE SENSORS (SWS)

In the present investigation, a sensor based on SW was developed [4], as schematically shown in Figure 17. It consists of two segmented waveguides sensors coupled to each other by the trench drilled in between and filled with MIP, which constitutes the segmentation of both cores. This sensor is based on the "attenuation of total reflection" (ATR) [6; 121; 136] by the coupling of the evanescent wave between the two fibers and the MIP layer segmentation [137]. The input power is driven by the POF_1 (Fig.16), in the sensing region of MIP which is able to recognize and capture the analyte present in the matrix solution. This produces an increase in the refractive index of the "cladding" (i.e. MIP), which enhances the modal mismatch and causes an optical power attenuation along POF1. The light which gets out of the POF_1 as radiative power (proportional to the "attenuation of the total reflection" of light in the POF_1), is recaptured into the guided mode of POF_2 after the interaction with the dielectric sensing layer. So, monitoring the output power of POF_1 and POF_2, the concentration of the analyte can be measured.

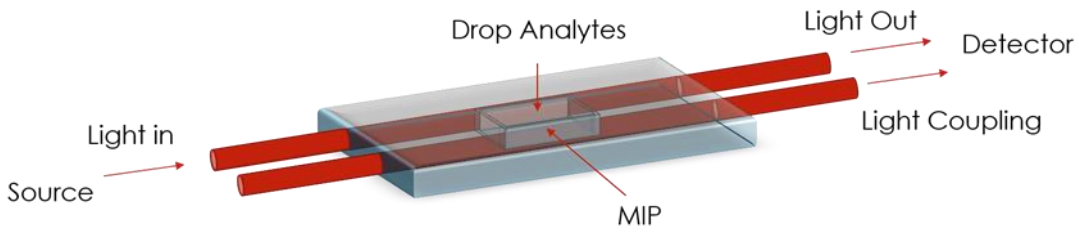

Figure 16: schematic view of the SWS platform

1.4.4.4.1 Fabrication of the sensor platform

The SW optical sensor platform can be built up in a few simple steps: in the first one, two POFs without jacket are embedded in a resin block, parallel and in tight contact; in the second one, a trench was fabricated between the two fibers by a computer numerical control (CNC) micro-milling machine using 1mm diameter end-mill. The two plastic optical fibers are made of a PMMA core of 980 µm and a fluorinated polymer cladding of 20µm, without the jacket, embedded in a resin block. The refractive index, in the visible range of interest, is about 1.49 for PMMA and 1.41 for the fluorinated polymer. The trench was about 6mm long, 1mm wide and 600µm deep (volume: 3.6 µl). A digital camera has been used to align the tip of the milling tool to the sample in

order to engrave the trench parallel to the fibers axis and equally wide across the fibers. The engraving parameters were optimized to reduce the surface roughness of the trench walls. The fabricated trench results in a sensing region of about 6 mm in length (see Fig.14). Finally, the prepolymer MIP solution was deposited in the trench by drop coating, and the polymerization was carried out as usual [10; 19; 135]. The same MIP used for other sensing platforms developed in this investigation was applied here too [134]. Thus its refractive index is about 1.42 in the visible range of interest.

It is particularly relevant that using this sensing method the normalization is particularly straightforward, and does not require any independent measurement. This point and the simple and cheap fabrication avoiding any irreproducibility due to the Au layer fabrication, make this platform really interesting for further investigation.

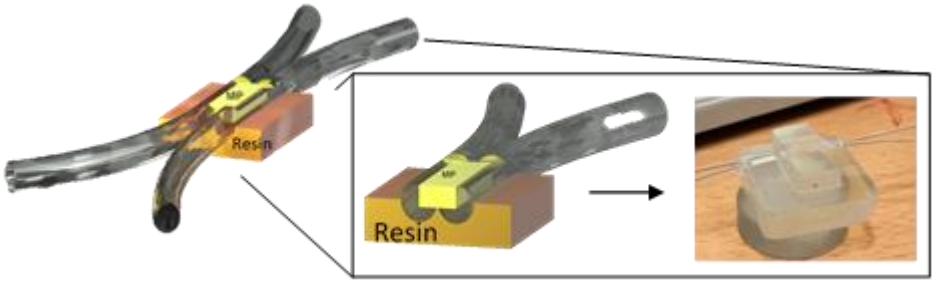

Figure 17. Optical chemical sensor based on two POFs coupled with a trench filled with a MIP receptor.

2 EXPERIMENTAL PROCEDURES

2.1 MATERIAL S AND SOLUTIONS

2.1.1 REAGENTS

The following reagents were used:

- Acetonitrile VWR Prolabo Chemicals®,
- Ethanol 96% vol VWR Prolabo Chemicals®,
- Dibenzyl disulfide 99% (DBDS) Sigma-Aldrich®,
- Diphenyl disulfide 99% (DPDS) Sigma-Aldrich®,
- Dibenzyl sulfide 99% (DBS) Alfa Aesar®,
- Methacrylic acid (MAA) 99% Sigma-Aldrich®,
- Divinyl benzene 80% (DVB) isomeric mixture Sigma-Aldrich®,
- Tetrabutylammonium perchlorate ($TBAClO_4$) Sigma-Aldrich®,
- Tridistilled H_2O,
- 2-Furaldehyde (2-FAL) 98% Alfa Aesar®,
- Furfuryl alcohol (FA) 98% Sigma-Aldrich®,
- 5-Hydroxymethyl-2-furaldehyde (HMF) 99% Sigma-Aldrich®,
- Ammonium perchlorate (NH4Cl) Sigma-Aldrich®,
- Ethylene glycol dimethacrylate (EGDMA) 98% Sigma-Aldrich®,
- Glycerine 88% Sigma-Aldrich®,
- D (-) - fructose 99% Sigma-Aldrich®,
- D(+) - Glucose monohydrate Polichimica s.r.l and Sigma-Aldrich®,
- L (+) - tartaric acid 99% Sigma-Aldrich®,
- (S)-(-)-Nicotine 98% Sigma-Aldrich®,
- Enzyme: horseradish peroxidase (HRP) with activity 2500 U/mL and glucose oxidase (GOD) with activity 5000 U/mL were purchased from Sigma Aldrich. Both the solutions were stored in a refrigerator.

- Dye for enzymatic assay: the chemicals 4-amino-antipyrine (A), 3,5-dichloro-2- hydroxy-benzenesulfonic acid (sodium salt, 99%) (B) were purchased from Sigma Aldrich.

All other reagents used were provided by Sigma-Aldrich® and were of analytical grade.

2.1.2 SOLUTIONS AND SAMPLES

- Mineral oil Nytro-Libra Trench,
- Synthetic wine: Batches of 250mL of synthetic wine are prepared as follows: 6.25g of fructose, 6.25g of glucose are dissolved in water, 1mL of glycerol and 1.25g of tartaric acid are added to the solution. Finally, 45mL of EtOH (18% v / v) is added, it is brought to volume with tri-distilled water and the pH adjusted to 3.3 with NaOH.
- Fibroin protein employed was extracted from the Native silk recovered from *B. mori* cocoons as exposed in the nature protocol [5]. Raw silk cocoons were purchased from SilkLab at TUFTS University in Boston (US).

2.2 ANALYTICAL INSTRUMENTATIONS AND PROCEDURES

2.2.1 EXPERIMENTAL SETUP FOR ELECTROCHEMICAL ANALYSIS

The electrochemical measurements were carried out using a PALMSENS analyzer controlled by the PalmSensPC PC software version 2.33 (2008), with the glass measuring cells of 25 mL volume.

The working electrode used was a glassy-carbon (BASI) of 3.0 mm diameter, platinum wire as counter-electrode and reference pseudo-electrode and Ag / AgCl / NaCl saturated (BASI) as reference electrode (E = 0.197 vs NHE)

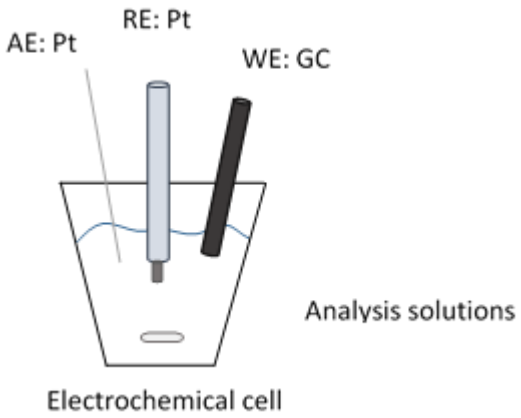

Figure 18. Schcematic view of the electrochemical measuring cell

In this work, three voltammetric analysis techniques have been employed: cyclic voltammetry (CV), differential pulse voltammetry (DPV) and squarewaves voltammetry (SWV). The conditions used are listed below:

Oxidation of DBDS:

CV:

E_vtx1	0 V
E_vtx2	2 V
E_step	0.01 V

E_start	0 V
E_cond	0 V
E_dep	0 V

Scanrate	0.1 V/s

N_scans	5
t_cond	0 s
t_dep	0 s
t_equi	2 s

DPV:

E_begin	1 V
E_end	2 V
E_step	0.01 V
E_pulse	0.025 V

E_cond	0 V
E_dep	0 V

scanrate	0.1 V/s
t_pulse	0.05 s

t_cond	0 s
t_dep	0 s
t_equi	2 s

Reduction of 2-FAL:

CV:

E_vtx1	0 V
E_vtx2	-2 V
E_step	0.01 V

E_start	0 V
E_cond	0 V
E_dep	0 V

scanrate	0.1 V/s

N_scans	5
t_cond	0 s
t_dep	0 s
t_equi	2 s

SWV:

E_begin	0 V
E_end	-2 V
E_step	0.01 V
E_pulse	0.025 V

E_cond	0 V
E_dep	0 V

Freq	25Hz

t_cond	0 s
t_dep	0 s
t_equi	2 s

2.2.2 ELECTROCHEMICAL PROCEDURE

The analyzes have been carried out by the electrochemical cell (described above 2.2.1.) as it follows: the solution to be analyzed, diluted if the case, is inserted into the measuring cell (usually 2 mL, always maintaining the volume ratio of solvent used in the analysis. Subsequently, the supporting electrolyte was added. The solvent for the analysis consists of AcN:EtOH=4:1 solution with $TBAClO_4$ 0.025 M as supporting electrolyte for one of the considered analytes, DBDS, which is poorly soluble in water. For 2-FAL, an analyte highly water-soluble, two different solutions have been considered, i.e H_2O:EtOH=75:25 with $NaClO_4$ 0.015M as supporting electrolyte and synthetic wine (prepared as described above 2.1.2.). Most often, the standard addition method was used for quantification. Between the measurements, the electrodes, the glass container, and the magnetic stirrer were washed with tap water, distilled water and conditioned with the solvent solution.

- DPV Standardization curves of DBDS

The standardization curve of the DBDS has been obtained by DPV analysis with the standard addition method. The standard additions have been performed of 20µL each in 2ml solution (5.3, 10.6 and 15.7 mg/L) with a DBDS standard solution at 540 mg/L in EtOH. Typical voltammograms obtained at different concentrations are shown in Figure 19.

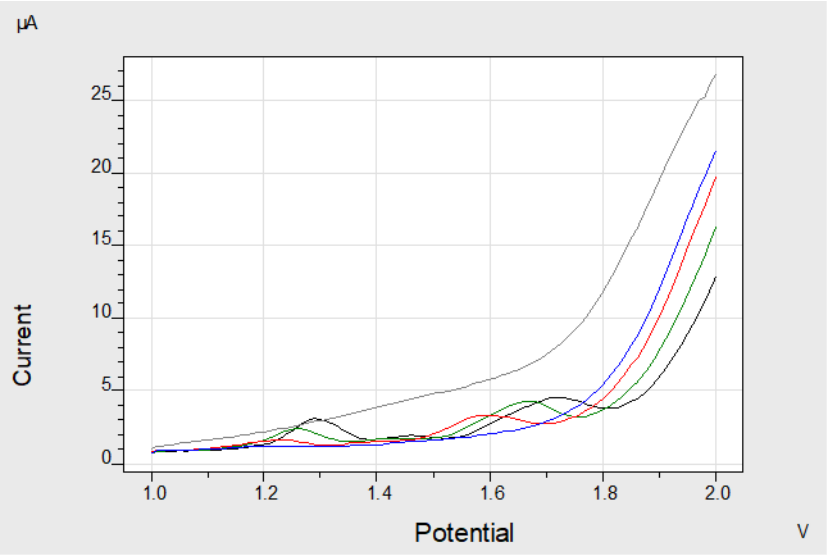

Figure 19. *DPV voltammogram of DBDS in AcN:EtOH=4:1, at different concentrations of DBDS. Potential (V) against current (µA).*

Two oxidation peaks are formed, with Ep increasing in the subsequent measurements. The peak height at 1.2-1.3 V increases linearly as the concentration of DBDS increases and is therefore considered as an analytical parameter for the quantitative determination of the DBDS.

The linear regressions parameters obtained from the standard additions method of DBDS, at the selected potential, are shown below in Table 1.

Table 1. *Linear regression parameters obtained by the standard additions method of DBDS; the slope and the ordinate origin are reported with the respective errors.*

Slope	Dev.st Slope	Ordinate Origin	Dev.st OO	r^2	sY/x
0,1	0,005	-0,17	0,06	0.999	0.024

The ordinate at the origin is negative and the phenomenon is still not clear. However numerous control standardizations have been carried out in standard AcN:EtOH=4:1 solution. The average obtained for the slopes and the ordinate origin is respectively 0.12 (3) and -0.1 (1), i.e. ordinate at the origin not significantly different from 0.

Since a strong irreproducibility has been observed during the electrochemical analysis, the solvent solution has been studied for the analysis with respect to the height of the peak signal obtained. It has been observed that the determinations carried out in acetonitrile solutions containing 20% by volume of ethanol, led to more reproducible and more sensitive signals than those in which pure acetonitrile, so the ratio 4:1 of AcN:EtOH has been employed. The concentration of $TBAClO_4$ employed has been studied by reporting different additions of $TBAClO_4$ in the standardization curves of DBDS. Based on the results, all the measurements were performed in $TBAClO_4$ 0.025 M since a linear response is obtained at higher concentrations than in different conditions.

- DPV standardization curves of substances with a structure similar to DBDS (interfering)

The electrochemical behavior of the interfering substances has been analyzed too.

The interferents considered are diphenyl disulfide (DPDS) and dibenzyl sulfide (DBS), given their molecular structural analogy with the DBDS.

The standardization curves have been obtained for both the substances by DPV in 2mL of AcN:EtOH=4:1 solvent with $TBAClO_4$ 0.025 M. The standard addition have been performed for DPDS with a standard at 610 mg/L (6, 11.9 and 17.8 mg/L), and for DBS with a standard at 515 mg/L (5, 10 and 15mg/L). The voltammograms are shown in Figure 20.

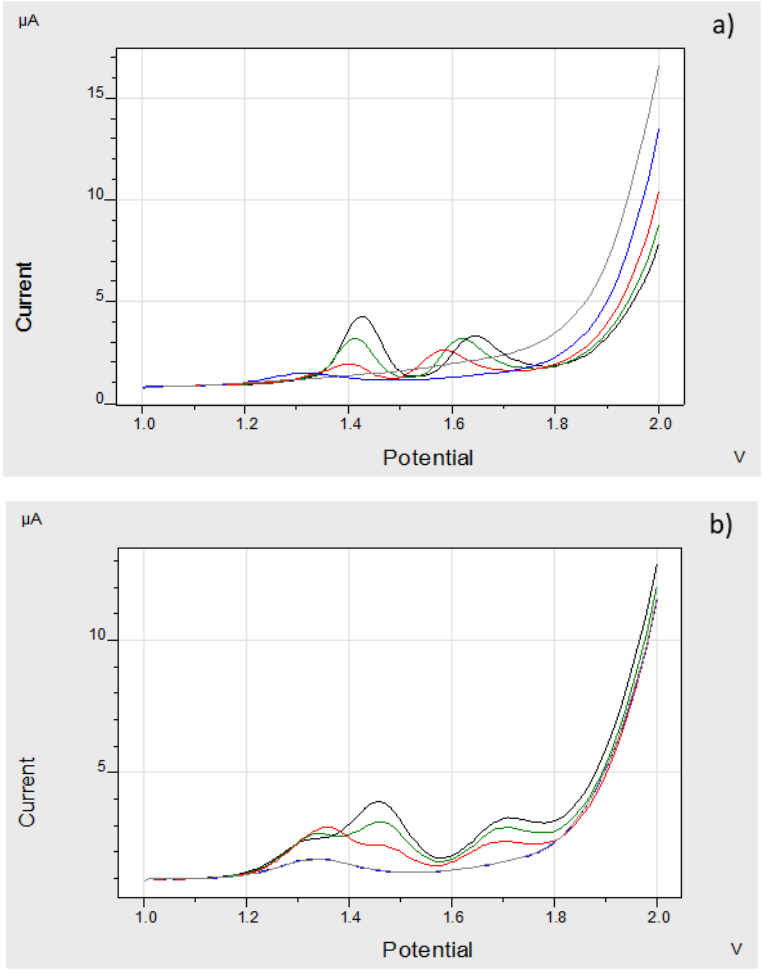

Figure 20. *DPV voltammograms of a) DPDS and b) DBS in AcN:EtOH=4:1, at different concentrations (standard addition method); potential (V) against current (μA).*

The related linear regressions parameters obtained from the standard additions method respectively of DPDS and DBS, at the selected potential, are shown below in Table 2 and Table 3.

Table 2. *Linear regression parameters obtained by the standard additions method of DPDS; the slope and the ordinate origin are reported with the respective errors.*

Slope	Dev.st Slope	Ordinate Origin	Dev.st OO	r^2	sY/x
0,195	0,01	-0,4	0,1	0,997	0.088

Table 3. *Linear regression parameters obtained by the standard additions method of DBS; the slope and the ordinate origin are reported with the respective errors.*

Slope	Dev.st Slope	Ordinate Origin	Dev.st OO	r^2	sY/x
0,152	0,008	0,08	0,09	0,997	0.057

The oxidation potential of the DPDS is between 1.4-1.43 V and that for the DBS is about 1.5 V. The voltammograms of the DPDS are close to those of the DBDS, as expected because of their similar molecular structure. It is noteworthy that even in the case of the DPDS the ordinate origin is significantly negative, as already observed in some standardizations of the DBDS.

- SWV Standardization curves of 2-FAL in H_2O:EtOH=75:25

The standardization curve of the 2-FAL has been performed by SWV with the standard addition method in 2mL of H_2O:EtOH=75:25 solution with $NaClO_4$ 0.01 M as supporting electrolyte. The standard additions have been performed at 5, 10 and 20 mg/L 2-FAL, from a 2-FAL standard solution at 580 mg/L in H_2O. Figure 21 shows a typical voltammogram obtained.

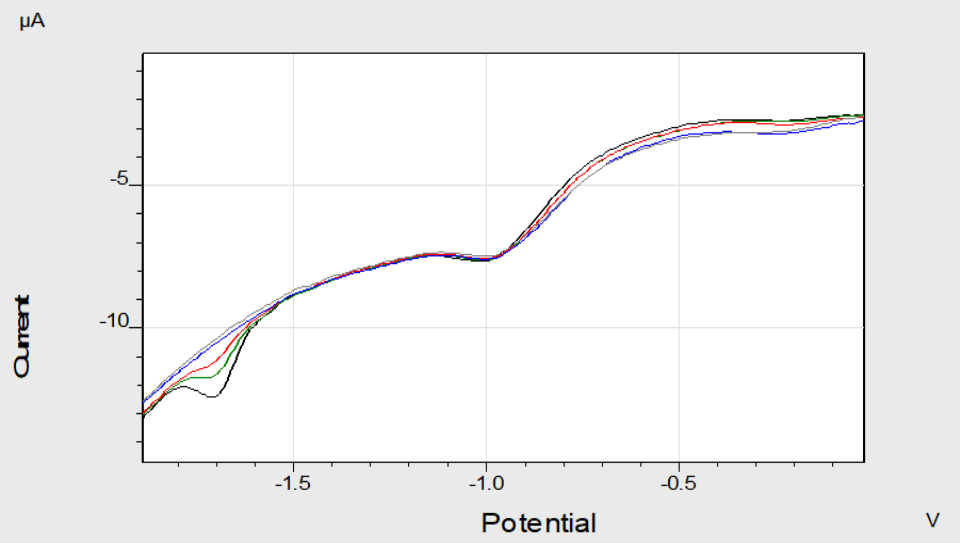

***Figure 21**. SWV voltammogram of 2-FAL in H_2O:EtOH=75:25, at different concentrations of 2-FAL. Potential (V) against the current (µA).*

The peak at -1 V is not due to the reduction of 2-FAL, since it is independent of the concentration, and therefore is attributed to impurities, probably present in the supporting electrolyte or on the surface of the GC.

A reduction peak is formed, with Ep at about -1.7V whose height increases linearly as the concentration of 2-FAL increases and is therefore considered as the analytical parameter for the quantitative determination of 2-FAL.

The linear regression parameters obtained from the standard additions method of 2-FAL, at the selected potential, are shown below in Table 4.

Table 4. Linear regression parameters obtained by the standard additions method of 2-FAL in H_2O:EtOH=75:25; the slope and the ordinate origin are reported with the respective errors.

Slope	Dev.st Slope	Ordinate Origin	Dev.st OO	r^2	sY/x
0,05	0,02	-0,04	0,26	0.968	0.144

The ordinate at the origin is negative but not significantly different from zero.

For comparison purposes, numerous control standardizations have been carried out in standard solutions H_2O:EtOH=75:25. The average slope value obtained is 0.05 (1). A certain irreproducibility has been observed probably due to a poisoning of the working electrode surface (GC) or because of the degradation of the 2-FAL standard which occur quikly in water solution [160]. The average obtained for the ordinates at the origin is 0.01(1). It is seen that the average of the ordinates at the origin is not significantly different from zero, although some values differ considerably due to uncontrollable experimental errors.

- SWV Standardization curves of 2-FAL in synthetic wine

The standardization curve of the 2-FAL has been performed by SWV with the standard addition method in 2mL of synthetic wine solution. The standard additions have been performed from 5 to 55 mg/L from a 2-FAL standard solution at 580 mg/L in H_2O. Figure 22 shows the voltammograms obtained.

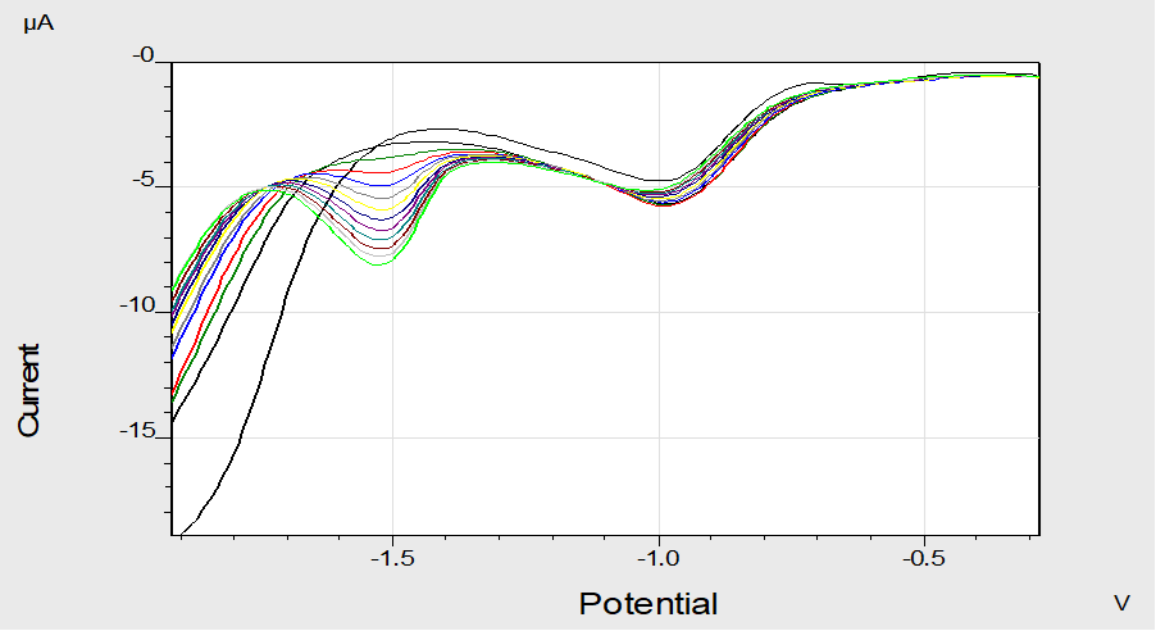

Figure 22. SWV voltammogram of 2-FAL in synthetic wine, at different concentrations of 2-FAL. Potential (V) against the current (µA).

The peak at -1 V is not due to the reduction of 2-FAL, since it is independent of the concentration, and therefore is attributed to the presence of impurities, probably present in the supporting electrolyte or on the surface of the GC.

A reduction peak is formed, at Ep of about -1.52V, the height of which increases linearly as the concentration of 2-FAL increases; therefore it was considered as an analytical parameter for the quantitative determination of 2-FAL.

The linear regression parameters obtained from the standard additions method of 2-FAL in synthetic wine, at the selected potential, are shown below in Table 5.

Table 5. *Linear regression parameters obtained by the standard additions method of 2-FAL in synthetic wine; the slope and the ordinate origin are reported with the respective errors.*

Slope	Dev.st Slope	Ordinate Origin	Dev.st OO	r^2	sY/x
0,071	0,001	-0,35	0,03	0.998	0.047

A certain irreproducibility has been observed even in the analysis performed in synthetic wine, however it is reduced respect to the water solution. It seems that the phenomenon of the 2-FAL degradation is slower in synthetic wine than in water solution as if the solution (pH , ethanol, ecc) or the components of synthetic wine can somehow stabilize this compound.

- SWV Standardization curves of substances with a structure similar to 2-FAL (interfering substances)

The interfering substances considered were the 5-hydroxymethyl-2-furaldehyde (HMF) and Furfuryl alcohol for their molecular structural analogy with 2-FAL.

The standardization curve of HMF has been obtained by electrochemical analysis with the standard addition method in 2 mL of H_2O:EtOH=75:25 solution. The standard additions have been performed with an HMF standard solution prepared at 500 mg/L in H_2O. Total addition of 80 µL corresponds to 40mg/L.

The voltammograms relative to the HMF shown below (Figure 23) are very similar to the voltammogram of 2-furaldehyde, as expected from their structural analogy.

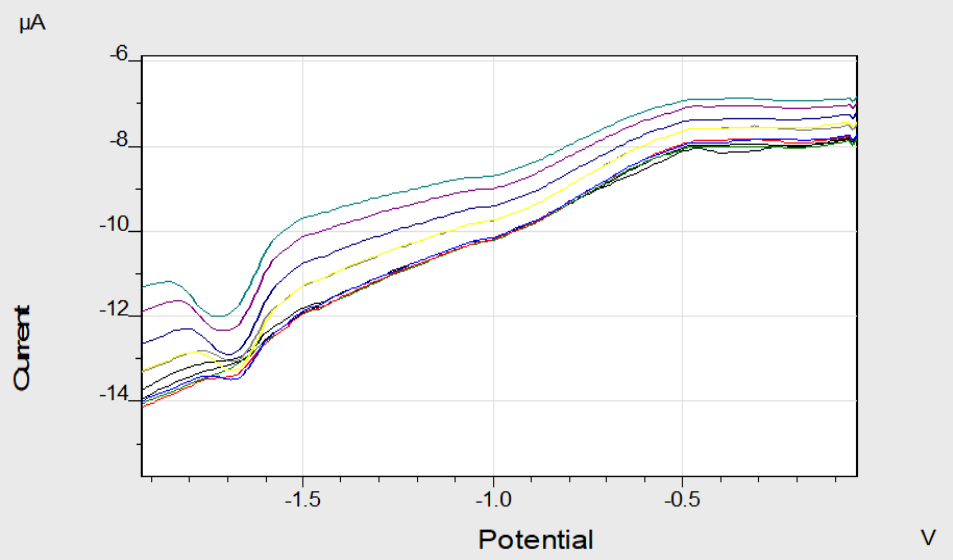

Figure 23. *SWV voltammogram of HMF in H_2O:EtOH=75:25, at different concentrations of HMF. Potential (V) against the current (µA)*

The reduction potential of HMF is between 1.68-1.70 V. In the example shown, the base current is very high, so the peak at about -1 V is partially reduced. However, a reduction peak is observed at around -1.7 V.

The linear regression parameters obtained from the standard additions method of HMF in H_2O:EtOH=75:25, at the selected potential, are shown below in Table 6.

Table 6. *Linear regression parameters obtained by the standard additions method of HMF in H_2O:EtOH=75:25; the slope and the ordinate origin are reported with the respective errors.*

Slope	Dev.st Slope	Ordinate Origin	Dev.st OO	r^2	sY/x
0,037	0,001	-0,06	0,05	0,986	0.062

Furfuryl alcohol has also been considered as a possible interfering agent. However, it has been observed that this substance is not reduced in the range of potentials considered. In fact, easily reducible groups such as the aldehyde group are not present in its structure.

2.2.3 EXPERIMENTAL SETUP FOR SPECTROPHOTOMETRIC ANALYSIS

2.2.3.1 Spectrophotometer

A spectrophotometer was used for the spectrophotometric analysis, Jas.Co V-750 spectrophotometer with two quartz cuvettes, 282 QS 1.000 and 283 QS 1.000.

The instrument is controlled using the Spectra Manager software.

The measurement conditions are:

Photometric mode	Abs
Uv/Vis bandwidth	1.0 nm
Uv/Vis response	0.06 s

Start	400 nm
End	200 nm
Data interval	1.0 nm
Scan mode	Continuous
Scan speed	400 nm/min

2.2.3.2 UV-VIS plate reader

A UV-VIS plate reader Synergy software version 2.00.18 with 96 well plates, type of reading “Endpoint” at wavelength 512, 513, 514nm was used. The temperature of the analysis range from 25 - 31°C.

2.2.4 UV-VIS PROCEDURE

The analyzes have been carried out by the UV/Vis Spectrophotometer (described above 2.2.3.) as it follows: As the first step, a baseline is recorded from the analysis of the solvent solution against the solvent. The solvent for the analysis consists of AcN:EtOH=4:1 solution fo the DBDS analyte, which is poorly soluble in water. For 2-FAL, an analyte highly water-soluble, two different solutions have been considered, i.e H_2O:EtOH=75:25 and synthetic wine (prepared as described in 2.1.2.). Subsequently, the solution to be analyzed, diluted if the case, is inserted into the measuring cuvette (usually 2 mL, always maintaining the volume ratio of solvent used in the analysis). The standard addition method was used for quantification. Between the analysis, the cuvette has been always washed with distilled water and finally conditioned with the solvent of analysis.

- UV Standardization curve of the DBDS

The standardization curve of the DBDS has been obtained by UV/Vis analysis with the standard addition method. The standard additions of DBDS have been performed of 10µL each in 2ml solution (2.7 mg/L) with a DBDS standard solution prepared at 540 mg/L in EtOH, up to a total addition of 200 µL, corresponding to 49mg/L. Typical UV spectra of absorption of DBDS obtained at different concentrations are shown in Figure 24.

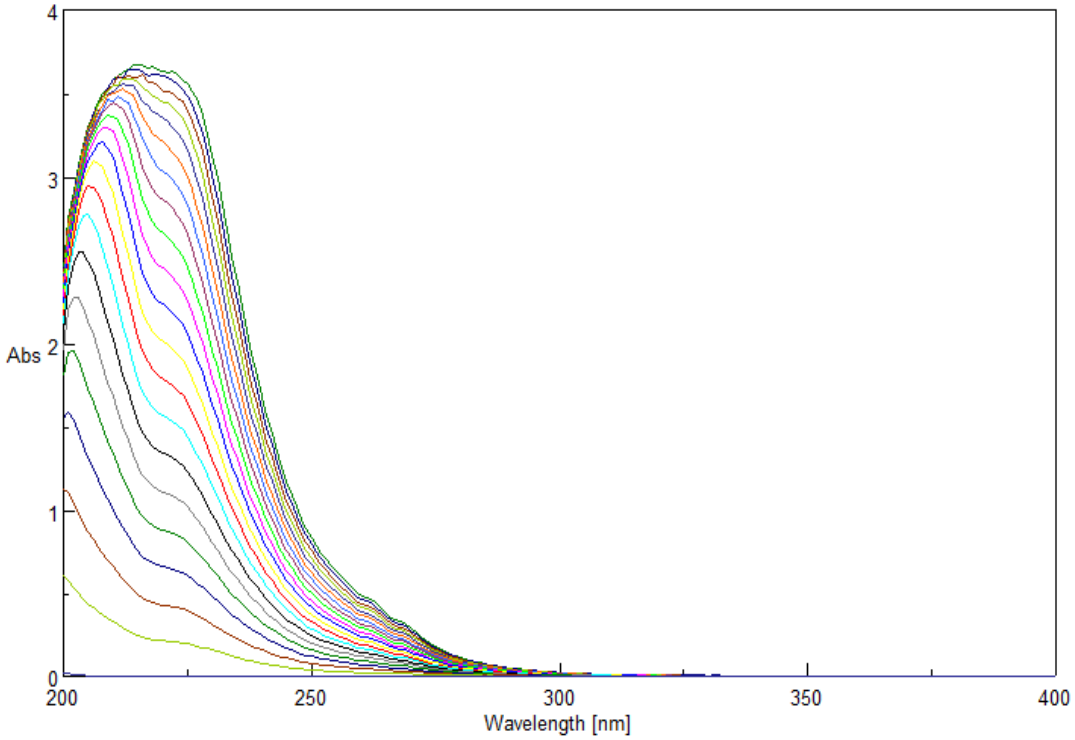

Figure 24. *UV spectra of DBDS in AcN:EtOH=4:1, at different concentrations of DBDS. Baseline registered against the same solvent.*

The absorbances at 220, 230, 250 and 270 nm were acquired. The linear regressions parameters obtained from the standard additions method of DBDS, at the selected wavelengths, are shown below in Table 7.

Table 7. *Linear regressions parameters calculated from the absorbances of DBDS at 220, 230, 250 and 270 nm. The slope and the ordinate at the origin are reported, for each absorbance, with the respective errors.*

	Slope	*Dev.st Slope*	*Ordinate Origin*	*Dev.st OO*	r^2	sY/x
A 220 nm	0,078	0,002	0,11	0,06	0.987	0.134
A 230 nm	0,0655	0,0003	-0,046	0,008	1.000	0.018
A 250 nm	0,0172	0,0001	-0,023	0,003	0.999	0.007
A 270 nm	0,00598	0.00004	-0,007	0,001	0.999	0.003

*Linear regression lines were obtained by the standard additions method

It is noted that the ordinate at the origin is significantly negative for wavelengths higher than 220nm. This phenomenon is still not clear and has not been further investigated.

- UV standardization curves of substances with a similar structure of DBDS (interfering substances)

The absorption behavior of the interfering substances has been analyzed too.

The interferents considered are diphenyl disulfide (DPDS) and dibenzyl sulfide (DBS), given their molecular structural analogy with the DBDS. The standardization curves have been obtained for both the substances by UV/Vis in 2mL of AcN: EtOH=8:2 solvent with the standard addition method.

DPDS

The standard additions of DPDS have been performed of 10µL each in 2ml solution (3 mg/L) with a DPDS standard solution prepared at 610 mg/L in EtOH, up to a total addition of 200 µL, corresponding to 55 mg/L. The UV spectra are shown in Figure 25.

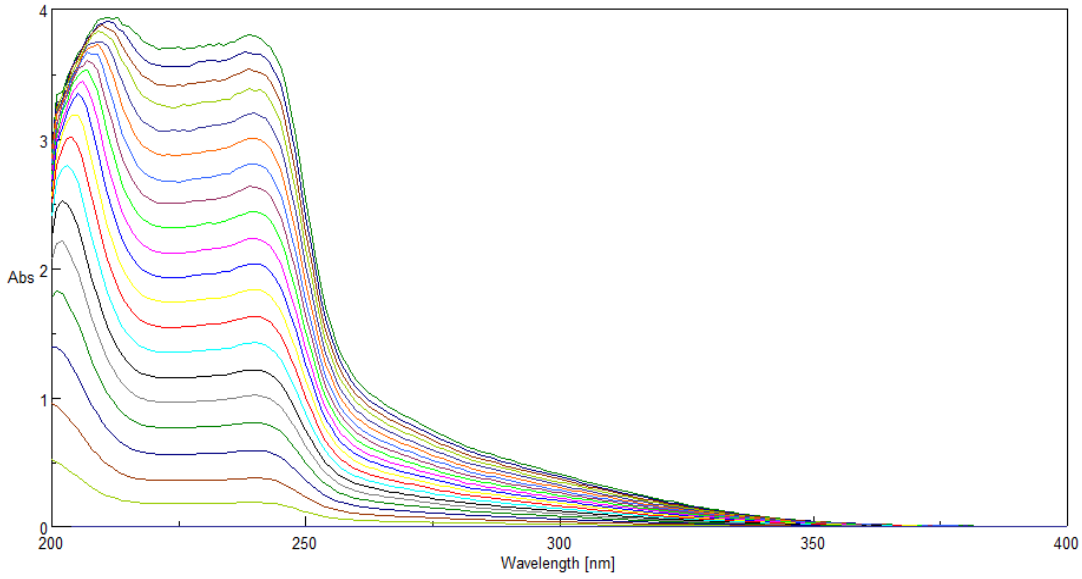

Figure 25. *UV spectra of DPDS in AcN:EtOH=4:1, at different concentrations of DBDS. Baseline registered against the same solvent.*

The absorbances at 220, 230, 250 and 270 nm were acquired. The linear regressions parameters obtained from the standard additions method of DPDS, at the selected wavelengths, are shown below in Table 8.

Table 8. *Linear regressions parameters calculated from the absorbances of DPDS at 220, 230, 250 and 270 nm. The slope and the ordinate at the origin are reported, for each absorbance, with the respective errors.*

	Slope	*Dev.st Slope*	*Ordinate Origin*	*Dev.st OO*	r^2	sY/x
A 220 nm	0,0689	0,0003	-0,054	0,009	1.000	0.020
A 230 nm	0,0690	0,0003	-0,053	0,009	1.000	0.019
A 250 nm	0,0461	0,0003	-0,06	0,01	0.999	0.021
A 270 nm	0,0154	0,0001	-0,023	0,004	0.999	0.008

*Linear regression lines were obtained by the standard additions method

Also in the case of the DPDS the ordinates at the origin are significantly different from 0.

DBS

The standard additions of DBS have been performed of 10µL each in 2ml solution (2.6 mg/L) with a DBS standard solution prepared at 515 mg/L in EtOH, up to a total addition of 200 µL, corresponding to 46 mg/L. The UV spectra are shown in Figure 26.

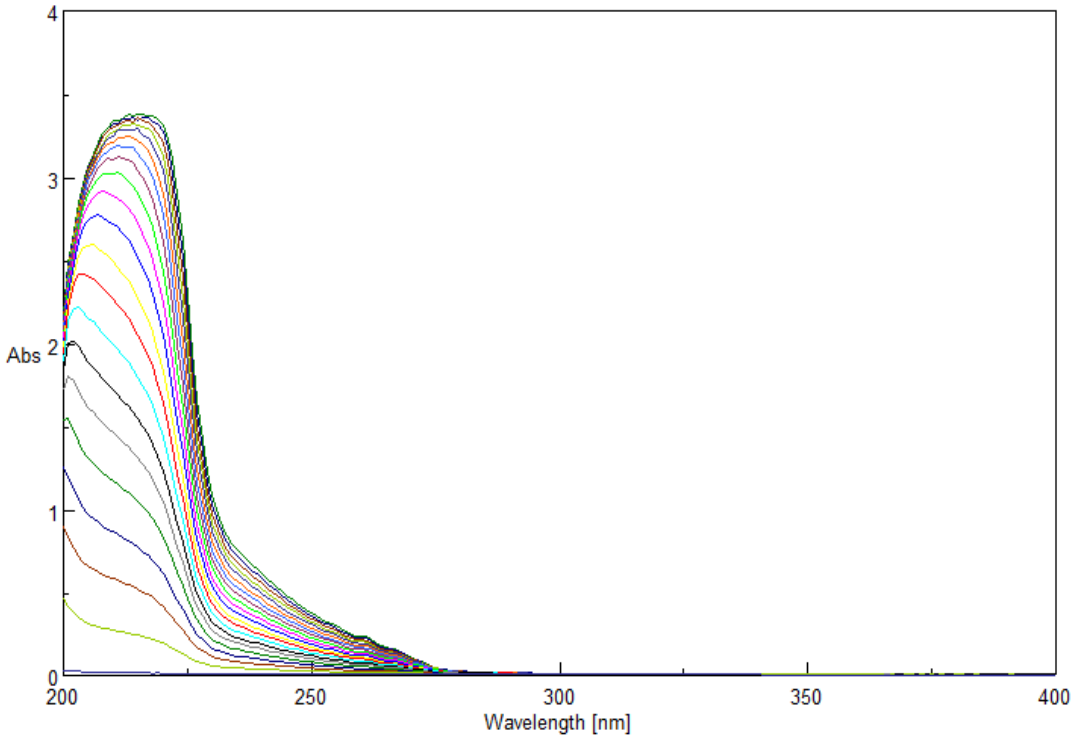

***Figure 26**. UV spectra of DBS in AcN:EtOH=4:1, at different concentrations of DBDS. Baseline registered against the same solvent.*

The absorbances at 220, 230, 250 and 270 nm were acquired. The linear regressions parameters obtained from the standard additions method of DBS, at the selected wavelengths, are shown below in Table 9.

Table 9. *Linear regressions parameters calculated from the absorbances of DBS at 220, 230, 250 and 270 nm. The slope and the ordinate at the origin are reported, for each absorbance, with the respective errors.*

	Slope	*Dev.st Slope*	*Ordinate Origin*	*Dev.st OO*	r^2	*sY/x*
A 220 nm	0,074	0,002	0,13	0,06	0.987	0.121
A 230 nm	0,0232	0,0002	-0,018	0,005	0.999	0.011
A 250 nm	0,00802	0.00006	-0,001	0,002	0.999	0.004
A 270 nm	0,00217	0.00002	0,0075	0,0005	0.999	0.001

*Linear regression line was obtained by the standard additions method

- UV standardization curves of 2-FAL

The standardization curve of the 2-FAL has been obtained by UV/Vis analysis with the standard addition method. The standard additions of 2-FAL have been performed of 10µL each in 2ml solution (2.9 mg/L) with a 2-FAL standard solution prepared at 580 mg/L in H_2O, up to a total addition of 40 µL, corresponding to 11.4 mg/L. Typical UV spectra of absorption of 2-FAL obtained at different concentrations are shown in Figure 27.

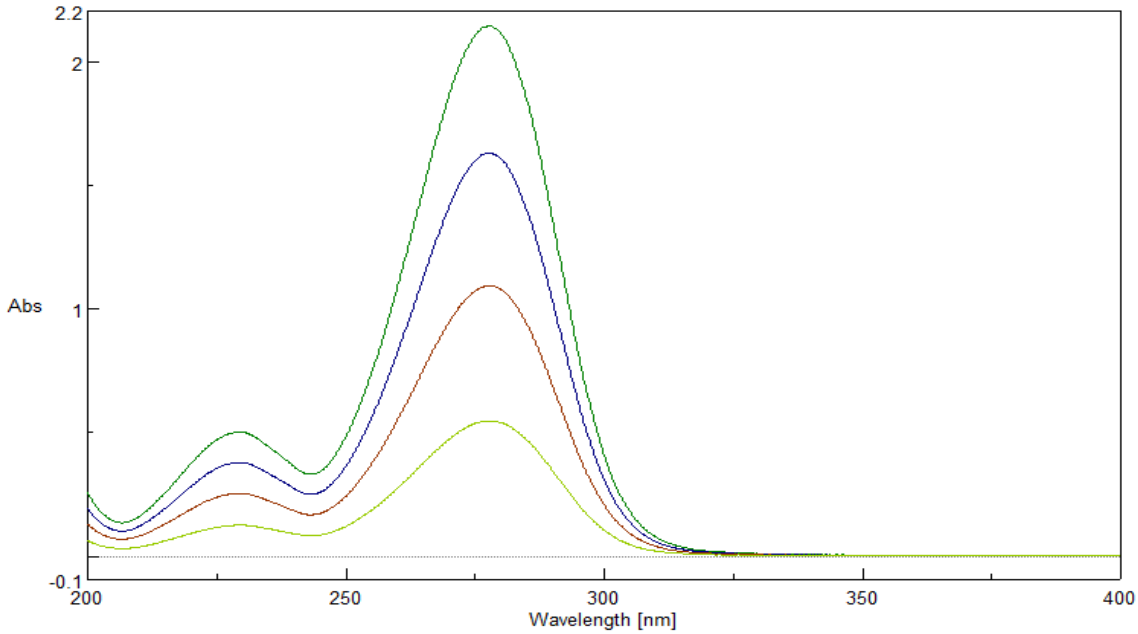

Figure 27. *UV spectra of 2-FAL in H_2O:EtOH=75:25, at different concentrations of 2-FAL. Baseline registered against the same solvent.*

The absorbances at 229nm and 278nm were acquired. The linear regressions parameters obtained from the standard additions method of 2-FAL, at the selected wavelengths, are shown below Table10.

Table 10. *Linear regressions parameters calculated from the absorbances of 2-FAL at 229nm and 278nm. The slope and the ordinate at the origin are reported, for each absorbance, with the respective errors.*

	Slope	*Dev.st Slope*	*Ordinate Origin*	*Dev.st OO*	r^2	*sY/x*
A 229 nm	0,0443	0,0002	-0,007	0,002	0.999	0.001
A 278 nm	0,188	0,001	0.003	0,009	0.999	0.008

*Linear regression line was obtained by the standard additions method

The absorbance at 278nm is used as an analytical parameter for the quantitative determination of 2-FAL.

- UV standardization curves of substances with a similar structure of 2-FAL (interfering substances)

The absorption behavior of the interfering substances has been analyzed too. The interferents considered are 5-hydroxymethyl-2-furaldehyde (HMF) and Furfuryl Alcohol (FA), given their molecular structural analogy with the 2-FAL. The standardization curves have been obtained for both the substances by UV/Vis in 2mL of H_2O:EtOH=75:25 solvent with the standard addition method.

HMF

The standard additions of HMF have been performed of 10µL each in 2ml solution (2.5 mg/L) with an HMF standard solution prepared at 500 mg/L in H_2O, up to a total addition of 40 µL, corresponding to 9.8 mg/L. The UV spectra are shown in Figure 28.

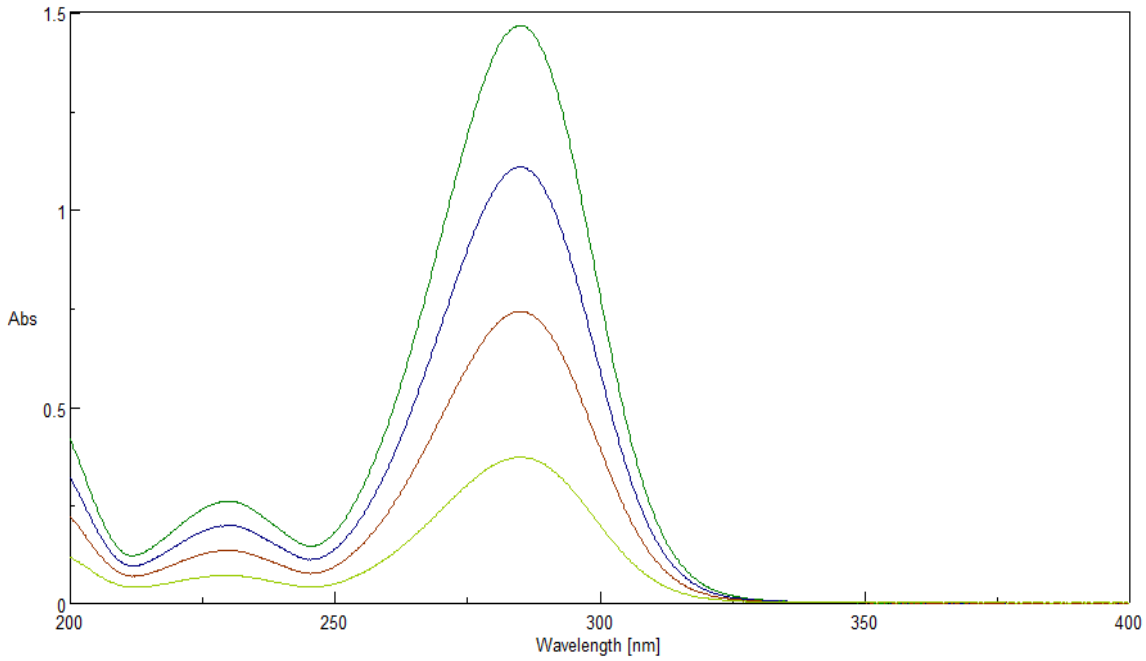

Figure 28. *UV spectra of HMF in H_2O:EtOH=75:25, at different concentrations of HMF. Baseline registered against the same solvent.*

The absorbances at 229nm and 285nm were acquired. The linear regressions parameters obtained from the standard additions method of HMF, at the selected wavelengths, are shown below in Table 11.

Table 11. *Linear regressions parameters calculated from the absorbances of HMF at 229nm and 285nm. The slope and the ordinate at the origin are reported, for each absorbance, with the respective errors.*

	Slope	*Dev.st Slope*	*Ordinate Origin*	*Dev.st OO*	r^2	sY/x
A 229 nm	0,02569	0,00002	0,0070	0,0001	0.999	0.0001
A 285 nm	0,1498	0,0002	-0.002	0,001	0.999	0.002

*Linear regression line was obtained by the standard additions method

The absorbance at 285nm is used as an analytical parameter for the quantitative determination of HMF. A probable deterioration of the HMF standard solution has been observed after about two months from preparation date. The analysis shows a peak of absorbance at 251nm and a value of absorbance at 229nm. The absence of the peak at 285nm has been noted. A probable degradation product of HMF is the levulinic acid [161].

The standardization curve obtained with the same methods described above with the standard of HMF suspected of being deteriorated is shown in the following Figure 29.

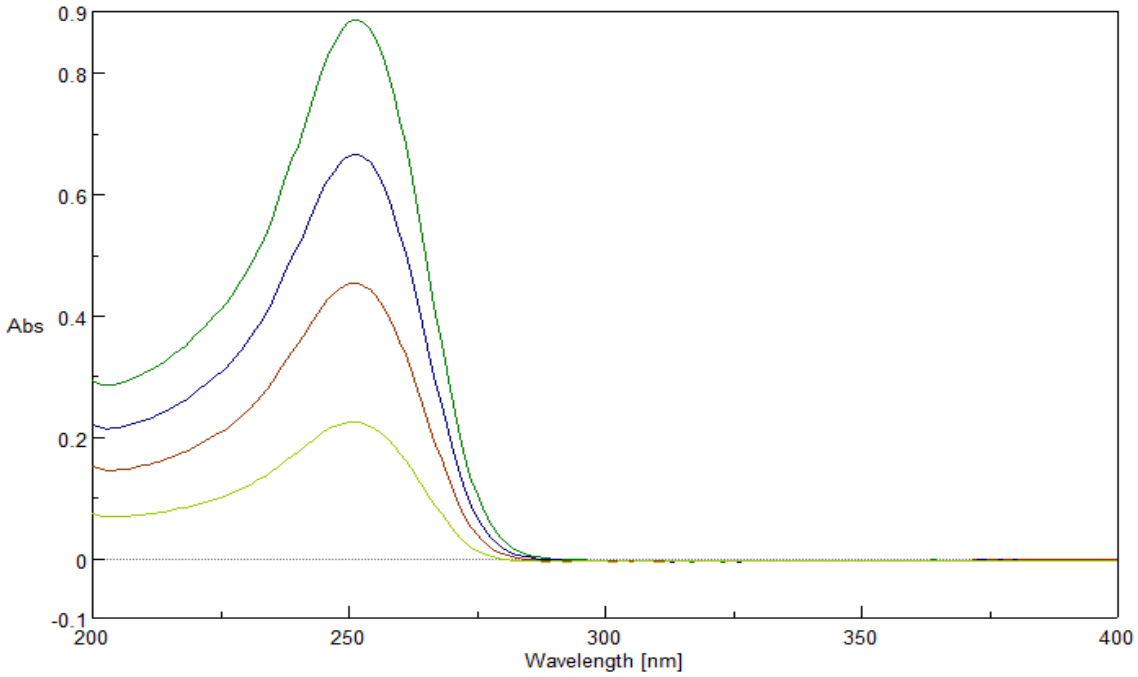

Figure 29. *UV spectra of HMF in H_2O:EtOH=75:25, at different concentrations of HMF. Baseline registered against the same solvent.*

The absorbances at 251nm was acquired. The linear regression parameters obtained from the standard additions method of HMF, at the selected wavelength, is shown below in Table 12.

Table 12. *Linear regression parameters calculated from the absorbance peak found on the suspected deteriored standard of HMF. The slope and the ordinate at the origin are reported, for each absorbance, with the respective errors.*

	Slope	*Dev.st Slope*	*Ordinate Origin*	*Dev.st OO*	r^2	sY/x
A 251 nm	0,0903	0,0008	0,001	0,005	0.999	0.003

*Linear regression line was obtained by the standard additions method

Furfuryl Alcohol

The standard additions of FA have been performed of 10µL each in 2ml solution (2.5 mg/L) with a FA standard solution prepared at 567.5 mg/L in H_2O, up to a total addition of 40 µL, corresponding to 11.1 mg/L. The UV spectra are shown in Figure 30.

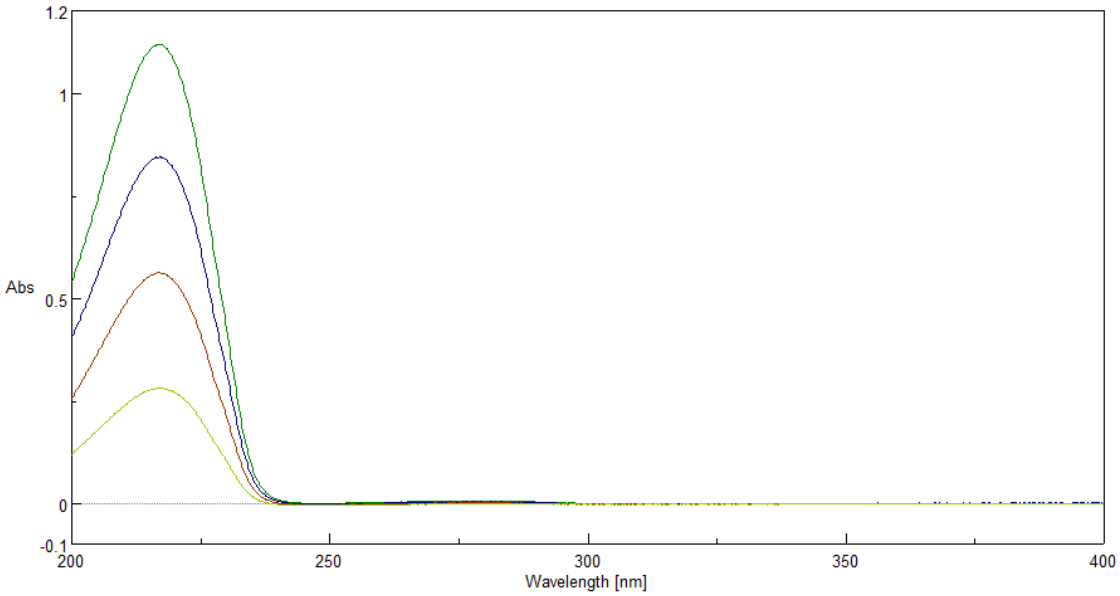

Figure 30. *UV spectra of FA in H_2O:EtOH=75:25, at different concentrations of FA. Baseline registered against the same solvent.*

The absorbances at 217nm were acquired. The linear regression line obtained by the standard additions method of FA, at the selected wavelength, is shown below Table 13.

Table 13. *Linear regression parameters calculated from the absorbance of FA at 217nm. The slope and the ordinate at the origin are reported, for each absorbance, with the respective errors.*

	Slope	*Dev.st Slope*	*Ordinate Origin*	*Dev.st OO*	r^2	*sY/x*
A 217 nm	0,1011	0,0002	-0,006	0,001	0.999	0.001

*Linear regression line was obtained by the standard additions method

2.2.5 ENZIMATIC ASSAY BY SPECTROPHOTOMETRIC DETECTION

A colorimetric enzymatic assay was employed for the analysis of the glucose concentration in the supernatant solution during the batch equilibration procedure for the characterization the molecular imprinting on silk fibroin protein which will be discussed in chapter 4. The enzymatic assay is the most commonly used for the glucose analysis in colorimetric sensors [162-164]. The analysis has been performed using a plastic 96 well plate with a 200µL volume on each well. The concentrations of the enzymes employed were 0.24 U/mL of GOD and 0.04 U/mL of HRP (ratio 6:1) in 30mM of phosphate buffer (pH 7). The dye ratio A/B used was 1:84 with a concentration of 0.05mM of 4-amino-antipyrine (A) and 4.2mM of 3,5-dichloro-2-hydroxy-benzenesulfonic acid (sodium salt, 99%) in 30mM of phosphate buffer (pH 7) (B) [165]. The analysis has been performed after an incubation time of 60min and 90min. Different concentration of glucose has been employed for standardization from 0-100 mg/L. The additions have been made by different dilution of a stock standard solution of glucose at 25000 mg/L in phosphate buffer (pH 7). A linear trend has been obtained with the described condition for the assay solution for glucose concentrations from 1 to 15 mg/L. So, further analysis of the supernatant solution obtained by the batch equilibration on fibroin sample has been diluted, if necessary, to enter in this linearity range. The maximum absorption of the dye has been found at about 512nm. The base line has been registered in a solution consisting of all the reagents without the analyte in the 30mM phosphate buffer.

- OPTIMIZATION OF THE ENZIMATIC ASSAY

The analysis method was optimized in regard to the enzymes ratio (GOD/HRP) and the Dye ratio (A/B). The analysis was performed in a 96 well plate with 200uL of the volume of analysis solution. The protocol of analysis was then tested and calibrated.

Some glucose standardization curve at different enzyme ratio GOD/HRP has been performed. The enzyme GOD/HRP ratios considered were 2:1 - 4:1 - 6:1 - 1:1 - 1:2. The different assay reagents were incubated at 32°C with a variable concentration of glucose, from 0-100 mg/L. The UV/Vis analysis was performed at different incubation time form 30 to 180 min; each acquisition was made after 30 min. At the end of each incubation period, the absorbance was measured. The first run has been performed on a full spectrum (200-800nm) to select the peak of absorbance. The maximum

value was found at three different wavelengths 512-513-514nm, so only an endpoint analysis on these wavelengths was than employed on further investigations. The results of the different glucose standardization curve have been compared obtain the best protocol with the more stable condition of analysis and the maximum value of the signal.

The dye used for the colorimetric enzymatic assay was constituted by A (AAP) 4-aminoantipyrine, B (DHBS) 3,5-dichloro-2- hydroxy-benzenesulfonic acid (sodium salt, 99%), it's the most typical employed for this type of enzymatic measurement [163; 165]. Many different dyes can be employed but this type was found to be the most sensitive since the color variation is from transparent to Bordeaux [162].

A preliminary comparison of the glucose standardizations curve at different enzyme and dye ratios have been performed to select the best assay protocol and wavelength of analysis (Figure 31). Also, to test the stability of the assays, subsequent analysis on the same solution was performed in the next two days as described in Figure 31.

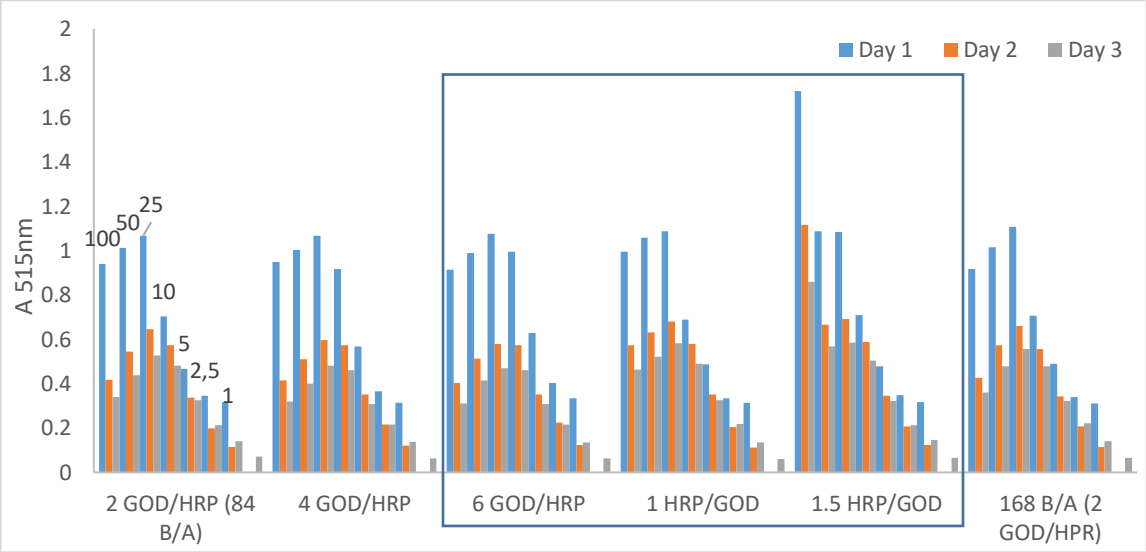

Figure 31. *Glucose Standardization on different GOD/HRP and A/B ratios, incubated at 31°C and analyzed after 1h and in the subsequent days as reported.*

The more intense signal has been observed for ratios 6:1 - 1:1 - 1:2 of GOD/HRP. Different concentrations of dye were tested too, with the ratio of A/B of 1:85 and 1:170, but no significant gain in signal was obtained; so it was maintained the ratio of 1:85 as exposed in the procedure [165].

Further, an investigation of the sensitivity of the different enzymatic assays obtained from the linear regression of the previous exposed standardization data has been performed and reported in Figure 31.

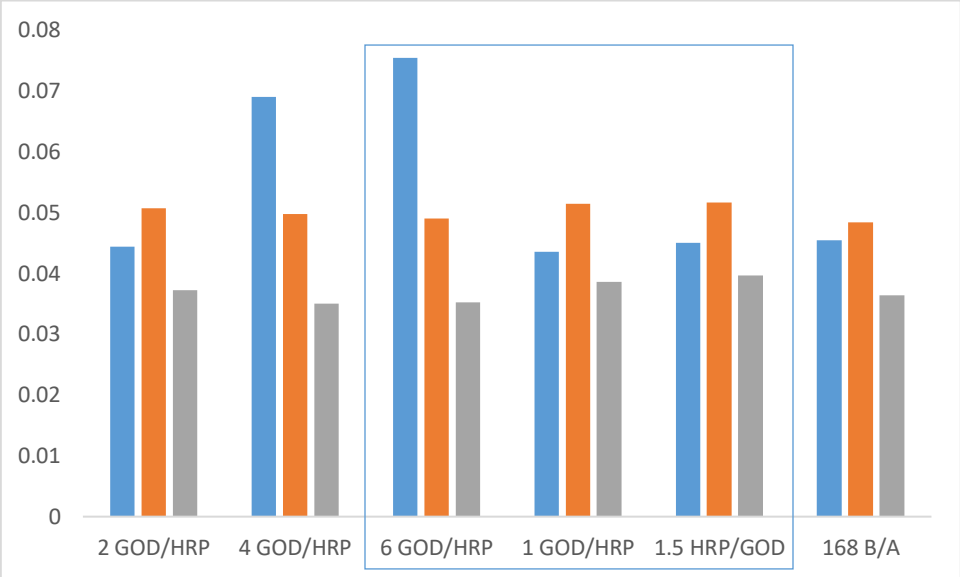

Figure 32. *Comparison between the sensitivities of the different enzymatic assay obtained from the linear regression on the different calibration curve of glucose from the absorption at 512nm.*

Data shows that the best reproducibility and the stability of the signal over time have been obtained for ratio 6:1 of GOD/HRP, so this assay has been chosen for the analysis of the absorption characterization of the imprinting of silk which will be exposed in chapter 4.

The standardization curve of the chosen assay with ratio 6:1 of GOD:HRP is reported in Figure 33 at different times, after 1h and in the subsequent two days.

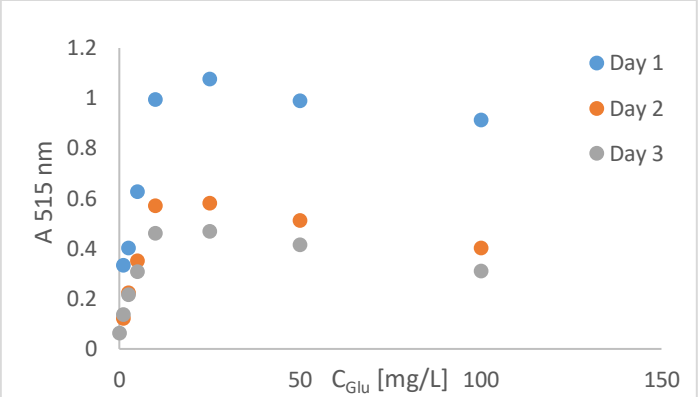

Figure 33. *Standardization curve of glucose by enzymatic colorimetric assay with GOD:HRP ratio of 6:1 at the different times, after 1h and in the subsequent two days.*

As it could be clearly seen, the saturation was reached in the condition considered, so for the further analysis on the analyte solution it was decided to maintain the concentration below 15 mg/L.

On the selected ratio of GOD/HRP=6:1 the reaction was studied at the wavelengths for which it was found the maximum absorbance (512-513-514nm) at the different times of reaction (30, 60, 90 and 120min). The results are reported in Fig.34.

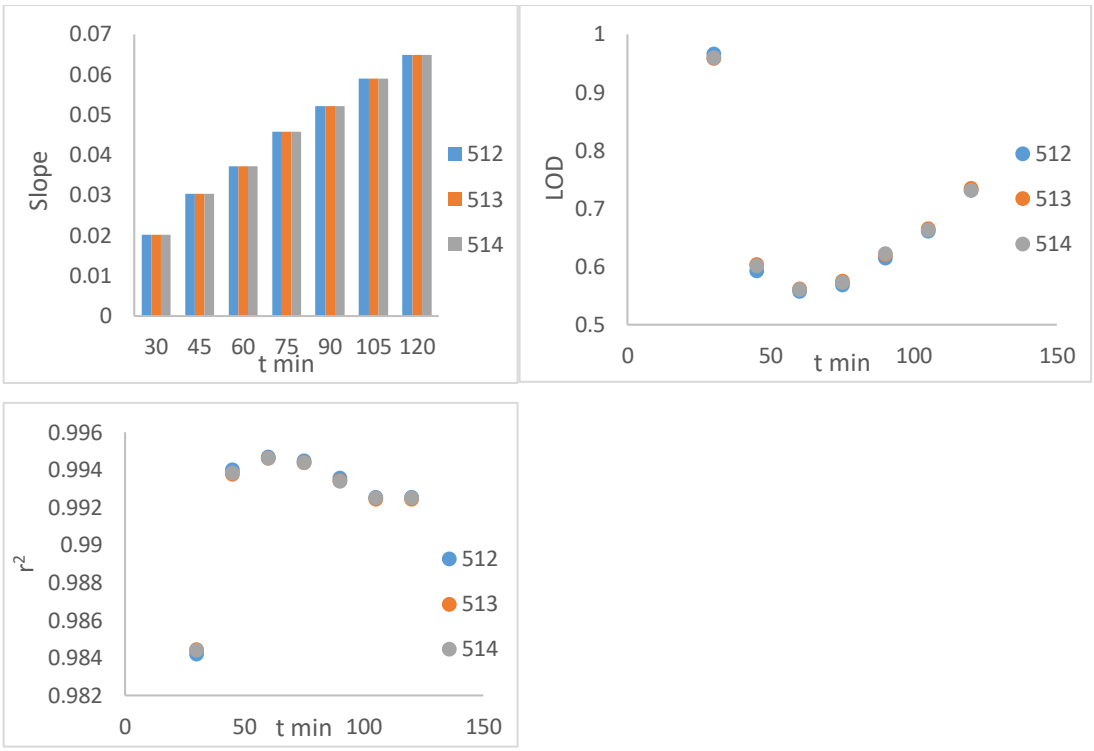

***Figure 34**. Study of the assay with GOD/HRP=6:1 at different wavelengths (512-513-514nm) a) comparison of the sensibility at different incubation time. b) LOD for different incubation time. c) R^2 of the linear regression on different incubation time.*

Even if the sensitivity seems to be higher for times of incubation above 90min, because of the intense coloration of the solution, a better LOD and the linearity was found for incubation time from 60 to 90min.

The best condition for the enzymatic assay was found in 200uL of analysis with a concentration of 0.04 U/mL of HRP and 0.24 U/mL of GOD (ratio 1:6 of HRP/GOD), a concentration of glucose ranging from 0-15 mg/L and a concentration of 0.05mM of 4-aminoantipyrine, and 4.2mM of 3,5-dichloro-2- hydroxy-benzenesulfonic acid (sodium salt, 99%) (ratio 1:84 of dye A/B) with an incubation time of 60-90min.

2.2.6 INSTRUMENTATION FOR OPTOELECTRONIC SENSORS

In all the optoelectronic systems considered in the present work, the simplest experimental setup consists of the following components, as shown in Figure 35:

- Light source: halogen lamp (HL–2000–LL, Ocean Optics) exhibiting a wavelength emission range from 360 nm to 1700 nm.
- Analyzer: Spectrophotometer a FLAME-S-VIS-NIR-ES with a detection range of 350÷ 1023 nm and a spectral resolution ($\delta\lambda_{DR}$) of 1.5 nm (FWHM). The spectral resolution of the spectrometer (USB2000 + UV–VIS spectrometer, Ocean Optics) was 1.5 nm ($\delta\lambda_{DR}$).
- The sensing platform.

Dedicated software: With SpectraSuite software most commonly the spectra have been acquired with an Integration time = 10 ms; Scans for media = 50. The transmission spectra of the SPR sensor prototypes were processed with the Matlab software.

Figure 35. Experimental instrumentation

The measurements with the sensor platform have been carried out in different ways, i.e. by a spectral or intensity amplitude approach.

In the SPR platforms (as for example D-shaped POF [1] and PMMA slab [20]) the shift in the resonance wavelength was considered i.e. a spectral approach was adopted. The configuration of the experimental setup, for the determination of the transmission spectrum by the intrinsic POF platform, is shown in Figure 36.

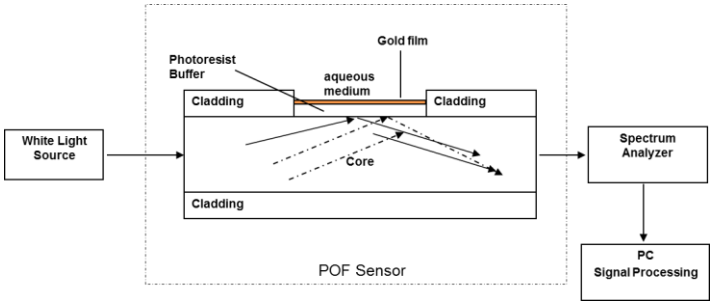

Figure 36. *Spectral approach configuration based on SPR*

In this case, the waveguide was the POF itself, while in the case of the PMMA slab platform the POFs are only employed for carrying the light to and from the waveguide (extrinsic configuration). The data have been collected as transmission spectrum in presence of the MIP receptor and normalized to the spectrum obtained in air before MIP deposition for the same platform and experimental setup, since not any plasmon resonance is excited in this case, due to the not appropriate refractive index of air [10; 19; 135].

The same configuration can be exploited for intensity measurements (Inkjet printed PET) [3]. In this case too the normalization is required for analytical application because of the irreproducibility of the light intensity in different experiments.

In the case, of the sensor based on evanescent wave coupling (EWC), an SWS platform has been developed as schematized in Figure 37 [2]. The experimental setup for acquiring the signal is composed of a light source which could be a white light lamp or LED, and two photodiodes, or an oscilloscope, for the signal registration (light intensity). This is reqired for the internal normalization of the signal, which is the ratio of the light intensity emerging from the injecting fiber and the colleting fiber. It is crucial to underline that in this case, the signal measured is independent of the input light. This analysis with a continuous on-line reference allows performing a better normalization of the signal, obtaining a more stable device with more consistent and reproducible results.

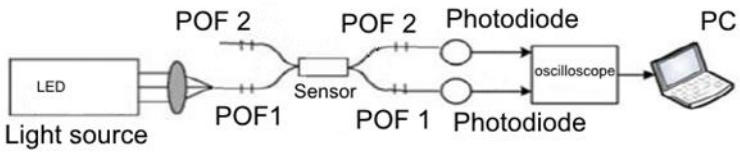

Figure 37. *Intentity approach configuration (ATR) based on EWC*

2.2.7 INVESTIGATION OF THE PERFORMANCE OF OPTICAL PLATFORMS

The characterization of the bare platform was performed by considering the most common performance parameters, as the sensitivity, the signal to noise ratio (SNR), and the resolution [148; 166-167].

The sensitivity is defined as the shift of the detected signal per unit change in physical property measured. For example, in the case of SPR sensors in spectral mode, the sensitivity (Sn) is defined as the shift in resonance wavelength $\delta\lambda_{res}$ per unit change in refractive index (nm/RIU) δn_s.

$$S_n = \frac{\delta\lambda_{res}}{\delta n_s}\left[\frac{nm}{RIU}\right] \qquad \textit{Eq. 3}$$

The Signal-to-Noise Ratio is defined as the ratio of the resonance wavelength shift induced $\delta\lambda_{res}$ and the full width at half maximum of the SPR dip δn_s. It depends on the refractive index of the sensing layer so it is an index of how accurately and precisely the sensor can detect the resonance wavelength.

$$SNR(n) = \left[\frac{\delta\lambda_{res}}{\delta\lambda_{SW}}\right]_n \qquad \textit{Eq. 4}$$

The resolution (Δn) of the SPR-based optical sensor can be defined as the minimum amount of change in refractive index detectable by the sensor. This parameter definitely depends on the spectral resolution (δλDR) of the spectrometer used to measure the resonance wavelength in a sensor scheme. Therefore, if there is a shift of δλres in resonance wavelength corresponding to a refractive index change of δns, then resolution can be defined as (eq.5)

$$\Delta n = \frac{\delta n_s}{\delta\lambda_{res}}\delta\lambda_{DR} \qquad \textit{Eq. 5}$$

In order to improve this factor, a number of different setup and structure of sensors have been largely studied.

The characterization of the bare platform is useful to identify the resonance wavelength as a function of the refractive index of the platform. This can be an indication of the reproducibility of the different platforms (for example the small differences in thickness of the gold layer) and the correct functionality of the platform.

2.2.8 SEM (Scanning electron microscopy) AND EDS (Energy Dispersive X-ray Spectrometry)

ZEISS EVO 10 SEM equipped with INCA software for EDX have been employed.

2.2.9 ELLIPSOMETER/REFRACTOMETER

The Metricon Model 2010/M Prism Coupler utilizes advanced optical waveguiding techniques to rapidly and accurately measure both the thickness and the refractive index/birefringence of dielectric and polymer films as well as refractive index of bulk materials.

2.2.10 ELECTROPHORETICAL SEPARATION (SDS-PAGE PROTOCOL)

Running Buffer (10 X concentrated): 700 mL of nanopure water add, 30.0 g of Tris-Base (buffer sol), 144 g of glycine (avoid the stacking of strains), 10.0 g of SDS (sulfactant denaturate the protein), Adjust pH to 8.3 with NaOH or HCl, Mix until fully dissolved, Bring volume to 1000 mL. Store at room temperature

Loading Buffer (4 X concentrated): 3.1 mL of nanopure water., 4.0 mL of glycerol (very viscous, may need a syringe or positive-displacement pipette. useful to rise up the viscosity of solution), 2.4 mL of 1 M Tris-HCl (pH 6.8), 0.8 g of SDS, 4.0 mg of bromophenol blue (indicator of the running front), 0.5 mL beta-mercaptoethanol (break the s-s bond of protein), Mix by vortexing until fully dissolved, Make 1 mL aliquots and store at -20 °C

Sample Preparation: Dilute 10 µL of 7.0% w/v silk fibroin solution with 2090 µL of nanopure water to create a 0.33 mg/mL solution (Final volume is 2100 µL). Mix 15 µL of dilute silk solution with 5

µL of 4 X loading buffer. Heat sample to 60 °C for 10 minutes then place on ice until ready to load samples.

Colloidal Strain solution: 20mL of strain solution + 80mL MilliQ (1:5), 25mL of MeOH to 1x sol, strain for 2h

Destrain 1° prepare 250mL tot: rinse for 60 sec. 10% Glacial Acetic Acid (25mL), 25% MeOH (62,5mL) and 162,5mL H_2O.

Destrain 2° methanol sol at 25% and rinse for 24h (62,5 methanol mL / 187,5mL H_2O)

Performing Gel Electrophoresis

This procedure uses NuPAGE™ 3-8% Tris-Acetate Protein Gels, 1.0 mm 10 well comb. It was prepared 1000 mL of 1 X running buffer by diluting 100 mL of 10 X running buffer with 900 mL of nanopure water gel cassette was removed from the pouch and rinse with nanopure water, the comb was removed gently to avoid the damaging of the wells. It was rinsed 3 times with 1 X running buffer and discard the rinses.

The gel cassette was posed in the electrolysis chamber (assuring the right position of the electrophoresis goes in at the opposite if the polarity is inverse). The chamber was filled with a small amount of 1 X running buffer and check for leaks. If the position was right so no leak is registered, it was filled by the running buffer enough to cover the wells in front and back.

The samples wells were loaded, in the first with 10 µL of protein standard (ladder) solution and the other with 20 µL of prepared samples mixed with loading buffer. It must be done carefully without spilling the loading sample solution outside the wells.

The run was made by applying 150 V for 1 hour. (the current in the right condition should rise at 40-55 mA).

Considering the end the electrophoresis if the loading dye reaches the bottom of the gel.

It was removed the gel carefully from the inside of the cassette and placed into a staining container.

Staining and Destaining

To strain the gel, pour in 100 mL of staining solution or more, ensuring that the gel is completely covered. Place the gel on an orbital rocker and let sit for 1 hour. Decant the staining solution and rinse thoroughly with nanopure water. Place gel in a destaining container and add 100 mL of destaining solution. The destaining process depends on the amount and spread of the proteins and as such times for destaining can vary greatly. Longer destains will remove the background staining but will also lower the intensity of the stain in the protein bands. Check the gel after 2-3 hours, if too much background is still present then allow the gel to destain overnight. When the desired level of background is reached, decant the destaining solution and rinse the gel thoroughly with nanopure water. Image gel on a gel imager, store in water if additional imaging will be needed.

2.3 METHODS

2.3.1 CHARACTERIZATION OF ADSORPTION BY BATCH EQUILIBRATION

The adsorption equilibria on MIP in form of small particles or beads is characterized by batch equilibration procedures. Once the MIP polymer has been properly washed (as described in the washing procedure of the polymer) and dried, if necessary by placing it in the oven for a few minutes, the adsorption of the analyte of interest (A) has been studied by equilibrating weighted amounts of polymer (usually 0.04 g) with measured volumes (usually 3 mL) of solutions with known concentrations of A (mg_A/L). The solution spiked with the analyte is contacted with MIP for a time sufficient to achieve the adsorption equilibrium, typically for 14 hours. The analysis of the supernatant solution at equilibrium condition has been performed by electrochemical or spectrophotometric methods, as described in paragraphs 2.2.2. and 2.2.4. The supernatant solution is separated by centrifugation (usually 10min at 4000rpm) to separate the solid polymer powder and to obtain a clear solution for the analysis. The MIP is collected for re-extraction of the adsorbed molecules. This procedure allows determining the analyte (2-FAL or DBDS) adsorption isotherms on the different MIPs, i.e. the curves showing the concentration of the adsorbed substance (normally in mg_A/g_{MIP}) as a function of the concentration of the substance in solution (in mg_A/L).

The concentration of the analyte in solution [A] is experimentally determined with the selected analytical procedure (see 2.2.2. and 2.2.4.). The concentration in the polymer phase [RA] is determined by the difference of the concentration in solution and the total added concentration or by re-extraction with a suitable solvent, as the released amount in the eluting solution.

The adsorbing properties of MIPs are commonly determined by the Langmuir adsorption model or equivalent models [168-172], in which the following adsorption mechanism is considered:

$$A + R \leftrightarrow AR \qquad K_{aff} = \frac{[RA]}{[R][A]} \quad \textit{Eq. 6}$$

R represents the selective site for A in the polymer, obtained by the molecular imprinting method. [R] is the concentration of the free sites and [RA] is the concentration of the R sites occupied by the analyte A. The concentrations [R] and [RA] are referred to the "polymer" phase, and the latter is expressed as $mg_{A\ adsorbed}/g_{MIP}$. The following relationships hold:

$$c_R = [RA] + [R] \qquad \textit{Eq. 7}$$

$$c_A = [A] + \frac{[RA]g}{V} \qquad \textit{Eq. 8}$$

c_R is the concentration of specific sites in MIP, expressed as $mg_{A\ adsorbable}/g_{MIP}$. The Langmuir sorption isotherm corresponds to the following relationship, which can be easily obtained from the equations reported above:

$$[RA] = \frac{K_{aff} c_R [A]}{1 + K_{aff}[A]} \qquad \textit{Eq. 9}$$

The parameters of this relation can be determined by non linear regression, available in the common statistical pakages, in particular the Hill equation from the software OriginPro 2016 b9.3.226 has been used in this study to fit the experimental data.

Alternatively, some linearized relationships have been proposed for the evaluation of the parameters, as for example:

$$[A] = -\frac{1}{K_{aff}} + \frac{[A]}{c_A - [A]} c_R \frac{g}{V} \qquad \textit{Eq. 10}$$

Another linearization model of the Langmuir isotherm is the double reciprocal equation reported below:

$$\frac{1}{[RA]} = \frac{1}{K_{aff} c_R [A]} + \frac{1}{c_R} \qquad \textit{Eq. 11}$$

It is also worthwhile to remember that an approximate value of K_{aff} can be obtained considering that when half of the receptor sites (the imprinted sites) are combined with A, the following relation is verified:

$$K_{aff} = 1/[A] \qquad \textit{Eq. 12}$$

A complete investigation of the adsorption equilibria requires to consider a large concentration range up to saturation of the solid phase.

The Langmuir adsorption isotherm is widely used for adsorption on a solid phase containing interaction sites, as for example is reported [168-172].

Since the adsorption capacity is defined as the maximum amount of the substance of interest which can be adsorbed on MIP at the considered conditions if the adsorption takes place according to the Langmuir sorption isotherm, this situation is reached when [A]>>Kaff. If the determination of only the adsorption capacity is required, only one equilibration at a concentration sufficiently high to saturate the MIP is needed.

The aspecific adsorption on the corresponding NIP was examined in the same way. This experiment gives useful information about the specificity of the considered MIP.

The specificity index is measured as the imprinting factor IF at saturation, i.e. at high concentration:

$$IF = \frac{[RA]_{max,MIP}}{[RA]_{max,NIP}} \qquad \textit{Eq. 13}$$

It must be underlined that IF at high concentration is that involving the less strong and probably less specific interaction sites. Much higher values can be determined at lower concentrations.

The adsorption of substances other than the template has been examined in the same way in order to establish the selectivity of the adsorbing solid.

After the adsorption, a re-extraction test has been also carried out in the same not spiked solvent. Successive extractions are often needed to completely extract the previously adsorbed template.

2.3.2 INVESTIGATION OF THE ADSORPTION ON MIP BY FLOW METHODS

In this work, some experiments of adsorption by flow methods on MIP as stationary phase has been performed as an alternative method for the characterization of the polymer by batch equilibration. This method presents some advantages, for example the phase separation is not required. Each column was created in the following way: a weighted amount of bulk MIP, porous or non-porous, previously grounded and sieved, was introduced into a Pasteur pipette, with a cutted tip and a septum of glassy wool of 1cm to sustain powder particles of the polymer. Figure 34 shows a sketch of the column:

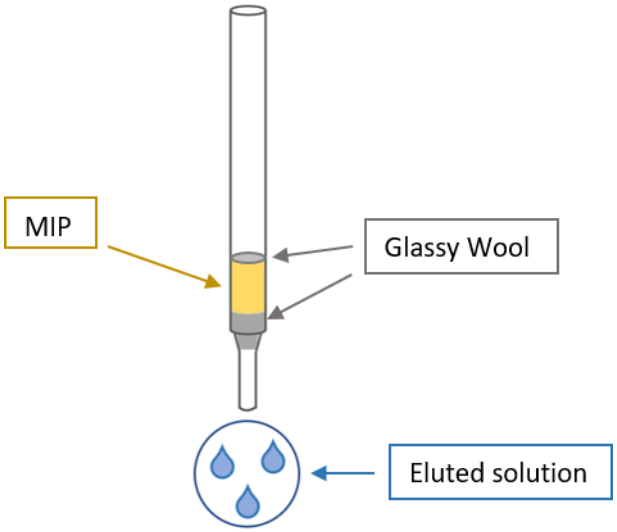

Figure 38. *Column for adsorption in flow with MIP cartidge.*

Adsorption has been characterized by determining the breakthrough curves, by continuous flow injection of DBDS solutions at a known concentration.

Subsequently, an eluting solution is passed through the column, collected in glass test tubes and analyzed spectrophotometrically and electrochemically, in order to quantify the release of the considered analute and verify the interferents.

The breakthrough curve shows the concentration of the adsorbate eluted from the column as a function of the sample solution volume. The curve has a sigmoidal shape: initially, the analyte is

completely adsorbed and retained into the stationary phase and therefore the concentration emerging from the column is 0. The concentration in the eluted portion increases up to the concentration of the injected solution when the MIP solid phase is completely saturated. The breakthrough volume (V_R) is the eluted volume for which a low fraction of the analyte emerges from the column. Various numerical models have been proposed for the breakthrough curves, based on adsorption isotherms as the Langmuir isotherm, giving a good reproduction of the elution profiles [173-175]. The retention volume (V_R), corresponding to the inflection point of the bt curve and the mass transfer kinetics which determines its shape depends on thermodynamic parameters.

A similar but simpler model is applied for describing the elution profile [176-178]. Two macroscopic parameters characterize the BT curves, related respectively to the adsorption equilibrium and kinetics, as in the model mentioned above. The first one is the retention volume (V_R), i.e. the volume required to half of the original analyte concentration to emerge from the column [179-181]. It is related to the distribution coefficient D by the following relationship (Eq.14) [182]:

$$V_R = V_m + DV_s \quad \textit{Eq. 14}$$

this relation has been successfully used in several chromatographic techniques, as for example for the reversed phase partition chromatography [183]. D is the distribution coefficient, i.e. the ratio of the concentration of the analyte in the solid phase (in mmol/mLs) and in the solution (in mmol/mL). Vm and Vs are the mobile and solid phase volume in the column.

The distribution coefficient is an equilibrium parameter, describing the distribution equilibrium between two phases, which is most often obtained by the Langmuir isotherms. However the parameters of the Langmuir equation depend on the conditions, so they are not really predictive.

The simplified Thomas and Adams-Bohart models have been successfully used to describe the sorption in different systems as for example neutral molecules (phenol) on activated sludge [184], and metal ions on strong cation exchanging resins [177].

In this case, it has been assumed that the rate determining step of the sorption process of the analyte in the ion exchange resin is [177-178]:

$$2\bar{B} + M^{2+} \leftrightarrow \bar{M} + 2B^{+} \qquad \textit{Eq 15}$$

M is the free ion metal and $\bar{M}$ is the portion of metal adsorbed in the resin; B is the cation exchanged in the resin.

Analogously, assuming that the MIP behaves like a complexing resin the BT curve can be modelled by the proposed relation and the parameters of the adsorption equilibrium and kinetics can be obtained as exposed by Pesavento et all. [185]. So the relationship relating the eluted volume V with the concentration is [177-178]

$$\frac{C}{C_0} = \frac{1}{1+exp\left[\left(\frac{k\times C_0}{Q}\right)\left(\left(\frac{q_e\times w}{C_0}\right)-V\right)\right]} \qquad \textit{Eq. 16}$$

C is the analyte concentration at eluted volume V, C_0 is the injected concentration (mmol mL^{-1}, ug ml^{-1} (mg/L)…), w is the amount of MIP resin in the column (ml_{res}=g_{res}/$d_{res.}$) it corresponds to Vs in eq.14 , Q is the volumetric flow rate (mL min^{-1}) and q_e (mmol ml_{res}^{-1}) is the analyte concentration in the resin (MIP) at the equilibrium with the concentration C_0 in the solution.

Equilibrium parameter: $q_e w / C_0$ (mL) is the volume for which $C/C_0 = 0.5$, i.e. the retention volume $V_{0.5}$. It is related to the distribution coefficient D (ml/ml_{res}= ml d_{res}/g_{res}; d_{res} is the density of the resin in g/ml) by the following relationship:

$$V_{0.5} = \frac{q_e w}{C_0} = DV_s \qquad \textit{Eq. 17}$$

which is equal to Eq.15 if V_m is negligible with respect to DV_s, as it is usually the case.

Kinetic parameter: kC_0/Q, depends on the adsorption kinetics. kC_0 has the dimension of a first order rate constant (min^{-1}).

The adsorbing capacity of the column in flow conditions is determined from the inflection of the breakthrough curve.

2.3.3 CHARACTERIZATION OF ADSORPTION ON MIP LAYER BY ELECTROCHEMICAL SENSOR

An electrochemical sensor is a sensor that uses an electrode as a transducer, so the signal can be a potential, a current or an impedance depending on the technique used for transduction. Electrochemical sensors have high sensitivity, ease of use and low cost. They are chemically modified electrodes (CME), at the surface of which some species capable of interacting with the desired analyte are fixed [57].

Intensive research in the field of sensors based on MIP has been carried out in the Department of Chemistry of the University of Pavia. MIP sensors have been developed for the determination of atrazine and dopamine by potentiometric transduction [131, 186] and for the determination of 2,4,6 trinitrotoluene (TNT) by voltammetry [57]. In the case of dopamine and TNT, MIP was deposited on screen printed cells (SPC). The possibility of using the sensor approach for the characterization of adsorption characteristics of MIPs has been demonstrated [57].

In MIP sensors a signal from a variation in the physical properties of the receptor layer is measured, which is directly related to the binding event of the analyte in the receptor layer. The relation between the concentration of the analyte absorbed [RA] and the signal S is given by the following equation:

$$S=k[RA] \qquad \textit{Eq. 18}$$

According to eq. 19, the Langmuir equation (eq.9) can be transformed in the following way:

$$S = \frac{kK_{aff}c_R[A]}{1+K_{aff}[A]} \qquad \textit{Eq. 19}$$

A common linearization form of the equation reported above for the Langmuir model (Scatchard model) is:

$$\frac{i_p}{[A]} = kK_{aff}c_R - i_pK_{aff} \qquad \textit{Eq. 20}$$

It is possible to evaluate K_{aff} but not C_R, at least if k (the proportionality constant of the signal) is unknown. The maximum signal is obtained when [A]>>K_{aff}, so the relation can be simplified and the signal is constant in function of increasing concentration, $S_{max}=kc_R$. When [A] is much lower than K_{aff} the relation between S and [A] is linear.

In this work the MIP interactions with the template have been investigated by the electrochemical sensor approach. The sensor is created in a simple way by depositing a MIP layer over the electrochemical cell. The signal is the peak current (i_p) obtained by voltammetry, which is directly proportional to the analyte concentration in the layer near to the working electrode. This method make it possible to study the MIP exactly in the form of a thin layer as it is used in the optical devices investigated in the present work. On the contrary the batch equilibration method described above requires MIPs in small particles, i.e. in a completely different shape. Another advantage with respect to other investigation methods as for example the batch equilibration, consists of a noticeable improvement of the detection limits, due to the fact that the template is preconcentrated at the electrode surface when it combines with the imprinted sites. As a proof of principle, 2-FAL and Nicotine were considered as template in water or in complex aqueous matrices (i.e. synthetic wine). These substances present an electrochemical activity which can be used for analytical purposes.

The voltammetric SPC-MIP sensor is based on a commercially available screen printed cell, with graphite ink working and auxiliary electrodes, and a silver ink quasi-reference electrode (Figure 35). The analysis was performed by square wave voltammetry (SWV), so the peak current is evaluated in function of concentration [57].

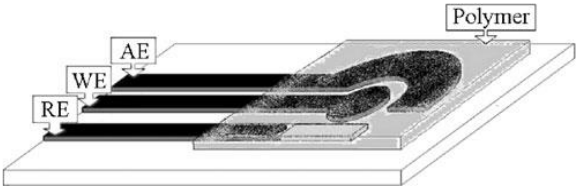

***Figure 39**. Voltammetric sensor based on MIP on screen printed cell (SPC)*

The condition employed for the electrochemical of 2-FAL and Nicotine analytes on the screen-printed cell are listened:

<u>Reduction of the 2-FAL:</u>

(Instrument: Palmsense)

CV:

E_vtx1	0 V	**E_start**	0 V	**scanrate**	0.1 V/s	**N_scans**	5
E_vtx2	-2 V	**E_cond**	0 V			**t_cond**	0 s
E_step	0.01 V	**E_dep**	0 V			**t_dep**	0 s
						t_equi	2 s

SWV:

E_begin	0 V	**E_cond**	0 V	**Freq**	22.5Hz	**t_cond**	0 s
E_end	-2 V	**E_dep**	0 V			**t_dep**	0 s
E_step	0.03 V					**t_equi**	2 s
E_pulse	0.065 V						

Oxidation of L-Nicotine:

(Instrument: Metrohm 757 VA Computrace)

CV:

E_vtx1	0 V
E_vtx2	2 V
E_step	0.01 V

E_start	0 V
E_cond	0 V
E_dep	0 V

scanrate	0.1 V/s

N_scans	5
t_cond	0 s
t_dep	0 s
t_equi	2 s

DPV:

E_begin	0.5 V
E_end	1.2 V
E_step	0.01 V
E_pulse	0.025 V

E_cond	0 V
E_dep	0 V

scanrate	0.1 V/s
t_pulse	0.09 s

t_cond	0 s
t_dep	0 s
t_equi	2 s

2.4 SYNTHESIS OF IMPRINTED COPOLYMERS

During this thesis work, MIPs have been synthesized as thin layers to be used in direct connection with the optical transducers considered, but also as bulk solids in several forms with the aim of a better characterization of the properties of the polymers. MIPs were synthesized as non-porous and porous bulk polymer and beads; while NIP only in the form of the porous bulk polymer. The molar composition used, was the same previously proposed for other MIPs (1:4:40 = template:functional monomer:cross-linker), already successfully employed for sensing applications [10; 135]. Moreover, two different cross-linkers have been considered. Bulk polymers have been synthesized, both in porous and non-porous form, for DBDS and 2-FAL. MIPs, as a bulk polymer layer, were synthesized on sensors for DBDS, 2-FAL, and Nicotine.

The prepolymer mixtures had the following compositions:

For **DBDS:**

- DVB (cross-linker, CL), methacrylic acid (functional monomer, MAA), DBDS and AIBN (radical initiator) at molar ratios 1: 4: 40 = TEMPLATE: MAA: CL.
- EGDMA (cross-linker, CL), methacrylic acid (functional monomer, MAA), DBDS and AIBN (radical initiator), at molar ratios 1: 4: 40 = 2-FAL: MAA: CL

For **2-FAL**:

- DVB (cross-linker, CL), methacrylic acid (functional monomer, MAA), 2-FAL and AIBN (radical initiator), at molar ratios 1: 4: 40 = 2-FAL: MAA: CL
- EGDMA (cross-linker, CL), methacrylic acid (functional monomer, MAA), 2-FAL and AIBN (radical initiator), at molar ratios 1: 4: 40 = 2-FAL: MAA: CL

For **NICOTINE**:

- DVB (cross-linker, CL), methacrylic acid (functional monomer, MAA), Nicotine and AIBN (radical initiator), at molar ratios 1: 4: 40 = 2-FAL: MAA: CL

Before any synthesis , the cross-linker and the functional monomer were purified by an alumina column, in order to eliminate the polymerization inhibitors (quinones, hydroquinones). Different forms of the polymer have been obtained using different % of solvent (acetonitrile, AcN) during the polymerization.

2.4.1 MIP BULK

The non-porous bulk MIP was the first type of polymer synthesized since the previous application for sensing purposes demonstrated the effectiveness of this type of formulation as a receptor layer [10; 135]. The procedures for the different templates are here reported:

DBDS:

- **Prepolymer mixture:** in a test tube, 1.156 mL of DVB crosslinker have been added to 55 µL of functional monomer MAA; the solution was deaerated with nitrogen for about 5 minutes. In case of EGMA as CL 1.224mL has been used. Subsequently, 40 mg of DBDS (0.162 mmol) was added to the solution and the solution was stirred until complete dissolution. Finally, 17 mg of AIBN (0.105 mmol) was added and dissolved. Not any porogen solvent was used in the prepolymer mixture. All the components were sufficiently soluble in DVB at the suggested proportions.
- **Polymerization:** The prepolymer mixture was thermally polymerized at 75 °C for 16 hours, in an open container.
- **Recovery:** At the end of the polymerization, the MIP results as a massive block (bulk) of transparent yellow glassy appearance. The polymer mass was recovered and finely grounded in a mortar. The mass of the MIP product was almost equal to that of the prepolymer mixture. In sensors, MIP results as a uniform layer (bulk) of transparent glassy appearance which covers the sensing area of the sensor.

2-FAL:

- **Prepolymer mixture:** in a test tube, 688µL of DVB cross-linker has been added to 41µL of functional monomer MAA; the solution was deaerated with nitrogen for about 5 minutes. In the case of EGMA as CL 911 µL has been used. Subsequently, 10µL of 2-FAL (0.121 mmol) was added to the solution and the solution was stirred until complete dissolution. Finally, 15 mg of AIBN (0.09 mmol) was added and dissolved. Not any porogen solvent was used in the prepolymer mixture. All the components were sufficiently soluble in DVB at the suggested proportions.

- **Polymerization:** The prepolymer mixture was thermally polymerized at 75 °C for 16 hours, in an open container.
- **Recovery:** At the end of the polymerization, the MIP results as a massive block (bulk) of transparent yellow glassy appearance. The polymer mass was recovered and finely grounded in a mortar. The mass of the MIP product was almost equal to that of the prepolymer mixture. In sensors, MIP results as a uniform layer (bulk) of transparent glassy appearance which covers the sensing area of the sensor.

NICOTINE:

- **Prepolymer mixture:** in a test tube, 0.709 mL of DVB crosslinker has been added to 42 µL of functional monomer MAA; the solution was deaerated with nitrogen for about 5 minutes. Subsequently, 20µL of Nicotine (0.124 mmol) was added to the solution and the solution was stirred until complete dissolution. Finally, 15 mg of AIBN (0.09 mmol) was added and dissolved. Not any porogen solvent was used in the prepolymer mixture. All the components were sufficiently soluble in DVB at the suggested proportions.
- **Polymerization:** The prepolymer mixture was thermally polymerized at 75 °C for 16 hours, in an open container.
- **Recovery:** At the end of the polymerization, the MIP results as a uniform layer (bulk) of transparent yellow glassy appearance which covers the sensing SPC electrodes.

2.4.2 POROUS BULK MIP AND NIP

DBDS:

- **Prepolymer mixture:** 0.5 mL of the prepolymer MIP DBDS mixture, prepared in the same way as that for the non-porous bulk MIP, was added with 1 mL of acetonitrile, as a porogenic solvent (67% of the final mixture). The solution was deaerated with nitrogen for 5 minutes; finally, 7 mg of AIBN was added and completely dissolved.
- **Polymerization:** the prepolymer mixture solution was placed in an oven at 75 ° C for 15 hours, in an open glass test tube.
- **Recovery:** the polymerization produced a non-homogeneous solid with a glassy layer on the surface and white, fine particles internally. This effect is probably due to the slower evaporation of the solvent in the internal mass.

The second portion of porous MIP had been synthesized with the same procedure, with the addition of a higher amount of solvent, at 75% as the final percentage. The solid obtained was similar to that previously synthesized.

2-FAL:

- **Prepolymer mixture:** 0.5 mL of the prepolymer mixture bulk MIP-2-FAL, was added with 1.5 mL of acetonitrile (75% of the final mixture), as a porogenic solvent (solvent volume/prepolymer mixture volume= 3). The solution was placed under nitrogen for about 5 minutes; 13mg of AIBN (0.07854mmol) were then added and completely dissolved.
- **Polymerization:** Finally, the prepolymer mixture solution was placed in an oven at 75 ° C for 15 hours, in an open glass test tube.
- **Recovery:** the polymerization produced a non-homogeneous solid with a glassy layer on the surface and white, fine particles internally. This effect is probably due to the slower evaporation of the solvent in the internal mass.

NIP:

The NIP (non-imprinted polymer) was synthesized in the same way and under the same conditions, but without analyte (i.e. DBDS or 2-FAL). The polymerization produced a non-homogeneous solid with a glassy layer on the surface and white, fine particles internally, visually very similar to the MIPs described above.

2.4.3 MIP BEADS

MIP as spherical microparticles was obtained by precipitation polimerization [187-189]. The same solution prepared for the porous bulk MIP, described above, was thermally polymerized in a closed container for 16 hours at 72 °C. The MIP synthesized appears as a fine white powder dispersed in the solvent. The particles were separated according to their size by decanting. A larger amount of porous solvent was used in case of EGDMA cross-linker than with DVB to obtain disaggregated particles.

2.4.4 MIP LAYER

- *MIP LAYER INTEGRATED IN OPTICAL SENSORS*

The thin MIP layer over the transduction devices was obtained by dropping 40µL of the not porous bulk-MIP prepolimer mixture (par. 2.4.1.) over the sensing surface and spinning at 750 rpm for 2min. Thermal polymerization was then carried out for 14 h at 72 °C in the air [1-2]. The gold planar surface on the chip (SPR active surface) was washed with ethanol and dried in a thermostatic oven at 60 °C prior to the prepolymer mixture deposition over the sensing region (gold film). The template was extracted by successive washings with EtOH 96%.

The NIP layer was obtained with the same procedure used for the MIP layer.

- *MIP LAYER DEPOSITION ON ELECTROCHEMICAL DEVICES (SPC)*

8 µl of prepolymer mixture was dropped over the whole SP cell and polymerized at 72°C in an oven (in air). The template was extracted by successive washings with EtOH 96%. Thermal polymerization was then carried out for 14 h at 72 °C [57]. The three electrodes of SPC are completely covered with a thin layer of MIP. In this way, the "electrolytic medium" is the polymeric layer, which at the same time ensures the selectivity.

3 RESULTS

3.1 MOLECULAR IMPRINTEDN SYNTHETICAL CO-POLYMERS

3.1.1 COMPUTATIONAL MODELING FOR IMPRINING EVALUATION

Computational method (Gaussian 09) has been used to test the interaction between functional monomer and template with the hybrid function at B3LYP / 6-311 + G ** level. The calculation was refined in a Continuous Model of Polarization (PCM) to evaluate the solvent effect.

The calculation was performed only on DBDS, since for the other analytes, 2-FAL, and nicotine, previously considerations were done on the prepolymer mixture, which lead to a successful MIP receptor [57; 135].

In the case of DBDS, two different functional monomers have been considered, MAA and VPy. It has been found that the interaction between MAA and DBDS takes place through hydrogen bonding, while other interactions are not relevant, at least in a low polarity solvent. This could be not true in a solvent with high polarity. VPy showed no significant interaction. Moreover, it was found that the crosslinker EGDMA is not suitable for this analyte, since it creates more stable hydrogen bonds with the functional monomer than with DBDS, thus hindering the proper formation of the complex. This effect has been confirmed by experimental results. Therefore, DVB was selected as a cross-linker in the case of DBDS. In the case of furfural, both DVB or EGDMA can be used. An analog of cross-linker (DVB or EGDMA) was considered as the solvent since this is employed in the synthesis as a solvent.

The most common formulation of MIPs considered in the present work is based on methacrylic acid (MAA) as the functional monomer. This functional monomer was selected since already successfully employed for an analyte in insulating transformer oil, i.e. 2-FAL [19]. It must be underlined that DBDS is a molecule with highly hydrophobic properties and low polarity. Different functional monomers have been considered, i.e. Vinyl pyridine (even in the protonate state).

Consequently, a computational method by the Gaussian program has been employed by the hybrid functional “B3LYP”, in which the electronic energies were calculated through the density functional theory. The calculation was made with the hybrid function at B3LYP / 6-311 + G ** level which

considers Non-covalent interactions (such electrostatic or hydrogen bond) between MAA and the template molecule (DBDS). The Geometry optimization was performed at the B3LYP/6-31G(d) level. The binding energy of template–monomer complexes, ΔE, was calculated as previously described (1.2.2.).

The sketches of the adducts in the more stable optimized configuration calculated are reported in Fig 40.

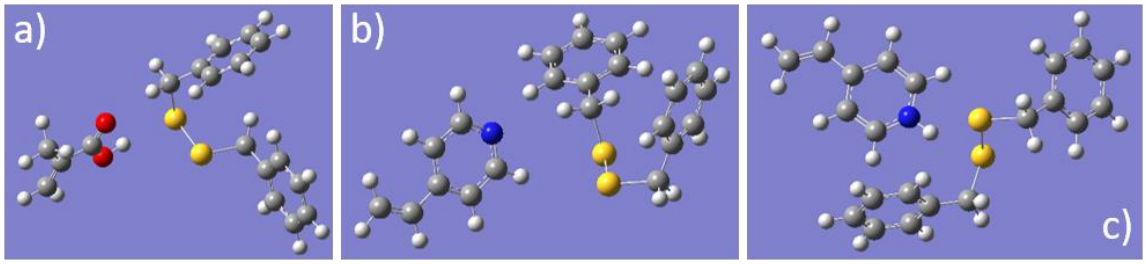

Figure 40: Adducts in the more stable configuration calculated by DFT method. a) MAA-DBDS b) 4-Vpy-DBDS, c) 4-Vpy⁺-DBDS

The related stabilization energy of the adducts calculated is reported as an example in the following Table 14:

Table 14. Interaction energies for adduct template- functional monomer. The interaction energies are expressed in kcal mol^{-1}

Stabilization Energies of Adducts

Complex	GAS (kcal/mol)	ACN (kcal/mol)
DBDS-MAA	-7.39	-1.85
DBDS-VPy	-3.74	0.78
DBDS-VPy+	-17.11	1.55

It was found that the interaction between MAA and DBDS takes place through a hydrogen bond, in a solvent with low polarity; while other types of hydrophobic interactions, π-π stacking, etc., are not found to be relevant even at an intramolecular level.

Among other reasons, EGDMA is considered as cross-linker due to the RI lower than DVB, which could be useful in SPR. Since the polar nature of EGDMA and MAA, the possible interaction of the

two compounds have been investigated as reported in Figure 41 and the results are shown in the relative Table 15.

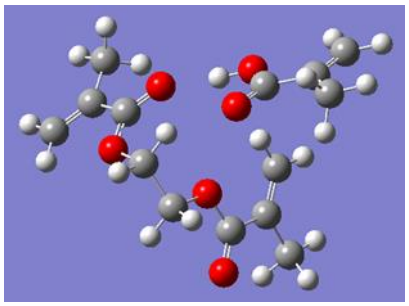

Figure 41. Adducts EGDMA-MAA calculated by DFT method.

Table 15. Interaction energies for EGDMA cross-linker and MAA monomer. The interaction energies are expressed in kcal mol^{-1}.

Stabilization Energy of the adduct		
Complex	GAS (kcal/mol)	ACN (kcal/mol)
EGDMA-MAA	-10.89	-3.00

As it can be clearly seen, EGDMA gives stronger interaction with MAA than DBDS, hindering the formation of complex MAA-template so finally only DVB was used. Another functional monomer, the vinylpyridine in its protonated state, was considered instead of MAA but weaker interactions were found than using MAA, so it was not considered anymore.

This also indicates that the formation of 1:2 complexes could be expected since two sulfur atoms are present in DBDS. Notice that the formation of a 1:2 complexes have been shown to considerably decrease the energy of the system [60-61]. Further investigation on this point will be performed by mechanical computation.

The evaluation of the solvent effect by the refinement of the calculation with the Continuous Model of Polarization (PCM) for the adduct DBDS-MAA is reported in Table 16 considering solvents of different polarity.

Table 16. Stabilization energy of the adduct DBDS-MAA in solvents with decreasing polarity

MAA-DBDS Stabilization energy in solvents with decreasing polarity				
Complex	GAS (kcal/mol)	ACN (kcal/mol)	EtOAc (kcal/mol)	C_6H_6 (kcal/mol)
DBDS-MAA	-7.39	-1.85	-2.48	-3.46

It has been found that the stabilization of the adduct DBDS-MAA, with respect to individual moieties (MAA and DBDS), is significant in the vacuum, but not significant in a polar solvent like acetonitrile. The important point is that despite the low polarity of DBDS, an interaction takes place with the considered functional monomer at least in a low polarity solvent. This could be not true in a solvent with high polarity as acetonitrile. Thus, it could be used for the washings. It must be underlined that the solvent in which the coordination of the functional monomer around the template actually takes place, when not any porogen solvent is used, is the cross-linker itself, the polarity of which is pretty low, ensuring the formation of the pre-assembly. As a matter of fact, the cross-linker represents a large part of the polymeric structure, being present at a molar ratio 10:1 with respect to the functional monomer, and 40:1 with respect to the template.

3.1.2 CHARACTERIZATION OF MORPHOLOGY AND MICROSTRUCTURE

Different kinds of MIPs have been synthesized, considering different cross-linkers (DVB and EGDMA) and variable percentage of porogenic solvent AcN. Moreover, MIPs have been prepared in different forms. The polymers synthesized in during this research work were analyzed by optical microscopy and scanning electron microscopy.

3.1.2.1 Bulk MIP

The not-porous Bulk-MIP-DVB-DBDS was synthesized using the bulk polymerization method described above (2.4.1.). The obtained polymer is finely ground into a mortar. Figure 42 shows the pictures of the non-porous bulk MIP imprinted for DBDS after the synthesis a) and after the grinding process in an agate mortar b). An image of the ground Bulk-MIP-DVB-DBDS particles by an optical microscope is shown c).

Figure 42. *Images of the Bulk-MIP-DVB-DBDS a) after polymerization in the oven; b) ground; c) ground powder by an optical microscope with 10x magnification.*

A glass-like polymer is formed, with some cracks due to the rapid evaporation of the solvent during the polymerization.

Figure 43 shows two pictures of the surface shape and details magnification of the Bulk-MIP-DVB-DBDS by electronic scanning microscope: one with a 250x magnification and one with a 20.00Kx. This image shows a very low porosity onto the surface.

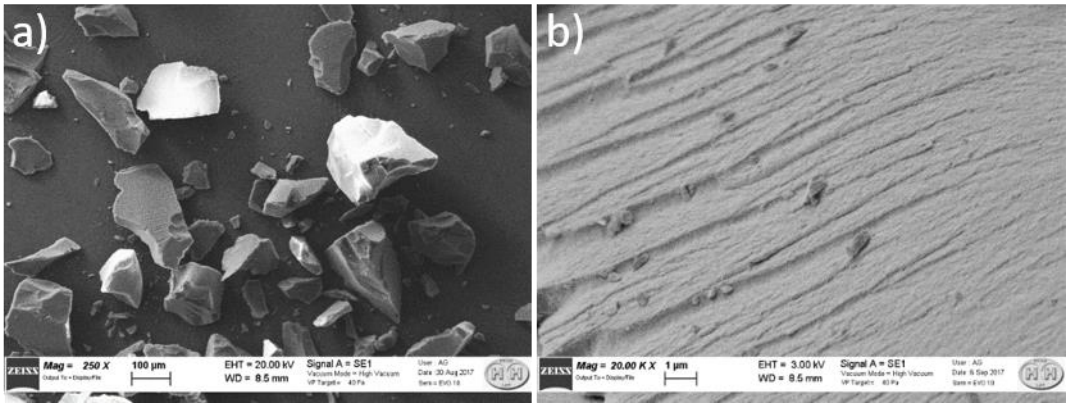

Figure 43. *SEM images of Bulk-MIP-DVB-DBDS: a) at 250x magnification; b) at 20.00Kx magnification.*

3.1.2.2 Porous MIP

- **Porous-MIP-DVB-DBDS1:**

The porous bulk MIP-DVB imprinted for DBDS was synthesized using the polymerization method described above (2.4.2.). The obtained polymer is finely ground into a mortar. Figure 40 shows the pictures of the Porous-MIP-DVB-DBDS after the synthesis a) and after the grinding process in an agate mortar b). An image of the ground Porous-MIP-DVB-DBDS particles by an optical microscope is shown c).

Figure 44. *Images of the Porous-MIP-DVB-DBDS1 a) after polymerization in the oven; b) ground; c) ground powder by an optical microscope at 10x magnification.*

The formation of a glassy layer on the surface of the polymer is due to the rapid evaporation of the solvent during the polymerization. Internally, the polymer is a very fine white powder composed by a cluster of particles.

Figure 45 a) shows the SEM image of this polymer after a dimensional separation. The separation is carried out as follows: the polymer is placed in contact with different solvents and left to deposit by sedimentation. The opalescent supernatants containing the suspended particles of smaller dimension were eliminated in each sedimentation. The solvents employed were water, AcN, and EtOH. Subsequently, the last portion was filtered on Gooch G-3 from water, ethanol, and acetonitrile. The sedimented heavier particles were analyzed by SEM (Figure 45).

Figure 45 shows two pictures of the surface shape and details magnification of the dimensionally sieved powder of Porous-MIP-DVB-DBDS1 polymer by electronic scanning microscope: one with a

250x magnification and one with a 20.00Kx. It can be noted that the surface of this polymer is more porous than that of the polymer synthesized in absence of the porogenic solvent.

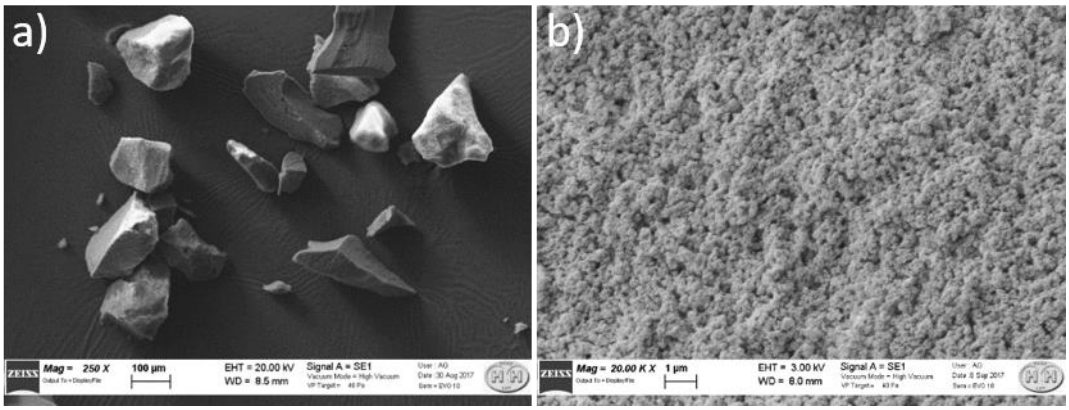

Figure 45. *SEM images of the Porous-MIP-DVB-DBDS1 after the sieving procedure a) at 250x magnification; b) at 20.00Kx magnification.*

- **Porous-MIP-DVB-DBDS2.**

The second portion of the Porous-MIP-DVB-DBDS was synthesized using the polymerization method described above (2.4.2.) in an open container. The obtained polymer is finely ground into a mortar. The images obtained by the optical microscope on the Porous-MIP-DVB-DBDS2 synthesized with a higher amount of porogen solvent in an open container, after the grinding process in an agate mortar, is shown in Figure 46.

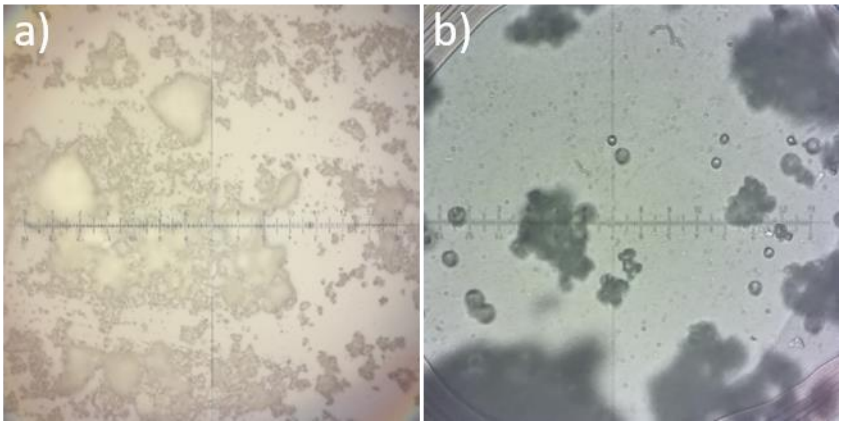

Figure 46. Images of the Porous-MIP-DVB-DBDS2 by optical microscope a) at 10x magnification; b) at 100x magnification.

From these images, it is possible to notice the difference found between this porous MIP (Porous-MIP-DVB-DBDS2) and the first one: at high magnification, spherical particles or their aggregates can be seen, with a lower glassy fraction compared to the previous one. This may be due to the fact that, with respect to the first polymerized porous bulk MIP, a higher amount of AcN has been added. If the evaporation rate is lower than the polymerization rate, maybe the first particles formed are precipitated in a spherical form in the solvent phase, as in the synthesis by precipitation polymerization in a closed tube for the MIP beads (see the 3.1.2.4 paragraph).

- **Porous-MIP-DVB-2-FAL**:

The porous MIP-DVB imprinted for 2-FAL was synthesized using the polymerization method described above (2.4.2.) in an open container. The obtained polymer is finely ground into a mortar. Figure 43 shows the pictures of the Porous-MIP-DVB-2-FAL after the synthesis a) and after the grinding process in an agate mortar b). An image of the ground MIP-DVB-2-FAL particles by an optical microscope is shown c).

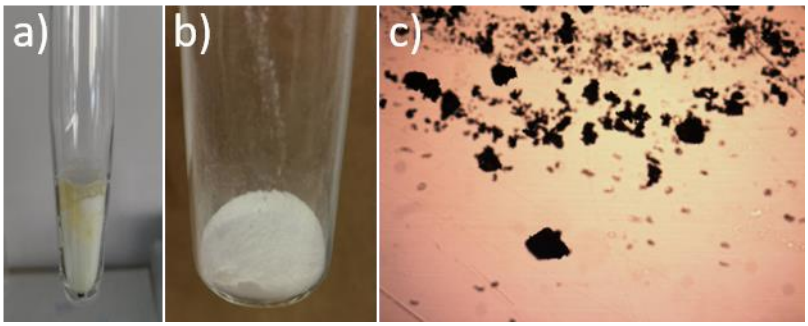

Figure 47. *Images of the porous-MIP-DVB-2-FAL a) after polymerization in the oven; b) ground; c) ground powder by an optical microscope at 200x magnification*

The formation of a glassy layer on the surface of the polymer is due to the rapid evaporation of the solvent during the polymerization. Internally, the polymer is a very fine white powder composed by a cluster of particles.

Figure 48 shows the magnified surface of the porous-MIP-DVB-2-FAL by SEM respectively at 100x magnification and 10.00Kx magnification. From the image, it is possible to notice the porosity of this type of polymer.

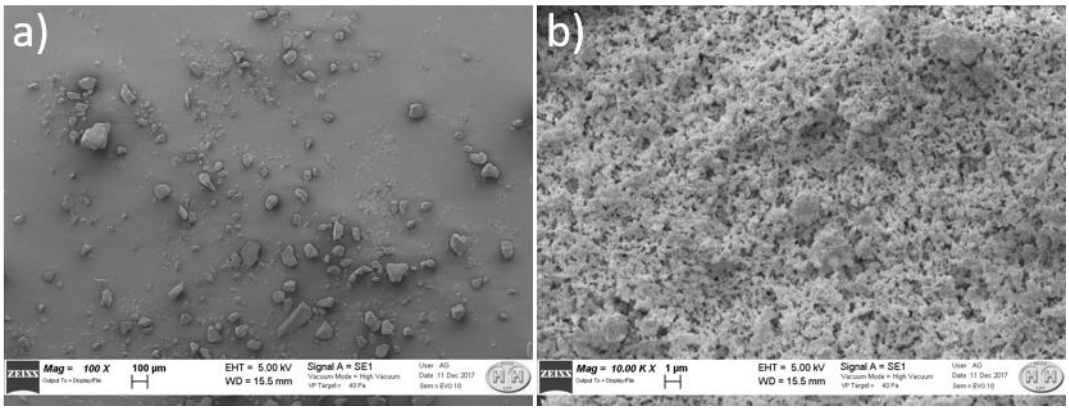

Figure 48. *SEM image of the Porous-MIP-DVB-2-FAL after the sieving procedure a) at 250x magnification; b) at 20.00Kx magnification.*

- **Porous-MIP-EGDMA-2-FAL1:**

The porous MIP-EGDMA imprinted for 2-FAL was synthesized using the polymerization method described above (2.4.2.) in an open container. The obtained polymer is finely ground into a mortar. Figure 49 shows the pictures of the porous-MIP-EGDMA-2-FAL1 after the synthesis a) and after the grinding process in an agate mortar b). An image of the ground MIP-EGDMA-2-FAL1 particles by an optical microscope is shown c).

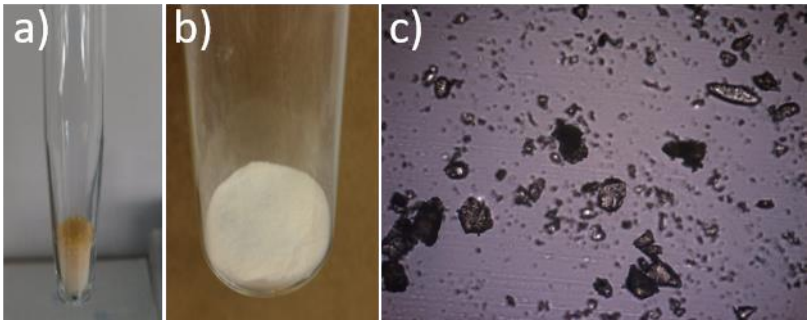

Figure 49. *Images of the porous-MIP-EGDMA-2-FAL1 a) after polymerization in the oven; b) ground; c) ground powder by an optical microscope at 200x magnification.*

The formation of a glassy layer on the surface of the polymer is due to the rapid evaporation of the solvent during the polymerization. Internally, the polymer is a very fine white powder composed by a cluster of particles.

Figure 50 shows the magnified surface of the porous-MIP-EGDMA-2-FAL1 by SEM respectively at 250x magnification and at 20.00Kx magnification. From the image, it is possible to notice the porosity of this type of polymer.

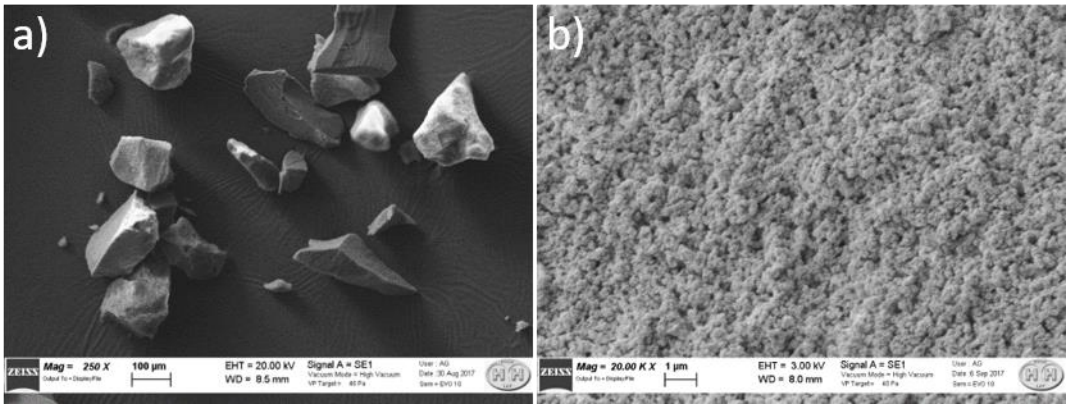

Figure 50. *SEM image of the porous-MIP-EGDMA-2-FAL1 after the sieving procedure a) at 250x magnification; b) at 20.00Kx magnification.*

The porous-MIP-DVB-2-FAL and the porous-MIP-EGDMA-2-FAL1 are morphologically very similar.

- **Porous-MIP-EGDMA-2-FAL2:**

The second portion of the porous-MIP-EGDMA imprinted for 2-FAL was synthesized using the polymerization method described above (2.4.2.) in a closed container. The obtained polymer is finely ground into a mortar. Figure 51 shows the pictures of the porous-MIP-EGDMA-2-FAL2 after the synthesis a) and after the grinding process in an agate mortar b). An image of the ground MIP-EGDMA-2-FAL2 particles by an optical microscope is shown c).

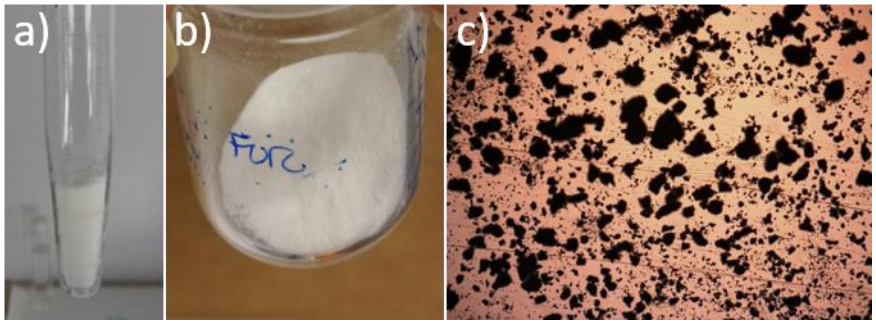

Figure 51. *Images of the porous MIP-EGDMA-2-FAL2 a) after polymerization in the oven; b) ground; c) ground powder by an optical microscope at 200x magnification.*

In this case, the formation of the glassy-like portion over the polymer was not observed, as it was for the porous-MIP-EGDMA-2-FAL1 with polymerization in an open vessel. Not any residual solvent was found in the container after the polymerization, which was probably absorbed into the porous structure of the solid. This phenomenon was verified by weighing the solid. The exceeding solvent in the polymer structure was eliminated by drying in the oven. The complete drying was verified by weighing the polymer powder after the treatment.

Figure 52 shows the magnified surface of the porous bulk MIP-EGDMA-2-FAL2 by SEM respectively at 500x magnification and at 20.00Kx magnification. From the image, it is possible to notice the porosity of this type of polymer.

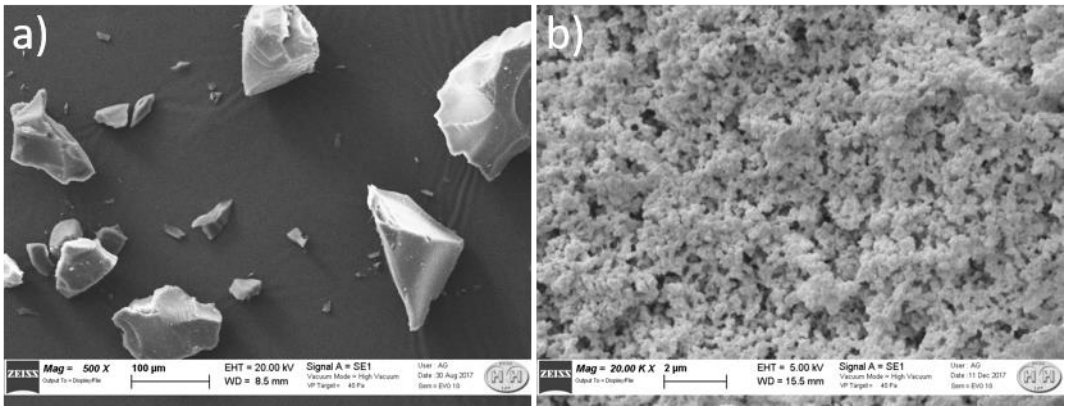

Figure 52. *SEM images of the porous MIP-EGDMA-2-FAL2 after the sieving procedure a) at 500x magnification; b) at 20.00Kx magnification.*

It is possible to notice that the ground polymer particles are not beads; moreover, high porosity is observed onto the surface, greater with respect to the porous-MIP-EGDMA-2-FAL1 previously described, ie. in the presence of a lower amount of solvent and polymerized in an open container.

3.1.2.3 Porous NIP

The porous bulk NIP-DVB was synthesized with the same procedure and conditions of the correspondent MIP-DVB, but without the analyte (DBDS or 2-FAL). NIPs obtained shows the same morphological characteristics of the correspondent MIP.

Figure 53 shows the pictures of the Porous-NIP-DVB after the synthesis a) and after the grinding process in an agate mortar b). An image of the ground Porous-NIP-DVB particles by an optical microscope is shown c)

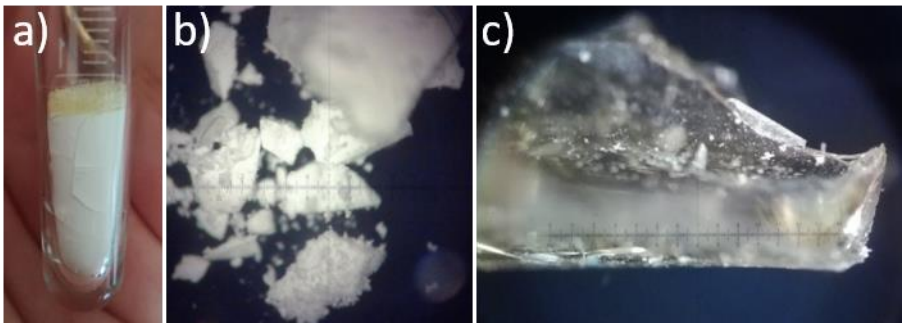

Figure 53. *Images of the Porous-NIP-DVB a) after polymerization in the oven; ground powder by an optical microscope b) at 10x magnification and c) at 100x magnification.*

3.1.2.4 Beads

- **Beads-MIP-DVB-DBDS:**

The Beads-MIP-DVB imprinted for DBDS was synthesized using the polymerization method described above (2.4.3.) in a closed container. The obtained polymer is finely ground into a mortar. Figure 54 shows the pictures of the Beads-MIP-DVB-DBDS after the synthesis 54a). An image of the Beads-MIP-DVB-DBDS particles by an optical microscope is shown 54b.

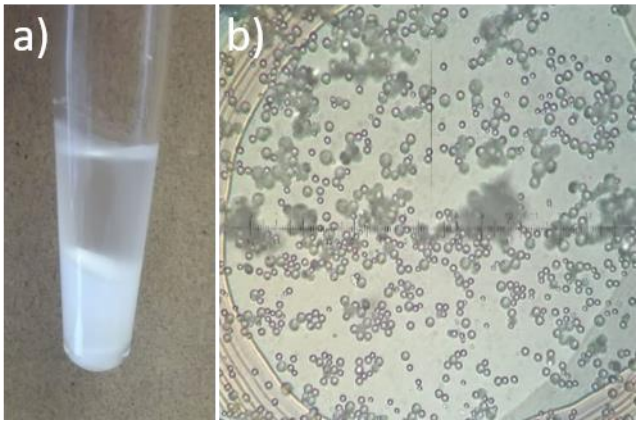

Figure 54. Image of Beads-MIP-DVB-DBDS a) after polymerization in the oven a); b) ground powder by an optical microscope at 100x magnification

From the image 54a. it can be noticed that the particles are precipitated in the reaction tube which still contains the solvent of polymerization. These particles are spherical 54b. and the surface is different porous bulk MIP obtained by the same prepolymer mixture but in an open container. This result is better shown in Figure 55, in which the SEM images are reported.

Figure 55 shows the magnified surface of the Beads-MIP-DVB-DBDS by SEM respectively at 5.00 kx magnification and at 20.00Kx magnification. From the image, it is possible to notice the shape, size and low porosity of this type of polymer.

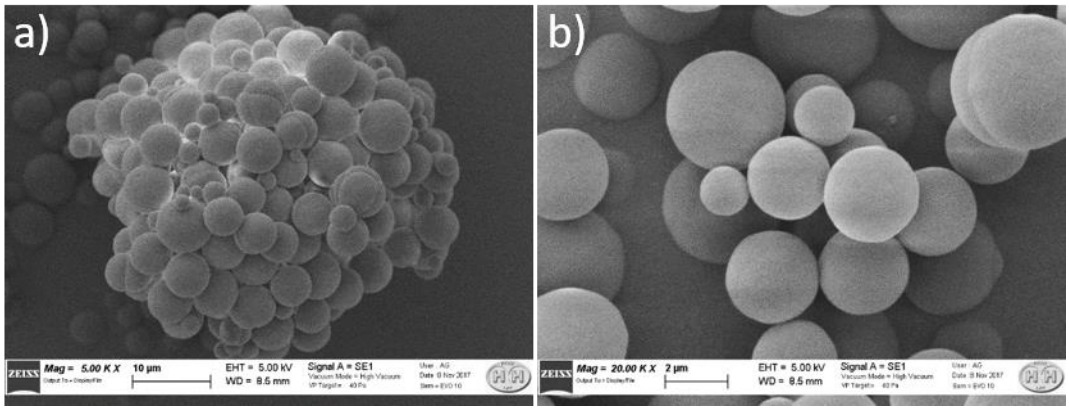

Figure 55.SEM images of the Beads-MIP-DVB-DBDS after the sieving procedure a) at 5.00 kx magnification; b) at 20.00Kx magnification

From the magnified images it is clearly seen that the surface of these particles is not porous. The particle size ranges from 0.2 to 5 µm.

- **<u>Beads-MIP-EGDMA-2-FAL:</u>**

The Beads-MIP-EGDMA imprinted for 2-FAL was synthesized using the polymerization method described above (2.4.3.) in a closed container. The obtained polymer is finely ground into a mortar. Figure 56 shows the pictures of the Beads-MIP-EGDMA-2-FAL after the synthesis 56a. An image of the Beads-MIP-EGDMA-2-FAL particles by an optical microscope is shown 56b.

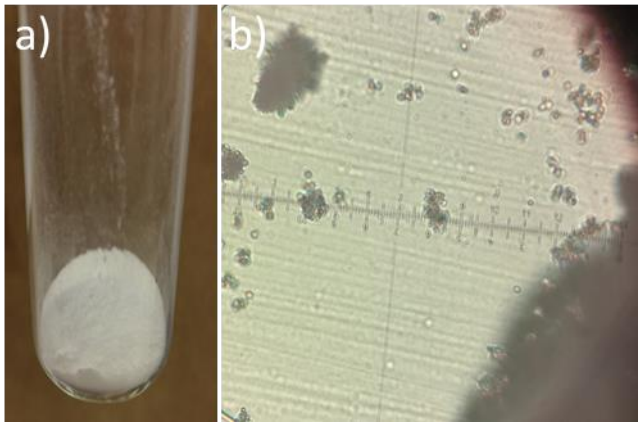

Figure 56. *Images of Beads-MIP-EGDMA-2-FAL: a) after polymerization in the oven a); b) ground powder by an optical microscope at 100x magnification*

From the image obtained under an optical microscope it can be seen that unlike other polymers, this MIP is in the form of beads. The largest particles are aggregates of beads. From the magnified images, shown in Figure 56b.

From the image 56. it can be noticed that the particles are spherical form the magnified image 56b, it seems, that the surface of these particles is not porous and with a glassy appearance as in the case of the Beads-MIP for DBDS prepared with DVB as cross-linker. The particle size instead is smaller than the Beads-MIP-DVB-DBDS (around 0.2 µm). This is evidently due to the different type of cross-linker employed, i.e. EGDMA instead of DVB.

From the optical microscope images, it can be seen that all the MIPs polymerized in a closed container with a sufficiently high amount of solvent have the form of beads. The largest particles

are aggregates of beads but the radius of the single beads is around 2µm. This particles size result too small for an application in SPE cartridges. However, even with this small size, the Beads-MIPs can be used for batch experiments and characterizations. Further study on the conditions for precipitation polymerization will be performed in order to increase the beads dimension. In parallel, other methods will be studied, i.e. surface imprinting.

3.1.3 MORPHOLOGY AND MICROSTRUCTURE ANALYSIS OF THE MIP LAYER ON TOP OF THE SENSOR

In Figure 57 a schematic picture of the sensing layer is reported. The MIP layer with its specific sites, the dielectric matrix containing the analytes and the gold film, needed to obtain the SPR phenomena, are shown.

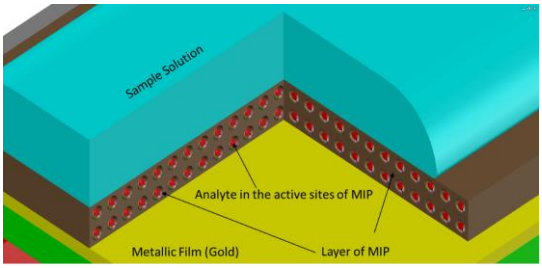

Figure 57. Schematic picture of the MIP sensible layer structure on the top of a sensor platform

The MIP layer was commonly obtained on optical platforms by the deposition of the bulk prepolymer mixture over the gold layer. The prepolymer mixture is spinned before polymerization.

Typical layer deposition on the Au surface of SPR sensors is reported. In Figure 58 the images of a Slab platform covered by a gold layer, 58a) before and 58b) after the MIP deposition are reported. A SEM image of the microstructure of the MIP over the gold layer is also shown 58c).

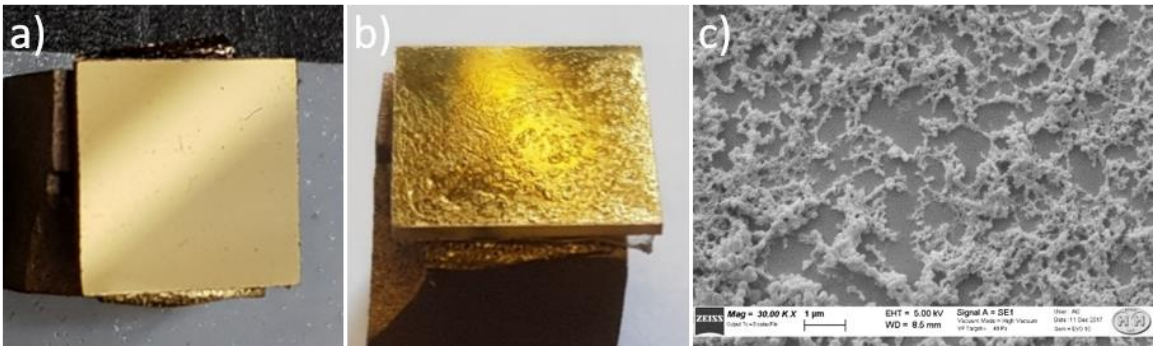

Figure 58. *Image of a Au-Slab a) before and b) after the MIP layer formation. A SEM analysis of a Bulk-MIP-DVB-DBDS layer, deposed on gold layer is reported.*

The spin coating deposition of the bulk MIP-DVB pre-polymeric mixture over an Au-platform lead to the formation of a thin layer of the polymer after the thermal polymerization. By the use of the bulk prepolymer mixture, as it is shown in the SEM image, the layer obtained is highly crosslinked but not completely homogeneous over the surface. This effect is probably due to the more rapid evaporation of the solution, during the thermal polymerization, with respect to the polymerization reaction.

3.1.4 WASHING PROCEDURE

A crucial step in MIP preparation is the extraction of the template from the solid polymer to expose the complementary structure of the imprinted sites and to eliminate the not-imprinted fraction by a washing procedure. At the same time, this washing step eliminates the non-fully polymerized monomers and/or oligomers which could interfere in the further employment of the polymer.

Washing was performed by simply contacting the solid with a proper solvent in the case of MIPs which employs non-covalent binding. However, the effectiveness of the procedure must be carefully studied to avoid any interference from the imprinted material. This control was made only on polymers in form of particles since a relatively large amount of material is required.

The study of the washing procedure for the particles was performed as it follows: the solid was weighed and placed in a glass container, provided with a plastic cap, containing a known volume of washing solution. The contact was maintained for about 10 hours, under stirring with a magnetic stir bar. The liquid phase was separated by centrifugation and analyzed, and the solid was extracted again with a new fresh solvent portion with the same procedure. The procedure was repeated until the complete washing was observed. The supernatants of the different portions were analyzed both spectrophotometrically and electrochemically, after appropriate dilution with the solvent.

- *Washing of MIP and NIP for DBDS*

The solvent used for the extraction of the template was typically EtOH, while the solvent employed in the analysis and dilution was AcN:EtOH=4:1.

Different conditions have been employed by varying the ratio of polymer quantity (mg) - the volume of extractant (mL) for example from 116.4 mg/mL, to 60mg/mL and 13.3mg/mL for the bulk MIP-DVB-DBDS, in order to find the best proportion.

For each washing portion, the absorbance at 270 nm was measured, after appropriate dilutions. As an example, the spectra of the subsequent washings of the porous MIP are reported in Figure 59.

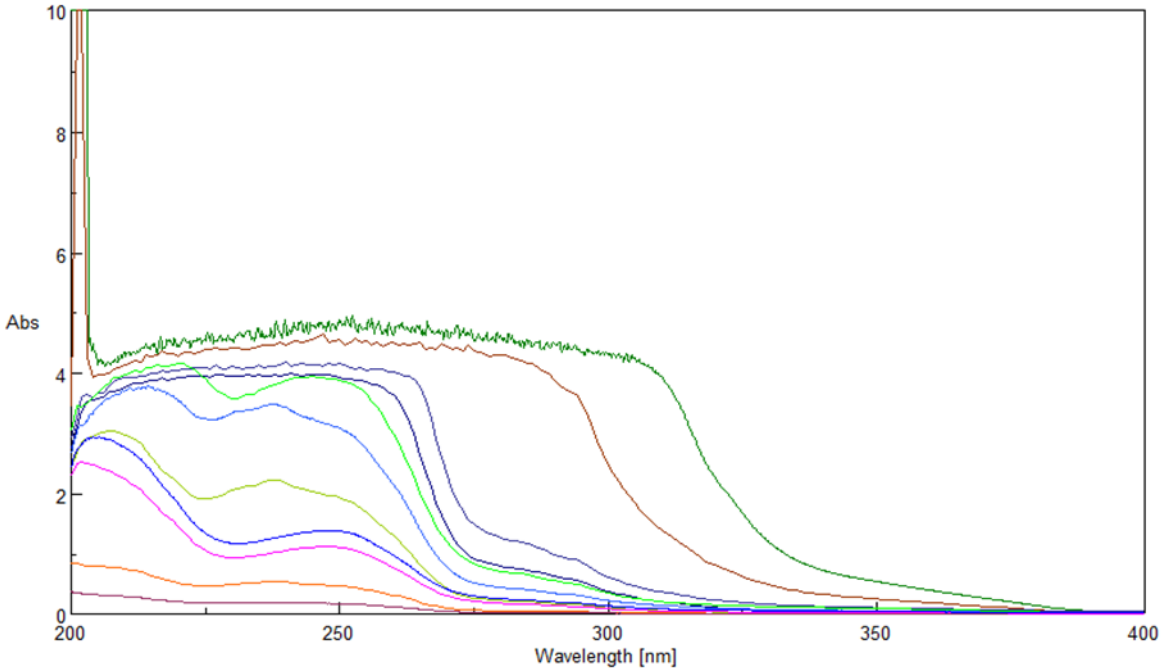

Figure 59. Spectra of the consecutive washings of porous MIP-DVB-DBDS2 at 60 $mg_{MIP}/mL_{solvent}$ ratio. I-II-III washing: ethanol 96 %; IV washing: AcN:EtOH=4:1; V-X washing: ethanol 98%.

An overview of the results obtained with different polymers is reported in the following Figure 60:

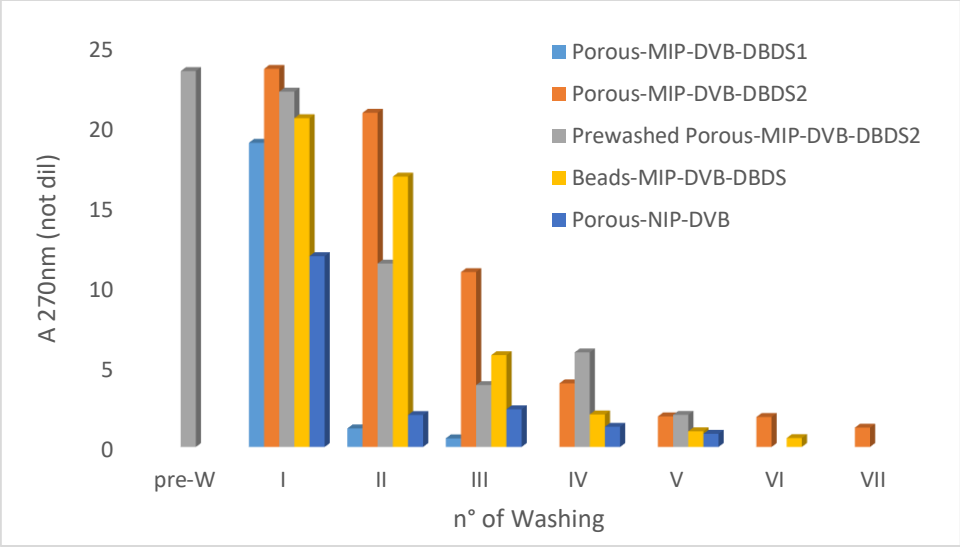

Figure 60. *Overview of the washings of different MIPs imprinted for DBDS and NIP, analyzed spectrophotometrically at 270 nm. $mg_{MIP}/mL_{solution}$: 13.3 porous MIP-DVB-DBDS1; 60 porous MIP-DVB-DBDS2; 60 pre-washed porous MIP-DVB-DBDS2, 60 Beads-MIP-DVB-DBDS, 13.3 porous NIP-DVB.*

The absorbance at 270nm is probably due to a large number of different compounds, in addition to DBDS, extracted with ethanol in the considered conditions. These are probably monomers or oligomeric fragments not completely polymerized, which have a certain solubility in the employed extraction solvent. Such components seem to prevent the quantification of DBDS by UV spectroscopy. Unfortunately, the same is true for the electrochemical analysis. The standard addition method applied to the first washing liquid showed a low sensibility and a negative ordinate at the origin even in highly diluted samples (1:50-1:100). After 2 or 3 washings the electrochemical sensibility obtained by the standard additions method, reach a similar value to that of the standardization curve, which means that the interfering substances are effectively washed out during the extraction of the template.

In conclusion, the effectiveness of the extraction procedure of the template can not be investigated by classical analytical methods, such as spectrophotometry and voltammetry. A different approach will be described below.

From the experimental data in Figure 60, it is seen that the use of only ethanol, like a washing solvent, is a good choice for washing since it extracts some interferents that are present in the polymer in only a few consecutive extractions. At the end of the process, the polymer can be

considered clean, presenting a very low UV and electrochemical signals, which do not interfere with the ensuing determinations.

In some trials, to confirm the complete extraction, further extraction has been performed in a different solvent (AcN, MeOH, Hexane, MeOH:CH_3COOH). In one case, with porous MIP-DVB-DBDS2, a pre-washing in AcN was made, which seems to extract a lower amount of compounds than the successive extractions with EtOH (Fig 60). It has been observed that the use of the acetonitrile-ethanol solution 4:1 in the washing results in the extraction of other interferents which are not washed out only by ethanol. This is clearly visible by comparing the spectra obtained with the two different washing solvents in Figure 56 and can be relevant when samples with this solvent are examined.

It can be noted that porous NIP-DVB releases a lower amount of substances than the corresponding MIP. This difference is only partially ascribable to the absence of DBDS in NIP and is probably due to the less porous structure of NIP than of MIP.

An important factor for an efficient extraction is the ratio mg of resin/ml of solvent and the structure of the resin.

The efficient template extraction could not be determined by the classical analytical methods, so this parameter was investigated by EXD analysis.

As an example, EXD analyses of bulk-DVB-DBDS before and after washing with ethanol are reported respectively in Fig 61 and in Fig 62:

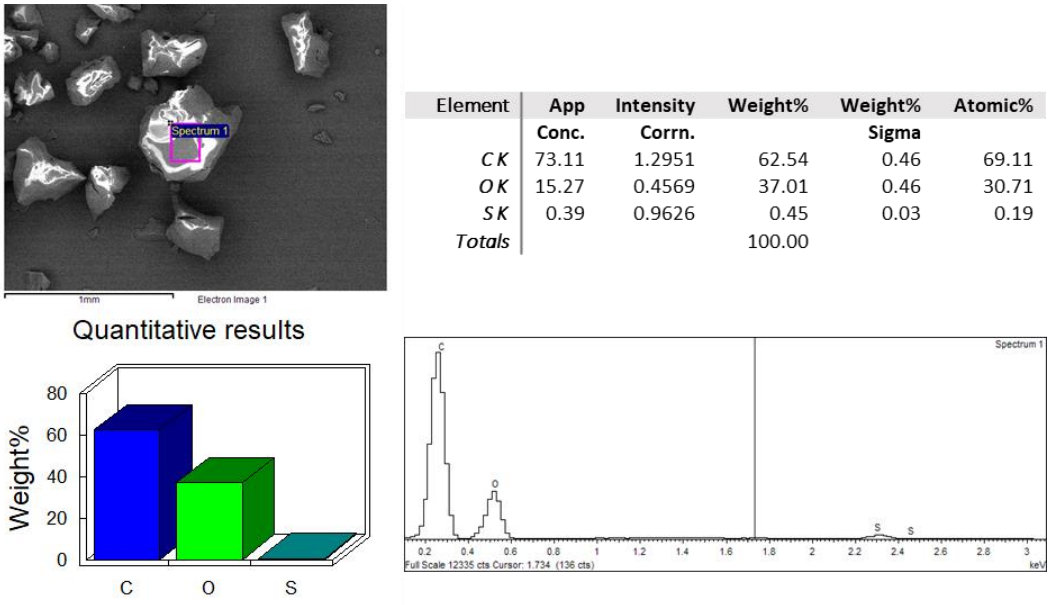

Element	App Conc.	Intensity Corrn.	Weight%	Weight% Sigma	Atomic%
C K	73.11	1.2951	62.54	0.46	69.11
O K	15.27	0.4569	37.01	0.46	30.71
S K	0.39	0.9626	0.45	0.03	0.19
Totals			100.00		

Figure 61. *EDX analysis of the bulk MIP-DVB-DBDS powder before the washing.*

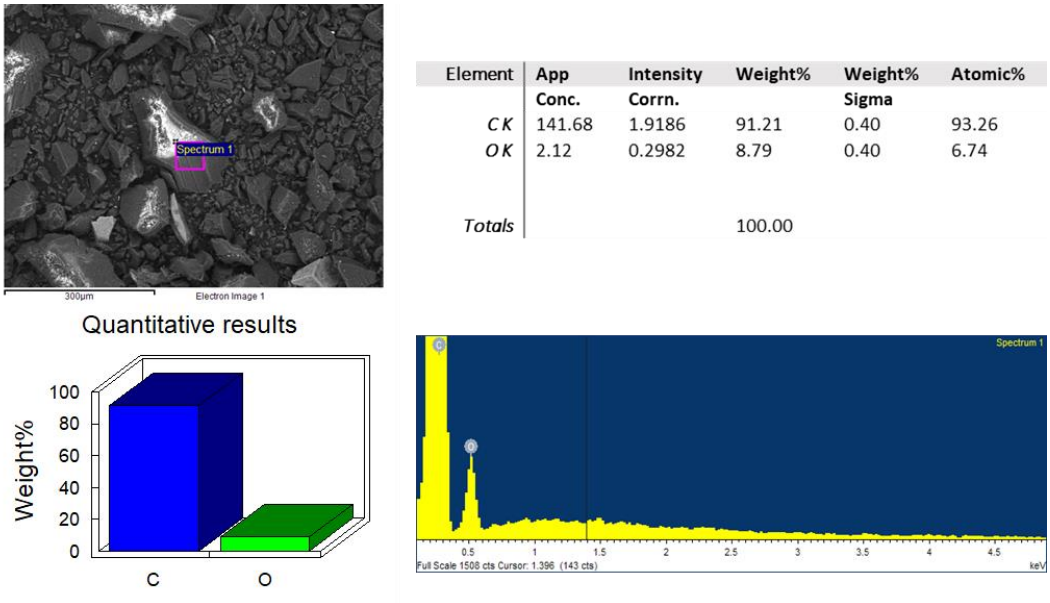

Element	App Conc.	Intensity Corrn.	Weight%	Weight% Sigma	Atomic%
C K	141.68	1.9186	91.21	0.40	93.26
O K	2.12	0.2982	8.79	0.40	6.74
Totals			100.00		

Figure 62. *EDX analysis of the powder bulk MIP-DVB-DBDS after the washing.*

The analysis was performed by following the Kα X-Ray emission of the S atom which is present only in the DBDS, the template compound. The EDX results show that after washing, only a small, practically negligible amount of S is present in the big agglomerate.

- *Washing of MIP and NIP for 2-FAL*

The solvent used for the extraction of the template was EtOH, while the solvent employed in the analysis and dilution was H_2O:EtOH=75:25. The washing has been performed maintaining the same ratio condition of polymer quantity (mg) - volume of extractant (mL) equal to 13,3 mg/mL. For each washing portion, the absorbance at 278 nm was measured, after appropriate dilutions. An overview of the results obtained with different polymers is reported in the following figure (Fig.63):

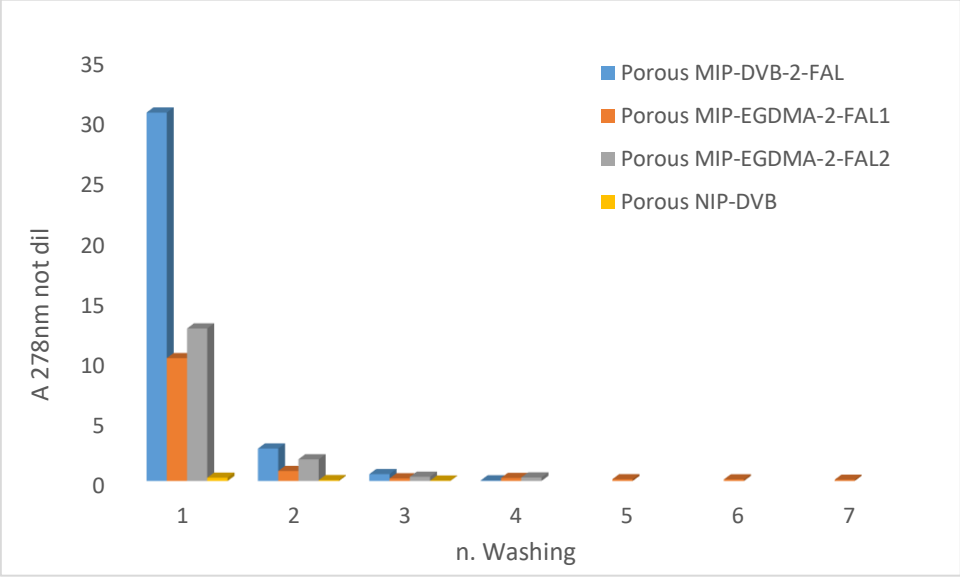

Figure 63. *Overview of the washings of different MIPs imprinted for 2-FAL and NIP, analyzed spectrophotometrically at 278 nm.* $mg_{MIP}/mL_{solution}$*: 13.3*

For all the fraction of MIP considered the total recovery is reported in table 17.

Table 17. *Value of recovery and absorbance of 2-FAL in the washing procedure with EtOH for the different MIP and NIP considered.*

Polymer Type	2_FAL Recovery %	A 278 (nm)
Porous MIP-DVB-2-FAL	97.7	30.6
Porous- MIP-EGDMA-2-FAL1	42.1	10.3
Porous-MIP-EGDMA-2-FAL2	52.6	13.0
Porous-NIP-DVB	0	0.271 (no peak)

The absorbance at 278nm is probably due to a large number of different compounds, in addition to 2-FAL, extracted with ethanol in the conditions considered. These are probably monomers or oligomeric fragments not completely polymerized, which have a certain solubility in the considered extraction solvent. Such components do not seem to interfere in the UV determination of 2-FAL, while they probably interfere in the SWV determination. The standard addition method applied to the first washing liquid showed a low sensibility and a negative ordinate at the origin even in highly diluted samples (1:50-1:100). After 2 or 3 washings the electrochemical sensibility obtained by the standard additions method rises up to a value similar to that of the standardization curve, which means that the interfering substances are effectively washed out during the extraction of the template.

According to the results of the spectrophotometric analysis, It should be noted that the recovery of 2-FAL obtained for MIP EGDMA is noticeably lower than that obtained for MIP-DVB. A very close quantity of 2-FAL has been recovered (11.39mg) in respect to that introduced for the imprinting (11.62mg) in case of MIP-DVB-2-FAL, with a recovery of 98%. The recovery was almost quantitative in the first extraction and in maximum three extractions it can be considered as complete. In some trials, to confirm the complete extraction, further extraction has been performed in a different solvent (AcN, MeOH:CH_3COOH).

In general, it was found as important factors the formulation of the resin, i.e. the cross-linker employed in the polymerization. Even the presence of the imprinted sites was found to be relevant in the capacity of retaining the analyte, as can be seen by the comparison between the extractions from the MIP and NIP.

The compounds extracted from the NIP gives an absorbance at 278nm considerably lower in respect to that of the corresponding MIP under similar conditions assimilable to 0. This is expected since the NIP does not contain 2-FAL. On contrary, at lower wavelengths, as for example at 210 nm, the A is remarkably high, demonstrating that even in the case of the NIP, various non-fully polymerized substances were released.

3.1.4.1 Washing of the MIP layer on the sensing platform:

The template was extracted from the polymer by ten washes with 96% ethanol [135]. In each washing operation, one drop of ethanol was contacted with the platform for a few seconds, and then fluxed away with fresh ethanol. The sensor was finally dried in an oven at 60°C.

Due to the very small amount of polymer in the sensing layer, it is evidently impossible to check the effectiveness of the washing procedure as reported in the case of the bulk equilibration procedure. However, the extraction of the template and of other components of the polymer soluble in the considered solvent can be checked by registering the sensor signal. As an example,

Figure 64 shows the normalized spectra of the SPR resonance obtained in the case of a D-shaped POF sensor with bulk MIP-DVB-2-FAL layer in H_2O before and after the MIP washing procedure. The spectrum obtained using the platform without MIP (bare platform) in water is reported for comparison in the same Figure 64.

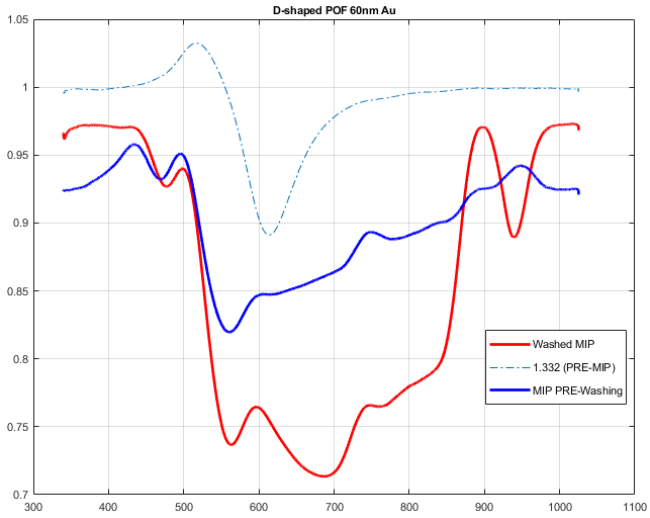

Figure 64. *Normalized spectra of the SPR resonance from a D-shaped POF sensor with bulk MIP-DVB-2_FAL layer in H_2O before and after the MIP washing procedure.*

The consistent variation in the spectral shape and intensity by washing procedure is clearly seen. This is probably due to a variation of the RI of the polymeric layer due to the extraction of

substances which, as in the MIP washing by batch equilibration reported above, were extracted from the MIP together with the template by the washing operations. The spectra are always normalized on the bare platform in the air. A difference in the resonance wavelength of the bare platform in water from the SPR on the bare platform in water and after the MIP deposition in water is seen too. A large redshift is observed for the resonance peak of the bare platform in water (RI=1.33) to the peak on washed MIP in water, as expected since MIP has an RI of 1.42 [1; 4], much higher than that of water. This resonance peak is not even seen on the not washed MIP sensor, probably because it was shifted out of the analytical wavelength window because of the very high RI of the non-washed MIP.

Other peaks which are visible in the spectrum of the MP sensor, before and after washing, could be due to the different coupling of light and in most of the cases, they are not even resonance peaks, since they do not change with RI of the medium. Notice that the peak at about 470 nm is only seen in the case of the MIP sensor, and it is red-shifted after washing. It could be ascribed to the presence of some gold nanostructures at the metal surface, formed after deposition of the polymer layer.

3.1.5 CHARACTERIZATION OF THE MIPs BY BATCH PROCEDURE

The adsorbing properties of MIPs were firstly characterized by the batch equilibration procedure described in “Methods” (par. 2.3.1). The results for different MIP and NIP are reported in Tables below in this paragraph 3.1.5., which show the mg of analyte absorbed in the MIP phase, the total percentage recovery, the imprinting factor (IF) and the affinity constant (K_{aff}).

The mg of analyte absorbed in the MIP phase is the quantity of the target substance recovered in the consecutive extractions. The recovery is obtained from the value of the absorption and the extractions, respect to the total amount in the system. The loading capacity, as mg of analyte per g of MIP ($mg_{Analyte}/g_{MIP}$), is evaluated from the total amount of analyte recovered in the extractions. This is an estimate of the amount of MIP active sites, assuming that the MIP has reached the saturation during the absorption phase, at high concentration of the template. The affinity constant (K_{aff}) can be calculated by considering that the equilibrium is reached in the first extraction where a fraction of the sites are occupied by the target substance and the other is empty. The results obtained by UV spectrophotometry are reported as: absorbance (A) of the supernatant solution at the analyte absorption wavelength, i.e. 278nm for 2-FAL and 270 for DBDS, measured after dilution to have A lower than about 2.5, but reported to the non-diluted value, and concentration of analyte in the supernatant (in mg/L) calculated from the absorbance of the liquid phase both in the adsorption and the extraction.

The results obtained by the electrochemical method are also shown for comparison. The following quantities are shown: the concentration of analyte (2-FAL or DBDS in mg/L) in solution evaluated experimentally by the standard addition method, the slope and the ordinate origin of the standard addition curve, with the respective error.

3.1.5.1 Characterization of MIP for DBDS

The experiment procedure is as follows: 40 mg of washed and dried polymer is placed in a glass container, with a plastic cap; then the solvent AcN: EtOH=4:1 (usually 3mL) spiked with a concentration of 90 mg/L of DBDS (0.27mg) for each analysis was added. The solubility of DBDS in this solvent high. The spiked solution is left in contact with MIP (40mg) for 10 hours under very mild stirring, in order to achieve the equilibrium condition. Re-extractions of DBDS from MIP has been carried out with the same procedure of the absorption employing the same volume of non-spiked solvent. The MIP powder was recovered from the absorption supernatant separating the two phases by centrifugation (10min at 4000rpm). Successive extractions are carried out, until not any more DBDS was extracted. The adsorption and the subsequent re-extraction of DBDS have been carried out with Bulk-, Porous- and Beads-MIP-DVB-DBDS. Also, the adsorption of similar substances to DBDS (DPDS, DBS) has been considered, on the same type of polymers and analyzed by the same procedure. The analysis of the supernatant solutions has been performed spectrophotometrically and in some cases electrochemically. The results are reported in Table 18.

Table 18. Batch characterization (adsorption and subsequent re-extraction) of DBDS form Bulk-, Porous- and Beads-MIP-DVB-DBDS (40 mg of polymer, 3 ml of solvent). Spectrophotometric and Electrochemical results.

	Bulk-MIP-DVB-DBDS in AcN:EtOH=4:1						
	UV			**DPV**			
	C tot (mg/L)	A 278 no dil	C surnat. (mg/L)	C tot (mg/L)	Slope	OO	C surnat (mg/L)
Reads	90	0,456	76,345	90	0,113(6)	2,32(6)	82,032
		C_{ads} (mg_{DBDS}/g_{MIP})	1.045				0.598

	Porous-MIP-DVB-DBDS1 in AcN:EtOH=4:1						
	UV			**DPV**			
	C tot (mg/L)	A 278 no dil	C surnat (mg/L)	C tot (mg/L)	Slope	OO	C surnat (mg/L)
Reads	90	0.2897	48,48	90	0,054(3)	0,16(3)	60,99
		C_{ads} (mg_{DBDS}/g_{MIP})	3.11				2.176

	Porous-MIP-DVB-DBDS2 in AcN:EtOH=4:1						
	UV			DPV			
	C tot (mg/L)	A 278 no dil	C surnat (mg/L)	C tot (mg/L)	Slope	OO	C surnat (mg/L)
Reads	90	1.08817	182.1012	90	0.0877(2)	0.615(2)	140.215
I Ext		0.0779201	13.03964		0.0867(8)	0.003(9)	0.0355
II Ext		0.0709307	11.87		0.089(2)	-0.09(3)	-0.989
III Ext		0.0635321	10.63186		0.104(4)	-0.19(5)	-1.856
DBDS ext (mg)			0.107				0.0001
C_{ads} (mg_{DBDS}/g_{MIP})			2.67				0.003
Recovery %			242%				0.04%
K_{aff} (M^{-1})			$3.26\ 10^4$				$6.93\ 10^9$

	MIP Beads-DVB-DBDS in AcN:EtOH=4:1						
	UV			DPV			
	C tot (mg/L)	A 278 no dil	C surnat (mg/L)	C tot (mg/L)	Slope	OO	C surnat (mg/L)
Reads	90	0.490722	82.120	90	0.109(2)	0.46(2)	84.809
I Ext		0.0585553	9.799		0.089(8)	0.11(9)	1.233
II Ext		0.0522859-	8.75		0.111(3)	-0.15(4)	-1.375
III Ext		0.0463395	7.755		0.120(5)	-0.19(5)	-1.590
DBDS ext (mg)			0.079				0.004
C_{ads} (mg_{DBDS}/g_{MIP})			1.97				0.092
Recovery %			120%				96%
K_{aff} (M^{-1})			$6.6\ 10^4$				$5.55\ 10^6$

Multiple extractions are needed to desorb the DBDS in the conditions considered. Other extractions have been carried out on a portion of the polymer employing different solvents i.e. AcN, MeOH:CH_3COOH=9:1, hexane, to verify that all the DBDS adsorbed was extracted; however no further recovery of the target compound has been observed. The bulk-MIP-DVB-DBDS and porous-MIP-DVB-DBDS seem to be only slightly affected by the interfering substances, as it could be seen from the good agreement of the recovery evaluated by electrochemical and UV analysis. The absorption of DBDS corresponds to the saturation of the imprinted sites at the considered conditions and is lower in the case of the bulk polymer than of the porous polymer. In the third case presented on Porous-MIP-DVB-DBDS2, the evaluated concentration of DBDS in the supernatant after equilibration was much higher than the total concentration, indicating the presence of interfering substances. For this reason, the adsorbed DBDS was evaluated by re-extraction, as reported in Table 18. The loading capacity is near to that of porous-MIP-DVB-DBDS1, as expected

from the fact that the two polymers have been synthesized with the same amount of porogenic solvent. The higher total interfering substances concentration is probably due to the fact that in this case a much higher total amount of polymer has been synthesized, about three times. The Porous-MIP-DVB-DBDS polymer appears to reach the saturation at around 2.67 mg_{DBDS}/g_{MIP} (0,011 mmol/g), while the Beads-MIP-DVB-DBDS at approximately 1.97 mg_{DBDS}/g_{MIP} (0,008 mmol/g), so the porous MIP has a slightly higher capacity probably due to a higher porosity than the Beads-MIP which actually is less porous, as it is seen by SEM analysis.

The polymers synthesized using EGDMA as cross-linker were not able to adsorb any DBDS. This behavior could be attributed to the phenomenon of the association between EGDMA and MAA which could reduce the concentration of MAA available for the coordination of the template in the prepolymer mixture, as it was calculated by computational model calculation.

It can be observed that the results obtained by UV and DPV are different and that the electrochemical analysis seems to be more affected by the interfering substances. Often, the characterization by electrochemistry was impossible to perform or a negative ordinate at the origin was found by the standard addition method.

The loading capacity of MIP is relatively low, particularly considering the total amount used for the imprinting. Moreover, this low capacity could be ascribed to the fact that DBDS can decompose at high temperature into a sulphur compounds, so during the thermal polymerization [190-191]. The affinity constant obtained for the porous-MIP-DVB-DBDS and Beads-MIP-DVB-DBDS are in an acceptable agreement. The approximated affinity constant K_{aff} calculated in AcN:EtOH=4:1 by spectrofotometc method is 3.26 10^4 M^{-1}. This is only an indicative value since the very low reproducibility of the analytical measurement made the calculation of a more precise value impossible. The value is low enough to make it possible to use AcN:EtOH=4:1 as a solvent for washing.

The Bulk-MIP-DVB-DBDS polymer was also used to realize the receptor layer on the SPR sensor (see chapter). The K_{aff} evaluated through the optical sensors (SPR or EWC) in another solvent , is much higher compared to the value found in batch procedure here described, respectively about 5.16 10^6 M^{-1} in D-shaped POF platform and 8.8 10^6 M^{-1} for SWS polatform. This seems to indicate that there are different and stronger sites in MIP, which can be investigated only by the use of more sensitive methods, as the sensor method described in the next chapter. According to the good results

obtained, in this case, it seem that the polymerization of thin layer occur before the thermal decomposition of the DBDS which moreover can protect and stabilize the compound in the active sites.

The imprinting factor (I.F.) cannot be obtained, no extraction on the NIP has been performed.

3.1.5.2 Characterization of MIP for 2-FAL

The experiment procedure is as follows: 40 mg of washed and dried polymer is placed in a glass container, with a plastic cap; then the solvent (usually 3mL) spiked with different 2-FAL concentrations for each analysis were added. For each polymer, two solvents have been considered, i.e. pure water and synthetic wine. The concentration of 2-FAL employed was 104.4 mg/L in some cases and 50 mg/L in other. A re-adsorption test at a low concentration of 2-FAL (5 mg/L) has also been performed. This value corresponds to the quantification limit of the UV technique used.

The spiked solution is left in contact with MIP (40mg) for 10 hours under very mild stirring, in order to achieve the equilibrium condition. Re-extractions of 2-FAL from MIP has been carried out with the same procedure of the absorption, employing the same volume of non-spiked solvent. The MIP powder was recovered from the absorption supernatant separating the two phases by centrifugation (10min at 4000rpm). Successive extractions are often carried out, until not any more 2-FAL was extracted. The adsorption and the subsequent re-extraction of 2-FAL have been carried out with the Porous-MIP-DVB, the Porous-MIP-EGDMAs, synthesized in an open container (porous MIP-EGDMA1) and in a closed container (porous MIP-EGDMA2), Beads EGDMA and NIP-DVB. Also, the adsorption of similar substances to 2-FAL (HMF, Furfuryl Alcohol) has been considered, on the same type of polymers and analyzed by the same procedure. The analysis of the supernatant solutions has been performed spectrophotometrically and in some cases electrochemically. The results are reported in Table 19.

As an example, in the following Figure 65, the UV absorption spectra of the re-adsorption of 2-FAL in synthetic wine and the two subsequent extractions in the same solvent are reported. The spectrum of the supernatant solution of a non-spiked synthetic wine (without the analyte) after

equilibration with the polymer is also reported for comparison.

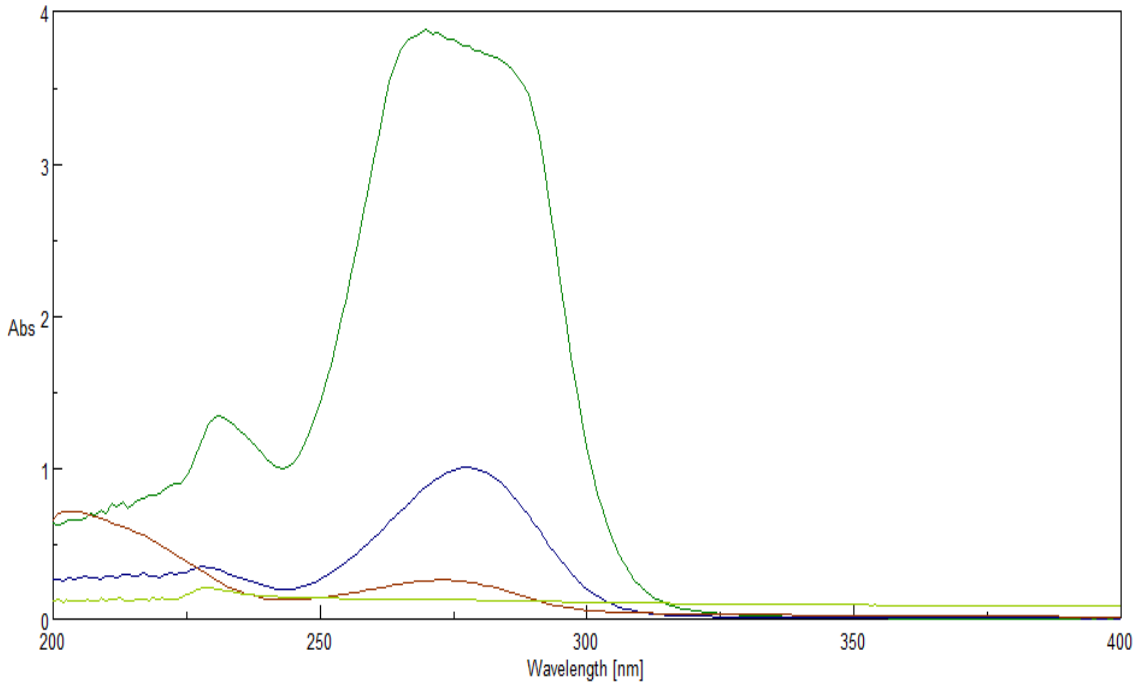

Figure 65. *UV absorption spectra of the re-adsorption of 2-FAL at 104.4 mg/L in synthetic wine(green line) and the two subsequent extractions in the same solvent are reported (blue and red lines). The spectrum of the supernatant solution of a non-spiked synthetic wine (without the analyte) after equilibration with the polymer is also reported for comparison. (light green line)*

From the UV spectra, it can be noted that the supernatant solution of the 2-FAL re-adsorption from synthetic wine experiment shows a well-defined peak at 278 nm, as well as the subsequent extractions in the same solvent. Instead, from the spectrum acquired on the solvent (without the analyte) left in contact for one night with the polymer, no peaks have been found at the wavelength of interest. Therefore, it can be assumed that the peak at 278nm is referred to furfural.

Table 19. *Batch Characterization (adsorption and subsequent re-extraction) of 2-FAL form the Porous-MIP-DVB-2FAL, the Porous-MIP-EGDMA-2FAL (1 and 2), Beads-EGDMA-2FAL and NIP-DVB. Spectrophotometric and Electrochemical results.*

	Porous-MIP-DVB-2FAL in water						
	UV			**SWV**			
	C tot (mg/L)	A 278 no dil	C surnat. (mg/L)	C tot (mg/L)	Slope	OO	C surnat (mg/L)
Reads	104,4	11,92	63,21	104,4	0,033(7)	0,7(1)	82,81
I ext		1,88	10,05		0,010(1)	0,3(3)	10,69
II ext		0,648	3,42		0,078(1)	0,155(8)	4,00
2-FAL ext (mg)			0,040				0.044
C_{ads} ($mg_{2\text{-}FAL}/g_{MIP}$)			1.010				1.102
Recovery %			73%				93%
K_{aff} (M^{-1})			$6.2\ 10^2$				$5.2\ 10^2$
I.F.			3.3				15

	Porous-MIP-DVB-2FAL in synthetic wine						
	UV			**SWV**			
	C tot (mg/L)	A 278 no dil	C surnat. (mg/L)	C tot (mg/L)	Slope	OO	C surnat (mg/L)
Reads	104,4	14	74,36	104,4	0,036(4)	0,1(2)	77,39
I ext		2,805	14,88		0,032	0,096	12,03
II ext		0,319	1,67		-0,03(3)	2,5(8)	-303,42
2-FAL ext (mg)			0,050				0.036
C_{ads} ($mg_{2\text{-}FAL}/g_{MIP}$)			1.241				0.902
Recovery %			87%				86%
K_{aff} (M^{-1})			$7.2\ 10^2$				$3.0\ 10^3$
I.F.			2.6				-

	Porous-MIP-DVB-2FAL in synthetic wine						
	UV			**SWV**			
	C tot (mg/L)	A 278 no dil	C surnat. (mg/L)	C tot (mg/L)	Slope	OO	C surnat (mg/L)
Reads	50	6,79	34,5	50	0,049(4)	0,3(2)	21,86
I ext		1,438	15,31		0,038(9)	-0,1(2)	-12,26
2-FAL ext (mg)			0,046				
C_{ads} ($mg_{2\text{-}FAL}/g_{MIP}$)			1.148				
Recovery %			100%				
K_{aff} (M^{-1})			$5.0\ 10^2$				
I.F.			2.4				

	Porous-MIP-EGDMA-2FAL1 in water						
	UV			SWV			
	C tot (mg/L)	A 278 no dil	C surnat. (mg/L)	C tot (mg/L)	Slope	OO	C surnat (mg/L)
Reads	50	5,31	28,22	50	0,078	0,495	25,24
I ext		1,176	6,25		0,048(4)	0,05(8)	4,16
II ext		0,016	0,08		0,066(3)	-0,04(4)	-2,13
2-FAL ext (mg)			0,019				0.012
C_{ads} ($mg_{2\text{-}FAL}/g_{MIP}$)			0.475				0.312
Recovery %			69%				59%
K_{aff} (M^{-1})			$2.5\ 10^4$				$6.9\ 10^4$
I.F.			2.37				1.2

	Porous-MIP-EGDMA-2FAL1 in synthetic vine						
	UV			SWV			
	C tot (mg/L)	A 278 no dil	C surnat. (mg/L)	C tot (mg/L)	Slope	OO	C surnat (mg/L)
Reads	50	6,084	32,32	50	0,037(1)	-0,13(2)	-14,32
I ext		1,122	5,96		0,068(4)	-0,37(6)	-21,33
II ext		0,269	1,43		0,081(7)	-0,0(1)	-0,49
III ext can		0,073	0,39				
IV ext 9MeOH:1CH3COOH		0,024	0,13				
2-FAL ext (mg)			0,022				
C_{ads} ($mg_{2\text{-}FAL}/g_{MIP}$)			0.583				
Recovery %			80%				
K_{aff} (M^{-1})			$2.9\ 10^4$				
I.F.			0.81				

	Porous-MIP-EGDMA-2FAL2 in water						
	UV			SWV			
	C tot (mg/L)	A 278 no dil	C surnat. (mg/L)	C tot (mg/L)	Slope	OO	C surnat (mg/L)
Reads	50	3,556	18,89	50	0,1039(9)	0,501(7)	19,28
I ext		1,648	8,75		0,114(4)	0,30(5)	10,56
II ext		0,532	2,83		0,071(4)	-0,03(6)	-1,47
2-FAL ext (mg)			0,035				0.032
C_{ads} ($mg_{2\text{-}FAL}/g_{MIP}$)			0.868				0.792
Recovery %			61%				60%
K_{aff} (M^{-1})			$9.8\ 10^3$				$5.1\ 10^3$
I.F.			4.375				3.2

	Porous-MIP-EGDMA-2FAL2 in synthetic wine						
	UV			SWV			
	C tot (mg/L)	A 278 no dil	C surnat. (mg/L)	C tot (mg/L)	Slope	OO	C surnat (mg/L)
Reads	50	5,016	26,64	50	0,024(3)	-0,13(4)	-21,56
I ext		0,944	5,01		0,010(3)	-0,06(4)	-25,66
II ext		0,344	1,83		0,005	-0,05	-44,62
			2-FAL ext (mg)	0,020			
			C_{ads} ($mg_{2\text{-}FAL}/g_{MIP}$)	0.513			
			Recovery %	67%			
			K_{aff} (M^{-1})	$4.4\ 10^4$			
			I.F.	0.741			

	Beads-MIP-EGDMA-2FAL in water						
	UV			SWV			
	C tot (mg/L)	A 278 no dil	C surnat. (mg/L)	C tot (mg/L)	Slope	OO	C surnat (mg/L)
Reads	50	5,14592	27,33	50	0,27(4)	2,0(6)	29,9
I ext		0,92252	4,90		0,31(3)	1,0(5)	12,57
II ext		0,19992	1,06		0,30(4)	0,7(6)	9,63
			2-FAL ext (mg)	0,019			0.067
			C_{ads} ($mg_{2\text{-}FAL}/g_{MIP}$)	0.447			0.943
			Recovery %	67%			104%
			K_{aff} (M^{-1})	$4.65\ 10^4$			$2.41\ 10^3$
			I.F.	2.4			1.7

	Beads-MIP-EGDMA-2FAL in synthetic wine						
	UV			SWV			
	C tot (mg/L)	A 278 no dil	C surnat. (mg/L)	C tot (mg/L)	Slope	OO	C surnat (mg/L)
Reads	50	7,5046	39,86	50	0,210(3)	2,17(5)	41,49
I ext		1,070176	5,68		0,28(3)	0,3(5)	4,41
II ext		0,42208	2,24		0,305(8)	0,1(1)	1,25
			2-FAL ext (mg)	0.024			0.017
			C_{ads} ($mg_{2\text{-}FAL}/g_{MIP}$)	0.594			0.424
			Recovery %	96%			94%
			K_{aff} (M^{-1})	$3.23\ 10^4$			$5.98\ 10^4$
			I.F.	0.89			0.42

It has been observed that the largest amount of absorbed 2-FAL is re-extracted in the first extraction. Other extractions have been carried out once on a polymer portion employing different solvents

i.e. AcN, 9MeOH:1CH_3COOH to verify that the whole 2-FAL adsorbed was extracted; however, no further recovery of the target compound has been observed. From the amount of 2-FAL extracted, it can be seen that the porous-MIP-DVB-2FAL polymer reached the saturation at around 1.24 $mg_{2\text{-}FAL}/g_{MIP}$ (0,013 $mmol_{2\text{-}FAL}/g_{MIP}$). This value has been obtained by the sum of the portions collected in the re-extractions both in H_2O or in synthetic wine. The results obtained by UV and SWV are in acceptable agreement. The porous-MIP-EGDMA-2FAL1 polymer seems to reach saturation at approximately 0.6 $mg_{2\text{-}FAL}/g_{MIP}$ (0,005 $mmol_{2\text{-}FAL}/g_{MIP}$). On the Beads-MIP-EGDMA-2FAL polymer, two readsorption tests and subsequent extractions have been carried out in H_2O or in synthetic wine. The first analysis shows saturation for H_2O corresponding to 0.45 $mg_{2\text{-}FAL}/g_{MIP}$ and in synthetic wine of 0.52 $mg_{2\text{-}FAL}/g_{MIP}$, which are not significantly different and are similar to the capacity of the Porous-MIP-EGDMA-2-FAL1. In the second use, however, the polymer seems to reach saturation at 0.225 $mg_{2\text{-}FAL}/g_{MIP}$ in H_2O and somewhat higher, 0.6 $mg_{2\text{-}FAL}/g_{MIP}$, in synthetic wine. Since this is in acceptable agreement with the first use, the result of the water extraction is probably to be ascribed to a difference in the equilibration time.

The polymers synthesized using EGDMA as cross-linker show a lower adsorbing capacity than the synthesized polymer using DVB. This behavior could be attributed to the phenomenon of association between EGDMA and MAA which could reduce the concentration of MAA available for the coordination of the template in the prepolymer mixture, as it was calculated by computational model calculation.

It can be observed that recoveries are 90% in the case of adsorption on porous MIP-DVB both from water and from synthetic wine, while they are around 70% in the case of MIPs with EGDMA. However, in this case too, the recovery from synthetic wine was larger than the recovery from water. Non-quantitative recovery is attributed to the fact that 2-FAL can decompose quite rapidly in aqueous solution [160]. Better results were found in the analyses performed under basic conditions. 2-FAL is not a very stable substance, particularly at high temperatures [160] and in an acidic environment. It should be noted that further extractions with water or synthetic wine have not led to further recovery. This phenomenon seems to be enhanced by the use of EGDMA polymers. MAA could play an important part in this catalysis, particularly in more polar environments, such as the polymer with EGDMA. A partial decomposition may, therefore, occur at the polymerization temperatures, in prepolymer mixture which employs EGDMA.

An approximated value of the affinity constant Kaff has been calculated as exposed above, the value calculated is 6.2 10^2 M^{-1} in water and 7.2 10^2 M^{-1} in synthetic wine for Porous-MIP-DVB-2FAL. So, the K_{aff} are in good agreement in the two different solvents. K_{aff} seems to be higher in polymers obtained with EGDMA as cross-linker, from one to two orders of magnitude (e.g 2.9 10^4 M^{-1} in Porous-MIP-EGDMA-2FAL).

The same adsorption experiments were carried out on the corresponding NIP at similar concentrations, obtaining only slightly lower adsorbed amounts (see results reported below). The imprinting factor (I.F.) obtained from the polymer synthesized with DVB as a cross-linker is 3, while the polymer synthesized with EGDMA has a lower I.F. equal to 2 in H_2O and to 1 in synthetic wine. These IF values obtained at relatively high concentrations confirm the formation of the specific sites, even if they are less concentrated than the aspecific sites, which are also saturated at the considered conditions.

Re-adsorption at lower concentration (5 mg/L of 2-FAL) has been carried out in synthetic wine too with subsequent spectrophotometric analysis on porous MIP-DVB and porous MIP-EGDMA synthesized in open and in closed vial. Only spectrophotometic analyses have been performed, since the LOQ was higher in voltammetric technique with respect to the concentration considered.

The results of the spectrophotometric analyses are reported in Table 20 below.

Table 20. Re-adsorption at lower concentration (5 mg/L of 2-FAL) in synthetic wine on porous MIP-DVB, porous-MIPs-EGDMA (1 and 2). Spectrophotometric results.

	Porous-MIP-DVB-2FAL in synthetic wine		
	UV		
	C tot (mg/L)	A 278 no dil	C supernat (mg/L)
Riads	5	0,78692	4,3476
I ext		0,2518588	1,3915
		2-FAL ext (mg)	0.004
		C_{ads} ($mg_{2\text{-}FAL}/g_{MIP}$)	0.1044
		Recovery %	115%
		K_{aff} (M^{-1})	1.93 10^4

	Porous-MIP-EGDMA-2FAL1 in synthetic wine		
	UV		
	C tot (mg/L)	A 278 no dil	C supernat (mg/L)
Riads	5	0,738332	4,07918
I ext		0,0663816	0,36675
		2-FAL ext (mg)	0.001
		C_{ads} ($mg_{2\text{-}FAL}/g_{MIP}$)	0.027
		Recovery %	89%
		K_{aff} (M^{-1})	1.02 10^5

	Porous-MIP-EGDMA-2FAL2 in synthetic wine		
	UV		
	C tot (mg/L)	A 278 no dil	C supernat (mg/L)
Riads	5	0,74056	4,09149
I ext		0,2219036	1,22599
		2-FAL ext (mg)	0.004
		C_{ads} ($mg_{2\text{-}FAL}/g_{MIP}$)	0.092
		Recovery %	106%
		K_{aff} (M^{-1})	2.32 10^4

Recovery at low concentrations is about 100%, sometimes even higher due to interferences. This means that at these concentrations the decomposition of 2-FAL is slower than that at high concentrations. The affinity constant, calculated as above, is an order of magnitude higher, about 1.93 10^4 M^{-1}. This is only an indicative value since the very low reproducibility of the measurement made the calculation of a more precise value impossible. However, this value seems to indicate the presence of sites with a higher affinity. Actually, the Bulk-MIP-DVB-2FAL polymer was also used to realize the receptor layer on the SPR sensor (see 3.2.2). The characterization of the MIP through the SPR method, gives a much higher value for K_{aff}, about 10^6 M^{-1}. A similar value was also obtained in the characterization by the electrochemical sensor in par. 3.1.7. Therefore, it seems that there are different and even stronger sites, which can be investigated only by the use of more sensitive methods, as the sensor optical and electrochemical methods described elsewhere.

3.1.5.3 Characterization of aspecific adsorption on NIP with batch procedure

The study of the adsorption of the analyte (2-FAL or DBDS) on NIP (non-imprinted polymer) allows to highlight any aspecific adsorption and to evaluate the imprinting factor, i.e. the capacity of adsorption on specific sites of MIP. This can also be considered a measure of the specificity of the polymer for the template (the analyte).

The analyses have been performed with the same procedure used to characterize the corresponding MIP for the imprinted template (DBDS or 2-FAL), on the supernatant after equilibration, both spectrophotometrically and electrochemically.

3.1.5.3.1 In the case of DBDS

The adsorption of DBDS has been performed on the washed and dried Porous-NIP-DVB. The results obtained by spectrophotometric and electrochemical analysis are reported in Table 21.

Table 21. Adsorption of DBDS on Porous-NIP-DVB from a solution of AcN:EtOH=4:1 at 90 mg/L of DBDS. Spectrophotometric and electrochemical results.

	Ads DBDS on Porous-NIP-DVB in AcN:EtOH=4:1						
	UV			**DPV**			
	C tot (mg/L)	A 278 no dil	C supernat (mg/L)	C tot (mg/L)	Slope	OO	C supernat (mg/L)
Ads	90	0.765668	128,132	90	0,0773(4)	1,781(5)	92.2078

Despite the fact that the recovery is higher than 100% due to interfering substances, it can be clearly seen that no aspecific absorption of DBDS occurs in the Porous-NIP-DVB. So, it can be concluded that the absorption of DBDS which was found in MIPs imprinted for DBDS (exposed above in Table 21) occurs by combination with specific imprinted sites. This confirms the findings by calculations, that the interaction DBDS-MAA was very weak. The results obtained by the two methods of analysis spectrophotometric and electrochemical are in a good agreement, even if a stronger influence from

interfering substances was observed in the adsorption analysis of porous-NIP-DVB. These substances were released from NIP in AcN:EtOH=4:1 as it was already observed for MIPs. No extraction have been performed on NIP since the total recovery of the analyte employed for the absorption was found in the analysis of the supernatant solution after the equilibration.

3.1.5.3.2 In the case of 2-FAL

Three different types of NIP where synthesized and characterized: a porous NIP-DVB, a porous NIP-EGDMA, and a bulk-NIP-EGDMA. The washed and dried NIPs polymers have been used to carry out adsorption of 2-FAL both in water and in synthetic wine, with the same procedure employed for the corresponding MIPs. An extraction test has been also performed with the same procedure. The results obtained by spectrophotometric and electrochemical analysis are reported in Table 22.

Table 22. Adsorption of 2-FAL on Porous-NIP (DVB and EGDMA) and Bulk-NIP-EGDMA from a solution of H_2O:EtOH=75:25 or synthetic wine both at 50 mg/L of 2-FAL. Spectrophotometric and electrochemical results.

	Ads 2-FAL on Porous NIP-DVB in H_2O						
	UV			**SWV**			
	C tot (mg/L)	A 278 no dil	C supernat (mg/L)	C tot (mg/L)	Slope	OO	C supernat (mg/L)
Ads	50	1,848	9,81	50	0,078(4)	0,17(3)	8,5
I ext		0,759	4,03		0,0969(7)	0,027(9)	1,11
2-FAL ext (mg)			0.012				0.003
C_{ads} ($mg_{2\text{-}FAL}/g_{MIP}$)			0.302				0.083
Recovery %			28%				19%

	Ads 2-FAL on Porous-NIP-DVB in synthetic wine						
	UV			**SWV**			
	C tot (mg/L)	A 278 no dil	C supernat (mg/L)	C tot (mg/L)	Slope	OO	C supernat (mg/L)
Ads	50	4,812	25,55	50	0,034(2)	-0,17(3)	-19,62
I ext		1,228	6,52		0,029(4)	-0,18(6)	-25,15
2-FAL ext (mg)			0.019				
C_{ads} ($mg_{2\text{-}FAL}/g_{MIP}$)			0.489				
Recovery %			64%				

	Ads 2-FAL on Porous-NIP-EGDMA in H_2O						
	UV			**SWV**			
	C tot (mg/L)	A 278 no dil	C supernat (mg/L)	C tot (mg/L)	Slope	OO	C supernat (mg/L)
Ads	50	3,738748	19,86	50	0,197(7)	1,7(1)	33,73
I ext		0,510668	2,71		0,196(8)	0,2(1)	3,36
II ext		0,0092	0,05		0,256(2)	-0,93(2)	-14,58
2-FAL ext (mg)			0.008				0.01
C_{ads} ($mg_{2\text{-}FAL}/g_{MIP}$)			0.207				0.252
Recovery %			45%				74%

	Ads 2-FAL on Porous-NIP-EGDMA in synthetic wine						
	UV			**SWV**			
	C tot (mg/L)	A 278 no dil	C supernat (mg/L)	C tot (mg/L)	Slope	OO	C supernat (mg/L)
Ads	50	5,0344	26,74	50	0,054(6)	0,07(9)	5,18
I ext		1,130324	6,00		0,197(5)	-0,04(7)	-0,73
II ext		0,5572	2,96		0,155(1)	0,552(2)	13,34
2-FAL ext (mg)			0.027				0.04
C_{ads} ($mg_{2\text{-}FAL}/g_{MIP}$)			0.672				1.000
Recovery %			71%				37%

	Ads 2-FAL Bulk-NIP-EGDMA in H_2O						
	UV			**SWV**			
	C tot (mg/L)	A 278 no dil	C supernat (mg/L)	C tot (mg/L)	Slope	OO	C supernat (mg/L)
Ads	50	0,761016	4,04	50	0,18(1)	0,7(2)	16,48
I ext		0	0		0,19(2)	0,2(2)	5,07
II ext		0	0		0,145(6)	0,15(9)	4,02
2-FAL ext (mg)			0.0				0.027
C_{ads} ($mg_{2\text{-}FAL}/g_{MIP}$)			0.0				0.682
Recovery %			-				51%

	Ads 2-FAL on not porous NIP-EGDMA in synthetic wine						
	UV			SWV			
	C tot (mg/L)	A 278 no dil	C supernat (mg/L)	C tot (mg/L)	Slope	OO	C supernat (mg/L)
Ads	50	4,05916	21,56	50	0,141(3)	1,33(4)	37,77
I ext		0,63432	3,37		0,1335(9)	-0,61(1)	-18,35
II ext		0,29576	1,57		0,1111(8)	0,26(1)	9,51
2-FAL ext (mg)			0.015				0.028
C_{ads} ($mg_{2\text{-}FAL}/g_{MIP}$)			0.370				0.713
Recovery %			53 %				95

The concentration adsorbed is always higher from wine solution than water, and in Porous-NIP-EGDMA than in Porous-NIP-DVB. However the value of adsorption is not 0, this means that an aspecific absorption occurs in NIPs. This aspecific adsorption could be due to the polar nature of the analyte which probably can interact with the free functional groups of the constituent moieties of the NIP polymer, such as MAA in NIP-DVB or even the EGDMA in case of NIP-EGDMA. So, this effect is even greater in EGDMA.

3.1.5.4 Characterization of selectivity of MIP by batch procedure with substances of a similar structure to the analytes

3.1.5.4.1 Selectivity of MIP imprinted for DBDS

With the same procedure illustrated for batch equilibration of the analyte, it has been tested the re-absorption and extraction of similar substances to DBDS, i.e. Diphenyl Disulphide (DPDS) and Dibenzyl Sulphide (DBS) on bulk and porous MIP-DVB, in order to test the selectivity for possible employment in a real matrix.

The DPDS and DBS standards are respectively 610 mg/L and 545 mg/L in EtOH. The solvent of analysis was maintained AcN:EtOH=4:1.

The tables illustrated below contain the same type of data reported for the re-absorption and extractions of DBDS, reported above.

Table 23. Adsorption of the substances with a similar structure to DBDS (DPDS, DBS) on MIPs-DVB-DBDS. Spectrophotometric and electrochemical results.

- Adsorption on Bulk-MIP-DVB-DBDS

	Ads DPDS on Bulk-MIP-DVB-DBDS in AcN:EtOH=4:1						
	UV			**DPV**			
	C tot (mg/L)	A 278 no dil	C surnat (mg/L)	C tot (mg/L)	Slope	OO	C surnat (mg/L)
Ads	90	1.083356	70,092	90	0,200(5)	4,12(7)	82.626
		Cads (mg_{DPDS}/g_{MIP})	1.493				0.553

	Ads DBS on Bulk-MIP-DVB-DBDS in AcN:EtOH=4:1						
	UV			**DPV**			
	C tot (mg/L)	A 278 no dil	C surnat (mg/L)	C tot (mg/L)	Slope	OO	C surnat (mg/L)
Ads	90	0.235636	108,791	90	0,13(1)	3,5(1)	103.445
		Cads (mg_{DBS}/g_{MIP})	-				-

- Absorption on Porous-MIP-DVB-DBDS

	Ads DPDS on Porous-MIP-DVB-DBDS1 in AcN:EtOH=4:1						
	UV			**DPV**			
	C tot (mg/L)	A 278 no dil	C surnat (mg/L)	C tot (mg/L)	Slope	OO	C surnat (mg/L)
Ads	90	1.36649	88.410	90	0,171(3)	0.60(3)	69.815
I Ext		0.1716	11.102		0.170(6)	-0.19(7)	-
II Ext		-	-		0.179(8)	-0.4(1)	-
		DPDS ext (mg)	0.033				
		Cads (mg_{DPDS}/g_{MIP})	0.833				
		Recovery %	111%				
		K_{aff} (M^{-1})	$6.76\ 10^4$				

	Ads DBS on Porous-MIP-DVB-DBDS2 in AcN:EtOH=4:1						
	UV			DPV			
	C tot (mg/L)	A 278 no dil	C surnat (mg/L)	C tot (mg/L)	Slope	OO	C surnat (mg/L)
Reads	90	0.374687	172.769	90	0,141(3)	0.71(3)	101.016
I Ext		0.114394	52.747		0.133(5)	0.20(5)	1.492
II Ext		-	-		0.1585(4)	0.152(5)	0.958
DBS ext (mg)			0.158				0.007
Cads (mg_{DBS}/g_{MIP})			3.956				0.184
Recovery %			251%				115%
K_{aff} (M^{-1})			$4.0\ 10^{3}$				$1.44\ 10^{5}$

- Absorption on Beads-MIP-DVB-DBDS

	Ads DPDS on Beads-MIP-DVB-DBDS in AcN:EtOH=4:1						
	UV			DPV			
	C tot (mg/L)	A 278 no dil	C surnat (mg/L)	C tot (mg/L)	Slope	OO	C surnat (mg/L)
Ads	90	1.11844	72.362	90	0,184(3)	0.68(3)	73.525
I Ext		0.0758654	4.908		0.191(4)	-0.055(6)	-0.287
II Ext		-	-		0.201(5)	-0.47(6)	-2.346
DPDS ext (mg)			0.015				
Cads (mg_{DPDS}/g_{MIP})			0.368				
Recovery %			86%				
K_{aff} (M^{-1})			$1.49\ 10^{6}$				

	Ads DBS on Beads-MIP-DVB-DBDS in AcN:EtOH=1:4						
	UV			DPV			
	C tot (mg/L)	A 278 no dil	C surnat (mg/L)	C tot (mg/L)	Slope	OO	C surnat (mg/L)
Ads	90	0.168878	77.870	90	0,160(7)	0.81(8)	101.982
I Ext		0.0618831	28.534		0.14(1)	-0.3(1)	-2.158
II Ext		-	-		0.18(1)	-0.1(1)	-0.712
DBS ext (mg)			0.086				
Cads (mg_{DBS}/g_{MIP})			2.140				
Recovery %			118%				
K_{aff} (M^{-1})			$2.2\ 10^{3}$				

It is deduced that the MIP synthesized is selective towards the DBS, which is not adsorbed in all the MIPs formulation considered. For the Porous MIPs and Beads MIP, an absorption of DBS was observed in the spectrophotometric analysis, but a really low Kaff was found. So, this effect could be due to an aspecific absorption on the higher surface of the two MIPs formulation with respect to the not porous Bulk-MIP. This is also shown by the low values of concentration of DBS adsorbed on MIPs (0.184mg_{DBS}/g_{MIP}), obtained in the electrochemical measurements on the extractions and, for which, also a quantitative recovery was observed during the absorption analysis. A lower K_{aff} was found with the electrochemical method in respect to spectrophotometric analysis. As it happens in case of DBDS analysis, the peak of UV absorption of DBS (around 270nm) was affected by interfering substances co-extracted preventing the precisely spectrophotometric measurement (e.g. the DBS recovery on Porous-MIP-DVB-DBDS was 251%). All the MIPs-DVB-DBDS does not seem to be selective for the DPDS, since in all the three formulations it was observed an adsorption of this compound. However, the concentration of DPDS adsorbed (C_{ads}=mg_{DPDS}/g_{MIP}) found is lower in respect to that found on DBDS adsorptions (Table 18.) in the case of Porous- and Beads-MIP-DVB-DBDS, i.e. respectively 0.833 mg_{DPDS}/g_{MIP} and 0.368 mg_{DPDS}/g_{MIP} in case of DPDS and 2.67 mg_{DPDS}/g_{MIP} and 1.97 mg_{DPDS}/g_{MIP} in case of DBDS. Only in the case of Bulk-MIP-DVB-DBDS polymer was found a similar value of adsorption of DBDS and DPDS, i.e. respectively 1,045 mg_{DPDS}/g_{MIP} and 1,49 mg_{DPDS}/g_{MIP}.

The approximated K_{aff} calculated for DPDS on Porous-MIP-DVB-DBDS formulation was similar to that found for DBDS on the same MIP considered (Tab.18), i.e 3.26 10^4 M^{-1} with DBDS analyte and 6.76 10^4 with DPDS analyte. However, for Beads-MIP-DVB-DBDS a greater value of K_{aff} was found for DPDS than DBDS i.e. 1.49 10^6 M^{-1} and 6.6 10^4 M^{-1}. Even in this case is possible that the DPDS determination was not precise due to the interferents compounds released by the polymer. The high absorption of DPDS is imputed to the really close structure of the compound with the analyte DBDS, which contain the same disulphur bridge. In fact, previous evaluations made by calculation showed that the strongest interaction of the considered functional monomer (MAA) occurred at the two S atoms of the DBDS.

3.1.5.4.2 Selectivity of the absorption on MIP imprinted for 2-FAL

With the same procedure illustrated for batch equilibration of the analyte, it have been tested the re-absorption and extraction of similar substances to 2-FAL, i.e., 5-hydroxymethyl-2-furaldehyde (HMF) and furfuryl alcohol (FA) on Porous-MIP-DVB-2FAL, on Porous-MIPs-EGDMA (1 and 2), and Porous-NIP-DVB in order to test the selectivity for a possible employment in a real matrix. In view of possible employment in a real matrix, the synthetic wine was considered as a solvent for the analysis. The HMF and FA standards were prepared respectively at 500 mg/L and at 565.5 mg/L in H_2O. In some cases 104.4 mg/L of interfering were considered, for a total of 0.3132 mg of 2-FAL added in the system (3mL of solvent); in other cases 50.0 mg/L of interferer were added, for a total of 0.15 mg added in the system.

The tables that will be illustrated below contain the same type of data reported for the re-adsorption of 2-FAL and for the subsequent extractions listed above.

The characterization by spectrophotometric analysis is reported. The electrochemical analysis results impossible due to interferences which gave an ordinate at the origin negative. Also, the Furfuryl Alcohol is not electroactive.

Table 24. Adsorption of HMF and FA from synthetic wine both at 104.4 mg/L on Porous-MIP-DVB-2FAL. Spectrophotometric results.

	Porous MIP-DVB in synthetic wine					
	HMF			**FA**		
	C tot (mg/L)	A 285 no dil	C surnat. (mg/L)	C tot (mg/L)	A 217 no dil	C surnat. (mg/L)
Ads	104,4	12,303	82,13	104,4	6.044	59,75
I ext		1,44	9,62		3.5	34,60
		HMF ext (mg)	0.029		**FA ext (mg)**	0.104
		C_{ads} (mg_{HMF}/g_{MIP})	0.721		**C_{ads} (mg_{FA}/g_{MIP})**	2.595
		Recovery HMF %	88%		**Recovery FA %**	90%
		K_{aff} (M^{-1})	$6.1\ 10^3$		**K_{aff} (M^{-1})**	$2.8\ 10^3$

	Porous MIP-EGDMA in synthetic wine					
	HMF			**FA**		
	C tot (mg/L)	A 285 no dil	C surnat. (mg/L)	C tot (mg/L)	A 217 no dil	C surnat. (mg/L)
Ads	50.0	3.892	43.10	50.0	3.704	36.62
I ext		0.604	6.69		1.544	15.26
		HMF ext (mg)	0.020		**FA ext (mg)**	0,046
		C_{ads} (mg_{HMF}/g_{MIP})	0.502		**C_{ads} (mg_{FA}/g_{MIP})**	1.144
		Recovery HMF %	100%		**Recovery FA %**	104%
		K_{aff} (M^{-1})	$1.6\ 10^4$		**K_{aff} (M^{-1})**	$5.2\ 10^2$

	Porous MIP-EGDMA2 in synthetic wine					
	HMF			**FA**		
	C tot (mg/L)	A 285 no dil	C supernat. (mg/L)	C tot (mg/L)	A 217 no dil	C supernat. (mg/L)
Ads	50.0	4.112	45.54	50.0	3.244	32.07
I ext		0.796	8.82		1.316	13.01
		HMF ext (mg)	0.026		**FA ext (mg)**	0.039
		C_{ads} (mg_{HMF}/g_{MIP})	0.661		**C_{ads} (mg_{FA}/g_{MIP})**	0.976
		Recovery HMF %	109%		**Recovery FA %**	90%
		K_{aff} (M^{-1})	$7.87\ 10^3$		**K_{aff} (M^{-1})**	$1.99\ 10^3$

	Porous NIP-DVB in synthetic wine					
	HMF			**FA**		
	C tot (mg/L)	A 285 no dil	C supernat. (mg/L)	C tot (mg/L)	A 217 no dil	C supernat. (mg/L)
Ads	50.0	4.156	46.03	50.0	3.916	38.71
I ext		0.356	3.94		1.112	10.99
		HMF ext (mg)	0.012		**FA ext (mg)**	0.033
		C_{ads} (mg_{HMF}/g_{MIP})	0.295		**C_{ads} (mg_{FA}/g_{MIP})**	0.824
		Recovery HMF %	100%		**Recovery FA %**	99%

Form the results, it is clearly seen that both the interferences substances are absorbed in all the considered MIPs imprinted for 2-FAL. This is due to the really similar structure of the 2-FAL with these two other compounds considered (i.e. HMF and FA). The concentration adsorbed (C_{ads}) of the FA it was found to be higher than HMF in all the MIPs imprinted for 2-FAL considered. However, in case of Porous-MIP-DVB-2FAL and Porous-MIP-EGDMA-2FAL1, the C_{ads} of HMF found in the extractions (Tab. 24) was lower than that found in the case of 2-FAL (Tab 21.); i.e. respectively 1.24

$mg_{2\text{-}FAL}/g_{MIP}$ and 1.47 $mg_{2\text{-}FAL}/g_{MIP}$ for 2-FAL, 0.721 mg_{HMF}/g_{MIP} and 0.502 mg_{HMF}/g_{MIP} for HMF. Only in the case of Porous-MIP-EGDMA-2-FAL2 the C_{ads} was slightly higher for HMF in respect to the case of 2-FAL, i.e. 0.513 $mg_{2\text{-}FAL}/g_{MIP}$ for 2-FAL, 0.661 mg_{HMF}/g_{MIP} for HMF.

In case of FA, the C_{ads} found was higher than that of the analyte 2-FAL (even used as template) in almost all the MIPs considered; i.e. 2.59 mg_{FA}/g_{MIP} in case of Porous-MIP-DVB-2-FAL and 0.976 mg_{FA}/g_{MIP} in case of Porous-MIP-EGDMA-2-FAL1 and 2.59 mg_{FA}/g_{MIP} Porous-MIP-EGDMA-2-FAL2.

It must be underlined that the wavelength of absorption of the FA is affected by absorption of the interfering substances, so this prevents its precise evaluation.

Moreover, an aspecific absorption of the two furanic compounds was observed, as exposed in the results on Porous-NIP-DVB. The C_{ads} value found for NIP were only slightly lower than that found on the MIPs in the adsorption of this substances, so this means that the binding take places mostly by the aspecific adsorption than through the imprinted sites. This is even confirmed by the lower K_{aff} values observed for the furans on Porous-MIPs-EGDMA in respect K_{aff} obtained considering 2-FAL on the same Porous-MIPs-EGDMA; i.e. for example 4.4 10^4 M^{-1} for 2-FAL, 7.87 10^3 M^{-1} for HMF and 1.99 10^3 M^{-1} for FA on Porous-MIP-EGDMA.

Lower value of K_{aff} were found in case of Porous-MIP-DVB-2FAL than the porous polymer with EGDMA cross-linker; however the values of K_{aff} were comparable between 2-FAL and furans considered, i.e. 7.2 10^2 M^{-1} for 2-FAL, 6.1 10^3 M^{-1} for HMF and 2.8 10^3 M^{-1} for FA.

It must be underlined that these values are only approximated value of Kaff. It can be seen a difference between the adsorption of the various furans considered in the case of the polymer with EGDMA compared to that with DVB. Evidently, the interaction with the carboxyl groups is more specific in a more polar environment. This is even confirmed by the K_{aff} which are lower in the case of for Porous-MIPs-EGDMA in respect to the Porous-MIP-DVB.

3.1.6 CHARACTERIZATION OF THE MIP ADSORPTION BY DYNAMIC FLOW PROCEDURE ON COLUMN (SPE)

3.1.6.1 Breakthrough Curve

Figure 66 shows the breakthrough curve on the adsorption of a solution at 32.4 mg/L of DBDS in AcN:EtOH=4:1 solvent on non-porous bulk MIP. The column consists of a 600 mg of MIP cartridge (volume of 2.3 cm^3). Seven portions of 0.5 ml each have been eluted: the first three were collected consecutively, then a night have been waited, before both the collections, of the second set of three portions and of the last portion.

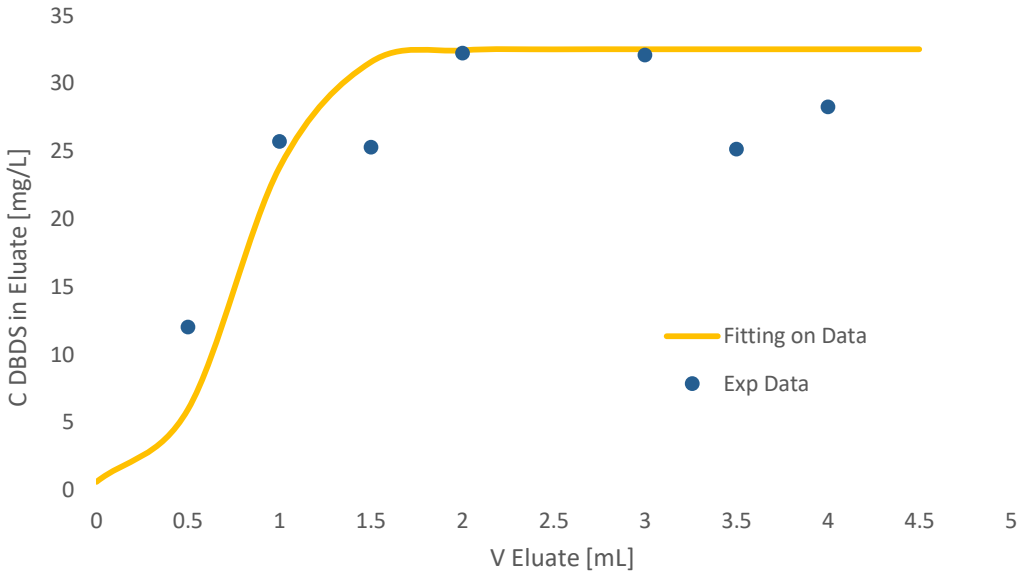

Figure 66. *The Breakthrough curve obtained form the absorption of a solution at 32.4 mg/L of DBDS in 8AcN: 2EtOH solvent on a SPE with 600 mg of Bulk-MIP-DVB-DBDS.*

The column capacity of 0.7 mL has been determined by the curve of the breakthrough curve and it corresponds to the adsorption of 22.7 µg of DBDS on a column of 600 mg of bulk MIP-DVB (0.113 mg_{DBDS}/g_{MIP}). The capacity of this MIP observed is lower in flow adsorption than in batch (0.56 mg_{DBDS}/g_{MIP} for non-porous MIP in Table 18). It is probably due to the kinetic process where only the more easily accessible sites can rapidly interact during the flow in the column.

3.1.6.2 Adsorption of DBDS from transformer oil

MIP has shown promise for the selective detection of our analyte DBDS, since no adsorption on the NIP has been observed. The MIP has been employed as sorbent phase in order to investigate the non-specific adsorption which could occur in complex matrices, i.e. transformer oil.

A particular oil of electric transformers, the "Nytro Libra", was considered. The investigation was conducted by pouring aliquots of oil into two columns, prepared one with 200 mg of non-porous bulk-MIP-DVB-DBDS (volume of the MIP column: 0.196 cm^3) and the other with 27.7 mg of porous-MIP-DVB-DBDS (volume of the MIP column: 0.057 cm^3) as previously described (the columns have a volume of 2.3 cm^3). The column consisting of the low-porosity bulk MIP-DVB-DBDS in particles obtained by grinding is packed with hexane. The sample mixture was prepared: 1:1 of oil:hexane at 25 mg/L of DBDS. A standard solution of DBDS at 540 mg/L in hexane have been used for the addition. 1 mL of the sample solution was injected in the column. The first drops which came out of the column consisted of the oil-hexane mixture and was discarded, whereby the column could be considered saturated with the oil-hexane mixture. Five portions of 2 mL each of eluate were collected, by flowing a solution of AcN:EtOH=4:1 at 0.2 mL / min. Each eluate was analyzed by UV spectroscopy and electrochemically, in order to determine the content of DBDS.

Figure 67 shows the mg of DBDS extracted after insertion of the mixture oil: hexane strengthened with the analyte vs the eluted volume.

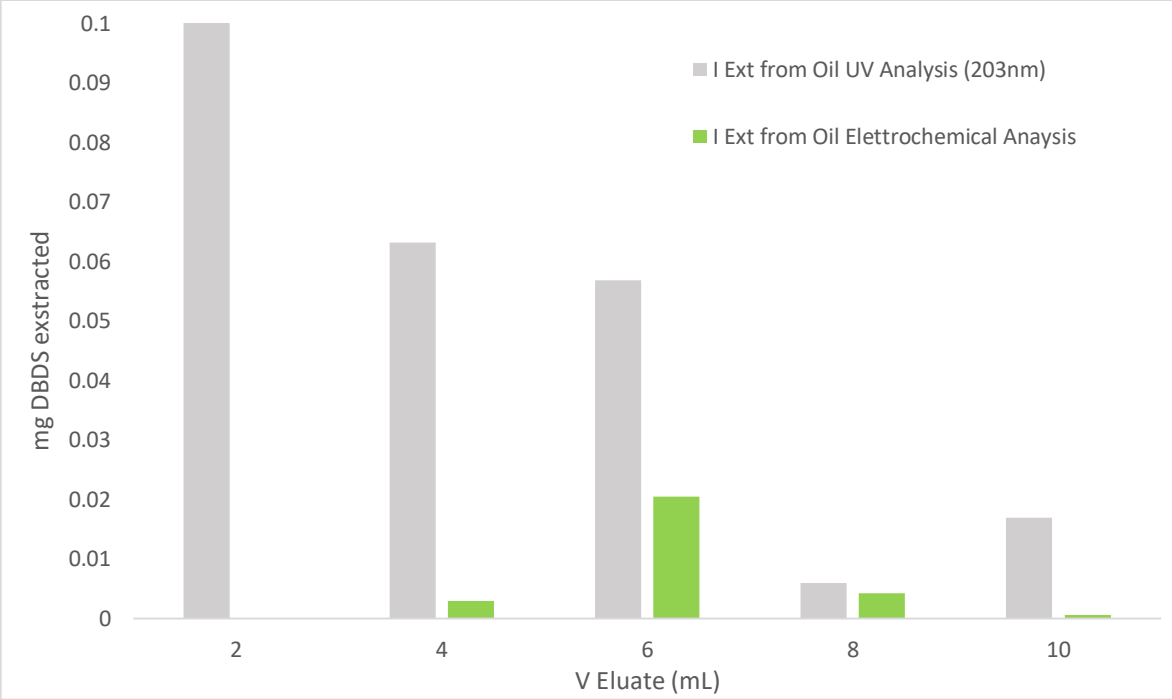

Figure 67: Extractions of DBDS from oil:hexane through the cartridge with non-porous bulk MIP (200mg). Eluent: AcN: EtOH=4:1 ; green bars: electrochemical analysis; gray bars: spectrophotometric analysis.

The amount of DBDS extracted in each eluent fraction is determined electrochemically by the standard addition method.

According to the electrochemical results on the extractions, it is possible to notice a Gaussian curve of elution; a very close quantity of DBDS has been recovered (0.022 mg) in respect to that introduced (0.025 mg), with a recovery of 88%. On contrary, strong interferences were observed by applying the spectrophotometric method which prevents the determination. These are probably the oil components adsorbed in MIP and co-eluted DBDS in the considered solvent, which however do not affect the electrochemical characterization.

The DBDS inserted in the column exit from the column after 6 mL of elution. The peak of elution can be considered as the retention volume (Vr), we can roughly evaluate the distribution coefficient between the two phases (solvent eluent and MIP) and a K_{aff} of the DBDS for the considered MIP (low-porosity bulk), since the column used can be considered more a cartridge for an SPE than a real chromatographic column for separations. It has been employed the relation (Eq.14) explained in the methods (par. 2.3.2.). K_D is equal to 41 $mL_{Solvent}/g_{MIP}$ ($25mg_{MIP}/mL_{solvente}$). As mentioned

previously, the constant results lower in the absorption in flow in respect to that obtained by batch procedure of 73 $mL_{solvent}/g_{MIP}$ ($13.3mg_{MIP}/mL_{solvente}$) since in the column only the most easily accessible sites can interact. Electrochemical and UV/Vis analysis confirm the possibility of the use of MIP as sorbent phase in SPE method with oil matrix. These SPE method opportunely tuned can lead to a percentage of recovery almost quantitative. However, for the employs with real oil matrix, further investigation to clean the eluted solution is needed, because of the interfering compound eluted, which enhance of the background current and made difficult to read the peak current of the analyte in the electrochemical analysis.

3.1.6.3 Unspecific adsorption on MIP of matrices compounds of the transformer oil

An additional column was considered to study the co-elution of interfering substances from oil. It was decided to investigate the porous-MIP as this polymer has a higher DBDS loading capacity than the bulk-MIP and seems to adsorb larger amounts of oil components. The column consisting of 27.7 mg of sieved porous-MIP packed with hexane. The column is loaded with 100uL of transformer oil, not containing DBDS. Then is was eluted 6 portions of 0.5 mL each of AcN:EtOH=4:1, maintaining a flow of 0.2 mL / min. Each of these aliquots was analyzed in the spectrophotometer.

Figure 68 shows the spectrum of the consecutive eluted portion from the SPE with porous MIP-DVB-DBDS after the saturation with oil in absence of DBDS.

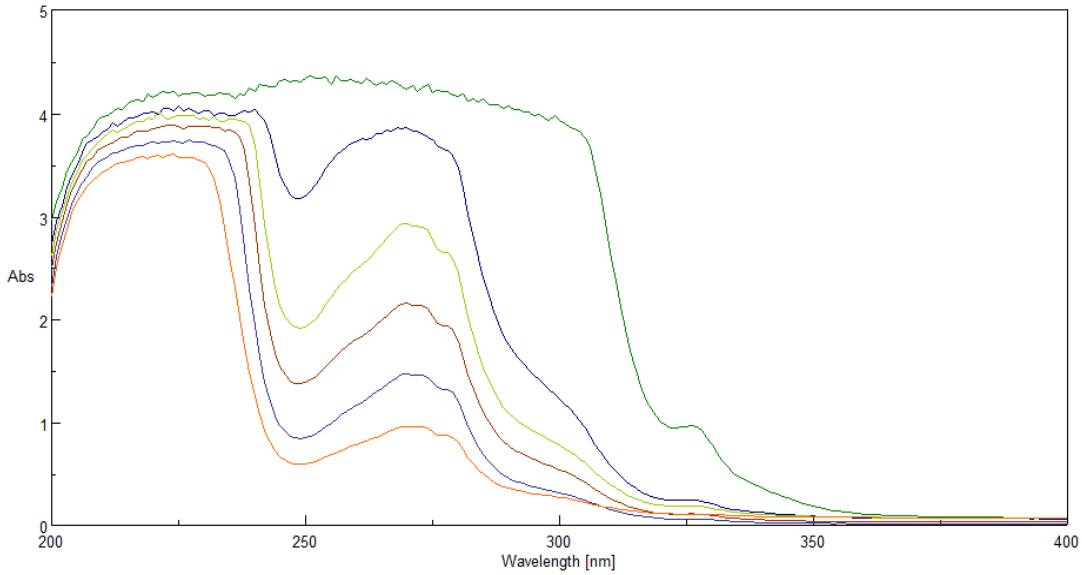

Figure 68. *UV spectra of the eluted portions form SPE with porous-MIP-DVB-DBDS collected with AcN:EtOH=4:1 after the saturation with oil in the absence of DBDS. All the portion were diluted 1:4 with AcN:EtOH=4:1 before the analysis.*

Table 25 shows the absorbtion at 270 nm of the diluted and undiluted eluates collected after saturation of the SPE-porous-MIP-DVB-DBDS column with oil not containing DBDS up to the saturation.

Table 25. *Spectrophotometric analysis at 270nm on the eluted portions form SPE-porous-MIP-DVB-DBDS diluted 1:4 with AcN:EtOH=4:1 and undiluted, after the saturation with oil in the absence of DBDS.*

n. elution	A 270 nm	A 270nm not dil
1 Elu	4,23614	16,94456
2 Elu	3,85859	15,43436
3 Elu	2,15082	8,60328
4 Elu	2,92627	11,70508
5 Elu	1,46938	5,87752
6 Elu	0,9598	3,8392

The first eluates show a very high absorbance in the UV region, far higher than that obtained from the washed MIP (as reported in 3.1.4.). This demonstrate the elution in AcN:EtOH=4:1 of a large

number of different substances absorbed in a non-specific way on the considered MIPs from oil. These substances interfere in the spectrophotometric determination since a high absorption peak was registered at the same absorption wavelength of the DBDS compound. Each eluted solution after oil saturation was also electrochemically analyzed by the standard addition method; the dose-response curves of are shown below in Figure 69.

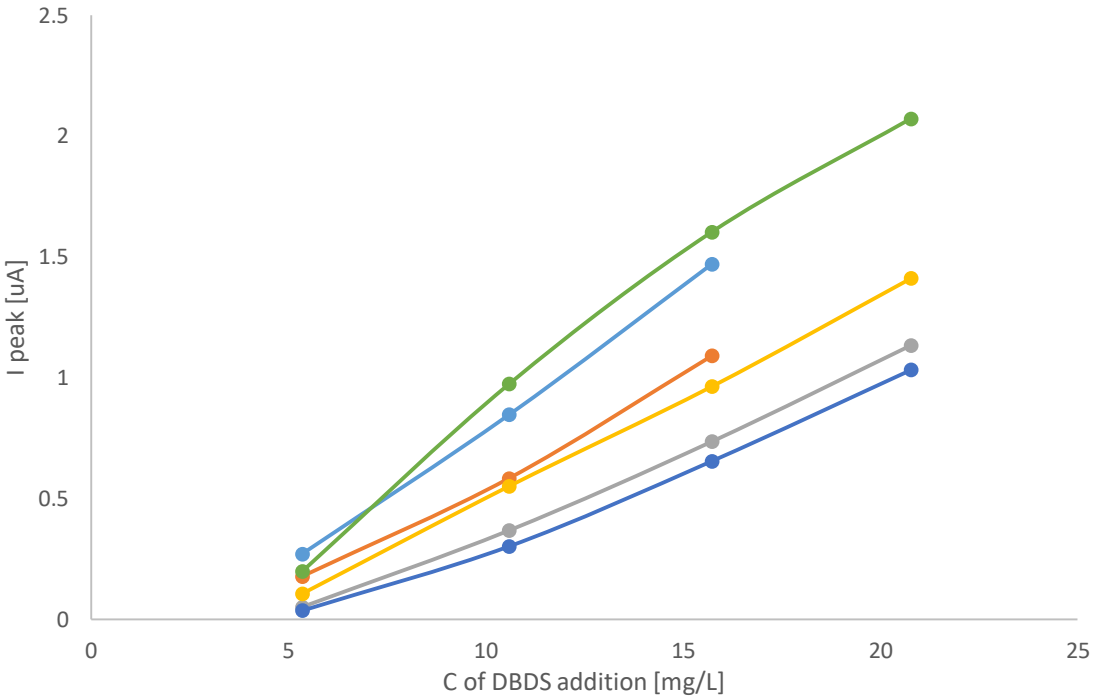

Figure 69. *Dose-response curves in the subsequent eluates of AcN: EtOH=4:1 from SPE-porous-MIP-DVB-DBDS column, after saturation with oil with no addition of DBDS. V eluted 0.5 mL, dilution 1:4.*

It can be clearly seen that all the aliquots show a negative ordinate at the origin preventing the electrochemical analysis.

3.1.7 CHARACTERIZATION OF THE ADSORPTION ON A MIP LAYER BY ELECTROCHEMICAL TRANSDUCTION

The adsorption on MIP can be characterized by batch equilibration as described in the corresponding paragraph 2.3.1. The experimental procedure is quite long and demanding since for example the phase separation is required. Moreover, in that case, the polymer is in form of small particles or beads, which is completely different from the MIP layer in a sensor. As a matter of fact, the adsorption on the polymer in this form is better characterized by a sensor in which the receptor in form of a layer is in contact with a suitable transduction method. In this way, the characteristics of the receptor can be evaluated exactly in the form which will be used in the sensor, this method of characterization of the MIP receptor layer is reported in the paragraph 2.3.3. Besides the characterization based on SPR, which is described in the relative chapter 3.2, other transduction methods can be applied. Electrochemical transduction is particularly suitable, since some electrochemical platforms, i.e. the screen printed cells, are not only robust, cheap and reproducible but also are easily derivatized with MIPs by a simple deposition procedure due to their flat shape [57; 135]. In this thesis, commercially available SPCs have been used, with comparable results obtained by SPR. To produce the receptor layer the prepolymer mixture is dropped over the whole SPC and polymerized at high temperature as described for the SPR sensors (par. 2.4.4). The extraction of the template is simply performed by successive flushing with 96% ethanol (par. 3.1.4). The measurements for characterization are performed with the robust and relatively cheap instrumentation required for amperometry or voltammetry and not any phase separation is required. When a MIP layer is present over the WE, or the whole cell, the electrochemical signal depends on the concentration of the electroactive substance in the layer, which is in immediate contact with the transductor, so that it can be used to characterize the adsorption reaction, as described in the paragraph 2.3.3. Two examples of this approach are here presented.

3.1.7.1 SPC with MIP imprinted for 2-FAL

The electrochemical sensor for investigating the adsorption characteristics of molecularly imprinted polymer for 2-FAL, in particular, the MIP-DVB-2-FAL deposited as a layer over an SPC has been realized by a simple procedure reported in 2.4.4., which has been previously described [57]. The prepolymer mixture composition employed for the deposition was the same reported in 2.4.1. for Bulk-MIP [57]. Square wave voltammetry was employed as the electrochemical technique in the condition described in 2.3.3. The measurements were performed taking advantage of the redox activity of 2-FAL. This has been demonstrated at a glassy carbon electrode, as reported in a different paragraph of this thesis (par. 2.2.2). The possibility of using an SPC with graphite ink as the working electrode (WE), derivatized with a MIP layer, has been here demonstrated. Measurements were performed in 5 ml of NaCl 0.1 M solution.

Typical Langmuir adsorption isotherms (dose-response curves) for different MIPs are reported in Fig.70, in terms of ip vs the concentration in solution phase ([A]/M). In the case of sensors [A] is equal to the total concentration of the analyte (c/M), due to the very small fraction adsorbed.

In Figure 70, Bulk-MIP-DVB-2FAL (MIP6), Bulk-NIP-DVB (NIP6), and Porous-MIP-DVB-2FAL (MIP5) are compared.

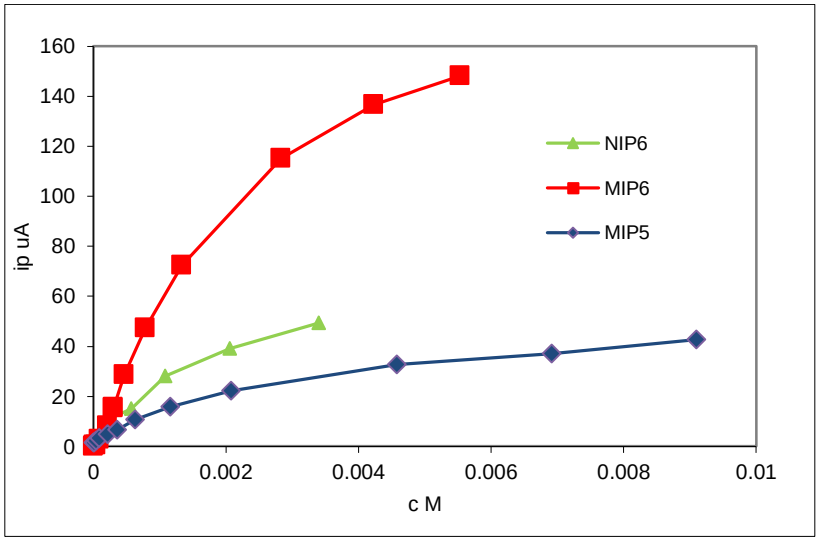

Figure 70: Langmuir adsorption isotherm on MIP6: Bulk-MIP-DVB-2FAL; NIP6: Bulk-NIP-DVB; MIP5: Porous-MIP-DVB-2FAL

The imprinting factor (see. Methods 2.3) is 2.6 for the Bulk-MIP-DVB polymer, and the adsorbing capacity is higher for Bulk-MIP-DVB than for Porous-MIP. The linearization of the Langmuir model equation by Scatchard equation (eq. 20) was employed to better define the MIP adsorption parameters. The Scatchard plots for the three considered sensors are reported in the following Figure 71.

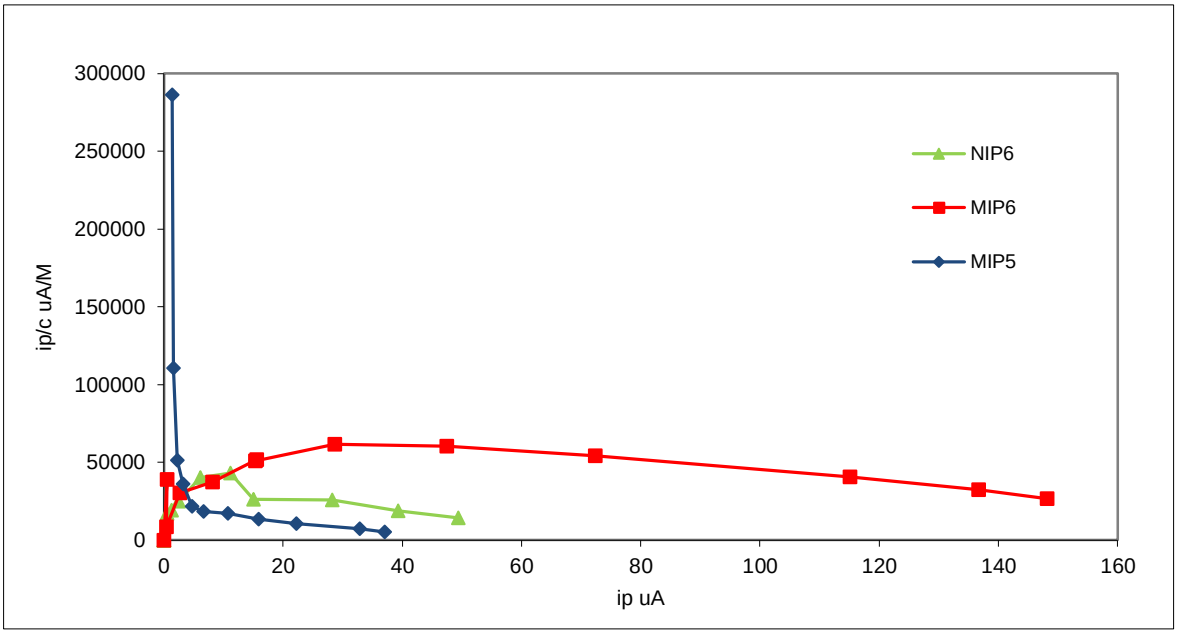

Figure 71. Scatchard plots for the three considered sensors MIP5: Porous-MIP-DVB-2FAL, MIP6: Bulk-MIP-DVB-2FAL; NIP6: Bulk-NIP-DVB;

The Scatchard fit is noticeably better in the case of MIP5 (porous polymer) as seen in Figure 71. It can be seen that only in the case of the sensor with MIP5 layer (the porous polymer) a curve with a negative slope is obtained, composed of two parts which are straight lines, according to the Scatchard plot when two kinds of sites with different affinity are present.

The Scatchard fitting of the two linear parts of the plot at low and high concentrations which consider sites of different affinity give are reported.

- Fit at high concentration:

$$\frac{i_p}{[A]} = -4.4(3) * 10^2 i_p + 21.8(8) * 10^3 \quad r^2 = 0.97 \qquad \text{Eq. 21}$$

- Fit at low concentration:

$$\frac{i_p}{[A]} = -2.5(1.5) * 10^5 i_p + 5{,}7(2{,}6) * 10^5 \quad r^2\ 0.73 \qquad \text{Eq. 22}$$

The parameters obtained by the Scatchard fittings are exposed in Table 26.

Table 26. Parameters from the Scatchard fitting at low and high concentration.

Scatchrad Fit	**K_{aff} (M^{-1})**	**Sensitivity with low c (µA/M)**	**kc_R**
c > 2 10^{-4} M	4.4(3) 10^2	2.18(8) 10^4	50
c < 2 10^{-4} M	2(1) 10^5	6(3) 10^5	2.4

The corresponding affinity constants (eq. 21 – 22) are 2.4(1.5) 10^5 M^{-1} and 4.4(3) 10^2 M^{-1} respectively at low and high concentration (Tab.26).

K_{aff} calculated at higher concentrations is very similar to that calculated for the sensors based on Bulk-MIP-DVB polymers (MIP6 and NIP6), while that at lower concentration could not be determined for the bulk polymers since they could not be fitted by the Scatchard plot (the slope was positive). Evidently, the WE is not accessible for low concentration of 2-FAL when the low porosity polymer is present over SPC. Notice that the stronger sites have K_{aff} about three magnitude orders higher than that of the weaker sites. On the other hand, the concentration of the stronger sites is about 20 times lower than that of the weaker sites.

By batch equilibration, only the weakest sites have been detected, because of the relatively high detection limits of the methods employed. Actually, the affinity constants of about 3 10^3 M^{-1} have been determined from water by the batch equilibration experiments (Tab.19 par.3.1.5). Only by the sensor method the stronger sites in MIP with 2.4 10^5 M^{-1} could be detected. By the SPR sensor sites with K_{aff} of 10^6 M^{-1} in water are detected, this affinity constant is not this different from that determined by the electrochemical sensor here presented.

3.1.7.2 SPC with MIP imprinted for Nicotine

A Bulk-MIP-layer for nicotine has been characterized by the same method previously described for the Bulk-MIP-layer for 2-FAL. The synthetic receptor for nicotine has been synthesized as reported in 2.4.4. The MIP layer has been prepared without any solvent, so to obtain a low porosity solid. The prepolymer mixture composition employed for the deposition was the same reported in 2.4.1. for Bulk-MIP [135]. The measurements were performed taking advantage of the ability of (–)nicotine (NICO) to be oxidized at carbon electrodes. Differential pulse voltammetry (DPV) was the electrochemical technique used for the preliminary investigation in the condition described in 2.3.3. Measurements were performed in water solution 0.1 M in KCl.

Some oxidation features appeared in the voltammograms which increased at increasing nicotine concentration, according to the Langmuir adsorption isotherm. The peak current (i_p) at around +0,7 V was measured at different concentrations (10^{-4} – 3 10^{-3} M), and the results were fitted by the Scatchard equation, obtaining the following parameters:

Table 27. The parameters obtained by the Scatchard fitting are reported.

K_{aff} (M^{-1})	**sensibility with low concentration (μA/M)**	**kc_R**
8(1) 10^3	2.2(3) 10^4	2.9

A constant i_p is obtained at a sufficiently high concentration of nicotine (from about 70mg/L), corresponding to the saturation of the imprinted sites in MIP. K_{aff} is not very high, as a consequence, the detection range is around 2 10^{-4} M. A similar affinity constant to that here obtained by the electrochemical sensor on the same Bulk-MIP-DVB of 7 10^{3} M^{-1} was determined by an SPR sensor in a previous investigation [135]. The concentrations lower than 10^{-4}M were not considered since the data cannot be fitted by the Langmuir sorption isotherm, as observed above in the case of Bulk-MIP-DVB-2-FAL for concentrations lower than about 4 10^{-4}M. Sites with much higher K_{aff}, of even several magnitude orders, could be characterized on a similar but porous MIP formulation. These results for the Bulk-MIP-DVB layer receptor for nicotine are similar to those obtained for Bulk-MIP-DVB layer receptor for 2-FAL, giving the proof of concept that using an electrochemical sensor for the characterization of the adsorption on MIP can be effective, both when the electrochemical reaction is a reduction or oxidation. The results obtained for Bulk-MIP-DVB for nicotine prove that relatively thick bulk (non-porous) layers can prevent the contact of the reactive substance with the WE.

3.2 OPTOELECTRONIC SENSORS BASED ON MOLECULARLY IMPRINTED POLYMERS

3.2.1 MULTIPLEXING SPR-MIP-POF D-SHAPED SENSORS

SPR sensors based on MIP have been successfully proposed for detection of target analytes in complex matrices, in several fields (see 1.4.2.). Different platform configurations have been proposed, among which a D-Shaped POF configuration has been successfully applied by our research group for several small molecules monitoring such 2-FAL [19], DBDS [14], TNT [10] or L-nicotine [135].

Platforms of this kind have a very good optical sensitivity of about 2500 nm RIU^{-1} at RI= 1.35 and a very good resolution of 0.0006 RIU, even with inexpensive instrumentation [18]. These platforms are rapid to prepare, not expensive, suitable for a convenient receptor deposition, and they make measurements at low concentration in small volumes possible. Moreover, these sensors are of small dimensions, so this makes them attractive for the multiplexing determinations. In this work, the possibility of employing the D-shaped POF platform in a multiplexing configuration has been investigated.

As a proof of principle, the possibility of the simultaneous determination of two analytes was investigated. Dibenzyl disulfide (DBDS) and furfural (2-FAL) in power transformer oil have been studied in consideration of their importance in quality control of this interesting matrix. Actually, DBDS is responsible for the corrosive properties of transformer oil and 2-FAL is a product of paper degradation in the insulant layer of a transformer, so both are used as a marker of the "health status" of a transformer [19; 134; 192-193].

The point is that the resonance wavelength of an SPR-MIP sensor scarcely depends on the chemical nature of the analyte, but mainly on the RI of the dielectric in contact with the gold layer, i. e. of the polymeric layer. The idea was to differentiate the resonance wavelength of the two analytes by considering different gold layer thickness [14-15]. Thus, preliminarily the performance of the D-shaped optical platforms with different gold film thickness was investigated, comparing two platforms with 30 nm and 60 nm thick gold layers.

The characterization of the SPR sensors has been performed in the same matrix in which the sensors will be used, i.e. a blank (=not containing the considered analyte) mineral transformer oil (Nytro Libra) spiked with different concentrations of the analytes, by determining the resonance wavelength variation with the analyte concentration, evaluated from the normalized transmission spectra. The experimental data have been treated considering the Langmuir adsorption isotherm, corresponding to a site by site adsorption. Thus, they could be fitted by the Hill equation to evaluate the affinity constant of the MIP sites and the dynamic range ($\Delta\lambda_{max}$) of the determination. The SPR transmission spectra were obtained by dropping 40 µl of the appropriate solution on the platforms with MIPs and without MIP (bare platforms), and incubating for 5 min. The platforms were rapidly washed with hexane after each measurement. Each experimental value is the average of 5 subsequent measurements, always taken after 5 min incubation with the respective standard deviations. The two bare optical platforms (configuration without MIP) with different gold layer thickness were characterized independently, using solutions of glycerin in water. They were characterized in terms of refractive index by using an Abbe refractometer. The MIP sensors were then simultaneously characterized in the cascaded configuration (see Fig. 13 Par. 1.4.4.1.2).

The possibility of performing measurement in a particularly convenient way for practical application, i.e. in a few µl drops, is offered by the shape of the optical platforms here proposed, which presents a flat surface and can be easily maintained in a horizontal position (see Fig. 13 Par 1.4.4.1.2).

The surface plasmon resonance wavelength spectra at the bare D-shaped POF optical platforms with different gold layer thickness have been obtained independently. They are reported in Fig. 72 for the platforms with 30 and 60nm gold layers (Au30nm and Au60nm, respectively) and for liquid dielectrics with different RI (mixtures glycerine/water). In Fig. 72 the variation of the resonance wavelength shift with the RI of the dielectric is reported.

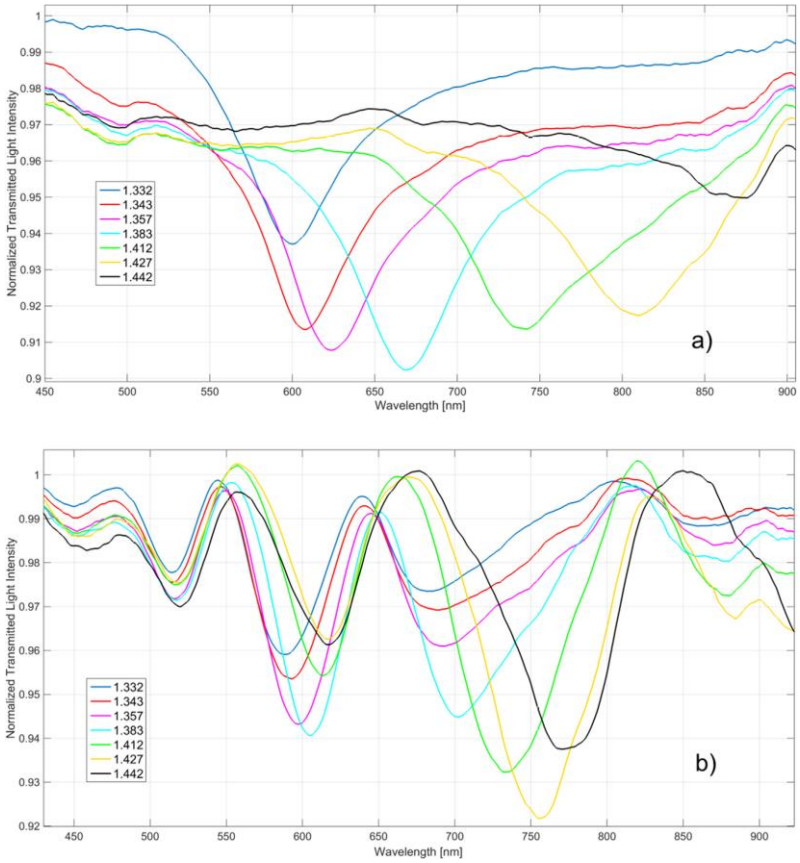

Figure 72. SPR transmission spectra, normalized to the spectrum in the air, for different liquid media with different refractive index (water-glycerol) of the aqueous medium. Configuration with 60 nm thick gold layer (a), and with 30 nm thick gold layer (b).

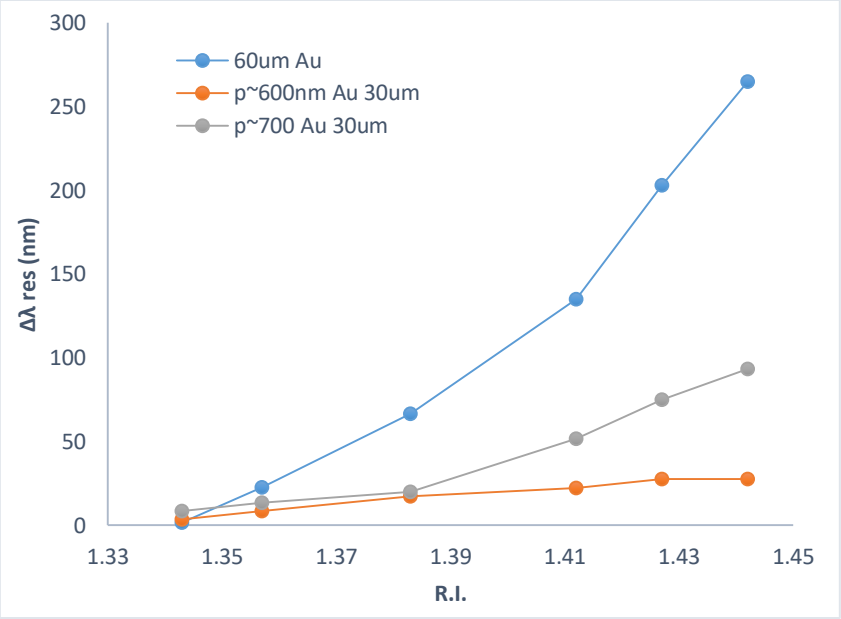

Figure 73. Overview of the variation of the resonance wavelength shift with the RI of the dielectric.

Wavelengths higher than about 950 nm should not be considered since in the experimental apparatus here used the transmittance results very low in that range [18]. Three main resonance dips are present for Au30nm, at around 510, 590, 690 nm in water, while only one for Au60nm, at 600 nm. All the minima are shifted toward higher wavelengths at increasing RI, i.e. the resonance wavelengths are red-shifted. The dependence of the shift (Δλ) on the RI of the sensing layer is linear only over small ranges. The optical sensitivity is higher at higher RI and noticeably different for the two platforms, being at RI=1.427, 270nm/RIU for the 30µm at 616.6nm and 2390nm/RIU for the 60µm at 809.5nm.

Especially at high RI, they are located at well different wavelengths. These characteristics are very promising for multianalyte detection based on in-series SPR-MIP sensors

The spectra obtained individually for the two MIP sensors are reported in Fig 74a and 74b. Fig.74a shows the absorption spectra of the SPR-MIP sensor for DBDS, with 30 nm thick gold layer. The transformer oil with different concentrations of DBDS is the liquid in contact with the MIP. It can be seen that only one dip is useful for detection, i.e. that at about 615 nm, which is red-shifted at increasing concentration of DBDS in the oil. In this case, the red-shifted SPR resonance is located in the middle of the spectral region of detection, i.e. at about 615 nm. Fig.74b shows the spectra of

the SPR-MP sensor for 2-FAL, with 60 nm thick gold layer. Here too only one useful resonance appears, at about 860 nm, which is red-shifted for increasing concentration of DBDS.

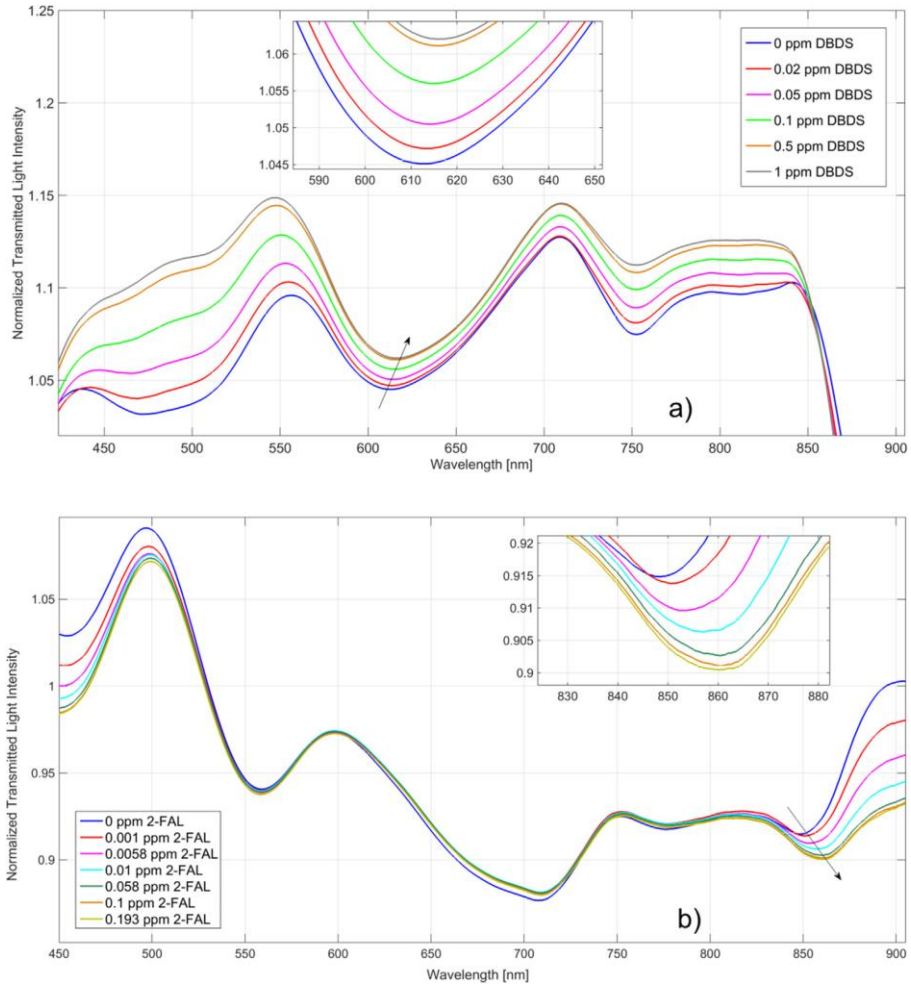

Figure 74. *a) POF-MIP sensor with 30 nm thick gold film: SPR transmission spectra for different concentrations of DBDS (mg/L) in oil. b) POF-MIP sensor with 60 nm thick gold film: SPR transmission spectra for different 2-FAL (mg/L) concentration in oil. Insets: zoom of resonance wavelengths.*

From the spectra in Fig.74, it can be seen that the resonance wavelengths of the two MIP sensors are very different. Noticeably, this is in agreement with the findings for bare platforms (Fig.72). Here too, for RI of the dielectric layer higher than 1.42, no resonance peaks appear around 615 nm for the Au60nm platform (see Fig. 72a) and no resonance peaks appear around 860 nm for the Au30nm case.

As previously described in the case of similar sensors [10; 135], the SPR wavelength shifts, with respect to the resonance wavelength at 0 mg/L, can be fitted by the Hill equation, in order to determine the affinity constant and other parameters of interest. In the case of DBDS the following values have been obtained at resonance wavelength around 610 nm: Kaff=5(1) 10^6 (M^{-1}); sensitivity at low concentration=2.3(7) 10^7 (nm M^{-1}); LOD = 7 10^{-8} (M). In the case of 2-FAL, the chemical parameters of interest, calculated by the Hill fitting, at resonance wavelength around 850 nm, are: K_{aff}=1.1(3) 10^7 (M^{-1}); sensitivity at low concentration = 5(2) 10^7 (nm M^{-1}); LOD = 3 10^{-8} (M). These parameters, obtained individually for DBDS and 2-FAL, are similar to the values determined by two optical platforms with 60 nm gold layer for DBDS and 2-FAL previously considered [134], independently of the fact that gold layers of different thickness have been used in the case of DBDS. It must be noticed that K_{aff} of 2-FAL from the oil matrix here considered is much higher than that from water, 1.1 10^{-6} M^{-1} [2].

In the multiplexing detection, the peak at around 615 nm (Au30nm sensor) can be used for the detection of DBDS. Whereas, 2-FAL can be determined with a MIP sensor with 60 nm thick gold layer positioned in series with the sensor for DBDS, on the basis of the red-shifted resonance at about 850 nm, since no resonance due to DBDS is present at this wavelength.

The normalized transmission spectra of the “in series” configuration, with the 2-FAL sensor following the DBDS one (see Fig. 13 par 1.4.4.1.2), are reported in Fig.75 for different 2-FAL and DBDS concentrations. Two resonance dips are formed at around 580 nm and 760 nm, which are ascribed to DBDS and 2-FAL, respectively. The dose-response curves at about 580 nm for DBDS and 760 nm for 2-FAL are shown in Fig. 75.

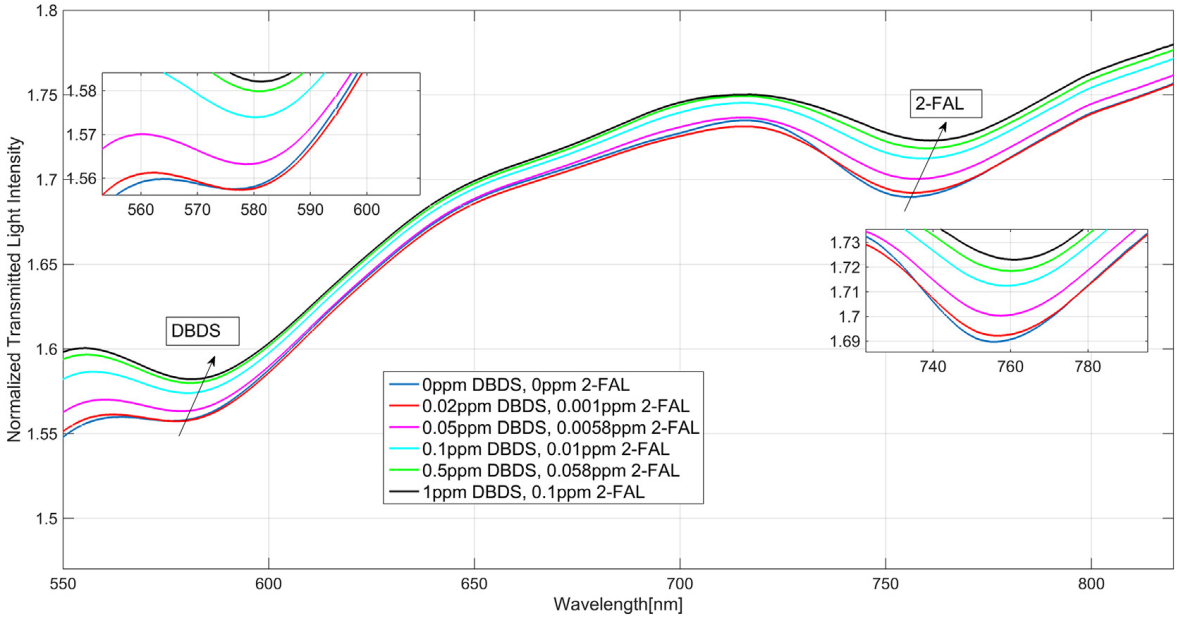

Figure 75.*The dose-response curves of DBDS at about 580 nm and for 2-FAL at 760 nm.*

Notice that the resonance wavelengths do not exactly correspond to those of the single platform (Fig. 75 and Fig. 74), due to the fact that higher order modes filtering of the multimode fiber are produced in the D-shaped POF waveguide.

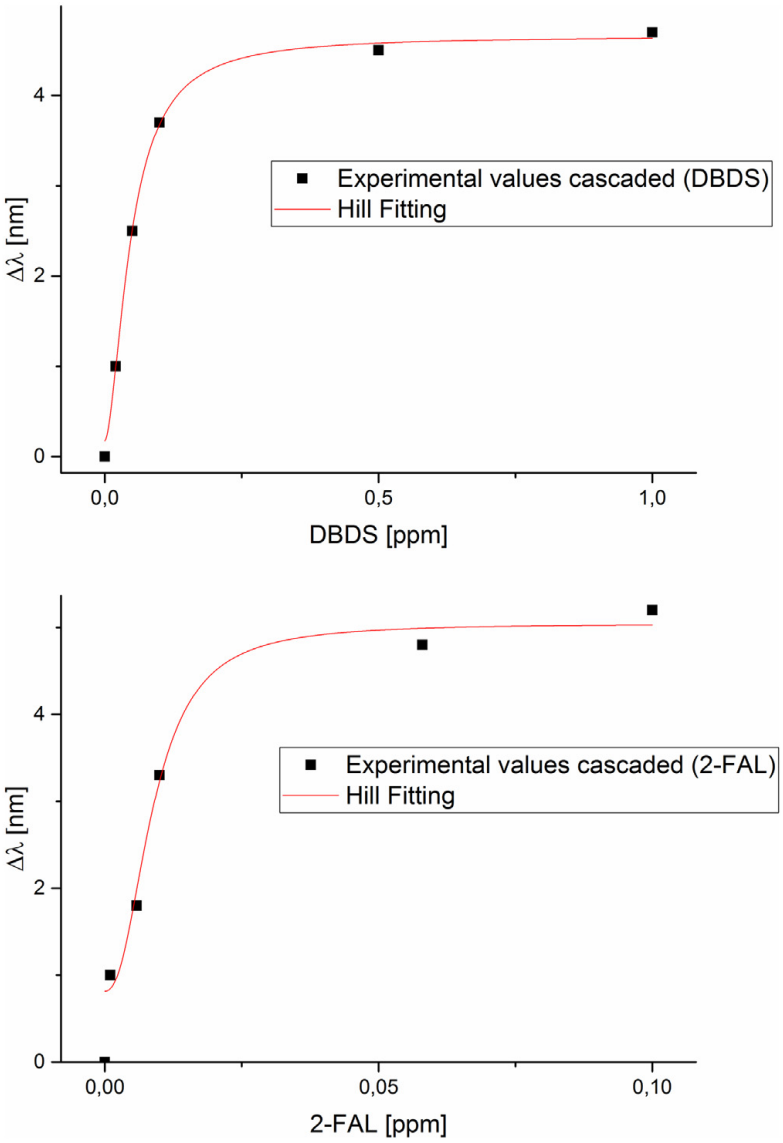

Figure 76. *Standardization curves for DBDS and 2-FAL, obtained from the resonance wavelengths of Fig.70.*

The chemical parameters obtained by the Hill fitting of the data obtained for the two analytes in the cascaded configuration are reported in Table 28.

Table 28. Parameters from the Hill fitting of the data of the two analytes in the cascaded configuration from mineral transformer oil.

Sensors	**$\Delta\lambda_{max}$(nm)**		**K_{aff}(M^{-1})**		**Sensitivity with low conc. (nm M^{-1})**		**LOD (M)**
	Value	Std. dev.	Value	Std. dev.	Value	Std dev.	Value
DBDS at 30nmAu	4.5	0.8	$5\ 10^{6}$	$1\ 10^{6}$	$2.3\ 10^{7}$	$0.7\ 10^{7}$	$7\ 10^{-8}$
2-FAL at 60nmAu	4.2	0.8	$1\ 10^{7}$	$3\ 10^{6}$	$5\ 10^{7}$	$2\ 10^{7}$	$3\ 10^{-8}$

The relevant parameters are not significantly different from those obtained from the single analyte experiments. The relevant parameters are not significantly different from those obtained from the single analyte experiments. However, the LOD of 2-FAL is significantly lower than that obtained by the individual experiments, probably due to the fact that here the resonance peak is in a much better position, i.e. near to the middle of the detectable resonance wavelength range.

The affinity constant (Kaff) of 2-FAL for the considered MIP from transformer oil is about one magnitude order higher than that from water [2]. Moreover, K_{aff} obtained from the SPR sensor is about three magnitude orders higher than those which have been determined by the batch equilibration procedure reported in par. 3.1.5, indicating that different sites are involved.

For both the sensing platforms used in this work, different substances were considered for testing the selectivity. There was not any specific adsorption of the considered substances on the MIP, because no resonance wavelengths shift was observed, although relatively high concentrations were considered. For example, in the detection of DBDS, furfural (2-FAL) and diphenyl disulfide (DPDS) are impurities likely present in used transformer oils, and for this reason, they are possible interfering substances. However, they do not produce any wavelength shift at POF-MIP-DBDS sensor, so indicating that they are not adsorbed. This shows that the sites with higher affinity are also those with the higher selectivity.

Experimental results of cascaded SPR-MIP sensors, for the detection of two markers (DBDS and 2-FAL) directly in transformer oil, have demonstrated an attractive feature for industrial application. Only one spectrometer is required in this new configuration, so obtaining a low cost multichannel optical chemical sensor system. Here, only the possibility of investigating two different analyte has been considered, but the concept could be extended to a larger number of analytes. However, the width of the resonance peaks limits the number of analytes which can be simultaneously determined. This aspect is very important when multimode plastic optical fibers are used because the FWHM is very large. However, it has been shown that, in the experimental set up here investigated, it is sufficiently narrow to allow at least two analytes to be simultaneously determined. It must be underlined that a low reproducibility has been found for D-Shaped POF sensors. One of the irreproducibility factors of the platform is due to the manual procedure of fabrication on D-shaped POF, (geometry and dimension of the sensing core exposed) in which the

geometry and the exposure dimension of the core are not always the same. The manual fabrication affects also the pattern of the gold layer, introducing an irreproducible roughness. It is well known that a shift on the SPR occurs on different thickness of the metal layer [14-15; 166] and that multiple resonance peaks could occur on a not uniform layer deposition. The spectrum is also affected by the MIP sensing layer deposition since a different thickness can cause a change in the mean refractive index of this dielectric. Both the factors (metal or dielectric thickness), could even lead to a shift of the SPR resonance peak out from the useful sensing region of the spectrum (450-800nm). A relevant problem related to the use of this platform concerns the signal normalization. The normalization is required to obtain the shift in the resonance wavelength and constitute an important aspect of the measurement particularly because the resonance shift is not an intense signal. The reference spectrum is the transmission spectrum obtained at the bare platform, before the MIP deposition, in the air in which not any plasmon resonance is expected to take place due to the low RI of air. Most of the issues are due to the coupling of light which can changes when the D-shaped POF platform is disconnected from the measurement setup since the coupling of the light depends on the axes on which the platform fiber is connected to the instrumentation. The reference is acquired on the same bare platform in the air before the MIP deposition. Then, the platform is removed to deposit the MIP layer. After the in situ polymerization and washing, the platform is reconnected to the lamp source, but a slight change in the position can variate the coupling of light, so the reference is not good anymore. Normalization has been also been considered by employing the spectrum registered on the platform after MIP deposition, in the air and/or in contact with the solvent without the analyte. If the RI change consistently by MIP deposition, an SPR signal is generated, so that the reference is not free from the plasmon resonance and the obtained peak is not a “resonance” peak, but a “resonance difference” peak, which is often poorly defined. An analysis based not on the shift of the resonance wavelength but on the intensity of the resonance peak was considered too. Unfortunately, this measurement was even more irreproducible than the analysis based on the resonance wavelength shift. For normalization, it requires a reference spectrum obtained exactly in the same conditions. To this aim, other types of platforms have been developed, which will be presented in a subsequent paragraph.

3.2.2 SPR PMMA SLAB WAVEGUIDE PLATFORM

A characteristics of the D-shaped POF optical platforms which is scarcely satisfactory is the poor reproducibility. In the present research work other platform configurations with a better expected reproducibility have been built up and tested for sensing application in connection with MIPs as receptors. Here, the results obtained by the PMMA slab waveguide based sensor described in paragraph 1.4.4.2 are reported. The experimental set up is shown in Fig.14. (par. 1.4.4.2).

This platform has been optically characterized in a previous research [20], in which its satisfactory sensitivity (1330 nm/RIU) and other optical characteristics have been determined. The prepolymer mixture for MIP for 2-FAL was prepared according to the procedure reported in 2.4.4. [19]. A platform with a non-imprinted polymer (NIP) was characterized too. The NIP composition (without the template) and the preparation method were the same previously described [19]. The measurements were carried out by dropping a small amount of solution, about 50 µL over the MIP layer of the sensor, which was kept in a perfectly horizontal position by the special holder (Fig.12). The spectrum was recorded after five minutes incubation. The SPR spectra along with data values were displayed on the computer screen and saved with the help of advanced software provided by Ocean Optics. The SPR transmission spectra were normalized to the reference spectrum by Matlab software. In particular, the transmission spectra were normalized to the spectra obtained in air before MIP deposition, in which not any plasmon resonance is excited [20]. Notice that the experimental procedure for obtaining the transmission spectra was exactly the same as that described in the case of the D-shaped POF platforms (3.2.1).

The dose-response curves were obtained by plotting the resonance wavelength variation ($\Delta\lambda_{res}$) or the resonance wavelength (λ_{res}) as a function of the total 2-FAL concentration.

The normalized transmission spectra obtained with the SPR-Slab-MIP sensor are shown in Figure 77.

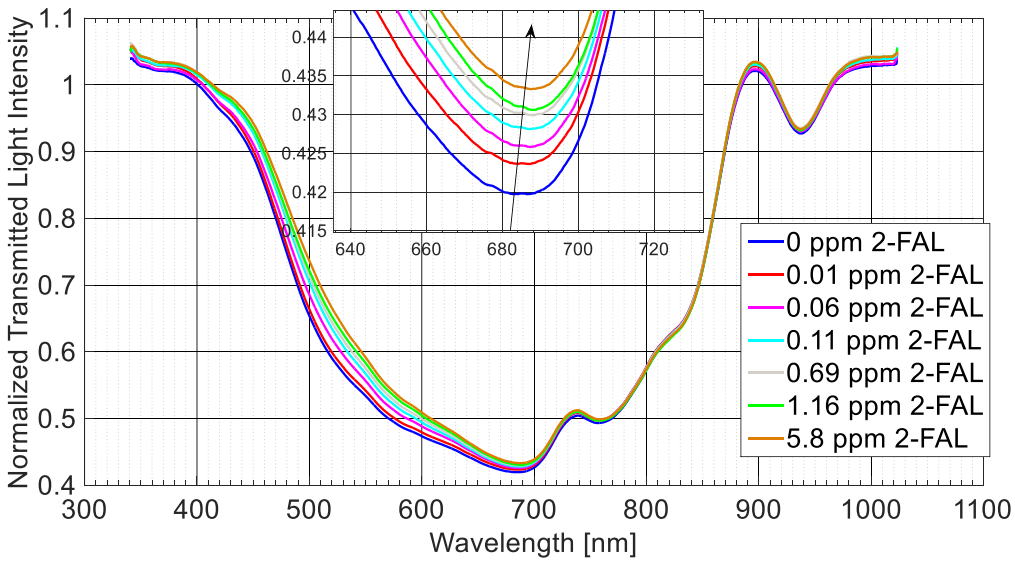

Figure 77. Normalized SPR spectra acquired by the SPR-Slab-MIP sensor for different furfural concentrations (in mg/L) in water. Inset: zoom of resonance wavelengths at 690 nm.

The spectra exhibit several transmission minima in the considered wavelength range (500–800 nm). The dip at around 690 nm is better defined than the other minima, and moreover, it depends on the 2-FAL concentration, as seen in the inset of Figure 77. There is a noticeable difference between the shape of the resonance peak, in particular the width at half height, of the platform in liquid dielectric [20] and that in the polymeric dielectric (MIP). This could be tentatively ascribed to the not perfect homogeneity of the polymeric layer opposite to the liquid layer. The resonance wavelength is shifted to higher values (redshift) when the 2-FAL concentration increases.

Figure 78 shows the resonance wavelength versus the analyte concentration (mg/L), on a semi-log scale. The fitting by the Hill equation [194] is reported below (Tab.29), which is satisfactory. Each experimental point (black square) is the average of 5 subsequent measurements and the error bars are the respective standard deviations (Fig.78).

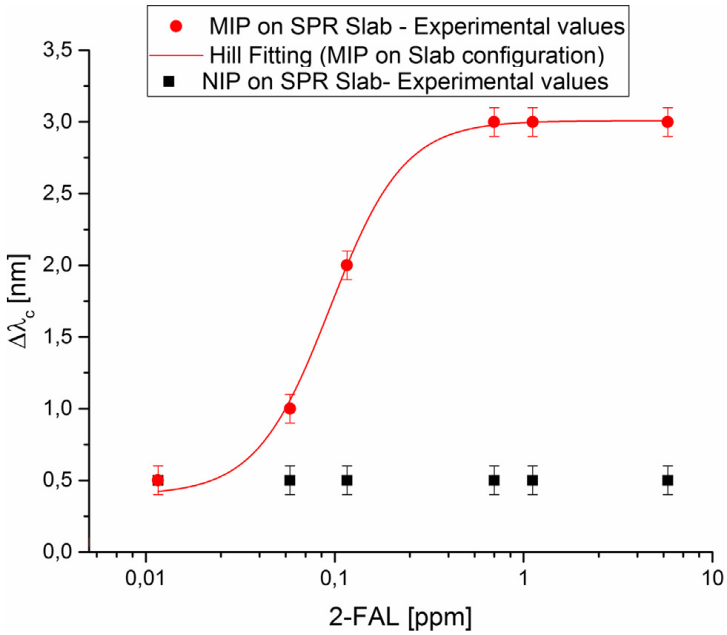

Figure 78. Resonance wavelength variation (with respect to blank 0 mg/L) versus 2-FAL concentrations, in semi-logarithmic axes, for SPR-Slab-MIP and SPR-Slab-NIP. The Hill fitting of the experimental values is also shown.

The parameters obtained and the associated standard errors are listed in Table 29.

Table 29. Chemical parameters from the Hill fitting of 2-FAL detection in water by a SPR-Slab-MIP sensor

Sensors	**$\Delta\lambda_{max}$(nm)**		**K_{aff}(M^{-1})**		**Sensitivity with low conc. ($nm\ M^{-1}$)**		**LOD (M)**
	Value	Std. dev.	Value	Std. dev.	Value	Std dev.	Value
SPR-Slab-MIP	3.0	0.1	$1.0\ 10^6$	$0.2\ 10^6$	$3.1\ 10^6$	$0.6\ 10^6$	$1.7\ 10^{-7}$

The affinity costant is $1.0\ 10^6\ M^{-1}$, i.e. very close to that found by the D-shaped POF SPR sensor [2]. The experimental results demonstrate that the proposed SPR platform is suitable for a chemical sensor based on MIP as receptor. It can be applied to the selective determination of 2-FAL in aqueous samples even at the low concentrations usually found, for example, in food or in environmental waters. For comparison a sensor based on a non-imprinted polymer (NIP) has also tested. The sensor based on a non-imprinted polymer (NIP) layer on the same SPR-Slab platform was examined by a similar procedure, but up to higher 2-FAL concentrations. Figure 75 shows the SPR transmission spectra, normalized to the reference spectrum (the transmission spectrum obtained in air before NIP deposition), for different 2-FAL concentrations (0-58 mg/L). A deep and

well defined peak is present, with a main resonance wavelength at around 521 nm, i.e. lower than that found on the MIP sensor. This indicates that the refractive index of the deposited NIP layer is different than that of the corresponding MIP layer. The most relevant information from Figure 75 is that the resonance wavelength is the same at different 2-FAL concentrations, indicating that 2-FAL is not adsorbed by the NIP, or if it is, it does not produce any refractive index variation of the polymer layer. Thus, aspecific adsorptions, i.e. those not involving the combination with the specific imprinted sites, are not relevant for the signal formation.

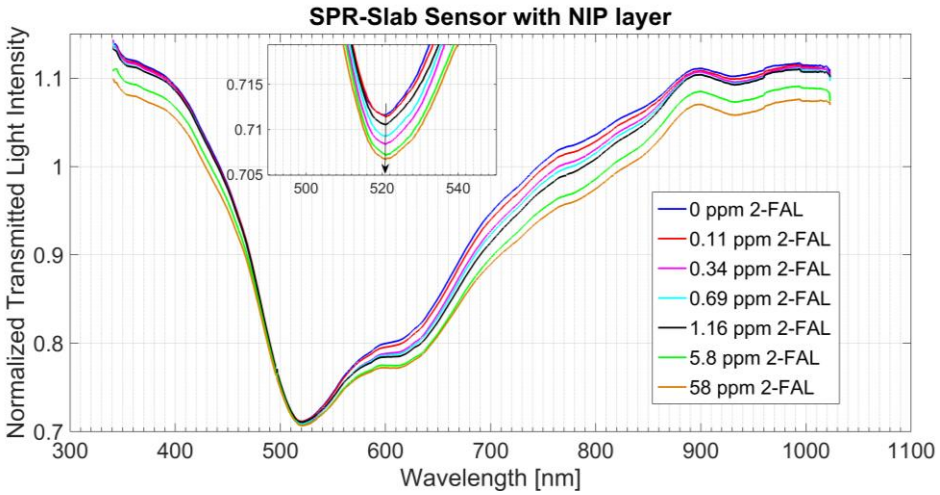

Figure 79. *Normalized SPR spectra acquired on the SPR-Slab-NIP sensor for different furfural concentrations (in mg/L) in water. Inset: zoom of resonance wavelengths.*

The advantage of this novel approach is the possibility of exploiting the input and output POFs to connect the equipment with the SPR sensor chip as waveguide. This has a better reproducibility from platform to platform, due to the better controlled thickness and roughness of the PMMA slab. Actually, not any manual operation is required for the preparation of the substrate, as for example a manual grinding of the fiber. Furthermore, the measurement itself is more reproducible since the connection of the input and output optical fibers is much more stable because of the holder. On the other hand, an irreproducibility due to gold layer formation and MIP deposition still persist.

3.2.3 INKJET PRINTED PET SLAB WAVEGUIDE PLATFORM

A different SPR waveguide has been developped, in which the metal layer was not obtained by sputtering, but by a different technique, i.e. Inkjet printing. This would ensure a more reproducible metal layer. Moreover, the metal layer can be deposited in different patterns. This preliminary investigation, carried out to demonstrate the principle of this transduction method, the pattern consisted of parallel lines. The substrate, which is also the waveguide, is a PET (polyethylene terephthalate) slab, with dimension 10x50x0.140 mm. The metal pattern was deposited by Inkjet printing, as described in par. 1.4.4.3. Since the metal is in form of nanoparticles, a L-SPR effect is expected to take place. On this pattern of silver nanoparticles the prepolymer mixture (200µL) was dropped and spinned for 2 min at 1000 rpm. Thermal polymerization was then carried out for 16 h at 80 °C. A non porous Bulk-MIP-DVB for 2-FAL layer was build up as a receptor over the optical platform as described in par 2.4.4. [2]

Two POFs (core of PMMA and cladding of fluorinated polymer, with 500µm of total diameter) connect the optical waveguide (PET layer covered with silver lines and MIP) with a light source and with a spectrometer, which is the same set up used for the D-shaped POF and the other platforms considered in the present investigation.

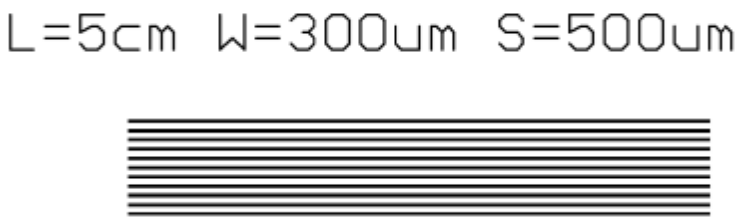

Figure 80. *The layout of the printed silver nanoparticles lines (the length (L) is 5cm, the spacing (S) is 500µm and the width (W) is 300µm).*

A schematic view of the platform with the connected POFs is reported in Fig.15 (par. 1.4.4.3*)*

The transmission spectra obtained at different concentrations of 2-FAL in water are reported as an example in Figure 81. These spectra were not normalized in view of the fact that the present study was only a preliminar investigation, aimed at demonstrating the possibility of building up optical

platforms of this type. When the concentration of the analyte increases, the output signal increases. It is evident that there is a significant modification of the sensor's output with analyte concentration in the wavelength range from 640 nm to 660 nm. Figure 81 shows the zoom of this wavelength range. The best sensitivity is clearly obtained when working at 652 nm.

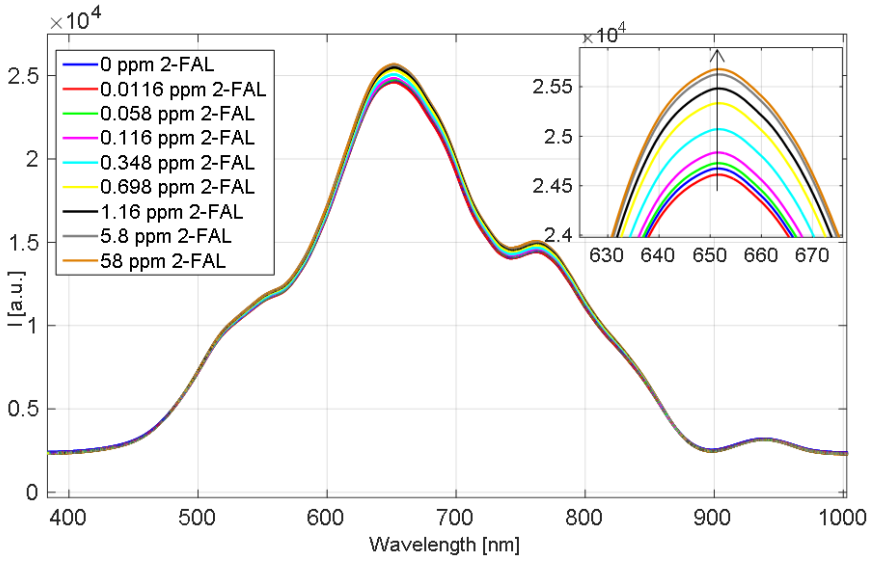

Figure 81. *Transmission spectra obtained by the Inkjet printed PET-MIP sensor for different furfural concentrations (in mg/L) in water. Inset: zoom of the wavelengths around at 650 nm*

Figure 82 shows the output values (I_{652nm}) versus 2-FAL concentration (mg/L) in semi-log scale and the Hill fitting to the experimental data at 652 nm. Each experimental point (black square) is the average of 5 measurements and the error bars are the respective standard deviations.

Figure 82 shows that the experimental data are well fitted by the Hill equation.

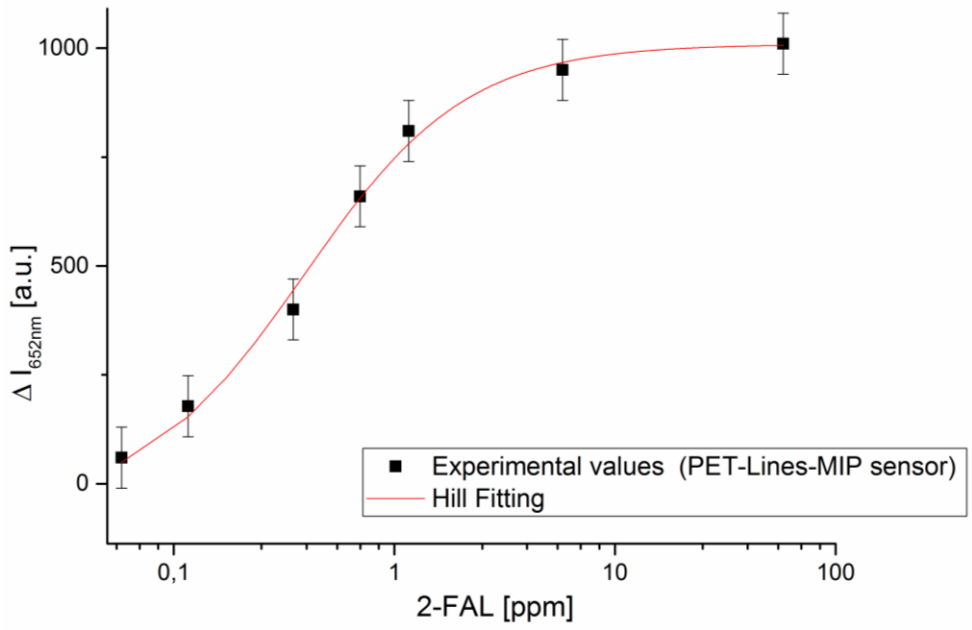

Figure 82. Inkjet printed PET-MIP sensor:Output variations (ΔI) as a function of 2-FAL concentrations (mg/L) in semi-log scale.

The parameters of the Langmuir isotherm obtained from the Hill fitting and the associated standard errors are listed in Table 30.

Table 30. Parameters obtained from the Hill fitting with the Inkjet printed PET-MIP sensor.

Sensors	**ΔI_{max}(a.u.)**		**K_{aff}(M^{-1})**		**Sensitivity with low conc. (a.u. M^{-1})**		**LOD (M)**
	Value	Std. dev.	Value	Std. dev.	Value	Std dev.	Value
Inkjet printed-PET-MIP	1009	32	$2.5\ 10^5$	$0.3\ 10^5$	$2.5\ 10^8$	$0.3\ 10^8$	$3.4\ 10^{-7}$

A similar sensor configuration, based on PET layer but without Inkjet printed lines of silver nanoparticles has been investigated for comparison. The experimental results obtained are shown in Figure 83. When the concentration of the analyte increases, the output signal, i.e. the intensity, decreases. It is evident that there is a significant modification of the sensor's output with analyte concentration, however, the effect is the opposite than that observed in the case of the platform with silver ink lines. This shows that the sensing mechanism is different in the two sensors, probably due to L-SPR in the case of the Inkjet printed PET-MIP, while to ATR attenuation in the case of PET slab [136].

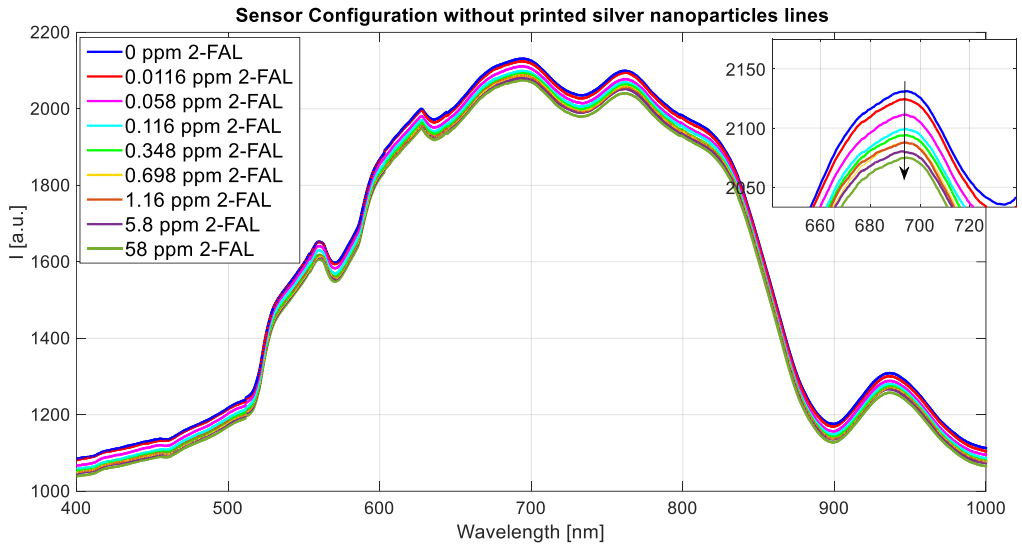

Figure 83. *Transmission spectra obtained by the PET-MIP sensor for different furfural concentrations (in mg/L) in water. Inset: zoom of the wavelengths around at 690 nm.*

Hill fitting of the experimental data is reported (Figure 84)

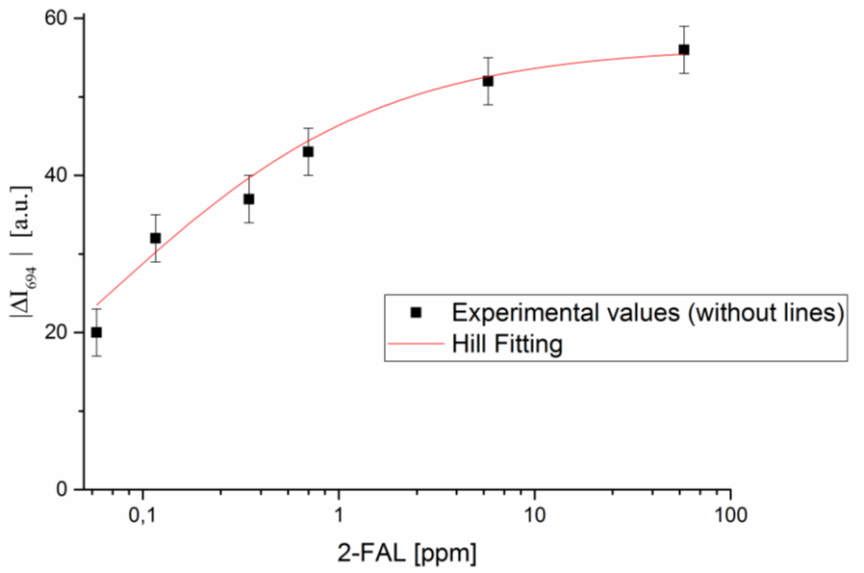

Figure 84. (PET-MIP sensor) Absolute value of the output variations (at 694 nm) as a function of 2-FAL concentrations, in semi-log scale, with Hill fitting of data.

The parameters obtained by the Hill fitting and associated standard deviations are reported in Table 31, in which they are compared with those by Inkjet printed PET-MIP.

Table 31. *Comparison between parameters obtained by Hill fitting on the Inkjet printed PET-MIP and PET-MIP sensors.*

Sensors	**ΔI_{max}(a.u.)**		**K_{aff}(M^{-1})**		**Sensitivity with low conc. (a.u. M^{-1})**		**LOD (M)**
	Value	Std. dev.	Value	Std. dev.	Value	Std dev.	Value
PET-MIP	56	6	$1.6\ 10^{6}$	$0.7\ 10^{6}$	$9\ 10^{7}$	$4\ 10^{7}$	$8.7\ 10^{-7}$
Inkjet printed-PET-MIP	1009	32	$2.5\ 10^{5}$	$0.3\ 10^{5}$	$2.5\ 10^{8}$	$0.3\ 10^{8}$	$3.4\ 10^{-7}$

From the data reported in Table 30, is it clearly seen that performances, in term of sensitivity at low concentration and LOD, obtained with the Inkjet printed PET-MIP sensor configuration, is better than PET-MIP sensor configuration. Obviously in this last case sensing is based on the evanescent wave attenuation, not on the SPR phenomenon. However, the latter sensing method can present some positive aspects such as the low-cost, simple and reproducible manufacturing procedure, due to the fact that not any metal layer or metal nanoparticle is present. In view of these promising results, a work aimed to improve the performances of the sensor, exploiting different geometries of printed silver nanoparticles lines, is presently in progress.

3.2.4 SWS OPTICAL PLATFORM

The schematic view of the fabricated optical platform is reported in Fig 16 (per. 1.4.4.4). A sensor for DBDS in transformer oil was developed as a proof of principle to demonstrate the operative possibilities of this type of platform. The proposed sensor could be viewed as two segmented waveguides coupled to each other, with the milled trench realizing the segmentation of both cores. The trench was filled with a MIP for 2-FAL, obtained by polymerization on site of the usual prepolymer mixture. The idea was to improve the repeatability of the platform by avoiding manual operations as far as possible while maintaining an easy and low-cost preparation method. Moreover, the problem of the normalization was here addressed by using two coupled optical fibers, the outputs of which were simultaneously measured. The experimental setup is schematically shown in Figure 85.

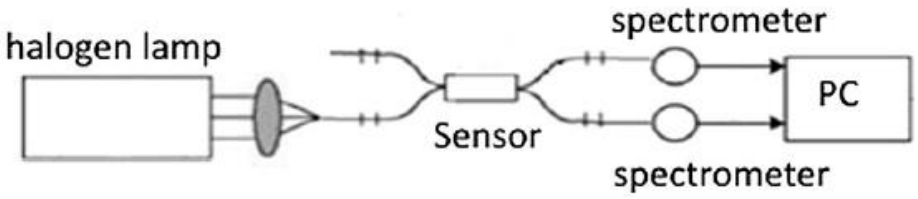

Figure 85. *Schematic wiev of the SWS platform experimental setup.*

A halogen lamp is connected to the input POF and the light intensity at the output (I_1) is measured and normalized to the light intensity coming out from the other POF (I_2). The analysis was performed by dropping 50 µL of sample solution over the MIP sensing region and waiting for the analyte to be absorbed on the MIP solid phase. When the refractive index of the MIP phase increases, because of the combination of the analyte with the receptive sites, the light intensity from the input POF (I_1) decreases while that at the output POF (I_2) increases. This approach permits to increase the sensitivity and to eliminate the irreproducibility introduced by the intensity fluctuations of the light source itself and the possible instability of the source to fiber coupling.

As an example, some results are reported in Figure 86, where the variation of the relative output ($S=I_1/I_2$) is plotted versus the log of the concentration of DBDS (mg/L), together with the fitting of the data by Hill equation.

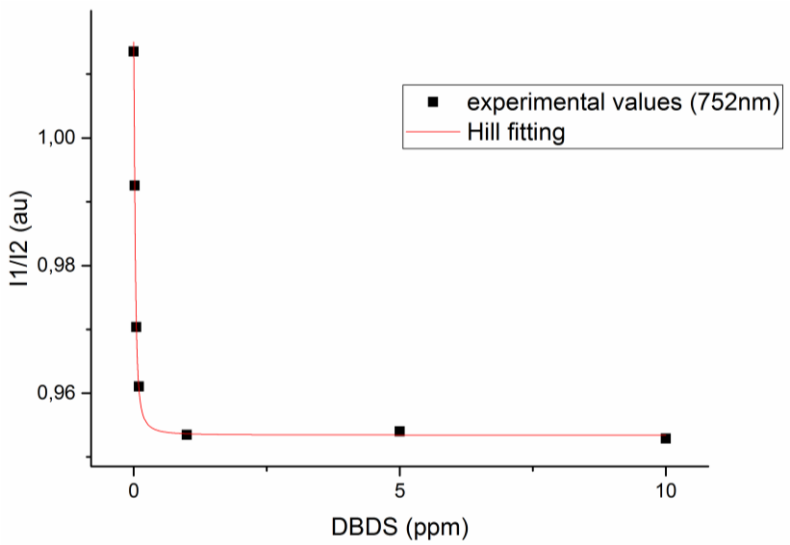

Figure 86. *Variation of the signal referred to the signal at 0 mg/L DBDS (ΔS) vs log of the concentration of DBDS [mg/L] and the fitting of the data by Hill equation. Data recorded at 752 nm.*

It is clearly seen that the relative output is decreased when the DBDS concentration increases, indicating that DBDS effectively combines with MIP from the oil matrix here considered by causing an increase of the refractive index of the polymeric phase. The light penetrating into the MIP phase is coupled to the second fiber.

The experimental points are well fitted by the Hill equation, confirming that adsorption takes place according to the Langmuir adsorption isotherm. The parameters evaluate by the Hill equation and the adsorption characteristics are summarized in Table 32.

Table 32 Parameters obtained from the Hill fitting with the SWS platform.

Sensors	**ΔY_{max}(a.u.)**		**K_{aff}(M^{-1})**		**Sensitivity at low conc. (a.u. M^{-1})**		**LOD (M)**
	Value	Std. dev.	Value	Std. dev.	Value	Std dev.	Value
MIP in SWS POF (752mn)	0.06	0.01	$8.8\ 10^6$	$0.2\ 10^6$	$5.2\ 10^5$	$2.4\ 10^5$	$5.3\ 10^{-8}$

It has been shown that this new sensor SWS Optical Platform can be used to monitor the refractive index variation of a MIP receptor layer as a function of the amount of adsorbed analyte. LOD of SWS platform of $5x10^{-8}$ M favorably compares with that of the SPR sensors as for example to those obtained with an SPR-POF-MIP sensor [1; 134]. The SWS platform could be more reproducible due to the simplicity of platform fabrication and to the absence of the Au layer. Moreover, the dimensions and geometry of this platform could be optimized in order to improve the sensitivity.

4 MOLECULAR IMPRINTING ON SILK REGENERATED FIBROIN

Recently, regenerated silk fibroin solutions derived from Bombyx mori cocoons have been used to form a variety of biomaterials, such as gels, sponges and films, for medical applications [195].

Moreover, it has been exploited as a scaffold biomaterial for cell culture and tissue engineering in vitro and in vivo [196]. In this work, the possibility of performing molecular imprinting on silk fibroin to develop a selective bioreceptor was investigated. The use of peptides as functional moieties for selective recognition of substrates has been presented in the literature [52-54]. In this work, we aim to use a protein instead of a peptide sequence to obtain the recognition of an analyte by exploiting non-covalent interactions usually not specific, but in which the selectivity is given by the precisely designed complementary structure. This could be obtained by the molecularly imprinting technique, exploiting the coordination of the substrate in solution with more molecular units either intramolecularly by the folding of the protein with a precise direction of the functional groups, or intermolecularly. Then the structure must be immobilized in a fixed structure complementary to that of the analyte, as it is done in the case of the molecularly imprinted polymers by polymerization in the presence of a cross-linker. In this case, the silk fibroin was used since this protein has been shown to be able to form insoluble thin layers suitable for application in optical sensors. As a proof of principle, a fibroin film imprinted for glucose has been prepared and preliminarily characterized.

The research was carried out at the SilkLab in the Biomedical Engineering Department at Tufts University in Boston. The idea is that a protein could adapt to a specific template by forming a pre-assembly of the functional groups around the template by electrostatic, H-bonds or other interactions. After formation, such specific sites should be able to maintain the shape even upon elution and rebinding. This possibility could be ensured by crystallizing the entire structure of the fibroin, containing the adduct pre-assembled moieties, into a solid phase with a designed structure [5; 197-198].

In fact, silk fibroin films, thanks to the appropriate optical (i.e. RI = 1.524 [108]) and mechanical properties, can be employed as a thin sensing layer on sensing devices with optical transduction, as for example those presented in this thesis, particularly those based on a flat sensing device. i.e D-shaped POFs or PMMA slabs. Other interesting complex optical structures such as gratings [5; 199], inverse opals [200-201] and waveguides [79], toroidal resonator [202], already developed with silk

fibroin have been considered in connection with optical transduction. Most of the preparations have been reported previously by the Silklab group. In this work, the possibility of obtaining molecularly imprinted structures on silk fibroin crystallized as a thin layer [5], with good affinity, selectivity, and capacity for a specific substrate has been preliminarily investigated.

In this investigation, as proof of principle, glucose has been considered as the template for the imprinting, considering its broad investigation with different transduction methods, even already approved in medical devices, as well as the compatibility with the various process required for the imprinting of fibroin [203]. Other analytes of interest in biomedical, biochemical and forensic fields can be considered too.

Native *B. mori* silkworm silk is composed of silk fibroin protein, the filament core protein, coated with sericin proteins, a group of soluble glycoproteins [204]. The silk fibroin consists of a light chain (Mw ~26 kDa) and a heavy chain (Mw ~390 kDa) linked by a disulfide bond [195]. Sericins are adhesive proteins and must be removed from the core fibroin fibers. Once this adhesive protein is removed, the fibroin fibers are dissolved into an aqueous solution that can be further processed into different materials. The protocols proposed by the Kaplan and Omenetto group [5] include methods to extract silk fibroin from *B. mori* cocoons and to fabricate hydrogels, tubes, sponges, composites, fibers, microspheres, and thin films. Silk fibroin is a polycrystalline copolymer composed of hydrophobic β-sheet crystallites embedded in an amorphous matrix of small hydrophilic linker segments [195]. Crystallinity can be induced via two methods, either by immersion in an alcohol such as methanol or ethanol or by water annealing. Water annealing is the process in which the silk materials are incubated in a humid environment for several hours [90-197]. The dominance of the β-sheet-forming regimes within the fibroin structure provides the protein-based materials with high mechanical strength and toughness. The toughness of silk fibers is greater than the best synthetic materials, including Kevlar [205]. In terms of strength, silkworm silk is superior to commonly used polymeric degradable biomaterials such as collagen and poly(l-lactic acid) (PLA).

4.1 ELABORATION OF THE SILK PROTEIN

The fibers of the silk need to be elaborated in order to obtain a solution useful for reshaping and chemical treatment; in our case the molecular imprinting. The process is summarized (Fig. 87) [5].

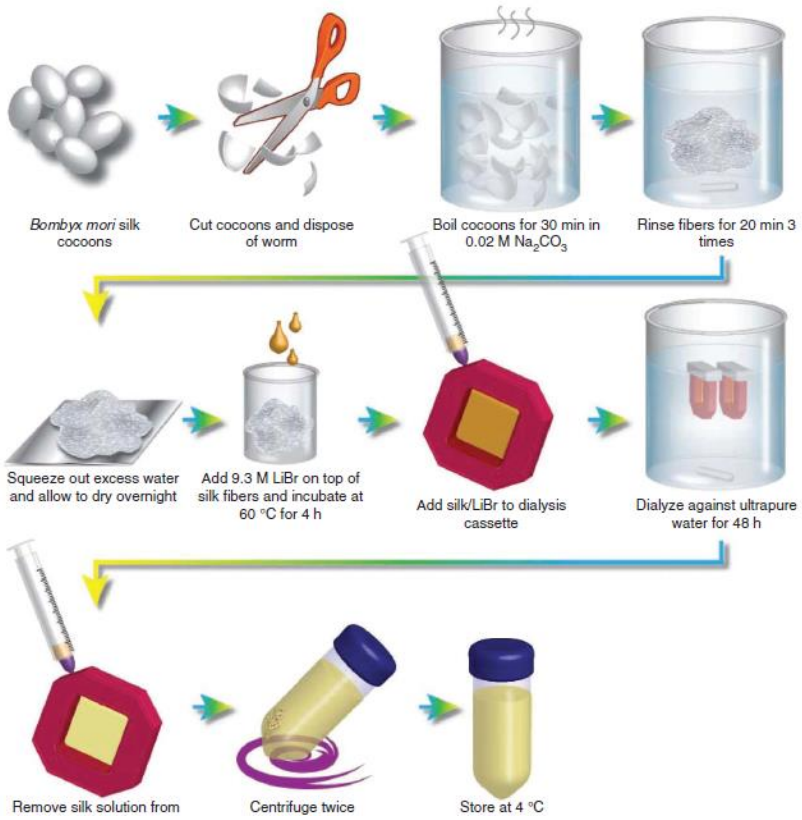

Figure 87. *Protocol of silk desolution [5]*

Briefly, the B. mori cocoons were shredded and boiled to degumming the fibroin fibers [5]. During this process, fibroin protein is denaturated and according to the boiling time, it is possible to obtain a different distribution of the molecular weight [50; 198; 203; 206]. In this work, 30min and 2h boiling were considered. Gel electrophoresis was performed to evaluate the molecular weight distribution. No separation of the strain has been performed after the boiling.

The procedure as it follows: 10.005g of shredder silk were placed in 4 mL of Millipore H_2O with 8.48g of Na_2CO_3 in a metal pot. boiled for the needed amount of time (2h or 30min) ensuring that the convective motion was achieved during boiling the process. The degumming was quenched under flowing water, and the silk was washed for 4 times by leaving the mass of silk in 4 liters of Milli-Q water under magnetic stirring and changing the water every 20min. this was the most critical part in the preparation of the pre-molecularly-imprinted solution since in this step the length of the biopolymer obtained is defined.

The drying process was performed under a hood or in a chamber with temperature and humidity controlled. In our case around 35°C and with a humidity of 21%, it was left until dry, usually for one day. The silk was left to drying on an aluminum foil.

A dissolving process was then performed in a LiBr solution 9.3 M, maintaining the temperature at 60°C for 4h. This process allows the fiber to be solubilized. The salt most probably can bring the fiber in solution by coordinating the Li^+ and the Br^- with the silk fiber on the protein end members (i.e. NH_4^+ and COO^-). LiBr solution was prepared to dissolve 14g of Silk dries fibers by dissolving 45,24g of LiBr in 56 mL H_2O of the final solution under stirring in a glass beaker. This solution is highly concentrated and allows a first separation of the not well-degummed fibers and that of extremely high M.W., which are not dissolved.

A dialysis was performed since it is necessary to eliminate the LiBr from the solution. It was performed by a dialysis membrane of 3.5 kDa with a capacity of 5mL/cm. The water have to be 200 times the amount of the silk solution, thus 5 L of Milli-q water were employed for 25mL of protein solution. Water was changed 6 times during 48h. At the end of the process, the solution was collected. A centrifugation and filtration was further required to eliminate the chain not dissolved or the aggregates. The centrifugation was performed at 4000 rpm/min for 20min refrigerated at 4°C and the filtration using a 0.04µm filter.

4.2 CHARACTERIZATION OF FIBROIN SOLUTION

4.2.1 DETERMINATION OF THE SOLUTION CONCENTRATION

The concentration was evaluated by a simple method. a known amount of volume of silk solution was deposed in a plastic weighing boat and dried in the oven. the product film obtained was weighed, obtaining the concentration. The result found for all the batches ranges from 6,6% and 6,8%.

4.2.2 CHARACTERIZATION OF THE M.W. OF THE PROTEIN

Gel electrophoresis was performed to test the MW distribution of the boiled batches (Fig.88).

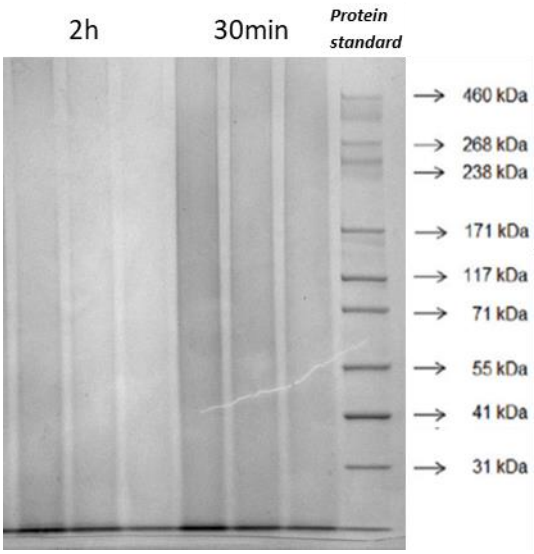

Figure 88. *Gel electrophoresis SDS-PAGE on fibroin batches boiled for 2h and 30min (each repeated 3 times).*

The boiling time influence the MW of the protein obtained as it clearly seen from the SDS-PAGE analysis and already know the literature [50; 198; 203; 206].

The calculation of the average MW present in the batches has been performed on SDS page by Image analysis with ImageJ. The protein standard intensity has been used to define the standard for the intensity of color in the image analysis as exposed in Figure 89.

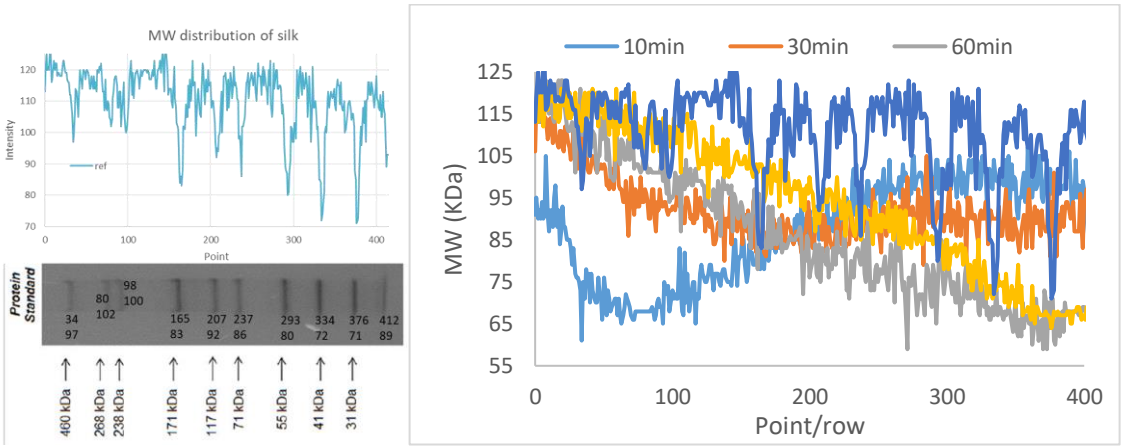

Figure 89. *a) Standard obtained from the analysis of SDS-PAGE, b) image analysis of the color intensity from the SDS-PAGE.*

From the analysis of image intensity of the grayscale on the SDS-PAGE, it was obtained the distribution of the different MW in the different sample. The MW distribution of the heavy fibroin should range from 31kDa at 268kDa for the 30min of degummed silk and is less than 55kDa for the silk boiled more than 90min, as know in the literature [203]. The results of the image analysis are reported in Figure 90 below:

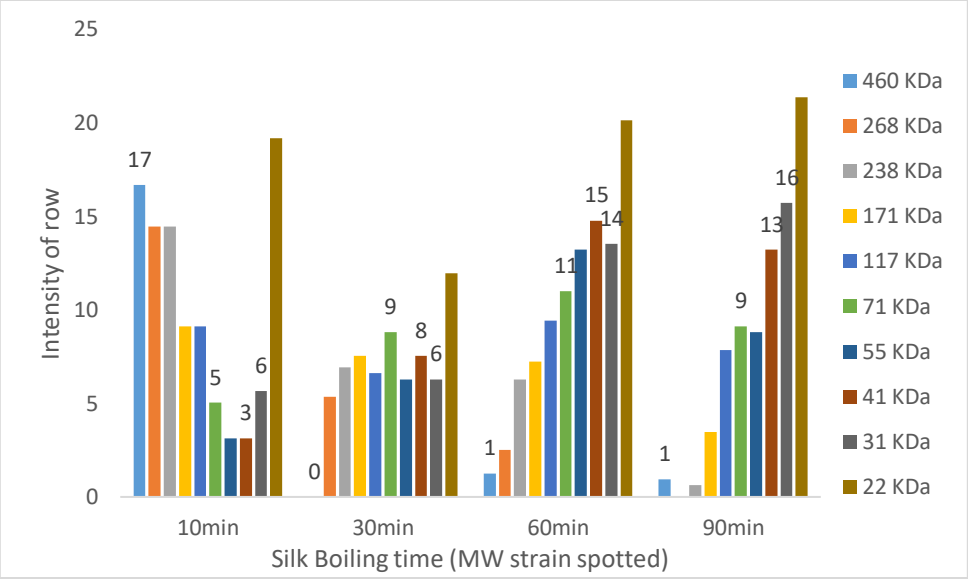

Figure 90. *MW distribution on the different batches for the increasing degumming time.*

The calculation of the weighted media on the MW distribution for the two batches employed was 69 kDa for the 30min degumming and 47 kDa for the 2h degumming.

4.3 MOLECULAR IMPRINTING OF THE FIBROIN (MIF)

4.3.1 COMPUTATIONAL MODELING OF THE RECEPTOR SITE

In MIP the functional monomers are used to create the pre-assembly with the site. In this case, we use a protein with a precisely given peptidic composition in which some peptide sequences can be recognized as “coordinating” moieties [54]. The most simple way to obtain a site is by folding the protein around the template establishing non-covalent interactions (hydrogen or electrostatic bonds) with the template. So, as a model, it was considered an intramolecular adduct by folding the peptide into a ring structure (Fig 91a). This could bestow the selectivity to the MIF sites, together with the thermodynamic stability of an intramolecular adduct. However, other intermolecular interactions are possible, due to the high concentration of the fibroin in the crystallized structure, so they were considered too (Fig.91b).

The silk fibroin protein derived from the B. *mori* silkworm has with well-defined amino acid sequences. The receptor binding site suggested considering the primary structure of silk fibroin as minimal coordinating moiety/block for the imprinting: [Gly-Ser-Gly-Ala-Gly-Ala] (M.W. 508.48 g/mol^{-1}).

Assuming that the site is formed by folding a determinate sequence i.e. the peptides of the primary structure (Fig. 91a), the block that coordinates can be modeled and the amount of imprinted site could be predicted.

Preliminary calculation by Density Functional Theory (DFT) function was performed to evaluate the binding capacity of this site (par. 1.2.2); the same calculation approach used for the MIP defining of the functional monomers for DBDS (par. 3.1.1).

Different models of coordination were considered based on intermolecular or intramolecular configuration, i.e. staking, sandwich or double-ring; an example of both the configuration is reported in Figure 91.

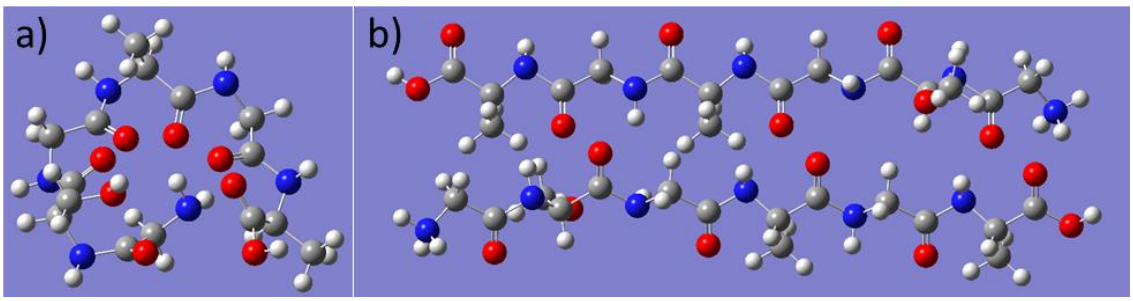

Figure 91. *Model of the adduct template-fibroin a) intramolecular (folded configuration), b) intermolecular (stacking configuration)*

Calculation of the thermodynamic stability of the models considered was performed. The optimized models calculated of the adducts glucose-fibroin with FOTP Method: RB3LYP Basis SET 6-311++G(d) in the vacuum are showed in Fig.92.

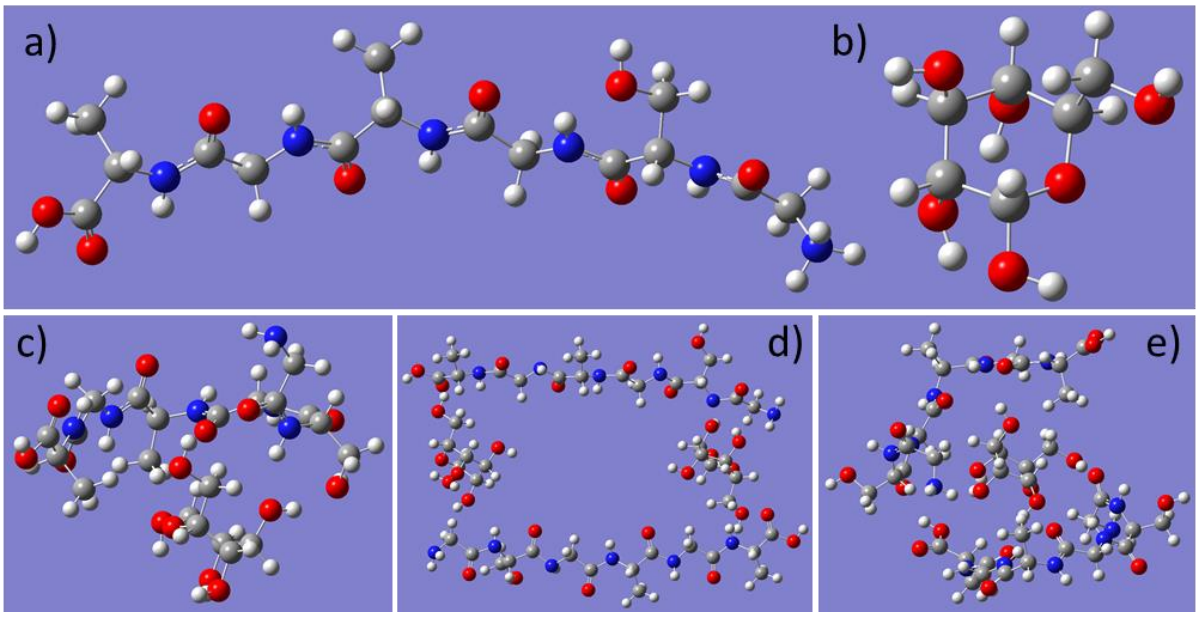

Figure 92. *Optimized models calculated of the adducts glucose-fibroin by DFT function on the two types of configurations (intermolecular and intramolecular) considered vs the fibroin and glucose in the vacuum. FOTP Method: RB3LYP Basis SET 6-311++G(d) a) Fibroin, b) Glucose, c) Intramolecular adduct Fibroin-Glucose, d) Intermolecular stacking (2xFibroin, 2xGlucose), e) Intermolecular sandwich (2xfibroin, 1xglucose)*

The relative stabilization energy of the optimized models calculated is reported in Table 33.

Table 33. Results on the optimized models calculated of the adducts glucose-fibroin by DFT function on the two types of configurations (intermolecular and intramolecular) considered vs the fibroin and glucose in the vacuum. FOTP Method: RB3LYP Basis SET 6-311++G(d) a) Fibroin, b) Glucose, c) Intramolecular adduct Fibroin-Glucose, d) Intermolecular stacking (2xFibroin, 2xGlucose), e) Intermolecular sandwich (2xfibroin, 1xglucose)

Stabilization Energies of Adducts	
Complex	GAS (kcal/mol)
Fibroin 1ststruct. (a)	-1518.59
Glucose (b)	-687.352
Folded add. (c)	-2205.44
Staking add. (d)	-4410.27
Sandwich add. (e)	-3723.44

Unfortunately, by the model employed no evidence of stabilization was found neither by the intermolecular or intermolecular structure considered. Most probably the site considered is not properly designed so, further study should be performed. An "**Adapting Biasing Force, ABF**" [207] calculation for a better understanding of the molecular folding and docking recognition will be carried out in the future.

The coordinating sites in protein strain calculated were 135 unit/fibroin molecule for the 30min boiled fibroin and 93 unit/ fibroin molecule for the 2h boiled fibroin. The concentration of the analyte for the imprinting was calculated in consideration of this ratio of the sites..

4.4 PREPARATION OF THE MOLECULARLY IMPRINTED FIBROIN FILM

The samples employ fibroin solutions at 6.6% concentration. Different molecular weights of the fibroin were employed obtained by different boiling times, in particular, 2h and 30min known in the literature to have a different molecular loss of the resulting chains [203] and yet characterized with gel electrophoresis to evaluate the effective range of the obtained molecular weights. An average value of 69kDa and 47kDa has been found respectively for 30min and 2h of boiled batches, in accordance with what reported in the literature [203]. The sample has been prepared by employing three different mixtures of molecular weight of the fibroin protein, a mixed solution with 47kDa and 69kDa and the other two batches with only one fibroin of molecular weight considered. The objective was to evaluate if the fibroin with lower molecular weight could be used as functional monomers to have high coordination.

The concentration of the template for the imprinting was calculated as a function of the estimated imprinting site (see 4.3.1.) as ratio Template:Silk coordinating site. Therfore, Glucose have been employed as analyte in three different concentration 137,5 mg/L – 260 mg/L – 350 mg/L for imprinting; all the film imprinted have been replied three times as statistic control. The standard was prepared from a glucose stock solution of 0,14M in a solution of PBS 30mM.

The solution was stirred by vortex for 3min. The aspecific adsorption was also evaluated through samples of not imprinted fibroin film (NIFF) with only boiled silk created in the same conditions of the imprinted film. In order to obtain reproducible films, the silk solution for obtaining films was deposited in a mold of PDMS with rectangular shape 4cmx2.8cm and 0.1cm thick. Total volume 1.12cm^2. For all the film the volume of deposition was 2mL. The drying was carried out in a drying chamber thermostated at 35°C and at a controlled humidity of 21%. The condition was optimized in terms of drying condition and size of deposition. The resulting film shows a small thickness, they were still transparent and with good mechanical properties to maintain the film shape during the batch analysis process; useful in view of possible use in sensors. The samples were treated by "water annealing" process to make them water resistant, inducing the transition from α-helix to β-sheets [197]. The "water annealing" was chosen with respect to the alcohol treatment or lyophilization already known in the literature [197-198] as it was considered to be less aggressive. Moreover, glucose used as the template is soluble in ethanol, i.e. the solvent used in the other treatment, so this certainly compromises the imprinting. The water annealing was performed by aqueous vapor,

in a closed oven at 70°C for 15h with controlled humidity. The vacuum was at -0.06Mpa. From literature, to complete the b-sheet formation of the film in this condition only 2h was necessary [197], to ensure the complete process it was left overnight. The water annealing step was found to be the most crucial and delicate during the synthesis of the sample, further efforts to improve this step should be investigated.

4.5 CHARACTERIZATION OF IMPRINTED FILM OF SILK (MIP-SILK AS FILM LAYER)

4.5.1 POROSITY AND MICROSTRUCTURE

The surface and porosity of the various films of not imprinted silk and imprinted silk were characterized by SEM imaging before and after the water annealing and after the dissolution of the analyte during the washing step. The use of AFM was also considered but no further information was discovered on the sample characterized. In bare-silk films, the surface is completely smooth and the porosity is absent. In the film with the analyte, a high superficial roughness and the presence of porosity are noted as a function of the different concentration of the analyte. However, the porosity is not proportional to the increase in the concentration of the analyte used in the imprinting solution. It is not clear whether the porosity is a function of the undesired crystallization of the analyte or derives from the incorrect water annealing which then causes a structural degradation during the dissolution phase of the analyte in the washings.

4.5.1.1 Morphologic and microstructure analysis by SEM

A SEM analysis was performed during the procedure of formation of the MIFF explained before, in order to characterize the effect of the various step on the microstructure.

A comparison of the MIFF and NIFF after the different steps of the formation procedure is reported in Figure 93.

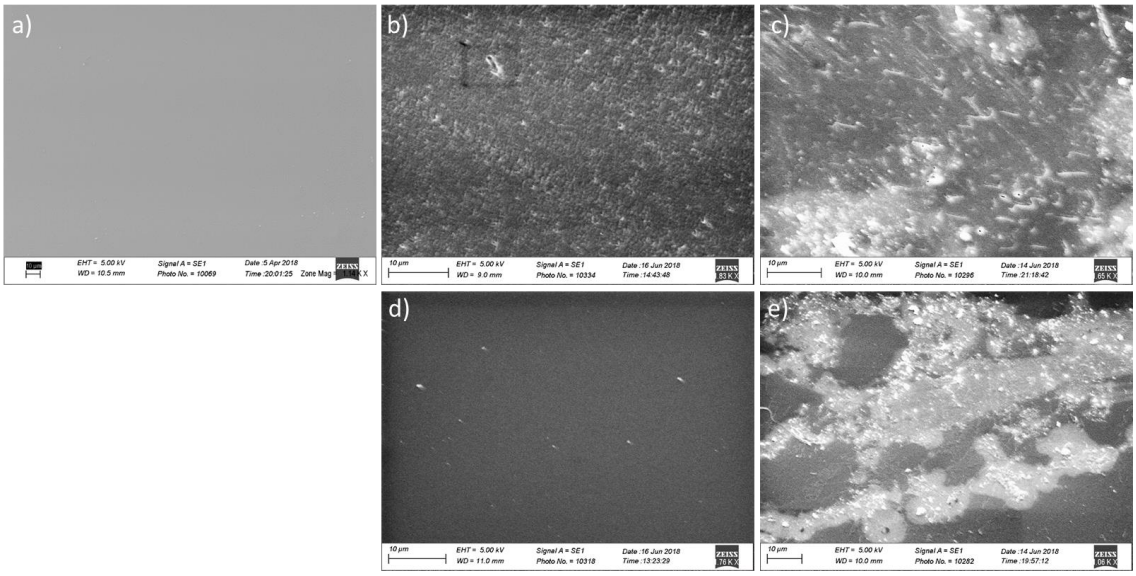

Figure 93. *Analysis of the microstructure of NIFF a) only dried film, b) after the water annealing, c) after the washing in PBS 30mM and MIFF d) after the water annealing, e) after the washing in PBS 30mM.*

The SEM analysis shows that the film of not imprinted fibroin after the drying is flat and without porosity a) while it became porous, with a rough surface right after the water annealing b). This effect could be due to a reorganization of the randomly distributed fibroin strands into crystalline β-domains. In the case of the imprinted fibroin, it was found that the compact and flat surface with a smooth surface still persists after the water annealing. This difference could be due to the glucose (template) which can be inserted in the structure and create a coordination plane which tends to compact the structure as exposed from Mason at all. (208).

After the washing, a diminish in the density of the structure have been observed, since the portion of fibroin which was not completely organized in β-sheets tend to dissolve (confirmed even by the FTIR analysis on the 4.5.1.2 below Fig. 97). A more uniform structure is observed in NIFF than MIFF. In the case of MIFF, the not uniformity of the structure could be due to the desorption of either the glucose and the fibroin not properly water annealed. An overview of the surface microstructure of

MIFF consisting of fibroin at different MW (47kDa, 47-69kDa, 69kDa) after the washing procedure is shown in Figure 94.

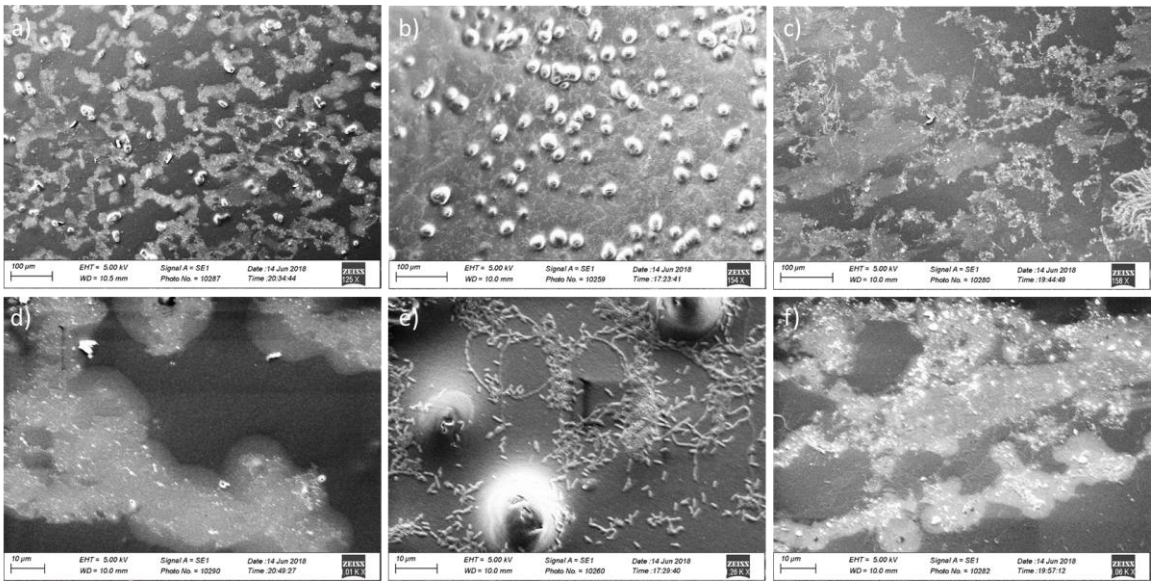

Figure 94. *SEM images of the sample at around 150x magnification of a) 47kDa, b) 47-69kDa, c) 69kDa; a magnified image of the same sample at around 1kx of c) 47kDa, d) 47-69kDa, e) 69kDa.*

The samples result to be different, a random distribution of bubbles was observed on the surface of the films, in particular in the case of the MIFF with mixed MW (47-69kDa). However, in the latter case, some structures are present on the surface (Fig 94e); this phenomenon is unknown. The presence of bubbles is probably due to the evaporation of the solvent during the water annealing.

4.5.1.2 Characterization of the Refractive index and thickness

The thicknesses and refractive index of the fibroin films have been characterized by 633nm Metricon instrument (see par.2.2.9) per literature [108]. Here is reported as exemplification a transmission spectra of a NIF film (Fig. 95).

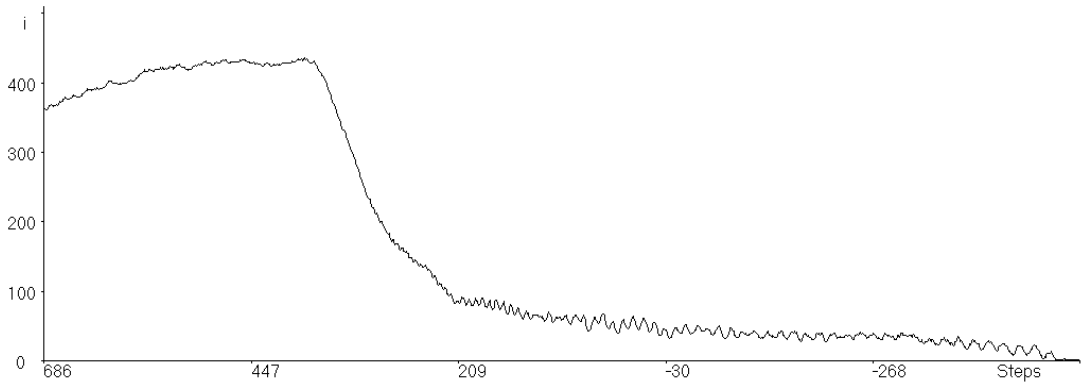

Figure 95. *Transmission Spectrum of a not imprinted fibroin film obtained by Metricon instrument.*

From the edge of the spectrum it can be calculated the RI and from the mode of the oscillations the thickness.

The thicknesses and refractive indices of the silk-only preliminary films of 2mL have been characterized by 633nm Metricon as per literature [108] and are between 40-60µm with an average RI at 1.54 value that coincides with that already found for regenerated silk fibroin obtained from cocoons of *B. mori* [108].

4.5.1.3 Evaluation of the water annealing (B-sheet content)

The formation of the β-sheet crystalline domains was evaluated by FTIR by analyzing the peaks in the region between 1616-1621 cm^{-1} of samples before and after the water annealing [108]. The increase in peaks recorded in this spectral region confirms the correct formation of the b-sheets.

A comparison of the spectra of NIFF samples before and after the water annealing is here reposted (Fig.96).

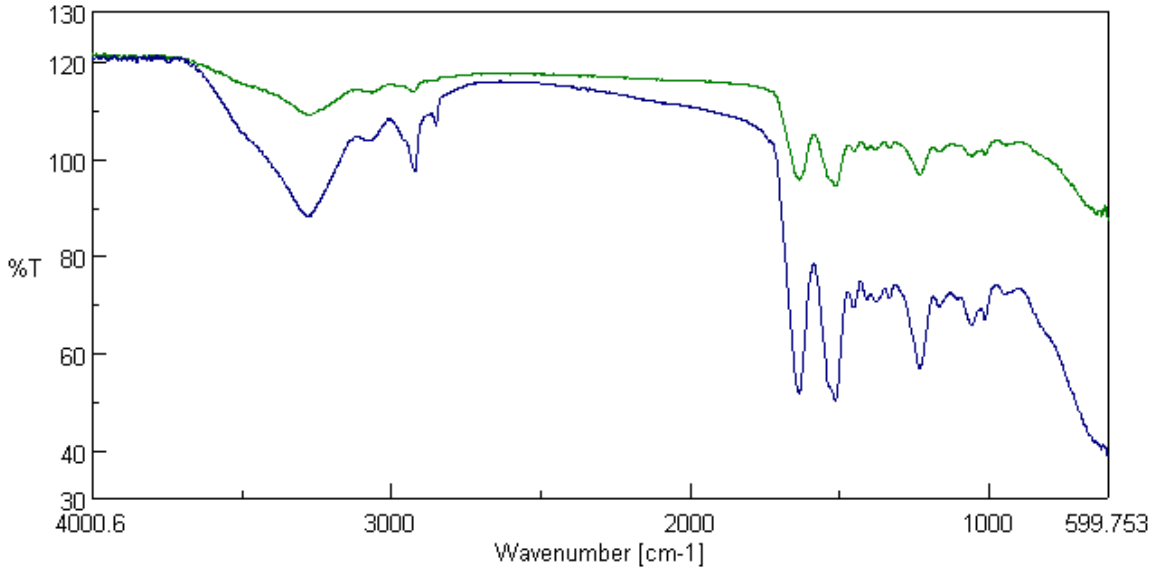

Figure 96. *FTIR Spectra of a NIFF before (green line) and after (blue line) the consequent water annealing.*

From the analysis of the peaks in the region between 1616-1621 cm^{-1} [108], the enhancement of the intensity of the peak corresponding to the formation of b-sheet domains in the water annealed sample is observed.

The analysis of the MIF after the washing consecutive to the water annealing is showed in Figure 97.

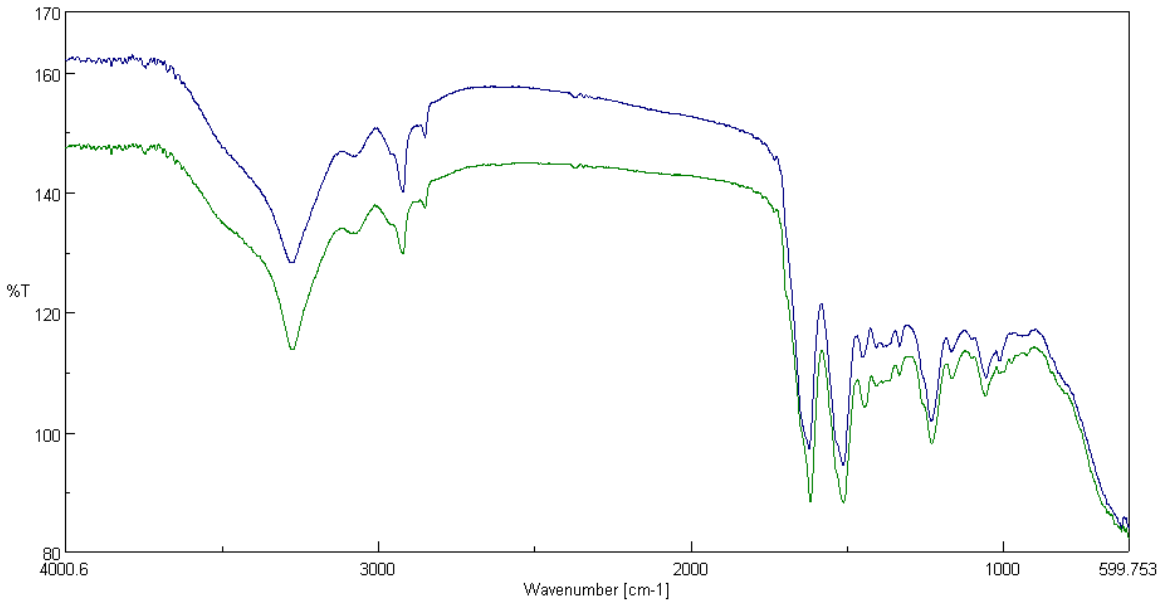

Figure 97. FTIR spectra of the MIFF a) after only the water annealing (blue line) and b) after the washing consequent to the water annealing (green line).

The transmittance intensity due to the global film structure diminishes; however, the intensity of the peaks due to the crystallinity domain remains unchanged. This is in accordance with SEM analysis, were the dissolution of the analyte and portion of the fibroin not completely crystallized occurs and a difference in the surface and microstructure has been observed too (par. 4.5.1.1)

4.5.2 WASHING OF THE FILM

The film has been washed with 5mL of an aqueous solution of PBS 30mM and left overnight in a sealed Petri dishes; this methodic was repeated 5 times. The content of the washing solution of the film was not quantified, only a qualitative method has been employed by visualizing the complete absence of the coloration in the enzyme assay.

4.5.3 INVESTIGATION OF THE ADSORBING PROPERTIES BY BATCH EQUILIBRATION

The adsorption properties of the MIFF were investigated by the batch equilibration method as described in the par. 2.3.1. The solvent used for adsorption and desorption was an aqueous solution of PBS 30mM. The silk film was left overnight in contact with 5mL of an appropriate solvent for adsorption or desorption (ensuring the complete soaking of the sample). The supernatant has been collected and analyzed by enzymatic assay, based on GOD/HRP.

The absorption procedure is as follows: the film sample was soaked into 5mL of 30mM of PBS solution spiked with glucose (at 157.5 mg/L– 270 mg/L – 350 mg/L). The samples weight were of around 0.1g after washing. For a shake of comparison and to evaluate the aspecific adsorption NIF has been tested too. In Fig. 98 the Langmuir adsorption isotherms obtained are reported. The loading capacity has been calculated as mg of glucose per g fibroin ($mg_{glucose}$ / $g_{fibroin}$) at saturation and the imprinting factor as the ratio of the recovered concentration on MIFF vs that on NIFF.

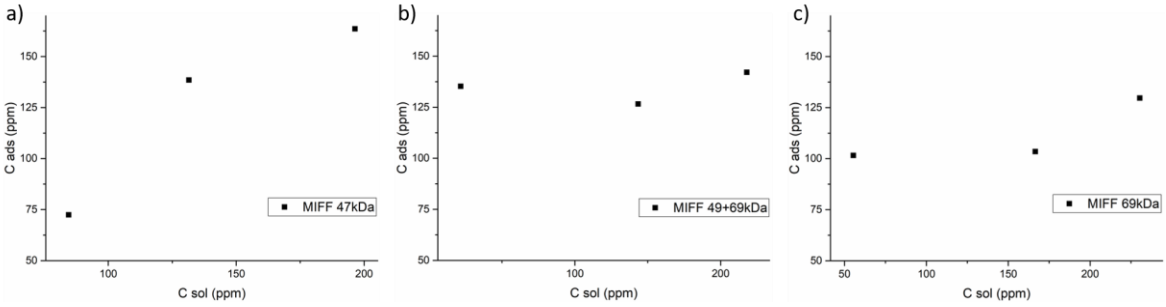

Figure 98. *Langmuir adsorption isotherms of glucose on MIF film at a) 47kDa+69kDa, b) 69kDa, c) 47kDa at a variable concentration at 157.5 mg/L, 270 mg/L and 350 mg/L of glucose in 30mM PBS.*

The relative parameters obtained from the Hill fitting on the previous Langmuir adsorption isotherms are exposed in Table 34.

Table 34. Parameters obtained by the Hill fitting and from the experimental data on the adsorption of glucose on MIF film at a) 47kDa+69kDa, b) 69kDa, c) 47kDa at a variable concentration at 157.5 mg/L, 270 mg/L and 350 mg/L of glucose in 30mM PBS

Results of the Adsorption										
Sample	**$K_{aff\ Hill}$ (mg/L^{-1})**		**$K_{aff\ Hill}$ (M^{-1})**		**$V_{max\ hill}$ (C_{ads} ,mg/L)**		**$C_{ads\ hill}$ (mg_{Ads}/g_{MIF})**		**$C_{ads\ exp}$ (mg_{Ads}/g_{MIF})**	
	Value	Err	Value	Err	Value	Err	Value	Err	Value	Err
(47+69)kDa (a)	35	-	$1.5\ 10^3$	-	142	-	7.1	-	5.7	0.3
47kDa (b)	117	-	$9.2\ 10^2$	-	164	-	8.2	-	5.6	0.7
69kda (c)	196	-	$5.1\ 10^3$	-	130	-	6.5	-	5.4	0.8

*hill fitting performed by OriginPro 2016

From the adsorption isotherm, an only approximated value can be calculated. While the difference can be not significant, the imprinted material obtained by the protein of mixed MW, seem to form sites with higher affinity. Further study of the equilibrium must be performed at lower concentrations. No difference in the loading capacity (C_{ads}) obtained experimentally was found by employing different MW of the fibroin protein. An IF of 1.8 was calculated for the 69kDa sample at the lowest concentration of 157 mg/L. This value confirms that some imprinting occurs, even if it is not very high at the considered concentration.

The high irreproducibility could be due to the method employed for the analysis, in which a high dilution has been used. Other possibly irreproducibility could be due to the water annealing and the washing procedures which affects the mechanical strength and structure of the film.

High absorption of glucose from PBS solution was observed but no glucose was desorbed with the same solution. Probably, a different solvent must be used for desorption, so a more detailed study must be performed on this regard. These results show the possibility to obtain an imprinting on silk derived fibroin. Further investigations are required to optimize this imprinting procedure. On the other hand, the physical characteristic, in particular, the refractive index, of the fibroin samples appear to be suitable for application in optical sensing.

5 CONCLUSIONS

The activity carried out during this research led to the creation of several selective optical sensors based on surface plasmon resonance (SPR) or on the evanescent wave coupling (EWC). SPR intrinsic devices directly developed on plastic optical fiber (POF) with the D-shaped profile have been previously proposed by the Zeni and Cennamo group [18]. This sensor consists of a plastic optical fiber (POF) deprived of the cladding, reduced to a D-profile by grinding and covered by a thin layer of Au in contact with the synthetic receptor (MIP). This platform is able to selectively detect the presence of DBDS or 2-FURin a real matrix, i.e. a mineral oil at a concentration as low as 6.7 10^{-8}M with a MIP K_{aff} of 5(1) $10^{6}M^{-1}$ [134]. The same device is able to detect the concentration of 2-FAL in the water down to 3 10^{-8} M, the affinity constant in water being noticeably lower than that in transformer oil K_{aff} =1.1(3) 10^{6} M^{-1}. In this investigation, D-shaped platforms of this kind have been implemented in multiplexing sensing devices, by coupling in series different sensors which differ because of the different thickness of metal layer [1]. Good results have been obtained for the simultaneous determination of two substances, DBDS and 2-FAL, in mineral oil, obtaining affinity constants, LOD, and detection range very similar to those of the single sensor. Despite these good results, intrinsic D-shaped platforms suffer from low reproducibility due to the manual fabrication procedure, in particular for the roughness of the surface platform which makes the homogeneous gold deposition very difficult. Consequently, SPR extrinsic configurations based on a plastic slab waveguide (PMMA or PET) were investigated, into which the light was injected by a POF, mainly in order to improve the reproducibility of the sensing device and develop more robust methods. Two kinds of sensing metal layers have been considered, i.e. a homogeneous thin gold film (50 nm) and a set of parallel silver nanoparticles printed lines [2-3] from which the enhancement of the signal was expected base on the L-SPR effect. The extrinsic SPR PMMA slab sensor consists of a PMMA slab as a waveguide, with a sputtered thin Au layer, in contact with MIP as the appropriate synthetic receptor [2]. The PMMA slab is commercially available and shows a reproducible surface roughness. Another extrinsic sensor was realized on a PET slab by the Inject printing technology, which ensures a high reproducibility in the deposition of the lines of silver nanoparticles [3]. The same molecularly imprinted polymer (MIP) for 2-FAL was used as a receptor in the two sensors. Both the proposed devices were able to selectively detect the 2-FAL in aqueous solution with comparable LOD and affinity constant for MIP to that obtained with the D-shaped configuration previously described.

The easy replacement of the chip allows a simplified measurement procedure, which results in an enhancement of the sensors reproducibility.

Other optical transductions have been considered in this investigation, based on the ATR principle which directly exploits the interaction of the evanescent wave. A segmented waveguide sensor and a PET-MIP sensor have been proposed. These methods have the extremely advantageous characteristic of avoiding the use of the metal layer with the related possible irreproducibility. The PET-MIP sensors consist in the same platform used for the Inkjet printing, but without the silver nanoparticle lines. It must be noted that in this case, the signal decreases opposite to that of the SPR-MIP-PET sensor, confirming that a different optical effect takes place in the two sensors [3]. The segmented waveguide sensor (SWS) is obtained by coupling POFs through a material of different RI in the middle [4]. Two parallel POFs were coupled through a trench drilled in between, filled with molecularly imprinted polymer. In this case, too, LOD and Kaff are comparable with that of SPR platforms but it is more reproducible due to the reduction of the manual fabrication procedures.

A noticeable advantage of the sensoristic methods based on POFs is related to the cheap and simple instrumentation required for the analysis, which can be miniaturized, in respect to the commercial devices based on prism configuration (Kretschmann configuration) [122]. It consists of a white light source emitting from 300 nm to 900 nm, i.e. the wavelength range of transmittance of the PMMA POF, or in some configurations even a LED; a spectrometer for the same wavelength range, and software for the data analysis. In the intrinsic D-shaped POF-SPR and extrinsic Slab-SPR sensors, the signal of analytical interest is the shift of the SPR resonance wavelength, which is evaluated in function of the analyte concentration, while in the extrinsic PET-line-MIP sensor and PET-MIP sensors, the intensity of light emerging from the platform is evaluated. Based on another concept of analysis, in the SWS platform the relative output, i.e. the ratio of the light intensity, emerging from the two fibers (I_2 /I_1), is measured in function of the concentration of the analyte.

All these sensors have been developed considering the possibility of employing MIPs as a receptor.

In this work, various MIPs have been synthesized with the aim of improving their performances as synthetic receptors in optical sensing devices. Even if a thin layer is actually the form in which the MIP is coupled to the optical sensing devices considered in the present work, MIPs in form of small particles and beads have been investigated as well for the sake of comparison.

In some cases, the identification of appropriate functional monomers for building up the appropriate MIP has been made by computational method (Gaussian 09).

The prepolymer solution of MIP has been prepared at molar ratio 1 (DBDS): 4 (MAA): 40 (DVB). The MIP composition was optimized for application as a receptor layer in sensors for different analytes detected in aqueous or organic solvents. Sensors based on MIPs of this kind coupled with optical transduction methods show high selectivity and low detection limit but have low dynamic range. The synthesis of MIP with a wide range of sites with a different affinity constant can extend the range of quantification toward the high concentrations. So, different formulations of MIP have been considered in order to obtain different porosity and enhance the MIP loading capacity.

In particular, the nature of the MIP formulation was investigated considering both the cross-linker and functional monomers, since it was found to be important in the case of the different polarity of the analytes considered.

Computational methods were employed at first to select the functional monomer in case of DBDS. Vinyl pyridine and MAA were considered, it was found that MAA gives the more stable adduct with DBDS. For 2-FAL only MAA was considered since this composition of the prepolymer mixture was already successfully employed for the imprinting of this analyte [19].

Another cross-linker was considered, i.e. EGDMA, instead of DVB, since it is promising for the somewhat higher RI (1.45). However, it has been calculated by the computational model that EGDMA can give stronger interactions with the MAA functional monomer than with DBDS template. This was confirmed by batch equilibration analysis, where the MIP-EGDMA imprinted for DBDS was not able to adsorb DBDS.

Besides the composition, the surface porosity of the polymer was found to be important too. In this research, MIPDVB polymers with different porosity and shape were investigated. A porous MIP has been synthesized by adding a porogen solvent (AcN) to the prepolymer solution in different ratios. Best result was obtained by the 1:3 ratio of solvent with respect to the prepolymer mixture. The porous-MIP-DVB-DBDS showed a loading capacity higher than the bulk MIP probably due to the higher polymer surface. In the case of both DBDS and 2-FAL, the porous MIP with the DVB cross-linker was found to be more suitable having a higher loading capacity than the polymers with EGDMA at the considered conditions. This is zero in the case of porous–MIP-EGDMA-DBDS and a half in the case of porous-MIP-EGDMA-2-FAL with respect to that of porous-MIP-DVB-2-FAL. MIP-

DVB-DBDS has been found to be specific, since not any adsorption of DBDS takes place on NIP-DVB, while some adsorption of 2-FAL on NIPs has been observed. In this case, the imprinting factor calculated for MIP-DVB was 3, while only 2 for MIP-EGDMA. This shows that the binding at the considered concentrations occurs with the imprinted sites and also aspecifically. Another MIP considered was the Beads MIP synthesized by precipitation polymerization, for which loading capacities similar to those of porous MIPs have been obtained.

A good selectivity was found in case of MIP-DVB imprinted for DBDS as for example a similar compound, DBS, was not found to be absorbed in all the MIP-DVB-DBDS formulation. However, for DPDS adsorption have been observed at the high concentrations considered, higher on porous-MIP-DVB than bulk-MIP-DVB, in agreement with the capacity for DBDS. In the case of porous-MIP imprinted for 2-FAL the adsorption of similar substances, such as FA and HMF, has been observed. However, the adsorption of both the templates (DBDS of 2-FAL) in all the MIPs formulation was found to be higher than that of the possibly interfering substances.

The most usual method for the characterization of the sorption on MIP is based on batch equilibration at different concentrations of the target substance, and determination of the target substance remaining in the solution phase. In this work this procedure has been applied to demonstrate that the sorption of the template on MIPs is in agreement with the Langmuir sorption isotherm, i.e it takes place by the combination on specific sites. The sites actually detected depend on the detection limits of the analytical technique used for the characterization and on the experimental conditions.

At concentration around 20-100 mg/L, the affinity constant has been found to be higher in the case of MIP-EGDMA-2-FALs than of MIP-DVB-2-FAL, about two orders of magnitude. However in this case too a similar K_{aff} of about 2 10^4 M^{-1} was obtained at lower concentration (5 mg/L). It must be noticed that the affinity constants determined by batch equilibration are much lower than those evaluated by the optical sensing methods considered in the present investigation, which were 10^5-10^7 M^{-1}.

This is due to the fact that the MIPs synthesized contain different types of sites, at low and high affinity. This effect is disadvantageous when MIP is employed for measurement in a small concentration range but can be advantageous where quantification in a broad range of concentration is needed.

Batch equilibration is an indirect measurement since the adsorption of an analyte in MIP was characterized by determining the concentration in the liquid phase at concentrations which depend on the detection limit of the analytical methods. In this way, all the sites, both at high and low affinity, are involved in the adsorption, without distinction. The concentrations at which the characterization of the sites at high affinity is possible are often below the LOD of the techniques employed in the batch analysis. In order to spot the high-affinity sites, sensoristic methods have been employed in this investigation, different from the optical ones. Voltammetric sensors based on screen printed cell (SPC) are particularly convenient for characterization, because of their low cost and very easy preparation. The SPC-MIP sensor considered in the present investigation was composed of a graphite ink working and an auxiliary electrode, and a silver ink quasi-reference electrode obtained by the screen printed technique, with a MIP layer deposed over the whole cell. Sensors of this kind have been developed for nicotine and 2-FAL, which have useful electrochemical characteristics. B this approach it was possible to detect sites with an affinity very similar to that detected by optical sensing. It is interesting to notice that the SPC-MIP-2-FAL sensor shows a LOD of 6 10^{-6}M for 2-FAL in water, which is almost one magnitude order higher than that obtained by the optical sensors here developed. On the other hand, the optical platforms seem not to give any response in the higher concentration range, i.e. for concentrations higher than about 1 mg/L, when the sites at low affinity are involved. An explanation can be that the RI variation is not sufficiently high in this case, neither for SPR or EWC.

Besides MIPs, new kinds of molecularly imprinted materials have been considered in order to improve the biocompatibility of the sensing devices. In particular silk fibroin has been examined for its good optical and mechanical characteristics. Moreover, it is a biomaterial already approved for biomedical applications. While sensors based on peptidic structures are well known in the previous literature, nothing is known about the possibility of “imprinting” a protein in order to improve its affinity and selectivity for a given substrate. Research for the development of an imprinted bioreceptor using the silk fibroin protein was carried out at Tufts University in Boston, aiming to an application in sensing devices exploiting the optical sensing platforms here proposed. The binding site has been evaluated considering the primary structure of the silk fibroin, as produced by an intermolecular folding of the protein around the template allowing non-covalent interactions. A study has been started on the thermodynamics by DFT calculations. [5]. Fibroin derived protein was employed exploiting different proteins with an average M.W. of 69kDa and 47kDa. Samples of imprinted fibroin film for glucose were obtained with different analyte concentration (140-260-350

mg/L in 2 mL of fibroin solution 6.6%). The films have been water annealed to obtain a water-resistant product. The characterization of the adsorption characteristic of fibroin films imprinted with glucose was performed by the batch procedure. A colorimetric enzymatic assay based on GOD/HRP enzymes was used to perform the quantitative analysis of glucose in solution after equilibration. Preliminary results on the imprinting of fibroin with glucose are promising, with an imprinting factor around 2. Moreover, the imprinted material can be easily obtained as a thin layer, which is particularly suitable for sensor development. A high loading capacity was found, around 5 ($mg_{analyte}/g_{fiborin}$), however, with high aspecific absorption, as seen from the IF. The approximate K_{aff} found of 10^3 M^{-1} is low, probably due to the high concentrations preliminarily considered in this investigation. Further investigations are required to optimize the imprinting procedure of this kind of material, before being able to combine it in sensing devices.

6 REFERENCES

[1]. **Pesavento M., De Maria L., Merli D., Marchetti S., Zeni L., Cennamo N.***, Towards the development of cascaded surface plasmon resonance POF sensors exploiting gold films and synthetic recognition elements for detection of contaminants in transformer oil,* Sens. BioSensing Res, 2017, 13, 128-135.

[2]. **Zeni L., Pesavento M., Marchetti S., Cennamo N.***, Slab plasmonic platforms combined with Plastic Optical Fibers and Molecularly Imprinted Polymers for chemical sensing,* Opt Laser Technol, 2018, 107, 484-490.

[3]. **Cennamo N., Zeni L., Andò B., Baglio S., Graziani S., Marletta V., Pistorio A., Pesavento M., Marchetti S.***, A novel chemical optical sensor based on molecularly imprinted polymer, optical fibers and inkjet printing technology,* I2MTC 2018 - 2018 IEEE International Instrumentation and Measurement Technology Conference: Discovering New Horizons in Instrumentation and Measurement, Proceedings, 2018, 1-5.

[4]. **Cennamo N., Testa G., Marchetti S., De Maria L., Bernini R., Zeni L., Pesavento M.***, Intensity-based plastic optical fiber sensor with molecularly imprinted polymer sensitive layer,* Sens Actuators B-Chem, 2017, 241, 534-540.

[5]. **Rockwood D. N., Preda R. C., Yücel T., Wang X., Lovett M. L., Kaplan D. L.***, Materials fabrication from Bombyx mori silk fibroin,* Nat. protoc., 2011, 6 (10), 1612-1631.

[6]. **Klantsataya E., Jia P., Ebendorff-Heidepriem H., Monro T. M., François A.***, Plasmonic Fiber Optic Refractometric Sensors: From Conventional Architectures to Recent Design Trends,* Sensors, 2017, 17 (1), 12.

[7]. **Gupta B. D., Shrivastav A. M., Usha S. P.***, Surface Plasmon Resonance-Based Fiber Optic Sensors Utilizing Molecular Imprinting***,** Sensors, 2016, 16 (9), 1381.

[8]. **Shrivastav A. M., Gupta B. D.***, SPR and Molecular Imprinting-Based Fiber-Optic Melamine Sensor With High Sensitivity and Low Limit of Detection,* IEEE J. Sel. Top. Quantum Electron., 2015, 22 (4), 1.

[9]. **Verma R. K., Sharma A. K., Gupta B. D.***, Modeling of Tapered Fiber-Optic Surface Plasmon Resonance Sensor With Enhanced Sensitivity,* 2007, 19 (22), 1786-1788.

[10]. **Cennamo N., D'Agostino G., Galatus R., Bibbò L., Pesavento M., Zeni L.**, *Sensors based on surface plasmon resonance in a plastic optical fiber for the detection of trinitrotoluene,* 2013, Sens. Actuators B-Chem., 188, 221-226.

[11]. **Andò B., Baglio S.,** *All-Inkjet Printed Strain Sensors,* Sensors, 2013, 13 (12), 8380.

[12]. **Hu M., Chen J., Li Z.Y., Au L., Hartland G.V., Li X., Marquez M., Xia Y.***, Gold nanostructures: engineering their plasmonic properties for biomedical applications,* Chem Soc Rev, 2006, 35 (11), 1084-1094.

[13]. **Cennamo N, Donà A, Pallavicini P, D'Agostino G, Dacarro G, Zeni L.***, Sensitive detection of 2,4,6-trinitrotoluene by tridimensional monitoring of molecularly imprinted polymer with optical fiber and five-branched gold nanostars,* Sens Actuat B Chem., 2015, 208, 291-298.

[14]. **Cennamo N., De Maria L., Pesavento M., Profumo A., Chemelli C., Zeni L.**, *Surface plasmon resonance in a D-shaped plastic optical fibre: influence of gold layer thickness in monitoring molecularly imprinted polymers.* Catania, Italy, IEEE Sensors Applications Symposium, 2016.

[15]. **Yuan Y., Wang L., Huang J.**, *Theoretical investigation for two cascaded SPR fiber optic sensors,* Sens Actuators B Chem, 2012, 161, 269– 273.

[16]. **Iga M., Sek A., Watanabe K.***, Gold thickness dependence of SPR-based heterocore structured optical fiber sensor,* Sens. Act. B: Chem., 2005, 106, 363–368.

[17]. **Van Lith J., Lambeck P. V., Hoekstra H. J. W. M., Heideman R. G., Wijn R. R.***, The Segmented Waveguide Sensor: Principle and Experiments,* J. lightwave technol, 2005, 1, 355-362.

[18]. **Cennamo N., Massarotti D., Conte L., Zeni L.***, Low Cost Sensors Based on SPR in a Plastic Optical Fiber for Biosensor Implementation,* Sensors, 2011, 11.

[19]. **Cennamo N., De Maria L., D'Agostino G., Zeni L., M. Pesavento.***, Monitoring of Low Levels of Furfural in Power Transformer Oil with a Sensor System Based on a POF-MIP Platform,* Sensors, 2015, 15, 8499-8511.

[20]. **Cennamo N., Mattiello F., Zeni L.***, Slab Waveguide and Optical Fibers for Novel Plasmonic Sensor Configurations,* Sensors, 2017, 17, 1488.

[21]. **Andò B., Marletta V.***, An All-InkJet Printed Bending Actuator with Embedded Sensing Feature and an Electromagnetic Driving Mechanism,* Actuators, 2016, 5 (3), 21.

[22]. **Polyakov, M.V.***, Adsorption properties and structure of silica gel,* Zhur Fiz Khim, 1931, 2, 799-805.

[23]. **Alexander C., Andersson H.S., Andersson L.I., Ansell R.J., Kirsch N., Nicholls I.A.***, Molecular imprinting science and technology: a survey of the literature for the years up to and including 2003,* J Mol Recognit, 2006, 19 (2), 106-80.

[24]. **Van Nostrum, C.F.***, Molecular imprinting: a new tool for drug innovation,* Drug Discov Today Technol, 2005, 2 (1), 119-24.

[25]. **Hilt J.Z., Byrne M.E.***, Configurational biomimesis in drug delivery: molecular imprinting of biologically significant molecules,* Adv Drug Deliv, 2004, 56 (11), 1599-620.

[26]. **Ye L., Mosbach K.***, The technique of molecular imprinting e principle, state of the art, and future aspects,* J Incl Phen Macrocycl Chem, 2001, 41 (1-4), 107-13.

[27]. **Byrne M.E., Park K., Peppas N.A.***, Molecular imprinting within hydrogels,* Adv Drug Deliv Rev, 2002, 54 (1), 149-61.

[28]. **Flavin K., Resmini M.**, *Imprinted nanomaterials: a new class of synthetic receptors,* Anal Bioanal Chem, 2009, 393 (2), 437-44.

[29]. **Huang Y.P., Liu Z.S., Zheng C., Gao R.Y.**, *Recent developments of molecularly imprinted polymer in CEC,* Electrophoresis, 2009, 30 (1), 155-62.

[30]. **Lee W.C., Cheng C.H., Pan H.H., Chung T.H., Hwang C.C.**, *Chromatographic characterization of molecularly imprinted polymers,* Anal Bioanal Chem, 2008, 390 (4), 1101-9.

[31]. **Maier N.M., Lindner W.**, *Chiral recognition applications of molecularly imprinted polymers: a critical review,* Anal Bioanal Chem, 2007, 389 (2), 377-97.

[32]. **Vlatakis G., Andersson L., Muller R., Mosbach K.**, *Drug assay using antibody mimics made by molecular imprinting,* Nature, 1993, 361, 645-647.

[33]. **Takatsy A., Vegvari A., Hjerten S., Kilar F.**, *Universal method for synthesis of artificial gel antibodies by the imprinting approach combined with a unique electrophoresis technique for detection of minute structural differences of proteins viruses and cells, (bacteria). Ib. Gel antibodies against proteins (hemoglobins),* Electrophoresis, 2007, 28 (14), 2345-50.

[34]. **Bolisay L.D., Culver J.N., Kofinas P.**, *Molecularly imprinted polymers for tobacco mosaic virus recognition,* Biomaterials, 2006, 27 (22), 4165-8.

[35]. **Seidler K., Lieberzeit P.A., Dickert F.L.**, *Application of yeast imprinting in biotechnology and process control,* Analyst, 2009, 134 (2), 361-6.

[36]. **Spivak D.A., Shea K.J.**, *Investigation into the scope and limitations of molecular imprinting with DNA molecules,* Anal Chim Acta, 2001, 435 (1), 65-74.

[37]. **Turner N.W., Jeans C.W., Brain K.R., Allender C.J., Hlady V., Britt D.W.**, *From 3D to 2D: a review of the molecular imprinting of proteins,* Biotechnol Prog, 2006, 22 (6), 1474-89.

[38]. **Takeuchi T., Hishiya T.**, *Molecular imprinting of proteins emerging as a tool for protein recognition,* Org Biomol Chem, 2008, 6 (14), 2459-67.

[39]. **Cenci L., Bertolla M., Anesi A., Ambrosi E., Guella G., Bossi A. M.**, *Micro- versus nano-sized molecularly imprinted polymers in MALDI-TOF mass spectrometry analysis of peptides,* Anal. Bioanal. Chem., 2017, 409, 26, 6253-6261.

[40]. **Bertolla M., Cenci L., Anesi A., Ambrosi E., Tagliaro F., Vanzetti L., Guella G., Bossi A. M.**, *Solvent-ResponsiveMolecularly Imprinted Nanogels for Targeted Protein Analysis in MALDI-TOF Mass Spectrometry,* ACS Appl. Mater. Interfaces, 2017, 9 (8), 6908–6915.

[41]. **Kempe M., Glad M., Mosbach K.**, *An approach towards surface imprinting using the enzyme ribonuclease A,* J Mol Recognit, 1995, 8 (1-2).

[42]. **Andersson L.I., Nicholls I.A., Mosbach K.**, *Molecular Imprinting: The Current Status and Future Development of Polymer-Based Recognition Systems,* Advances in Molecular and Cell Biology, 1996, 15, 651-670.

[43]. **Kempe M., Mosbach K.**, *Separation of amino acids, peptides and proteins on molecularly imprinted stationary phases,* J. Chromatogr. A, 1995, 691 (1–2), 317-323.

[44]. **Andersson L.I., O'Shannessy D.J., Mosbach K.**, *Molecular recognition in synthetic polymers: preparation of chiral stationary phases by molecular imprinting of ammino acid amides,* J Chromatogr, 1990, 513, 167-179.

[45]. **Sellergren B., Lepistoe M., Mosbach K.**, *Highly enantioselective and substrate-selective polymers obtained by molecular imprinting utilizing noncovalent interactions. NMR and chromatographic studies on the nature of recognition,* J. Am. Chem. Soc., 1988, 110 (17), 5853–5860.

[46]. **Andersson I.L., Mosbach K.**, *Enantiomeric resolution on molecularly imprinted polymers prepared with only non-covalent and non-ionic interactions,* J Chromatogr A, 1990, 516 (2), 313-322.

[47]. **Andersson L.I., Miyabayashi A., O'Shannessy D.J., Mosbach K.**, *Enantiomeric resolution of amino acid derivatives on molecularly imprinted polymers as monitored by potentiometric measurements,* J Chromatogr A, 1990, 516 (2), 323-331.

[48]. **Valdebenito A., Espinoza P., Lissi E.A., Encinas M.V.**, *Bovine serum albumin as chain transfer agent in the acrylamide polymerization. Proteine polymer conjugates,* Polymer, 2010, 51 (12), 2503-7.

[49]. **Dennis P. B., Walker A. Y., Dickerson M. B., Kaplan D. L., Naik R. R.**, *Stabilization of Organophosphorus Hydrolase by Entrapment in Silk Fibroin: Formation of a Robust Enzymatic Material Suitable for Surface Coatings,* ACS Biomacromolecules, 2012, 13(7), 2037-2045.

[50]. **Marelli B., Brenckle M. A., Kaplan D. L. , Omenetto F. G.**, *Silk Fibroin as Edible Coating for Perishable Food Preservation.* Sci. Rep., 2016, 6, 25263.

[51]. **Tao H., Kainerstorfer J.M., Siebert S.M., Pritchard E.M., Sassaroli A., Panilaitisa B.J.B, Brenckle M.A., Amsden J.J., Levitt J., Fantini S., Kaplan D.L., Omenetto F.G.**, *Implantable, multifunctional, bioresorbable optics,* PNAS, 2012, 109 (48), 19584-19589.

[52]. **Pavan S., Berti F.**, *Short peptides as biosensor transducers,* Anal Bioanal Chem, 2012, 402, 3055–3070.

[53]. **Karimzadeh A., Hasanzadeh M., Shadjou N., De La Guardia M.**, *Peptide based biosensors,* Trends Analyt Chem., 2018, 107, 1-20.

[54]. **Giovannoli C., Passini C., Volpi G., Di Nardo F., Anfossi L., Baggiani C.**, *Peptide-based affinity media for solid-phase extraction of Ochratoxin A from wine samples: Effect of the solid support on binding properties,* Talanta, 2015, 144, 496–501.

[55]. **Mayes A., Mosbach K.**, *Molecularly Imprinted Polymers: useful materials for analytical chemistry?,* Trends Analyt Chem., 1997, 16 (6), 321-331.

[56]. **Cenci L., Andreetto E., Vestri A., Bovi M., Barozzi M., Iacob E., Busato M., Castagna A., Girelli D., Bossi A. M.**, *Surface plasmon resonance based on molecularly imprinted nanoparticles for the picomolar detection of the iron regulating hormone Hepcidin-25,* J Nanobiotechnology, 2015, 13 (1), 51.

[57]. **Pesavento M., D'Agostino G. , Alberti G. , Biesuz R. , Merli D.**, *Voltammetric platform for detection of 2,4,6-trinitrotoluene based on a molecularly imprinted polymer,* Anal Bioanal Chem., 2013, 405 (11), 3559-3570.

[58]. **Karim K., Breton F., Rouillon R., Piletska E.V., Guerreiro A., Chianella I., Piletsky S.A.**, *How to find effective functional monomers for effective molecularly imprinted polymers?,* Adv Drug Deliv Rev, 2005, 57 (12), 1795-1808.

[59]. **Potyrailo R. A., Mirsky V. M.**, *Combinatorial Methods for Chemical and Biological Sensors,* SSBM, 2009, 135-158.

[60]. **Gholivand M. B., Karimian N., Malekzadeh G.**, *Gomputational design and synthesis of a high selective molecularly imprinted polymer for voltammetric sensing of propazine in food samples,* Talanta, 2012, 89, 513-520.

[61]. **Diñeiro Y., Menédez M. I., Blanco-López M. C., Lobo-Castañón M. J., Miranda-Ordieres A. J., Tuñón-Blanco P.**, C*omputational predictions and experimental affinity distributions for a homovanillic acid molecularly imprinted polymer,* Biosens Bioelectron, 2006, 22, 364-371.

[62]. **Nicholls I. A., Andersson H. S., Charlton C., Henschel H., Karlsson B. C., Karlsson J. G., O'Mahony J. W. S.**, *Theoretical and computational strategies for rational molecularly imprinted polymer design,* Biosens Bioelectron, 2009, 25, 43-55.

[63]. **Baggiani C., Giovannoli C., Anfossi L., Passini C., Baravalle P., Giraudi G.**, *A Connection between the Binding Properties of Imprinted and Nonimprinted Polymers: A Change of Perspective in Molecular Imprinting,* J. Am. Chem.Soc., 2012, 134, 1513-1518.

[64]. **Appel M., Jackson M. A., Wang L. C., Ho C. H., Mueller A.**, *Determination of fusaric acid in maize using molecularly imprinted SPE clean-up,* J. Sep. Sci, 2014, 37, 281-286.

[65]. **Wang X., Tang Q., Wang Q., Qiao X., Xu Z.**, *Study of a molecularly imprinted solid-phase extraction coupled with high-performance liquid chromatography for simultaneous determination of trace trichlorfon and monocrotophos residues in vegetables,* J. Sci. Food Agric., 2014, 94, 1409-1415.

[66]. **Nezhadali A., Feizy J., Beheshti H. R.**, *A molecularly imprinted polymer for the selective extraction and determination of fenvalerate from food samples using high-performance liquid chromatography,* Food Anal. Methods, 2015, 8, 1225-1237.

[67]. **Yan H., Yang C., Sun K. H. R. Y.**, *Ionic liquid molecularly imprinted polymers for application in pipette-tip solid-phase extraction with gas chromatography for rapid screening of dicofol in celery,* J. Chromatog. A, 2014, 1361, 53-59.

[68]. **Khan S., Bhatia T., Trivedi P., Satyanarayana G. N. V., Mandrah K., Saxena P. N., Mudiam M. K. R., Roy S. K.**, *Selective solid-phase extraction using molecularly imprinted polymer as a sorbent for the analysis of fenarimol in food samples,* Food Chem., 2016, 199, 870-875.

[69]. **Lung W., Wu X., Liu D., Li L., Chen L., Zhang X.**, *Multi-template imprinted polymers dor simultaneous selective solid-phase extraction of six phenolic compounds in water samples followed by determination using capillary electrophoresis,* J. Chromagr. A, 2017, 1483, 30-39.

[70]. **Malitesta C., Mazzotta E., Picca R., Poma A., Chianella I.**, *MIP sensors – the electrochemical approach,* Anal Bioanal Chem, 2015, 402 (5), 1827–1846.

[71]. **Pardeshi S., Singh S. K.***, Precipitation polymerization: a versatile tool for preparing molecularly imprinted polymer beads for chromatography applications,* RSC Adv., 2016, 6, 23525-23536.

[72]. **Vasapollo G., Sole R. D., Mergola L., Lazzoi M. R., Scardino A., Scarrano S., Mele G.***, Molecularly Imprinted Polymers: Present and Future Prospective,* Int. J. Mol. Sci., 2011, 12 (9), 5908-5945.

[73]. **Yoshimatsu K., Reimhult K., Krozer A., Mosbach K., Sode K., Ye L.**, U*niform molecularly imprinted microspheres and nanoparticles prepared by precipitation polymerization: the control size suitable for different analytical applications,* Anal Chim Acta., 2010, 657 (2), 215.

[74]. **Turner A., Uzun L.***, Molecularly-imprinted polymers sensors: realising their potential,* 2015, Biosens Bioelectron, 76, 131-144.

[75]. **Haupt K., Mosbach K.***, Molecularly Imprinted Polymers and Their Use in Biomimetic Sensors,* Chem Rev, 2000, 100, 2495-2504.

[76]. **Sellergren, B.***, Imprinted Polymers with Memory for Small Molecules, Proteins, or Crystals,* Angew Chem Int Ed Engl, 2000, 39, 1031-1037.

[77]. **Sellergren, B.***, Noncovalent molecular imprinting: antibody-like molecular recognition in polymeric network materials,* Trends Anal Chem, 1997, 16, 310-320.

[78]. **Omenetto F.G., Kaplan D.L.***, A new route for silk,* Nat Photonics, 2008, 2 (11), 641–643.

[79]. **Parker S.T., Domachuk P., Amsden J., Bressner J.,Lewis J. A., Kaplan D.L., Omenetto F.G.***, Biocompatible Silk Printed Optical Waveguides,* Advanced Materials, 2009, 21 (23) .

[80]. **Tao H., Kaplan D.L., Omenetto F.G.***, Silk materials-a road to sustainable high technology,* Adv Mater, 2012, 24 (21), 2824-37.

[81]. **Applegate M. B., Perotto G., Kaplan D. L., Omenetto F. G.***, Biocompatible Silk Step-Index Optical Waveguides,* Biomed. Biomed. Opt. Express, 2015, 6, 4221−4227.

[82]. **Howard D., Partridge K., Yang X., Clarke N. M. P., Okubo Y., Bessho K., Howdle S. M., Shakesheff K. M., Oreffo R. O. C.***, Immunoselection and adenoviral genetic modulation of human osteoprogenitors: In vivo bone formation on PLA scaffold,* Biochem Biophys Res Commun, 2002, 299 (2), 208–215.

[83]. **Partridge K., Yang X., Clarke N.M., Okubo Y., Bessho K., Sebald W., Howdle S.M., Shakesheff K.M., Oreffo R.O.**, A*denoviral BMP-2 gene transfer in mesenchymal stem cells: in vitro and in vivo bone formation on biodegradable polymer scaffolds,* Biochem Biophys Res Commun, 2002, 292 (1), 144-52.

[84]. **Stone K.R., Steadman J.R., Rodkey W.G., Li S.T.***, Regeneration of meniscal cartilage with use of a collagen scaffold. Analysis of preliminary data,* J Bone Joint Surg Am, 1997, 79 (12), 1770-7.

[85]. **Kim D.H., Viventi J., Amsden J.J., Xiao J., Vigeland L., Kim Y.S., Blanco J.A., Panilaitis B., Frechette E.S., Contreras D., Kaplan D.L., Omenetto F.G., Huang Y., Hwang K.C., Zakin M.R., Litt B., Rogers J.A.**, *Dissolvable films of silk fibroin for ultrathin conformal bio-integrated electronics,* Nat Mater, 2010, 9 (6), 511-7.

[86]. **Kim D.H., Lu N., Ma R., Kim Y.S., Kim R.H., Wang S., Wu J., Won S.M., Tao H., Islam A., Yu K.J., Kim T.I., Chowdhury R., Ying M., Xu L., Li M., Chung H.J., Keum H., McCormick M., Liu P., Zhang Y.W., Omenetto F.G., Huang Y., Coleman T., Rogers J.A.**, *Epidermal electronics,* Science, 2011, 333 (6044), 838-43.

[87]. **Viventi J., Kim D.H., Vigeland L., Frechette E.S., Blanco J.A., Kim Y.S., Avrin A.E., Tiruvadi V.R., Hwang SW., Vanleer A.C., Wulsin DF., Davis K., Gelber C.E., Palmer L., Van der Spiegel J., Wu J., Xiao J., Huang Y., Contreras D., Rogers J.A., Litt B.**, *Flexible, foldable, actively multiplexed, high-density electrode array for mapping brain activity in vivo,* Nat Neurosci, 2011, 14 (12), 1599-605.

[88]. **Perry H., Gopinath A., Kaplan D.L., Dal Negro L., Omenetto F.G.**, *Nano- and Micropatterning of Optically Transparent, Mechanically Robust, Biocompatible Silk Fibroin Films,* Advanced Materials, 2008, 20 (16), 3070-72.

[89]. **Lawrence B.D., Cronin-Golomb M., Georgakoudi I., Kaplan D.L., Omenetto F.G.**, *Bioactive silk protein biomaterial systems for optical devices,* Biomacromolecules, 2008, 9 (4), 1214-20.

[90]. **Hu X., Shmelev K., Sun L., Gil E.S., Park S.H.,Cebe P., Kaplan D.L.**, *Regulation of Silk Material Structure by Temperature-Controlled Water Vapor Annealing,* Biomacromolecules, 2011, 12, 1686–1696.

[91]. **Palermo G., Barberi L., Perotto G., Caputo R., De Sio L., Umeton C., Omenetto F.G.**, *Conformal Silk-Azobenzene Composite for Optically Switchable Diffractive Structures,* ACS Appl. Mater. Interfaces, 2017, 9, 30951 - 30957.

[92]. **Altman G.H., Diaz F., Jakuba C., Calabro T., Horan R.L., Chen J., Lu H., Richmond J., Kaplan D.L.**, *Silk-based biomaterials,* Biomaterials, 2003, 24 (3), 401-16.

[93]. **Amsden J.J., Domachuk P., Gopinath A., White R.D., Dal Negro L., Kaplan D.L., Omenetto F.G.**, *Rapid Nanoimprinting of Silk Fibroin Films for Biophotonic Applications,* Adv Mater., 2010, 22 (13).

[94]. **White R.D., Gray C., Mandelup E., Amsden J.J., Kaplan D.L., Omenetto F.G.**, *Rapid nano impact printing of silk biopolymer thin films,* J Micromech and Microeng, 2011, 21 (11).

[95]. **Tsioris K., Tao H., Liu M., Hopwood J.A., Kaplan D.L., Averitt R.D., Omenetto F.G.**, *Rapid transfer-based micropatterning and dry etching of silk microstructures,* Adv Mater, 2011, 23 (17), 2015-9.

[96]. **Tsioris K., Tilburey G.E., Murphy A.R., Domachuk P., Kaplan D.L., Omenetto F.G.**, *Functionalized-Silk-Based Active Optofluidic Devices,* Adv Funct Mater, 2010, 20 (7), 1083-1089.

[97]. **Mondia J.P., Amsden J.J., Lin D., Negro L.D., Kaplan D.L., Omenetto F.G.**, *Rapid nanoimprinting of doped silk films for enhanced fluorescent emission,* Adv Mater, 2010, 22 (41), 4596-9.

[98]. **Tao H., Chieffo L.R., Brenckle M.A., Siebert S.M., Liu M., Strikwerda A.C., Fan K., Kaplan D.L., Zhang X., Averitt R.D., Omenetto F.G.**, *Metamaterials on paper as a sensing platform,* Adv Mater, 2011, 23 (28), 3197-201.

[99]. **Young S.L., Gupta M., Hanske C., Fery A., Scheibel T., Tsukruk V.V.**, *Utilizing conformational changes for patterning thin films of recombinant spider silk proteins,* Biomacromolecules, 2012, 13 (10), 3189-99.

[100]. **Galeotti F., Andicsova A., Yunusc S., Botta C.**, *Precise surface patterning of silk fibroin films by breath figures,* Soft Matter, 2012, 17.

[101]. **Wilz A., Pritchard E.M., Li T., Lan J.Q., Kaplan D.L., Boisona D.**, *Silk polymer based adenosine release: therapeutic potential for epilepsy,* Biomaterials, 2008, 29 (26), 3609–3616.

[102]. **Pritchard E.M., Kaplan D.L.**, *Silk fibroin biomaterials for controlled release drug delivery,* Expert Opin Drug Deliv, 2011, 8 (6), 797–811.

[103]. **Szybala C., Pritchard E.M., Lusardi T.A., Li T., Wilz A., Kaplan D.L., Boison D.**, *Antiepileptic effects of silk-polymer based adenosine release in kindled rats,* Exp Neurol, 2009, 219 (1), 126-35.

[104]. **Zhang J., Pritchard E., Hu X., Valentin T., Panilaitis B., Omenetto F.G., Kaplan D.L.**, *Stabilization of vaccines and antibiotics in silk and eliminating the cold chain,* Proc Natl Acad Sci USA, 2012, 109 (30), 11981-6.

[105]. **Tsioris K, Raja W.K., Pritchard E.M., Panilaitis B., Kaplan D.L., Omenetto F.G.**, *Fabrication of Silk Microneedles for Controlled-Release Drug Delivery,* Adv Funct Mater, 2011, 22 (2).

[106]. **Seib F. P., Kaplan D. L.**, *Doxorubicin-loaded silk films: Drug-silk interactions and in vivo performance in human orthotopic breast cancer,* Biomaterials, 2012, 33 (33), 8442-8450.

[107]. **Seib F.P., Coburn J., Konrad I., Klebanov N., Jones G.T., Blackwood B., Charest A., Kaplan D.L., Chiu B.**, *Focal therapy of neuroblastoma using silk films to deliver kinase and chemotherapeutic agents in vivo,* Acta Biomaterialia, 2015, 20, 32–38.

[108]. **Perotto G., Zhang Y., Naskar D., Patel N., Kaplan D.L., Kundu S.C., Omenetto F.G.**, *The optical properties of regenerated silk fibroin films obtained from different sources,* Appl. Phys. Lett., 2017, 111, 103702.

[109]. **Guo, X.**, *Surface Plasmon Resonance Based Biosensor Technique: A.,* J. Biophotonics, 2012, 5, 483–501.

[110]. **Abdulhalim I., Zourob M., Lakhtakia A.**, *Surface Plasmon Resonance for Biosensing: A.* Electromagnetics, 2008, 28, 214–242.

[111]. **Homola, J.**, *Surface Plasmon Resonance Sensors for Detection of Chemical and Biological Species,* Chem. Rev., 2008, 108, 462–493.

[112]. *Surface Plasmon Resonance-Based Fiber Optic Sensors:.* **Gupta B., Verma R.** 979761, s.l. : J. Sens., 2009.

[113]. *Theoretical Modeling of a Localized Surface Plasmon Resonance Based Intensity Modulated Fiber Optic Refractive Index Sensor.* **Srivastava S. K., Verma R. K., Gupta B. D.** s.l. : Appl. Opt., 2009, Vols. 48, 3796–3802.

[114]. *Localized surface plasmon resonance spectroscopy and sensing.* **Willets K. A., Van Duyne R. P.** s.l. : Annual Review of Physical Chemistry, 2007, Vols. 58, pp. 267–297.

[115]. *Review of Surface Plasmon Resonance and Localized Surface Plasmon Resonance Sensor.* **Chen Y., Ming H.** s.l. : Photonic Sens., 2012, Vols. 2, 37–49.

[116]. *Refractometric Sensing Using Propagating versus Localized Surface Plasmons: A Direct Comparison.* **Svedendahl M., Chen S., Dmitriev A., Kall M.** s.l. : Nano Lett., 2009, Vols. 9, 4428–4433.

[117]. *Comparative Analysis of Localized and Propagating Surface Plasmon Resonance Sensors: The Binding of Concanavalin A to a Monosaccharide Functionalized Self-Assembled Monolayer.* **Yonzon C. R., Jeoung E., Zou S. L., Schatz G. C., Mrksich M., Van Duyne R. P.** s.l. : J. Am. Chem. Soc., 2004, Vols. 126, 12669–12676.

[118]. *Localized Surface Plasmon Resonance Biosensors.* **Zhao J., Zhang X., Yonzon C. R., Haes A. J., Van Duyne R. P.** s.l. : Nanomedicine 2006, 2006, Vols. 1, 219–228.

[119]. *Localized Surface Plasmon Resonance Sensors.* **Mayer K. M., Hafner J. H.** s.l. : Chem. Rev., 2011, Vols. 111, 3828–3857.

[120]. **Sharma A. K., Jha R., Gupta D.O.***, Fiber-Optic Sensors based on Surface Plasmon Resonance: A Comprehensive Review*, IEEE Sens J, 2007, 7 (8), 1118-1129.

[121]. **Liang G., Luo Z., Liu K., Wang Y., Dai J., Duan Y.**, *Fiber Optic Surface Plasmon Resonance–Based Biosensor Technique: Fabrication, Advancement, and Application,* Analytical Chemistry, 2016, 46 (3), 213-223.

[122]. **Kretschmann E., Raether H.***, The theory of plasma resonance radiation,* Z. Naturforsch, 1967, 22a, 1623.

[123]. **Jorgenson R.C., Yee S.S.**, A *fiber-optic chemical sensor based on surface plasmon resonance,* Sens. Act. B: Chem., 1993, 12, 213–220.

[124]. **Wang X.D., Wolfbeis O.S.***, Fiber-optic chemical sensors and biosensors 2008-2012,* Anal. Chem., 2013, 85, 487-508.

[125]. **Piliarik M., Homola J., Manikova Z., C˘tyroky´ J.**, S*urface plasmon resonance sensor based on a single-mode polarization-maintaining optical fiber,* Sens. Actuat. B Chem, 2003, 90, 236–242.

[126]. **Yola M.L., Atar N., Eren T.**, *Determination of amikacin in human plasma by molecular imprinted SPR nanosensor,* Sens Actuat B Chem., 2014, 198, 70-76.

[127]. **Abdin M. J., Altintas Z., Tothill I. E.**, *In silico designed nanoMIP based optical sensor for endotoxins monitoring,* Biosens Bioelectron, 2015, 67, 177-183.

[128]. **Scarano S., Vestri A., Ermini M.L., Minunni M.**, *SPR detection of human Hepcidin-25: a critical approach by immuno- and biomimetic-based biosensing,* Biosens Bioelectron., 2013, 40, 135-140.

[129]. **Tan Y., Jing ., Ding Y., Wei T.**, *A novel double-layer molecularly imprinted polymer film based surface plasmon resonance for determination of testosterone in aqueous media,* Appl Surf Sci, 2015, 342 (1), 84-91.

[130]. **Zhang Q., Jing L., Zhang J., Ren Y., Wang Y., Wang Y., Wei T., Liedberg B.**, *Surface plasmon resonance sensor for femtomolar detection of testosterone with water-compatible macroporous molecularly imprinted film,* Anal Biochem, 2014, 463, 7-14.

[131]. **Pesavento M., D'Agostino G., Biesuz R., Alberti G., Profumo A.**, *Ion Selective Electrode for Dopamine Based on a Molecularly Imprinted Polymer,* Electroanalysis, 2011, 24 (4), 813-824.

[132]. **Kara M., Uzun L., Kolayli S., Denizli A.**, *Combining molecular imprinted nanoparticles with surface plasmon resonance nanosensor for chloramphenicol detection in honey,* J Appl Polym Sci, 2013, 129 (4).

[133]. **Lavine B.K., Westover D.J., Kaval N., Mirjankar N., Oxenford L., Mwangi G.K.**, *Swellable molecularly imprinted polyN-(N-propyl)acrylamide particles for detection of emerging organic contaminants using surface plasmon resonance spectroscopy,* Talanta, 2007, 72 (3), 1042-1048.

[134]. **Cennamo N., De Maria L., Chemelli C., Profumo A., Zeni L., Pesavento M.**, *Markers Detection in Transformer Oil by Plasmonic Chemical Sensor System Based on POF and MIPs,* IEEE Sensors J., 2016, 16 (21), 7663-669.

[135]. **Cennamo N., D'Agostino G., Pesavento M., Zeni L.**, *High selectivity and sensitivity sensor based on MIP and SPR in tapered plastic optical fibers for the detection of l-nicotine,* Sens. Actuators B Chem., 2014, 191, 529–536.

[136]. **Sequeira F., Duarte D., Bilro L., Rudnitskaya A., Pesavento M., Zeni L., Cennamo N.**, *Refractive Index Sensing with D-Shaped Plastic Optical Fibers for Chemical and Biochemical Applications,* Sensors, 2016, 16, 2119.

[137]. **Lith J. V., Lambeck P. V., Hoekstra H. J. W. M., Heideman R. G., Wijn R. R.**, *The Segmented Waveguide Sensor: Principle and Experiments,* J Lightwave Technol, 2005, 23, 355-363.

[138]. **Lambeck P.V., van Lith J., Hoekstra H.J.W.M.**, T*hree novel integrated optical sensing structures for the chemical domain,* Sens. Actuators B Chem., 2006, 113, 718-729.

[139]. **Luff B.J., Harris R.D., Wilkinson J.S., Wilson R., Schiffrin D.J.**, *Integrated-optical directional coupler biosensor,* Opt. Lett., 1996, 21, 618–620.

[140]. **Lou J., Xu H., Xu B., Huang J., Li B., Shen W.**, *Fiber-optic evanescent wavesensor with a segmented structure,* Appl. Opt., 2014, 53, 4200–4205.

[141]. **Bilro L., Alberto N., Pinto J.L., Nogueira R.**, *Optical sensors based on plastic fibers,* 2012, 12 (9), 12184-207.

[142]. **Bilro L., Alberto N., Sa L. M., Pinto J. L., Nogueira R.***, Analytical Analysis of Side-Polished Plastic Optical Fiber as Curvature and Refractive Index Sensor,* J. Lightwave Technol, 2011, 29 (6), 864-870.

[143]. **Gowri A., Sai V.V.R.***, Development of LSPR based U-Bent Plastic Optical Fiber Sensors,* Sens. Actuators B Chem, 2016, 230, 536–543.

[144]. **Al-Qazwini Y., Noor A.S.M., Al-Qazwini Z., Yaacob M.H., Harun S.W., Mahdi M.A.***, Refractive index sensor based on SPR in symmetrically etched plastic optical fibers,* Sens. Actuators A Phys., 2016, 246, 163–169.

[145]. **Park J., Park, Y.J., Shin J.D.**, *Plastic optical fiber sensor based on in-fiber microholes for level measurement,* 028002, Jpn. J. Appl. Phys., 2015, 54.

[146]. **Cennamo N., Varriale A., Pennacchio A., Staiano M., Massarotti D., Zeni L., D'Auria S.***, An innovative plastic optical fiber based biosensor for new bio/applications. The case of celiac disease,* Sens. Act. B: Chem., 2013, 176, 1008–1014.

[147]. **Cennamo N., Pesavento M., Lunelli L., Vanzetti L., Pederzolli C., Zeni L., Pasquardini L.**, *An easy way to realize SPR aptasensor: a multimode plastic optical fiber platform for cancer biomarkers detection,* Talanta, 2015, 140, 88–95.

[148]. **Kanso M., Cuenot S., Louarn G.**, *Sensitivity of Optical Fiber Sensor Based on Surface Plasmon Resonance: Modeling and Experiments,* Plasmonics, 2008, 3, 49-79.

[149]. **Dwivedi Y. S., Sharma A. K., Gupta B. D.**, *Influence of Design Parameters on the Performance of a Surface Plasmon Sensor Based Fiber Optic Sensor,* Plasmonics, 2008, 3, 79-86.

[150]. **Sharma A.K., Gupta B.D.**, *On the sensitivity and signal to noise ratio of a stepindex fiber optic surface plasmon resonance sensor with bimetallic layers,* Opt. Commun., 2005, 245, 159–169.

[151]. **Liu Z., Wei Y., Zhang Y., Liu C., Zhang Y., Zhao E., Yang J., Yuan L.***, Compact distributed fiber SPR sensor based on TDM and WDM technology,* Opt. Express, 2015, 23, 24004-24012.

[152]. **Uzun L., Turner A.P.F.***, Molecularly-imprinted polymers sensors: realising their potential,* Biosens. Bioelectron., 2016, 76, 131–144.

[153]. **Mäntysalo M., Pekkanen V., Kaija K., Niittynen J., Koskinen S., Halonen E., Mansikkamäki P., Hämeenoja O.**, *Capability of Inkjet Technology in Electronics Manufacturing.* San Diego, CA, US : Electronic Components and Technology Conference, 2009.

[154]. **Unander T., Nilsson H. E.**, *Characterization of printed moisture sensors in packaging surveillance applications,* IEEE Sens. J., 2009, 9 (8), 922–928.

[155]. **Lakhmi R., Debeda H., Dufour I., Lucat C.,** *Force sensors based on screen-printed cantilevers,* IEEE Sens. J., 2010, 10 (6), 1133–1137.

[156]. **Jacq C., Lüthi B., Maeder T., Lambercy O., Gassert R., Ryser P.**, *Thick-film multi-DOF force/torque sensor for wrist rehabilitation,* Sens. Actuators A Phys., 2010, 162, 361–366.

[157]. **Andò B., Baglio S., Bulsara A.R., Emery T., Marletta V., Pistorio A.**, *Low-cost inkjet printing technology for the rapid prototyping of transducers,* Sensors, 2017, 17 (4), 748.

[158]. **Andersson H., Manuilskiy A., Unander T., Lidenmark C., Forsberg S., Nilsson H.E.**, *Inkjet printed silver nanoparticle humidity sensor with memory effect on paper,* IEEE Sens. J., 2012, 12 (6), 1901–1905.

[159]. **Crowley K., Morrin A., Hernandez A., O'Malley E., Whitten P. G., Wallace G. G., Smyth M. R., Killard A. J.**, *Fabrication of an ammonia gas sensor using inkjet-printed polyaniline nanoparticles,* Int. J. Pure Appl. Anal. Chem., 2008, 77 (2), 710–717.

[160]. **Dunlop, A. P.**, *Furfural formation and behavior,* Industrial and engineering chemistry, 1984, 40 (2), 204-209.

[161]. **Lamminp K., Ahola J., Tanskanen J.**, *Kinetics of furfural destruct ion in a formic acid medium*, RSC Adv., 60243, 2014, 4.

[162]. **Dungchai W., Chailapakul O., Henry C.S.**, *Use of multiple colorimetric indicators for paper-based microfluidic devices,* Analytica Chimica Acta, 2010, 674, 227–233.

[163]. **Zhu W.J., Feng D.Q., Chen M., Chen Z.D., Zhu R., Fang H.L., Wang W.**, *Bienzyme colorimetric detection of glucose with self-calibration based on tree-shaped paper strip,* Sens Actuators B Chem, 2014, 190, 414– 418.

[164]. **Grumann M., Steigert J., Riegger L., Moser I., Enderle B., Riebeseel K., Urban G., Zengerle R., Ducrée J.**, *Sensitivity enhancement for colorimetric glucose assays on whole blood by on-chip beam-guidance,* Biomed Microdevices, 2006, 8, 209–214.

[165]. **Fernando C. D., Soysa P.**, *Optimized enzymatic colorimetric assay for determination of hydrogen peroxide (H_2O_2) scavenging activity of plant extracts,* MethodsX, 2015, 2, 283-291.

[166]. **Y. S. Dwivedi, A. K. Sharma, B. D. Gupta.**, *Influence of Design Parameters on the Performance of a Surface Plasmon Sensor Based Fiber Optic Sensor,* Plasmonics, 2008, 3, 79-86.

[167]. **Homola J., Piliarik M.**, *Surface Plasmon Resonance (SPR) Based Sensors,* Springer Ser Chem Sens and Biosens, 2006, 4, 45-67.

[168]. **Xia L.X., Shen Z., Vargas T., Sun W.J., Ruan R.M., Xie Z.D., Qiu G.Z.**, *Attachment of acidithiobacillus ferrooxidans onto different solid substrates and fitting through langmuir and freundlich equations,* Biotechnol. Lett., 2013, 35, 2129-2136.

[169]. **Wyciszkiewicz M., Saeid A., Malinowski P., Chojnacka K.**, *Valorization of phosphorus secondary raw materials by acidithiobacillus ferrooxidans,* Molecules, 2017, 22, 473.

[170]. **Li R.J.U., Baxter S.C., Bode M., Berch J.K., Shah R.N., Shimizu K.D.**, *Application of the freundlich adsorption isotherm in the characterization of molecularly imprinted polymers,* Anal. Chim. Acta., 2001, 435, 35–42.

[171]. **And H.K., Spivak D.A.**, *New insight into modeling non-covalently imprinted polymers.* 11269, J. Am. Chem. Soc., 2003, 125.

[172]. **Umpleby R.J., Baxter S.C., Chen Y., Shah R.N., Shimizu K.D.**, *Characterization of Molecularly Imprinted Polymers with the Langmuir–Freundlich Isotherm,* Anal. Chem., 2001, 73 (19), 4584–4591.

[173]. **Sajonz P., Zhong G., Guiochon G.**, *Influence of the concentration dependence of the mass transfer properties on the chromatographic band profiles I. Apparent axial dispersion coefficient in frontal analysis,* J. Chromatogr. A, 1996, 728 (1-2), 15-23.

[174]. **Sajonz P., Kele M., Zhong G., Sellergren B., Guiochon G.**, *Study of the thermodynamics and mass transfer kinetics of two enantiomers on a polymeric imprinted stationary phase,* J. Chromatogr. A, 1998, 810 (1-2), 1-17.

[175]. **Andrzejewska A., Kaczmarski K., Guiochon G.**, *Theoretical study of the accuracy of the pulse method, frontal analysis, and frontal analysis by characteristic points for the determination of single component adsorption isotherms,* J. Chromatogr. A, 2009, 1216 (7), 1067-83.

[176]. **Ruiz M., Sastre A.M., Zikan M.C., Guibal E.**, *Palladium sorption on glutaraldehyde-crosslinked chitosan in fixed-bed systems,* J Appl Polym Sci, 2001, 81 (1), 153-165.

[177]. **Juang R.S., Kao H.C., Chen W.**, *Column removal of Ni(II) from synthetic electroplating waste water using a strong-acid resin,* Sep. Purif. Technol., 2006, 49 (1), 36-42.

[178]. **Lin L.C., Li J.K., Juang R.S.**, *Removal of Cu(II) and Ni(II) from aqueous solutions using batch and fixed-bed ion exchange processes,* Desalination, 2008, 225 (1-3), 249-259.

[179]. **Helfferich, F.** Ion Exchange (Chapter 5, p. 140). McGraw-Hill, New York, 1962.

[180]. **Pesavento M., Biesuz R., Alberti G., Sturini M.**, *Separation of copper(II) and aluminium(III) from fresh waters by solid phase extraction on a complexing resin column,* J. Sep. Sci., 2003, 26, 381.

[181]. **Pesavento M., Profumo, Sastre A.**, *Chromatographic behaviour of trace metal ions on a strong base anion exchange resin functionalized by azo ligands,* Talanta, 1994, 41 (10), 1689-1697.

[182]. **Helfferich, F.** Ion Exchange (Chapter 9, p. 466). McGraw-Hill, New York, 1962.

[183]. **Hennion M.C., Cau-Dit-Coumes C., Pichon V.**, *Trace analysis of polar organic pollutants in aqueous samples: Tools for the rapid prediction and optimisation of the solid-phase extraction parameters,* J. Chromatogr. A, 1998, 823 (1–2), 147-161.

[184]. **Aksu Z., Gonen F.**, *Biosorption of phenol by immobilized activated sludge in a continuous packed bed: Prediction of breakthrough curves,* Process Biochem., 2004, 39, 599-613.

[185]. **Pesavento M., Sturini. M., D'Agostino G., Biesuz R.**, *Solid phase extraction of copper(II) by fixed bed procedure on cation exchange complexing resins,* J. Chromatogr A, 2010, 1217 (8), 1208-1218.

[186]. **D'Agostino G., Alberti G., Biesuz R., Pesavento M.**, *Potentiometric sensor for atrazine based on a molecular imprinted membrane,* Biosens Bioelectron., 2006, 15 (22), 145-52.

[187]. **K. Yoshimatsu, K. Reimhult, A. Krozer, K. Mosbach, K. Sode, L. Ye.**, *Uniform molecularly imprinted microspheres and nanoparticles prepared by precipitation polymerization: the control size suitable for different analytical applications,* Anal Chim Acta., 2010, 657 (2), 215.

[188]. **G. Vasapollo, R. D. Sole, L. Mergola, M. R. Lazzoi, A. Scardino, S. Scarrano, G. Mele.** *, Molecularly Imprinted Polymers: Present and Future Prospective,* Int. J. Mol. Sci., 2011, 12 (9), 5908-5945.

[189]. **S. Pardeshi, S. K. Singh.**, *Precipitation polymerization: a versatile tool for preparing molecularly imprinted polymer beads for chromatography applications,* RSC Adv., 2016, 6, 23525-23536.

[190]. **Plaza S., GruziÏ íski R.**, *Homogenous and hetrogenous thermal decomposition of diphenyl disulfide,* Wear, 1996, 194, 212.

[191]. **Plaza S., Mazurkiewicz B., Gruziński R.***, Thermal decomposition of dibenzyl disulphide and its load-carrying mechanism,* Wear, 1994, 174, 209.

[192]. **Sevastyanova O., Pasalskiy B., Zhmud B.**, *Copper Release Kinetics and Ageing of Insulation Paper in Oil-Immersed Transformers,* Engineering, 2015, 7, 514-529.

[193]. **Dukhi V., Bissessur A., Martincigh B.**, *Formation of Corrosive Sulfur with Dibenzyl Disulfide in Fluid-Filled Transformers,* Ind. Eng. Chem. Res, 2016, 55 (11), 2911–2920.

[194]. **Burganov B.I., Lobanov A.V., Borisov I.A., Reshetilov A.N.**, *Criterion for Hill equation validity for description of biosensor calibration curves,* Anal. Chim. Acta, 2001, 427, 11–19.

[195]. **Vepari C., Kaplan D.L.**, *Silk as a biomaterial,* Prog. Poly. Sci., 2007, 32, 991–1007.

[196]. **Wang, Y.Z.**, *Stem cell-based tissue engineering with silk biomaterials,* Biomaterials, 2006, 27, 6064–6082.

[197]. **Lu Q., Hu X., Wang X., Kluge J. A., Lu S., Cebe P., Kaplan D. L.**, *Water-Insoluble Silk Films with Silk I Structure water annealing,* Acta Biomater., 2010, 6 (4), 1380-1387.

[198]. **Nam J., Park Y.H.**, *Morphology of Regenerated Silk Fibroin: Effects of Freezing Temperature, Alcohol Addition, and Molecular Weight,* J Appl Polym Sci, 2001, 81, 3008–3021.

[199]. **Kim S., Marelli B., Brenckle M.A., Mitropoulos A.N., Gil E.S., Tsioris K., Tao H., Kaplan D.L., Omenetto F.G.**, *All-water-based electron-beam lithography using silk as a resist,* Nat Nanotechnol, 2014, 9 (4), 306-10.

[200]. **Kim S., Mitropoulos A.N., Spitzberg L.D., Tao H., Kaplan D.L., Omenetto F.G.***, Silk inverse opals,* Nat Photon 2012, 6, 818–823.

[201]. **Diao Y.Y., Liu X.Y., Toh G.W., Shi L., Zi J.**, *Multiple Structural Coloring of Silk-Fibroin Photonic Crystals and Humidity-Responsive Color Sensing,* Adv Funct Mater, 2013, 23 (43).

[202]. **Xu L., Jiang X., Zhao G., Ma D., Tao H., Liu Z., Omenetto F.G., Yang L.**, *High-Q silk fibroin whispering gallery microresonator,* Optics Express, 2016, 24 (18), 20825-20830.

[203]. **Pritchard E. M., Hu X., Finley V., Kuo C. K., Kaplan, D. L.**, *Effect of Silk Protein Processing on Drug Delivery from Silk Films,* Macromol. Biosci., 2013, 13, 311-320.

[204]. **Craig C., Riekel C.**, *Comparative architecture of silks, fibrous proteins and their encoding genes in insects and spiders,* Comp. Chem. Physiol. B Biochem. Mol. Biol, 2002, 133, 493–507.

[205]. **Omenetto F.G., Kaplan D.L.**, *New opportunities for an ancient material,* Science, 2010, 329, 528–531.

[206]. **Hoa M.P., Wanga H., Lau K.T.**, *Effect of degumming time on silkworm silk fibre for biodegradable polymer composites,* Appl Surf Sci, 2012, 258, 3948– 3955.

[207]. **Babin V., Karpusenka V., M. Moradi, C. Roland, Sagui C.**, *Adaptively Biased Molecular Dynamics:An Umbrella Sampling Method With aTime-Dependent Potential,* Int J Quantum Chem, 2009, 109, 366-3678.

[208]. **Mason P.E., Lerbret A., Saboungi M.L., Neilson G.W., Dempsey C.E., Brady J.W.**, *Glucose Interactions with a Model Peptide,* Proteins, 2011, 79 (7), 2224–2232.

7 ACKNOWLEDGMENTS

I would like to thank all my group of research in particularly my Tutor the professor Maria Pesavento, for the kindness and the patience in supervision and teaching during all the Ph.D. path. A great thank goes to all the collaboration groups in particular to Luigi Zeni and Nunzio Cennamo of the Second University of Campania and Letizia De Maria of the RSE for allowing me to undertake this path which has been the most formative both at a personal and professional level. I would like to thank them even for the friendship and all the work which has been done together. A particular thanks go to Professor Fiorenzo Omenetto which hosted me in his research group, for making me feel like welcome and for giving me access to multiple resources. A big thank to his co-workers David Kaplan and Marco Liscidini for the disponibility and kindness in discussing the work. A great thanks to the professor and employee personal of the chemistry department of Pavia which help me with competence and instrumentation other than supporting me in a various way, Prof. Profumo, Prof. Alberti, Prof. Biesuz, Prof. Merli, Prof. Ghigna and Dr. Girella, Dr. Cucca. I thank my ex students Domingo, Rachele and Alessandra for the work did and the great time spent together and all the colleagues and friend with whom I have had the fortune to collaborate during these years. Last but not least all my enlarged family which is always present.